STUDIES ON GOLD(I) COMPLEXES: FROM CHIRAL CATALYSTS TO ELUSIVE INTERMEDIATES

Alba Helena Pérez Jimeno

UNIVERSITAT ROVIRA i VIRGILI

Studies on Gold(I) Complexes: from Chiral Catalysts to Elusive Intermediates

Alba Helena Pérez Jimeno

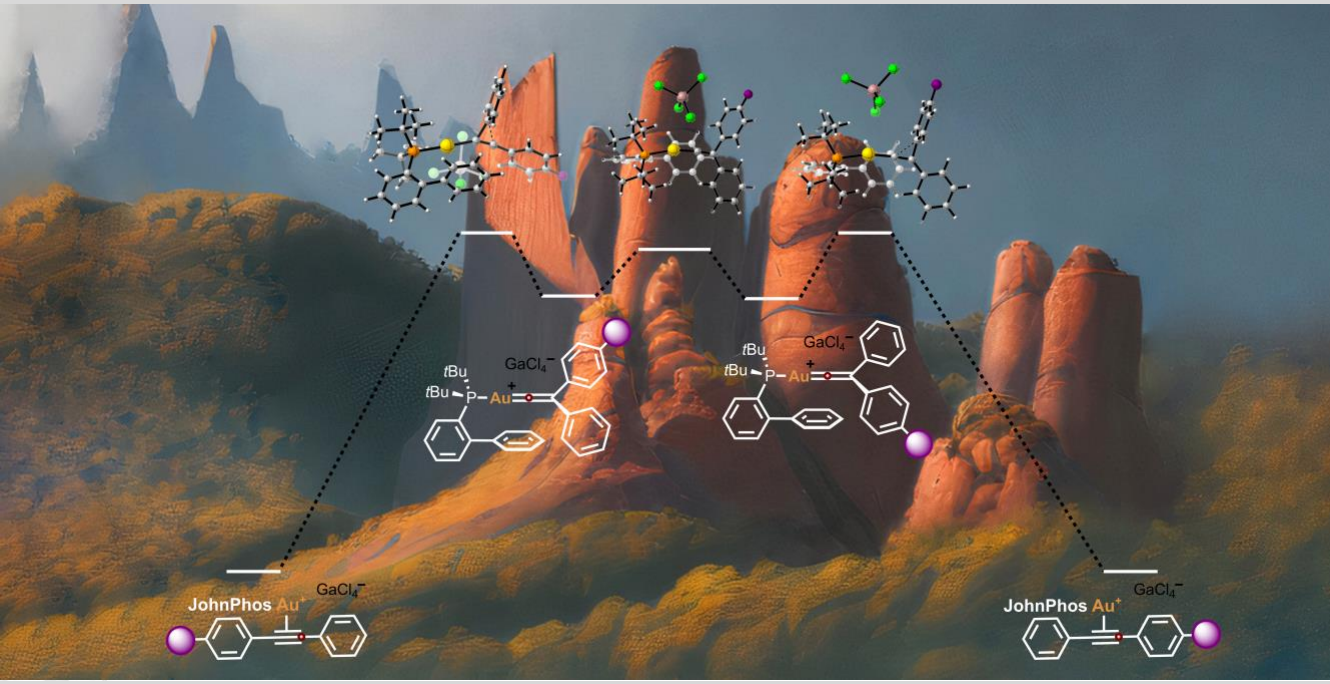

DOCTORAL THESIS
2023

Alba Helena Pérez Jimeno

Studies on Gold(I) Complexes: from Chiral Catalysts to Elusive Intermediates

DOCTORAL THESIS

Supervised by Professor Antonio M. Echavarren

Institut Català d´Investigació Química (ICIQ)

Tarragona 2023

ICIQ Institut Català d'Investigació Química

UNIVERSITAT ROVIRA i VIRGILI

I STATE that the present study, entitled "Studies on Gold(I) Complexes: from Chiral Catalysts to Elusive Intermediates", presented by Alba Helena Pérez Jimeno to award the degree of Doctor, has been carried out under my supervision at the Institut Català d´Investigació Química (ICIQ).

Tarragona, March 10th, 2023

Doctoral Thesis Supervisor

Prof. Antonio M. Echavarren Pablos

A mis padres

"Lo que conocemos es una gota, lo que no conocemos es un océano"

Isaac Newton

Acknowledgements

Quiero comenzar dando las gracias a mi director de tesis Antonio M. Echavarren, por darme la primera oportunidad como Summer Fellow, y todas las que vinieron después. Gracias a él, no solo he aprendido (mucha) química orgánica y organometálica, sino también toda clase de curiosidades insólitas acerca de aves, animales y, por supuesto, ópera. En estos años Antonio me ha ayudado a crecer personal y profesionalmente, ampliando no solo mi conocimiento sino también aportándome más confianza en mí misma y forjando mi espíritu crítico.

Además, esta Tesis no hubiera sido posible sin el respaldo de Sonia Gavaldá e Imma Escofet, miembros indispensables del grupo, que siempre están ahí para echar una mano y para ofrecerte un buen consejo en los momentos de duda. Además, quiero darte las gracias Imma por toda tu ayuda con los DFT.

I would like to thank Dr. Abraham Mendoza for the opportunity of joining his group during my short stay in the University of Stockholm. Additionally, I want to thank the people who made my stay warmer in such a cold place: Matteo, Alba, Bea, Stefanie and Emanuele.

I also want to thank the Research Support Area of ICIQ: Nuclear Magnetic Resonance, X-Ray Diffraction, High Resolution Mass Spectrometry, CHROMTAE and CRTU.

I would like to continue by thanking all the current and former members of the Echavarren group, for the moments shared in the lab, the interesting chemical discussions, and the continuous learning. Especially I want to thank those people with whom I have the pleasure to collaborate with: Dr. Giuseppe Zuccarello, Dr. Marc Montesinos, Dr. Cristina García and Dr. Inma Martín.

Quiero recalcar que de esta experiencia, además de compañeros de laboratorio, me llevo amigos. Gracias Joan, por integrarme y hacerme sonreir desde el pimer día, ha sido un placer ser vecinos de vitrina y compañeros de piso. Gracias Mauro e Inma, por ser un pack indivisible con respuesta para mis innumerables preguntas. Cristina, gracias por tus continuas enseñanzas, por las discusiones sobre “physical organic chemistry”, por motivarme día a día y por seguir apoyándome incluso desde lejos. Muchísimas gracias a las nuevas generaciones del laboratorio, Tania, Anna y Gala, por ser un soplo de aire fresco y convertir el laboratorio en una reunión de amigas, y a Laura, a la que con gusto acogemos en el 2.3 con la alegría que desprende. Finalmente, gracias, Ana, por dar cada paso junto a mí, por compartir nuestras frustraciones y dudas y por salir juntas de este lío en el que nos metimos en 2018.

Quiero dar las gracias a dos de mis postdocs favoritos, Leo y Marc, por animarme cuando no veía el final de la tesis, y por los buenos momentos pasados en el “piso de Marc”, los tiempos del covid hubieran sido mucho más duros sin vosotros. También quiero agradecer los momentos compartidos a Oti, Riccardo, Antonia, Andrea, Edu, Isa, Pablo, Àlex, Nico, Víctor y Eric (sí, ya estás adoptado en el grupo).

Además, me gustaría dar las gracias a aquellas personas que, sin compartir grupo de investigación conmigo, me han acompañado estos años, gracias, Ali, por siempre llevar la sonrisa puesta, gracias, Jana y Ángel, por ser los mejores y más ruidosos compañeros de piso. No me olvido del resto de los "lunchers" Bruna, Adi, Pablo, y Patri, que tantos buenos momentos me han dado. También quiero darle las gracias a Miguel Bernús y a los que se nos unieron después (Isa, Albert, Enric), por todas las cenas que han alegrado nuestras tardes más duras. Y por supuesto gracias, Alba Martínez Bascuñana, en estos años te has convertido en una amiga indispensable y una fuente continua de planes e ideas para solucionar los días. ¡Qué habría hecho yo sin ti!

En especial, quiero dar las gracias a mi mejor casualidad, David. Que me ha enseñado que sin agobiarse también se llega a los sitios, sólo que con menos disgustos, que siempre tiene una broma que hacerme para subirme el ánimo y a quien admiro profundamente, siempre un paso por delante de mí y tendiéndome una mano para ayudarme a pillarlo, te quiero.

Llegados a este punto, quiero dar las gracias a mis abuelos, por cuidarme y apoyarme siempre, a mi abuela Leticia, por su cariño incondicional, a mi abuela Micaela por siempre animarme a estudiar, a mi abuelo Miguel por quitarle hierro a todo y a mi abuelo Pepe por molestarse en entender lo que era una Tesis Doctoral para saber qué estaba haciendo yo en Tarragona.

Quiero extender mis agradecimientos a mi familia y amigos, por todos los buenos momentos vividos y el apoyo, aun no teniendo claro de qué va esto de la química organometálica.

Quiero terminar dando las gracias a los culpables de que esté escribiendo este manuscrito. Gracias, papá y mamá por ser mi soporte constante, por animarme a volar lejos cuando fue necesario y por enseñarme lo que es realmente importante. No hubiera llegado tan lejos sin vuestro apoyo, os quiero muchísimo.

This work was carried out with the support of the Ministerio de Ciencia e Innovación (PID2019-104815GB-I00/AEI/10.13039/501100011033, and FPU predoctoral fellowship (FPU18/03298) to A.H.P.J. from 2019 to 2023), the Severo Ochoa Excellence Accreditation 2020-2023 (CEX2019-000925-S), the AGAUR (2021 SGR 1256), the CERCA Program/Generalitat de Catalunya and the ICIQ foundation for financial support.

At the time of writing this thesis, the research summarized herein have been published in

"Dissecting Electronic and Steric Effects of Chiral Gold(I) Pyrrolidinyl-Biphenylphosphine Catalysts"

Zuccarello, G.; Escofet, I.; Nannini, L. J.; Arroyo-Bondía, A.; Fincias, N.; Arranz, I.; Pérez-Jimeno, A. H.; Peeters, M.; Martín-Torres, I.; Sadurní, A.; García, V.; Wang, Y.; Kirillova, M. S.; Caniparoli, U.; Núñez, G. D.; Maseras, F.; Besora, M.; Echavarren, A. M. *Manuscript in preparation*

In addition, other results which are not discussed in this thesis have been published in:

"***Enantioselective Folding of Enynes by Gold(I) Catalysts with a Remote C2-Chiral Element***" Zuccarello, G.; Mayans, J. G.; Escofet, I.; Scharnagel, D.; Kirillova, M. S.; Pérez-Jimeno, A. H.; Calleja, P.; Boothe, J. R.; Echavarren, A. M. *J. Am. Chem. Soc.* **2019**, *141*, 11858–11863. (Highlighted in *Synfacts* **2019**, *15*, 1135.)

Table of Contents

Prologue

This Doctoral Thesis manuscript has been divided into three main parts, a general introduction on gold(I) catalysis and two research chapters, which are preceded by the abstract and general objectives of the Thesis and followed by the overall conclusions of the work. Each research chapter contains five sections including a specific introduction on the research topic, the objectives, the discussion of the obtained results, the conclusions and the experimental section. The references and numbering are organized by chapters.

Chapter I, *"General Introduction"* provides an overview of the basic principles of homogeneous gold(I) catalysis including the cycloisomerizations of enynes. Additionally, the studies on gold(I) carbenes as intermediates in gold(I) catalysis is presented.

Chapter II, "*Expanding the Pyrrolidinyl-Biaryl Phosphine Gold(I) Complexes Family*" presents the design, synthesis and performance study of two new members of the family of chiral pyrrolidinyl-biaryl phosphine gold(I) complexes. The synthesis of the complexes was performed in collaboration with Dr. Marc Montesinos and Dr. Inma Martín. This work pretends to complete the project started during my master thesis done in collaboration with Giuseppe Zuccarello, Joan G. Mayans, Dr. Imma Escofet, Dr. Dagmar Scharnagel, Dr. Mariia S. Kirillova, Pilar Calleja and Jordan R. Boothe on the study of pyrrolidinyl-biphenyl phosphine gold(I) complexes family, published in *J. Am. Chem. Soc.* **2019**, *141*, 11858–11863.

Chapter III, "*On the Nature of Gold(I) Vinylidenes*" discloses a deep study on gold(I) vinylidenes, by presenting a new way for accessing them from gold(I) vinylidenoids. A strategy for the generation of gold(I) vinylidenoids has been developed together with the experimental study of their reactivity. DFT studies has been performed to support the mediation of gold(I) vinylidenes in these transformations. The project was started in collaboration with Dr. Cristina García-Morales.

List of Abbreviations and Acronyms

In this manuscript, the abbreviations and acronyms most commonly used in organic and organometallic chemistry have been used following the recommendations of "Guidelines of Authors" of the Journal of Organic Chemistry.

Additional abbreviations and acronyms used in this manuscript are listed below:

APCI	atmospheric pressure chemical ionization
BAr_4^{F-}	tetrakis[3,5-bis(trifluoromethyl)phenylborate]
BF4	tetrafluoroborate
BINAP	2,2'-bis(diphenylphosphino)-1,1'-binaphthyl
BINOL	1,1'-binaphthol
BIPHEP	(Biphenyl-2,2'-diyl)bis(diphenylphosphine)
dr	diastereomeric ratio
ee	enantiomeric excess
er	enantiomeric ratio
Diipf	*1,1′-Bis(diisopropylphosphino)ferrocene*
Dppf	1,1′-Bis(diphenylphosphino)ferrocene
ESI	electrospray ionization
JohnPhos	(2-biphenyl)di-tert-butylphosphine
IPr	1,3-bis(2,4,6-trimethylphenyl)imidazole-2-ylidene
L	ligand
MALDI	matrix assisted laser desorption ionization
MeOBIPEP	bis(diphenylphosphino)-6,6′-dimethoxy-1,1′-biphenyl
MeCN	acetonirile
MS	mass spectrometry/molecular sieves
MW	microwave irradiation
NBO	natural bond orbital
NHC	N-heterocyclic carbene
OTf^-	triflate
SFC	Supercritical Fluid Chromatography
TS	transition state

Abstract

Gold(I) was ignored in the chemistry world until the end of the 20th century. However, the special ability of gold(I) to activate unsaturated bonds compared to other transition metals caused an exponential growth in the use of gold(I) complexes as catalysts in different reactions. To develop the enantioselective version of these reactions, several strategies have been followed.

Our group developed a folding strategy via ligand design, which provides excellent results in the gold(I)-catalyzed enantioselective cyclization of enynes. The strategy is based on the ability of a family of JohnPhos gold(I) complexes containing C_2-symmetric *trans*-2,5-diaryl pyrrolidines to encapsulate the substrates, directing the nucleophilic attack. With the aim of expanding the applicability of these complexes, we have designed and synthesized two new members of this family of chiral gold(I) complexes by expanding the central ring of their structure (Scheme 1). The performance of the new complexes has been tested in five different reactions comparing their reactivity and enantioselectivity to the ones provided by the first generation of these pyrrolidinyl-biaryl phosphine gold(I) complexes.

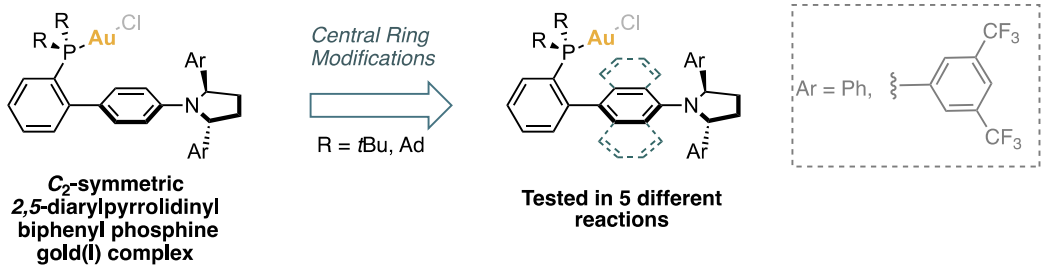

Scheme 1. Expansion of the pyrrolidinyl-biaryl phosphine gold(I) complexes family.

Mechanistic studies on gold(I)-catalyzed transformations are a hot topic in the field of gold(I) chemistry. In this context, gold(I) carbenes can be considered as the main characters and several groups have invested their efforts in the extensive study of these species. Among gold(I) carbenes, gold(I) vinylidenes are a specially intriguing type. Gold(I) vinylidenes have been proposed as intermediates of different gold(I)-catalyzed reactions. However, their high reactivity and lack of stability has limited evidence proving their existence. Based on the studies on gold(I) carbenes performed in our group, we have developed a methodology to access gold(I) vinylidenes from gold(I) vinylidenoids. To do so, we have synthesized a family of gold(I) vinylidenoids, which has shown vinylidene type reactivity (Scheme 2). This reactivity has been studied experimentally via NMR spectroscopy and by DFT, disclosing the influence of the gold(I) vinylidene intermediates in the outcome of the reaction. Additionally, the structural features of these computed gold(I) vinylidenes have been analyzed, revealing a major stabilization from the organic fragment over the one provided by the gold(I) unit.

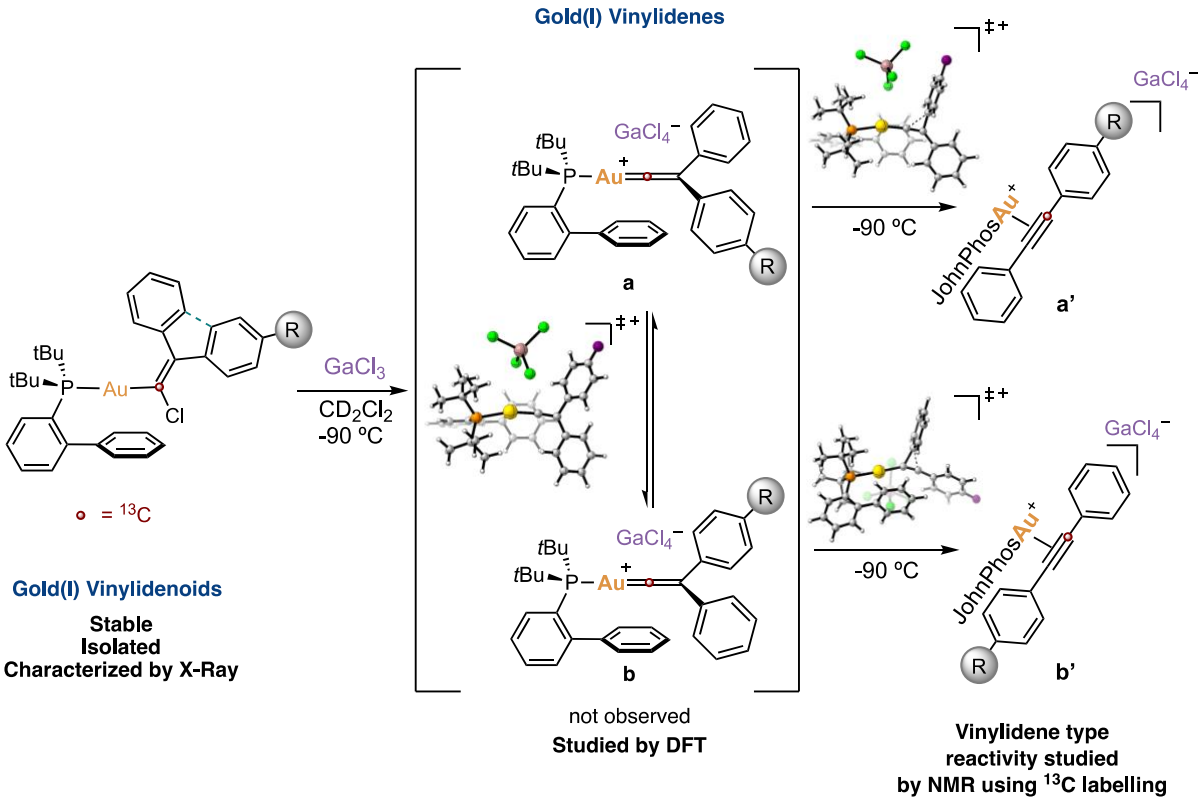

Scheme 2. Study of the connection between gold(I) vinylidenoids and gold(I) vinylidenes.

General Objectives

The aims of this Doctoral Thesis were the development of new gold(I) enantioselective complexes for their application in asymmetric gold(I)-catalyzed reactions and the study of gold(I) vinylidenes as gold(I) reactive intermediates. In particular, the objectives of this work were:

- The design and synthesis of new members of a family of pyrrolidinyl-biaryl phosphine gold(I) complexes together with the study of their performance in catalysis.
- The development of a new methodology for the generation of gold(I) vinylidenes and the study of these reactive intermediates by experimental and computational methods.

The objectives are described in more detail in each corresponding chapter.

Chapter I: *General Introduction*

Chapter I

The Dawn of Gold Chemistry

Gold is a well-known precious metal. It plays a major role in the world of jewellery and it has been associated with wealth and power along history. Despite its popularity, the scientific community ignored it for centuries, due to its stability on air and its lack of reactivity compared to other transition metals.

The origins of gold in chemistry date from 1931, when Kharasch achieved the auration of arenes by using gold(III) chloride.[1] However, the debut of gold in catalysis took place in the 80s, when metallic gold was used by the group of Hutchings as a heterogeneous catalyst for the formation of vinyl chlorides from acetylene. Parallelly, the group of Haruta found that, under similar heterogeneous conditions, this metal could catalyze the oxidation of carbon monoxide to carbon dioxide at room temperature.[2] Even so, gold did not participate in homogeneous catalysis until the end of the 20th century, when the groups of Teles[3] and Tanaka[4] reported the gold(I)-catalyzed selective addition of alcohols and water to alkynes.

These discoveries unlocked the research in homogeneous gold catalysis, which disclosed the unique ability of gold(I) complexes for the selective π-activation of unsaturated bonds (alkynes, allenes and alkenes).

Consequently, gold(I) catalysis has exponentially gained popularity in the last 20 years, providing access to otherwise difficult accessible carbon–carbon and carbon–heteroatom bonds in the synthesis of complex molecules. [5]

---

1 (a) Kharasch, M. S.; Horace; S. I. *J. Am. Chem. Soc*. **1931,** *53*, 3053-3059. (b) Carreras, J.; Echavarren A. M. *An. Quím.* **2014**, *110*, 140-143.

2 (a) Hutchings, G. J. J. *Catal.* **1985**, *96*, 292–295. (b) Haruta, M.; Kobayashi, T.; Sano, H.; Yamada, N. *Chem. Lett.* **1987**, *16*, 405–408. (c) Hutchings, G. J. *ACS Cent. Sci.* **2018**, 4, 1095–1101.

3 Teles, J. H.; Brode, S.; Chabanas, M. *Angew. Chem. Int. Ed*. **1998**, *37*, 1415–1418.

4 Mizushima, E.; Sato, K.; Hayashi, T.; Tanaka, M. *Angew. Chem. Int. Ed.* **2002**, *41*, 4563–4565.

5 (a) Hashmi, A. S. K. *Gold Bull*. **2003**, *36*, 3–9. (b) Hashmi, A. S. K. *Gold Bull*. **2004**, *37*, 51–65. (c) Furstner, A.; Davies, P. W. *Angew. Chem. Int. Ed.* **2007**, *46*, 3410–3449. (d) Hashmi, A. S. K. *Chem. Rev.* **2007**, *107*, 3180–3211. (e) Jiménez-Núñez, E.; Echavarren, A. M. *Chem. Rev.* **2008**, *108*, 3326–3350. (f) Fürstner, A. *Chem. Soc. Rev.* **2009**, *38*, 3208–3221. (g) Shapiro, N. D.; Toste, F. D. *Synlett*, **2010**, 675–691. (h) Obradors, C.; Echavarren, A. M. *Acc. Chem. Res.* **2014**, *47*, 902– 912. (i) Fensterbank, L.; Malacria, M. *Acc. Chem Res.* **2014**, *47*, 953–965. (j) Dorel, R.; Echavarren, A. M. *Chem. Rev.* **2015**, *115*, 9028–9072. (k) Day, D.P.; Chan, P.W. H. *Adv. Synth. Catal.* **2016**, *358*, 1368–1384. (l) Boyle, J. W.; Zhao, Y.; Chan, P.W. H. *Synthesis*, **2018**, *50*, 1402–1416.

General Aspects of Gold(I) Catalysis

The unique characteristics of gold, which differentiates its reactivity from the rest of the transition metals, has been ascribed to relativistic effects.[6] In the case of atoms with heavy nucleus, the electrons speed highly increases and, according to the special theory of relativity, this results in the increase of their mass. The increase of the mass causes the contraction of the *s* and *p* orbitals, rising the ionization energies of the atom. The contraction of the *s* and *p* orbitals causes a higher shielding of the electrons occupying the *d* and *f* orbitals, increasing the size of these orbitals and minimizing the repulsion between the electrons. Relativistic effects intensify with the filling of 4*f* and 5*d* orbitals reaching a maximum in the case of gold ([Xe] $4f^{14}\,5d^{10}\,6s^{1}$) (Figure 1).

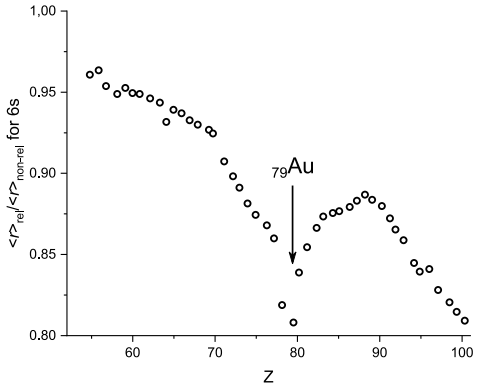

Figure 1. Calculated relativistic contraction of the 6s orbital of elements with Z 55 to 100.[7]

This phenomenon is responsible of the yellow colour of gold and of events like "aurophilicity", the attraction between two different Au(I) ions with a strength of the order of hydrogen-hydrogen bonds. Additionally, relativistic effects explain the highest electronegativity of gold among transition metals ($\chi = 2.4$), justifying its resistance to oxidation.

The exceptional ability of gold(I) to activate unsaturated bonds is also due to relativistic effects, which provides gold with a superior Lewis acidic character. The expansion of the filled *d* orbitals of gold(I) minimizes the electron-electron repulsion, allowing its interaction with the filled π orbitals of unsaturated bonds. This interaction is particularly noticeable in the activation of alkynes towards nucleophilic attack, phenomenon known as "alkynophilicity".

Finally, relativistic effects are also responsible of the preferred linear dicoordination of gold(I), since the contraction of the orbitals facilitates the *s/p* or *s/d* hybridizations.[8] This particular coordination trend

6 (a) Bartlett N. *Gold Bulletin*, **1998**, *31*, 22–25(b) Pyykk., P. *Angew. Chem. Int. Ed.* **2002**, *41*, 3573–3578. (c) Schwartz, H. *Angew. Chem. Int. Ed.* **2003**, *42*, 4442–4454. (d) Pyykk., P. *Angew. Chem. Int. Ed.* **2004**, *43*, 4412–4456. (e) Gorin, D.; Toste, F. D. *Nature*, **2007**, *446*, 395–403.

7 P. Pyykkö, J. P. Desclaux, *Acc. Chem. Res.* **1979**, *12*, 276.

8 Gimeno, M. C.; Laguna, A. *Chem. Rev.* **1997**, *97*, 511–522.

prevents gold to undergo elementary organometallic reactions, such as oxidative addition or *β*-hydride elimination. However, some examples of gold(I)/(III)-mediated cross coupling reactions have been reported. [9,10]

The reactivity of gold(I) complexes can be easily modulated by ligand design (Figure 2).[11] Thus, the use of highly donating *N*-heterocyclic carbenes generates less electrophilic gold(I) complexes while gold(I) complexes bearing less donating phosphite ligands present high electrophilicity. The use of bulky phosphines as ancillary ligands provides an intermedium electrophilicity which has been the most effective in a high number of gold(I)-catalyzed reactions.[12]

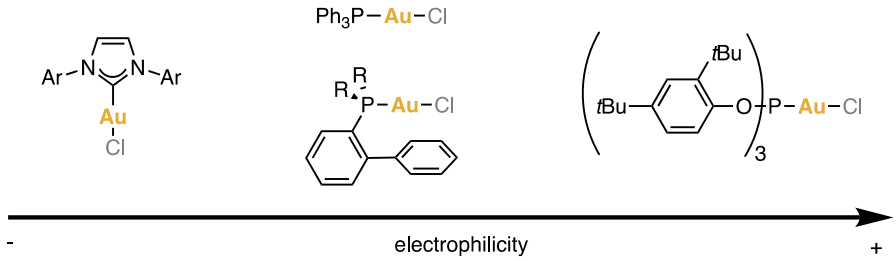

Figure 2. Electrophilicity modulation of gold(I) complexes via ligand design.

The generation of neutral gold(I) complexes can be easily achieved by directly treatment of the corresponding ligand with commercially available dimethylsulfide gold(I) chloride ($Me_2S{\cdot}AuCl$). However, these complexes need to be activated to enable coordination of gold(I) to the substrate.[13] With that aim, two main approaches have been addressed (Scheme 1). The first one is the *in situ* generation of the active complex using a chloride scavenger. However, this strategy can promote the formation of inactive chloride-bridged digold(I) species and side reactions derived from the chloride scavenger.[14] The second option is the formation of cationic complexes that substitutes the chloride by a labile ligand. In this sense, stable cationic complexes can be easily generated by treating gold(I) chloride complexes

9 (a) Livendahl, M.; Goehry, C.; Maseras, F.; Echavarren, A. M. *Chem. Commun.* **2014**, *50*, 1533–1536. (b)Joost, M.; Amgoune, A.; Bourissou, D. *Angew. Chem. Int. Ed.* **2015**, *54*, 15022– 15045. (c) Akram, M. O.; Mali, P. S.; Patil, N. T. *Org. Lett.* **2017**, *19*, 3075− 3078.

10 Chan, A.Y.; Perry, I. B.; Bissonnette, N. B.; Buksh, B.F.; Edwards, G. A.; Frye, L. I.; Garry, O. L.; Lavagnino, M. N.; Li, B. X.; Liang, Y.; Mao, E.; Millet, A.; Oakley, J. V.; Reed, N. L.; Sakai, H. A.; Seath, C. P.; MacMillan, D. W. C. *Chemical Reviews* **2022**, *122*,1485-1542.

11 (a)Hashmi, A. S. K.; *Chem. Rev.* **2007**, *107*, 3180–3211. (b) Gorin, D. J.; Sherry, B. D.; Toste, F. D. *Chem. Rev.* **2008**, *108*, 3351–3378. (b) Wang, W.; Hammond, G. B.; Xu, B. *J. Am. Chem. Soc.* **2012**, *134*, 5697–5705.

12 Zuccarello, G.; Zanini, M.; Echavarren, A. M. *Isr. J. Chem.* **2020**, *60*, 360–372.

13 Ranieri, B.; Escofet, I.; Echavarren, A. M. *Org. Biomol. Chem*. **2015**, 13, 7103–7118.

14 (a) Wang, D.; Cai, R.; Sharma, S.; Jirak, J.; Thummanapelli, S. K.; Akhmedov, N. G.; Zhang, H.; Liu, X.; Petersen, J. L.; Shi, X. *J. Am. Chem. Soc.* **2012**, *134*, 9012–9019. (b) Homs, A.; Escofet, I.; Echavarren, A. M. *Org.Lett.* **2013**, *15*, 5782−5785. (c) Franchino, A.; Montesinos-Magraner, M.; Echavarren, A.M. *Bull. Chem. Soc. Jpn.* **2021**, *94*, 1099–1117.

with a silver or sodium salt in the presence of nitriles.[15] With this strategy, gold(I) cationic complexes are isolated from the chloride salts, avoiding undesired side reactions. These cationic complexes can directly participate in the reaction after replacement of the labile ligand by the substrate through an associative ligand exchange mechanism.

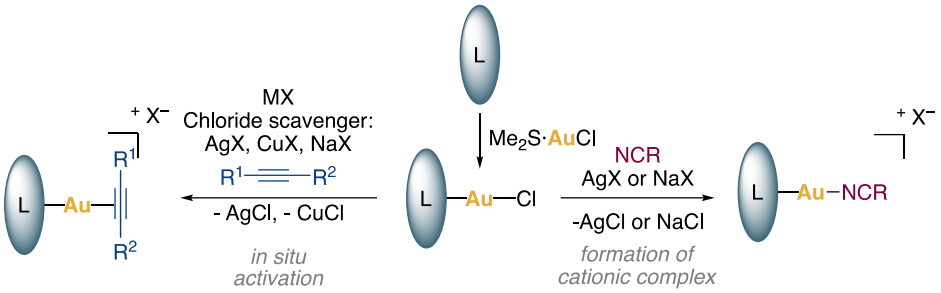

Scheme 1.Generation and modes of activation of gold(I) complexes.

Cycloisomerization of 1,*n*-Enynes

Alkynophilicity is one of the main reasons for the rapid rise in popularity of gold in organic chemistry.[16] Gold complexes activate alkynes through the formation of (η^2-alkyne)gold(I) species **1**, susceptible to nucleophilic attack. This nucleophilic attack usually happens via outer-sphere mechanism and following a Markovnikov selectivity, forming *trans*-alkenyl gold complexes **2** as intermediates in different reactions (Scheme 2).[16a,17]

Scheme 2. Trans nucleophilic addition to (η^2-alkyne) gold(I) complexes.

The activation of alkynes by gold has been key for the development of 1,*n*-enyne cyclization reactions, which give direct access to complex molecules from simple starting materials forming C–C and

15 (a) Nieto-Oberhuber, C.; López, S.; Muñoz, M. P.; Cárdenas, D. J.; Buñuel, E.; Nevado, C.; Echavarren, A. M. *Angew. Chem. Int. Ed.* **2005**, *44*, 6146–6148. (b) Amijs, C. H. M.; López-Carrillo, V.; Raducan, M.; Pérez-Galán, P.; Ferrer, C.; Echavarren, A. M. *J. Org. Chem*. **2008**, *73*, 7721–7730.

16 (a) García-Mota, M.; Cabello, N.; Maseras, F.; Echavarren, A. M.; Pérez-Ramírez, J.; López, N. *ChemPhysChem* **2008**, *9*, 1624 – 1629. (b) Hoffmann-Röder A.; Krause, N. *Org. Biomol. Chem*., **2005,** *3*, 387–391.

17 (a) Hashmi, A. S. K.; Weyrauch, J. P.; Frey, W.; Bats, N. W. *Org. Lett.* **2004**, *6*, 4391–4394. (b) Kennedy-Smith, J. J.; Staben, S. T.; Toste, F. D. *J. Am. Chem. Soc*. **2004**, *126*, 4526–4527.

C–heteroatom bonds.[18] Although these reactions were initially performed using different electrophilic metal salts and complexes, the use of gold successfully overcomes the performance of other systems.[19]

Among all 1,*n*-enyne cyclization reactions, cyclization of 1,6-enynes has been deeply studied, allowing the understanding of different mechanisms through which these substrates can evolve into diverse cyclized products depending on the enyne substituents and the reaction conditions (Scheme 3).[5h,19a,20]

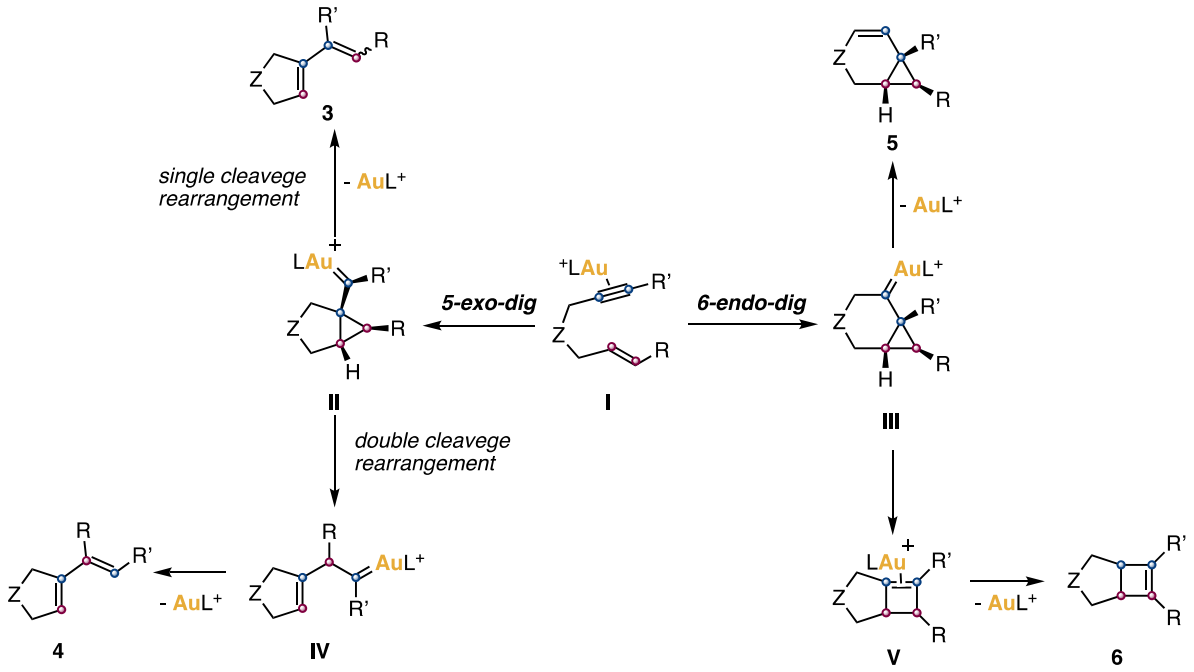

Scheme 3. Main pathways for the gold(I)-catalyzed cycloisomerization of 1,6-enynes.

In gold(I)-catalyzed 1,6-enyne cyclizations, Gold(I) complexes coordinate to the alkyne, forming (η^2-alkyne)gold complexes **I**, which can undergo 5-*exo*-dig cyclization to form cyclopropyl gold carbenes **II** or 6-*endo*-dig cyclization to cyclopropyl gold carbenes **III** after an intramolecular nucleophilic attack of the alkene. At this point, these intermediates can give different products depending on the presence

18 (a) Lloyd-Jones, G. C. *Org. Biomol. Chem*., **2003**, *1*, 215–236. (b) Aubert, C.; Buisine, O.; Malacria, M. *Chem. Rev*., **2002**, *102*, 813–834. (b) Diver, S. T.; Giessert, A. J. *Chem. Rev*., **2004**, *104*, 1317–1382. (c) Echavarren, A. M.; Nevado, C. *Chem. Soc. Rev*., **2004**, *33*, 431–436.

19 (a) Nieto-Oberhuber, C.; Muñoz, M. P.; Buñuel, E.; Nevado, C.; Cárdenas, D. J.; Echavarren, A. M. *Angew. Chem. Int. Ed.* **2004**, *43*, 2402–2406. (b) Nieto-Oberhuber, C.; Muñoz, M. P.; López, S.; Jiménez-Núñez, E.; Nevado, C.; Herrero-Gómez, E.; Raducan, M.; Echavarren, A. M. *Chem. Eur. J.* **2006,** *12*, 1677–1693. (c) Jiménez-Nuñez, E.; Echavarren, A. M. *Chem. Commun.* **2007**, 333–346.

20 (a) Nieto-Oberhuber, C.; López, S.; Muñoz, M. P.; Cárdenas, D. J.; Buñuel, E.; Nevado, C.; Echavarren, A. M. *Angew. Chem. Int. Ed.* **2005**, *44*, 6146–6148. (d) Ferrer, C.; Raducan, M.; Nevado, C.; Claverie, C. K.; Echavarren, A. M. *Tetrahedron* **2007**, *63*, 6306–6316. (e) Soriano, E.; Marco-Contelles, J. *Acc. Chem. Res.* **2009**, *42*, 1026–1036. (f) Escribano-Cuesta, A.; Pérez-Galán, P.; Herrero-Gómez, E.; Sekine, M.; Braga, A. A. C.; Maseras, F.; Echavarren, A. M. *Org. Biomol. Chem*. **2012**, *10*, 6105–6111.

of external nucleophiles. In the absence of nucleophiles, cyclopropyl gold carbenes **II** can evolve through a single cleavage rearrangement to form 1,3-dienes **3**.[21] In this process, it takes place a 1,3-migration of the alkene terminal carbon to the alkyne terminal carbon. Otherwise, intermediates **II** can rearrange into gold(I) carbenes **IV** by the formal insertion of the terminal alkene carbon into the alkyne carbons via a double cleavage rearrangement. Subsequent α-hydrogen elimination yields 1,3-dienes **4**.[22] By the other side, α–proto deauration in cyclopropyl gold(I) carbenes **III** will provide bicyclo[4.1.0]hept-2-enes **5**. These same intermediates **III**, can undergo ring expansion and isomerize to (η^2-cyclobutene) gold(I) complexes **V**. The isomerization and demetallation of **V** lead to cyclobutenes **6**.

The presence of external nucleophiles widely expands the possible reaction outcomes, giving access to alkoxy-, hydroxy- or aminocyclization products, after the nucleophilic attack of alcohols, water or amines to the cyclopropyl gold(I) carbene intermediates.[19a,b,20a]

Although we have centered our attention in 1,6-enynes, similar mechanisms have been observed for 1,5-enynes[23] and 1,7-enynes.[24] Additionally, macrocyclization of 1,n-enynes where $n \geq 7$ give access to larger cyclic molecules.[25]

Gold carbenes intermediates

As we have described above, gold carbenes are key intermediates in gold-catalyzed transformations.[26] Although we have introduced them in the context of 1,*n*-cyclizations (Scheme 3, Scheme 4a),[5h,19a,20] other common transformations generate gold(I) carbenes as the main intermediates. These

21 Cabello, N.; Jiménez-Núñez, E.; Buñuel, E.; Cárdenas, D. J.; Echavarren, A. M. *Eur. J. Org. Chem.* **2007**, 4217–4223.

22 (a) Ota, K.; Chatani, N. *Chem. Commun.* **2008**, 2906–2907. (b) Ota, K.: Lee, S. I.; Tang, J.-M.; Takachi, M.; Nakai, H.; Morimoto, T.; Sakurai, H.; Kataoka, K.; Chatani, N. *J. Am. Chem. Soc.* **2009**, *131*, 15203–15211.

23 (a) Zhang, L.; Kozmin, S. *J. Am. Chem. Soc*. **2004**, *126*, 11806–11807. (b) Soriano, E.; Marco-Contelles, J. *J. Org. Chem.* **2012**, *77*, 6231–6238. (c) Han, X.; Retailleau, P.; Gandon, V.; Voituriez., A. *Chem. Commun.* **2020**, *56*, 9457–9460.

24 (a) Cabello, N.; Rodríguez, C.; Echavarren, A. M. *Synlett* **2007**, 1753–1758. (b) Milián, A.; García-García, P.; Pérez-Redondo, A.; Sanz, R.; Vaquero, J. J.; Fernández-Rodríguez, M. A. *Org. Lett.* **2020**, *22*, 8464–8469.

25 Obradors, C.; Leboeuf, D.; Aydin, J.; Echavarren, A. M. *Org. Lett.* **2013**, *15*, 1576–1579.

26 For Reviews on this topic: (a) Y. Wang, M. E. Muratore, A. M. Echavarren, *Chem. Eur. J.* **2015**, *21*, 7332–7339; (b) R. J. Harris, R. A. Widenhoefer, *Chem. Soc. Rev*. **2016**, *45*, 4533–4551. (c) Navarro, M.; Bourissou, D. *Adv. Organomet. Chem.* **2021**, *76*, 101−144.

transformations include the decomposition of organic diazocompounds (Scheme 4b),[27] the ring opening of cyclopropenes (Scheme 4c)[28] or the retro-Buchner reaction of cycloheptatrienes (Scheme 4d).[29] Other examples are the 1,2-acyloxy migration of propargylic carboxylates or ethers (Scheme 4e),[30] the nucleophilic addition of *N*-oxides or sulfoxides to electrophilic (η^2-alkyne)gold(I) complexes (Scheme 4f)[31,32] and the cycloaddition of diene-allenes, which forms gold vinylidenes as intermediates (Scheme 4g)[33].

---

27 (a) Fructos, M. R.; Belderrain, T. R.; de Frémont, P.; Scott, N. M.; Nolan, S. P.; Díaz-Requejo, M. M.; Pérez, P. J. *Angew. Chem. Int. Ed.* **2005**, *44*, 5284– 5288 (b) Yu, Z.; Ma, B.; Chen, M.; Wu, H.-H.; Liu, L.; Zhang, J. *J. Am. Chem. Soc.* **2014**, *136*, 6904–6907. (c) Xi, Y.; Su, Y.; Yu, Z.; Dong, B.; McClain, E. J.; Lan, Y.; Shi, X. *Angew. Chem. Int. Ed.* **2014**, *53*, 9817–9821.

28 (a) Hadfield, M. S.; Bauer, J. T.; Glen, P. E.; Lee, A.-L. *Org. Biomol. Chem.* **2010**, *8*, 4090–4095; (b) Li, C.; Zeng, Y.; Wang, J. *Tetrahedron Lett.* **2009**, *50*, 2956–2959. (c) Li, C.; Zeng Y.; Zhang H.; Feng J.; Zhang, Y.; Wang J. *Angew. Chem. Int. Ed.* **2010**, *49*, 6413–6417. (d) For a review on gold-catalyzed transformations of cyclopropenes, see: Miege, F.; Meyer, C.; Cossy, J. *Beilstein J. Org. Chem.* **2011**, *7*, 717–734.

29 (a) Solorio-Alvarado, C. R.; Wang Y.; Echavarren, A. M. *J. Am. Chem. Soc.*, **2011**, *133*, 11952–11955. (b) Wang, Y.; McGonigal, P. R.; Herlé, B.; Besora, M.; Echavarren, A. M. *J. Am. Chem. Soc.*, **2014**, *136*, 801–809. (c) Leboeuf, D.; Gaydou, M.; Wang, Y.; Echavarren, A. M. *Org. Chem. Front.* **2014**, *1*, 759–764.

27 (d) Wang, Y.; Muratore, M. E.; Rong, Z.; Echavarren, A. M. *Angew. Chem. Int. Ed.* **2014**, *53*, 14022–14026. (e) For a review on this topic: Mato, M.; García-Morales C.; Echavarren A. M. *ChemCatChem* **2019**, *11*, 53–72.

30 (a) Gorin, D. J.; Dubé, P.; Toste, F. D.; *J. Am. Chem. Soc.* **2006**, *128*, 14480– 14481. (b) Marco-Contelles, J.; Soriano, E. *Chem. Eur. J.* **2007**, *13*, 1350– 1357. (c) Amijs, C. H. M.; López-Carrillo, V.; Echavarren, A. M. *Org. Lett.* **2007**, *9*, 4021–4024. (d) Li, G.; Zhang, G.; Zhang, L. *J. Am. Chem. Soc.* **2008**, *130*, 3740–3741. (e) Shapiro, N. D.; Toste, F. D. *J. Am. Chem. Soc.* **2008**, *130*, 9244–9245; (f) Correa, A.; Marion, N.; Fensterbank, L.; Malacria, M.; Nolan, S. P.; Cavallo, L.; *Angew. Chem. Int. Ed.* **2008**, *47*, 718–721. (g) Shapiro, N. D.; Shi, Y.; Toste, F. D.; *J. Am. Chem. Soc.* **2009**, *131*, 11654–11655; (h) Wang, S.; Zhang, G.; Zhang, L. *Synlett* **2010**, 692–706. (i) de Haro, T.; Gómez-Bengoa, E.; Cribiffl, R.; Huang, X.; Nevado, C. *Chem. Eur. J.* **2012**, *18*, 6811–6824. (j) Shiroodi, R. K.; Gevorgyan, V. *Chem. Soc. Rev.* **2013**, *42*, 4991–5001.

31 (a) Shapiro, N. D.; Toste, F. D. *J. Am. Chem. Soc.* **2007**, *129*, 4160–4161. (b) Ye, L.; Cui, L.; Zhang, G.; Zhang, L. *J. Am. Chem. Soc.* **2010**, *132*, 3258– 3259. (c) He, W.; Li, C.; Zhang, L. *J. Am. Chem. Soc.* **2011**, *133*, 8482–8485. (d) Noey, E. L.; Luo, Y.; Zhang, L.; Houk, K. N. *J. Am. Chem. Soc.* **2012**, *134*, 1078–1084; (e) Ji, K.; Zhang, L. *Org. Chem. Front.* **2014**, *1*, 34–38; (f) Vasu, D. Hung, H.-H. Bhunia, S. Gawade, S. A. Das, A. Liu, *Angew. Chem. Int. Ed.* **2011**, *50*, 6911–6914. (g) P. Nösel, L.; Nunes dos Santos Comprido, R.-S.; Lauterbach, T.; Rudolph, M.; Rominger, F.; Hashmi, A. S. K. *J. Am. Chem. Soc.* **2013**, *135*, 15662–15666. (h) Shu, C.; Liu, R.; Liu, S.; Li, J.-Q.; Yu, Y.-F; He, Q.; Lu, X.; Ye, L.-W.*Chem. Asian J.* **2015**, *10*, 91–95.

32 Schulz, J.; Jsíkovm, L.; Skríba, A.; Roithová, J. *J. Am. Chem. Soc.* **2014**, *136*, 11513–11523.

33 (a) Ye, L.; Wang, Y.; Aue, D. H.; Zhang, L. *J. Am. Chem. Soc.* **2012**, *134*, 31– 34. (b) Hashmi, A. S. K.; Braun, I.; Nösel, P.; Schädlich, J.; Wieteck, M.; Rudolph, M.; Rominger, F.; *Angew. Chem. Int. Ed.* **2012**, *51*, 4456–4460. c) Hashmi, A. S. K.; Wieteck, M.; Braun, I.; Rudolph, M.; Rominger, F.; *Angew. Chem. Int. Ed.* **2012**, *51*, 10633–10637. d) Hansmann, M. M.; Rudolph, M.; Rominger, F.; Hashmi, *A. S. K. Angew. Chem. Int. Ed.* **2013**, *52*, 2593–2598. e) Hansmann, M. M.; Rominger, F.; Hashmi, A. S. K. *Chem. Sci.* **2013**, *4*, 1552–1559. f) Hashmi, A. S. K. *Acc. Chem. Res.* **2014**, *47*, 864–876.

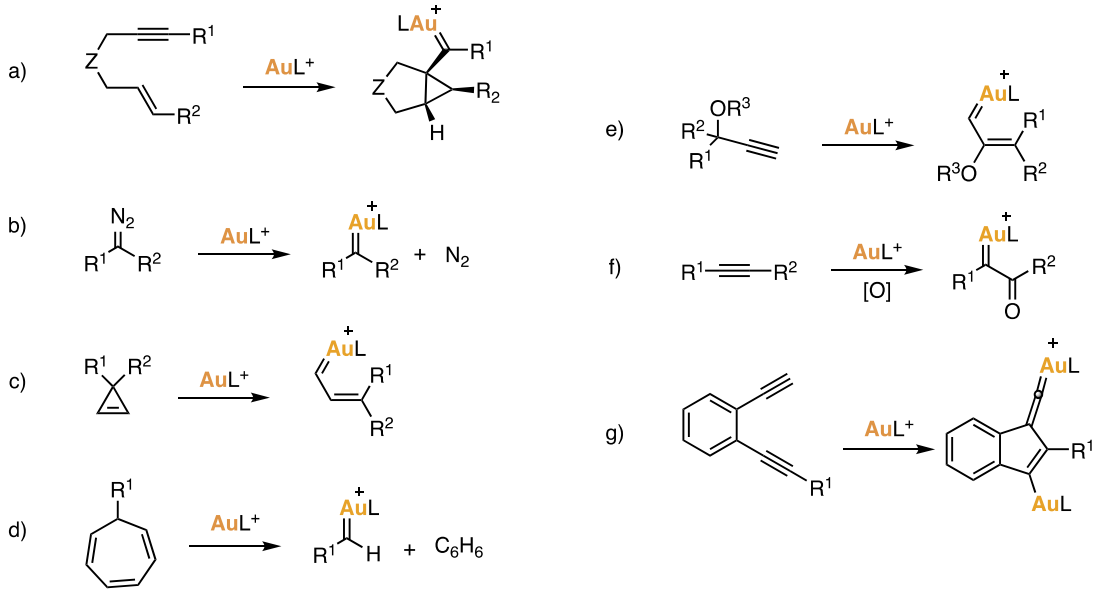

Scheme 4. Most general reactions with gold(I) carbenes as main intermediates.

Despite its ubiquity, the nature of these intermediates has been extensively questioned. However, in the last 10 years plenty of theoretical and experimental studies have been focused on unmasking these species and nowadays several groups have managed to characterize them in solution and even isolate gold carbenes in solid state.[26]

The structure of gold(I) carbenes is based on a three-center four-electron σ–hyperbond in which the two centers attached to gold compete for the π-back donation of the filled 5*d* orbitals of gold (Figure 3).[34]

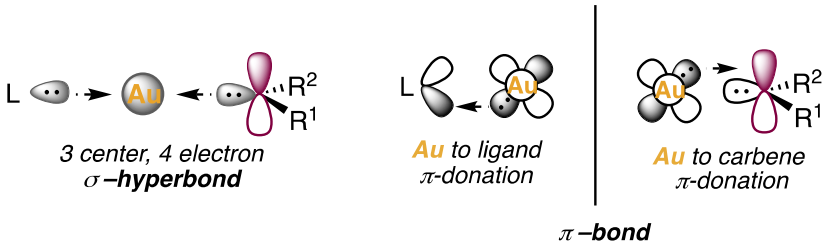

Figure 3. Bonding model for gold carbene complexes.

This situation exposes a great influence of the nature of both substituents on the bonding and reactivity of gold(I) carbenes and shows how, by tunning the ligand structure, carbene-like character can be modulated (Figure 4).

34 Benitez, D.; Shapiro, N. D.; Tkatchouk, E.; Wang, Y.; Goddard, W. A.; Toste, F. D. *Nat. Chem.* **2009**, *1*, 482–486.

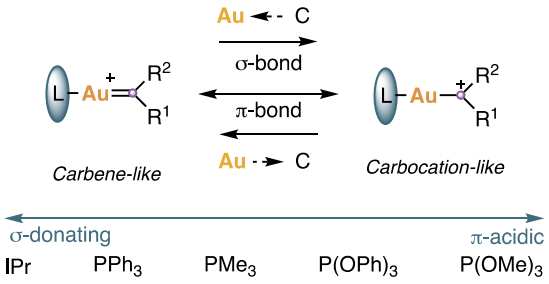

Figure 4. Influence of the ligand on the carbene/carbocation character of gold(I) carbenes.

Carbene-like character depends on the nature of the Au–C bond and it is improved when the gold-to-carbon σ-bonding is decreased and the π-bonding is increased. The electronic properties of the Au–C bond is contingent upon the Au–L bond. Thus, strongly σ-donating ligands, like NHC (*N*-heterocyclic carbenes), favour the carbene like character of gold complexes, while π-acidic phosphites ligands require from a higher π-back donation of gold to the ligand, which results in a lower Au–C π-bonding, enhancing the carbocation character. This carbene-carbocation character has been finally claimed as a mere representation of the two extreme situations, since the current interpretation of gold(I) carbenes was fully described by Toste and Goddard in 2009 as a continuum between these two edges.[32]

Gold(I) carbenes can be classified as highly electrophilic Fisher carbenes, considering the two types in which metal carbenes are divided.[35] Fischer carbenes are singlet derived carbenes with electrophilic character stabilized by the metal and the heteroatoms attached to the carbene. In this type of carbenes, the π-donating heteroatom group stabilizes the empty π orbital of the carbenes, making the metal-to-carbene π-back donation weak. The weakness of the π-back donation increases with the rise in electronegativity of the metal, becoming maximum in gold carbenes and causing their high electrophilicity. By the other side, Schrock carbenes are originated from triplet state carbenes which present nucleophilic character, derived from two covalent bonds stablished between the metal and the triplet carbene, which is more electronegative than the metal (Figure 5).

35 (a) Crabtree, R. H. in *The Organometallic Chemistry of the Transition Metals* (**2005**). John Wiley & Sons, Inc. 309–341. (b) Schubert, U. *Coord. Chem. Rev.* **1984**, *55*, 261–286. (c) Frenking, G.; Sola, M.; Vyboishchikov, S. F. J. *Organomet. Chem.* **2005**, *690*, 6178–6204.

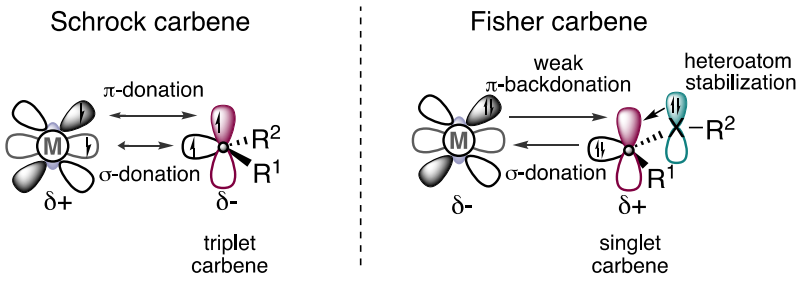

Figure 5. Types of metal carbenes.

Due to the weak π-backdonation of gold, some authors have recommended the use of the term gold(I) carbenoids to refer to gold(I) carbenes.[39] However, although both species displays similar reactivity, the difference between them can be stablished just by defining their structure (Figure 6). Carbenoids can be described as organometallic species with a similar reactivity to carbenes in which a sp^3 carbon is bonded to a metal (M) and a leaving group (X). The elimination of that leaving group will release the carbene species.[26a,36] Several studies on the synthesis and analysis of gold(I) carbenoids have been done,[37] however, in this introduction we will focus our attention on gold(I) carbenes.

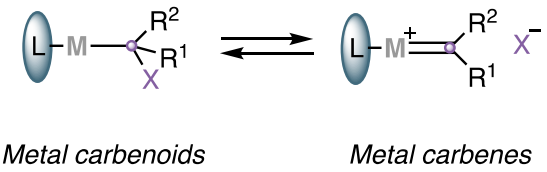

Figure 6. Structural relationship between metal carbenoids and carbenes.

To fully understand the nature of gold carbenes many groups have invested their efforts in the characterization and isolation of these important intermediates using different strategies.[24, 38] In this section the main findings in the study of Gold(I) carbenes will be exposed, evaluating the factors involved in their stability. To facilitate the understanding of this manuscript, alfa carbon in carbenes will be referred as C1 and represented as a lilac point.

36 (a) Closs, G. L.; Moss, R. A. *J. Am. Chem. Soc.* **1964**, *86*, 4042–4053. (b) Bernardi, F.; Bottoni, A.; Miscione, G. P. *Organometallics* **2000**, *19*, 5529–5532.

37 (a) Nesmeyanov, A. N.; Perevalova, É. G.; Smyslova, E. I.; Dyadchenko, V. P.; Grandberg, K. I. *Russ. Chem. Bull*. **1977**, *26*, 2417–2419. (b) Steinborn, D.; Becke, S.; Herzog, R.; Günther, M.; Kircheisen, R.; Stoeckli-Evans, H.; Bruhn, C. Z. *Anarg. Allg. Chem.* **1998**, *624*, 1303–1307. (c) Perevalova, E. G.; Struchkov, Y. T.; Dyadchenko, V. P.; Smyslova, E. I.; Slovokhotov, Y. L.; Grandberg, K. I. *Russ. Chem. Bull.* **1983**, *32*, 2529–2536.

38 Raubenheimer, H. G.; Cronje S. *Chem. Soc. Rev.*, **2008**, *37*, 1998–2011.

Synthesis and characterization of gold(I) carbenes

The first gold(I) carbene was generated in 1982 by Aumann and Fischer through a transmetalation protocol from tungsten carbene **7** (Scheme 5). [39] The use of dimethylamine and phenyl as the substituents directly attached to the carbenic carbon stabilized gold(I) carbene **8** enough to be isolated in solid state. However, the length of the Au–C1 bond (2.023 Å) typical from an Au–C(sp^2) single bond, indicated the absence of gold π-backdonation and high stabilization from the organic fragment.

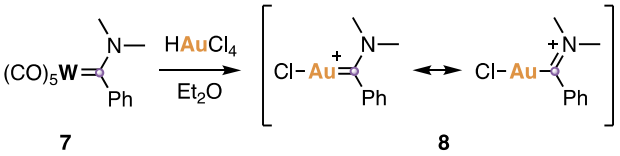

Scheme 5. First isolated Fischer type gold(I) carbene.

The transmetalation strategy was further extended by using chromium carbenes as starting materials, which allowed to expand the scope of heteroatom stabilized gold(I) carbenes. These carbenes **10** require stabilization from alkoxy groups as π-donating substituents and NHC or phosphines as ancillary ligands to gold (Scheme 6).[40] The alkoxy groups attached to C1 provide high stabilization to the gold(I) carbenes, making them stable to air, however it also prevents them from displaying any carbene like reactivity. The characterization of these species revealed extremely downfield resonance of the carbenic carbon (250-300 ppm) together with the expected linear geometry (L–Au–C1 ≈ 180º) and shortening of the C1–heteroatom bond, reinforcing the Fischer carbene nature of the synthesized structures.[33c]

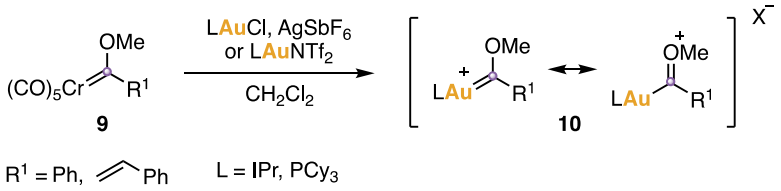

Scheme 6. Methoxy stabilized gold(I) carbenes.

In 2014, Broomer and Widenhoefer synthesized cyclopropyl methoxy carbene **12** via transmetalation from chromium carbenes. This structure was the first one in providing experimental evidence of the π-back donation of gold to the carbene, based on the bond length perturbations observed in the cyclopropyl ring. The comparison of this bond length perturbations with the ones in known cyclopropyl

39 Aumann, R.; Fischer, E. O. *Chem. Ber*. **1981**, *114*, 1853–1857.

40 (a) Fañanas-Mastral, M.; Aznar, F. *Organometallics*, **2009**, *28*, 666–668. (b) Seidel, G.; Gabor, B.; Goddard, R.; Heggen, B.; Thiel, W.; Fürstner, A. *Angew. Chem., Int. Ed*., **2014**, *53*, 879–882.

oxocarbenium ions, allowed to equate the stabilization provided by gold to the one provided by a cyclopropyl group (Scheme 7).[41]

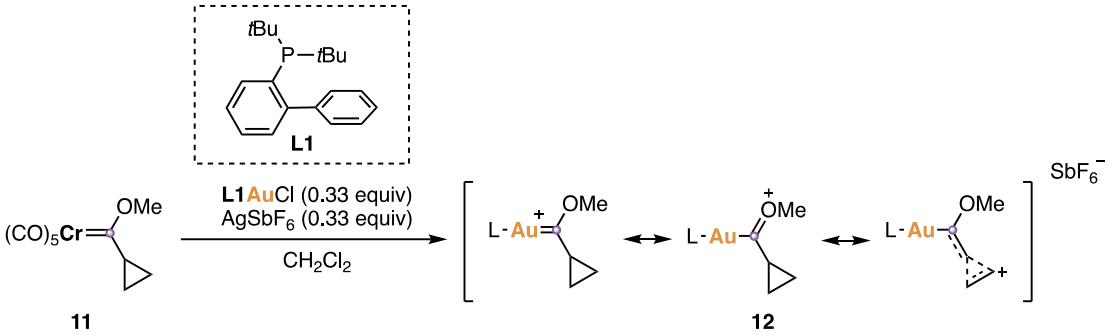

Scheme 7. Gold(I) Fischer-type carbene stabilized by π-backdonation of gold.

Although the synthesis of the above-mentioned gold(I) carbenes was crucial to elucidate their structure and properties, their stabilization via heteroatom substituents prevents their reactivity and alienate them from the gold(I) carbene intermediates typical of gold(I)-catalyzed reactions.

In 2014, Fürstner reported the synthesis and isolation of the first example of gold(I) carbene lacking π-conjugated heteroatoms directly attached to C1 (Scheme 8). [42] Gold(I) carbene **14** presented carbene reactivity leading to cyclopropanation reactions after treatment with electron-rich olefins, however the high electrodonating character of anisyl ring substituents prevented the detection of π-back donation from gold.

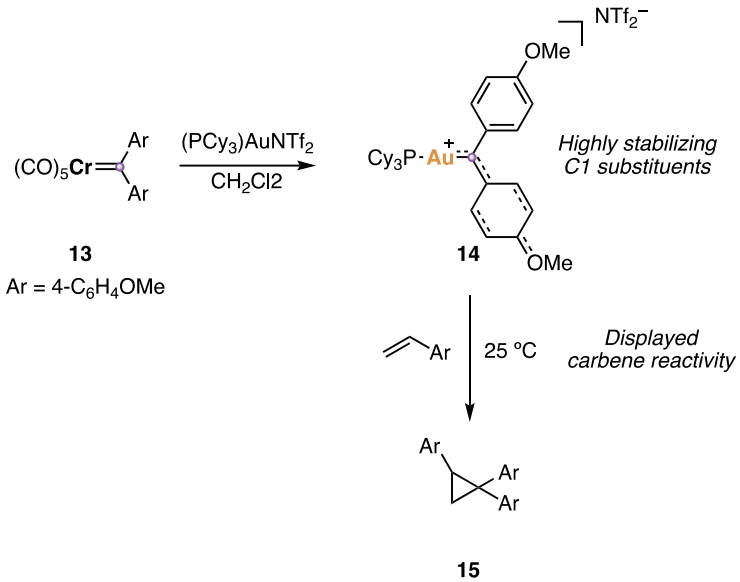

Scheme 8. Synthesis and reactivity of the first gold(I) carbene lacking π-conjugated heteroatoms.

41 Brooner, R. E. M.; Widenhoefer, R. A. *Chem. Commun*., **2014**, *50*, 2420–2423.

42 Seidel, G.; Fürstner, A. *Angew. Chem., Int. Ed.*, **2014**, *53*, 4807–4811.

According to the carbene model proposed by Toste,[32] this π-backdonation would increase with strongly σ-donating ligands attached to gold. This hypothesis was confirmed by Straub and Widenhoefer,[43] who pioneered in 2014 the synthesis and structural characterization of gold(I) carbenes lacking π-conjugated heteroatoms which evidenced the stabilization of the positive charge by the gold fragment. These gold(I) carbenes were synthesized following different strategies from the abovementioned transmetalation. Thus, Straub synthesized gold(I) carbene **17** via treatment of NHC gold cationic complex **16** with (dimesityl)diazomethane (Scheme 9). Parallelly, Widenhoefer generated cycloheptatrienylidene **19** via hydride abstraction (Scheme 10). Gold(I) carbene **17** was too stable to be reactive, however, the slightly shorter length of C1–Au bond (2.014 Å) in respect of Au–L bond (2.030), observed after X-Ray analysis, supported the carbene stabilization by gold. Additionally, the bathocromic shift of the esmerald-green gold(I) carbene **17** compared to the red–purple carbenium ion $[Mes^2CH]^+[HSO4]^-$ also evidenced the participation of gold fragment in the stabilization of the positive charge.

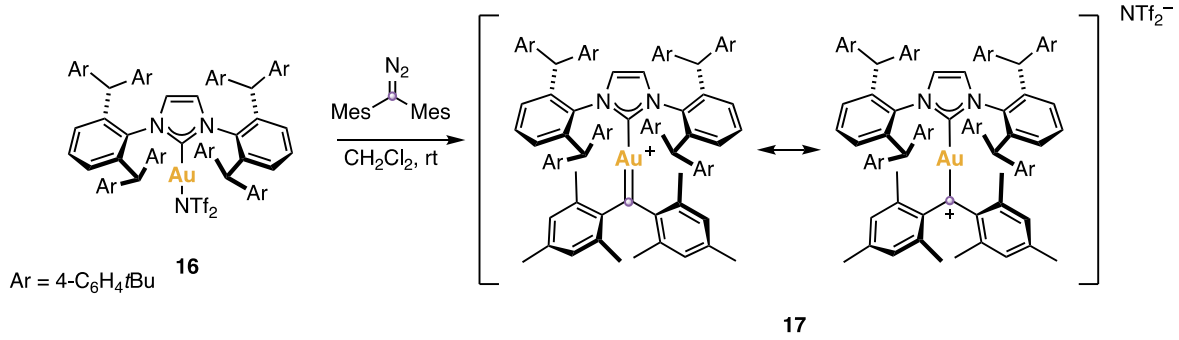

Scheme 9. Synthesis of gold(I) vinylidene 12 via treatment with diazomethane compounds.

In gold(I) carbene **19**, Widenhoefer and co-workers exploited the aromatic stabilization provided by cycloheptatrienyl ligand and set JohnPhos as the ancillary ligand to gold, commonly used in gold(I)-catalyzed 1,*n*-enynes cyclizations. Thus, they managed to stabilize gold(I) carbene **19** enough to be characterized but also reactive, undergoing reduction or oxidation when treated with hydride donors or oxidants. X-Ray analysis of **19** evidenced the contribution of gold in the stabilization of the intermediate.

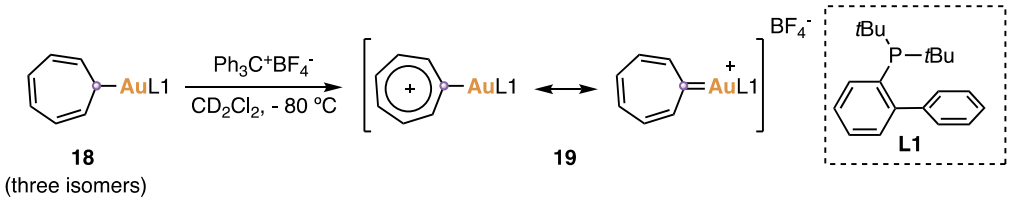

Scheme 10. Synthesis of gold(I) Vinylidene 14 via hydride abstraction.

43 (a) Hussong, M. W.; Rominger, F.; Kräner, P.; Straub, B. F. *Angew. Chem. Int. Ed.* **2014**, *53*, 9372–9375. (b) Harris, R. J.; Widenhoefer, R. A. *Angew. Chem., Int. Ed*., **2014**, *53*, 9369–9371.

In a similar manner to Straub, Bourissou reported the synthesis and characterization of the first tricoordinated gold diphenylcarbene complex **21**, which presented the shortest Au–C bond length reported so far (1.984 Å), indicating a significant Au–C1 back donation also supported by DFT calculations and Natural Bond Orbital analysis.[44] Taking advantage of the high stabilization provided by the dicoordination of *o*-carboranyl diphosphine to gold, the group of Bourissou reported in 2018 the synthesis and characterization of the first highly electrophilic α-oxo carbene gold(I) complex **22** (Scheme 11),[45] intermediates in carbene transfer and coupling reactions catalyzed by gold(I).[46]

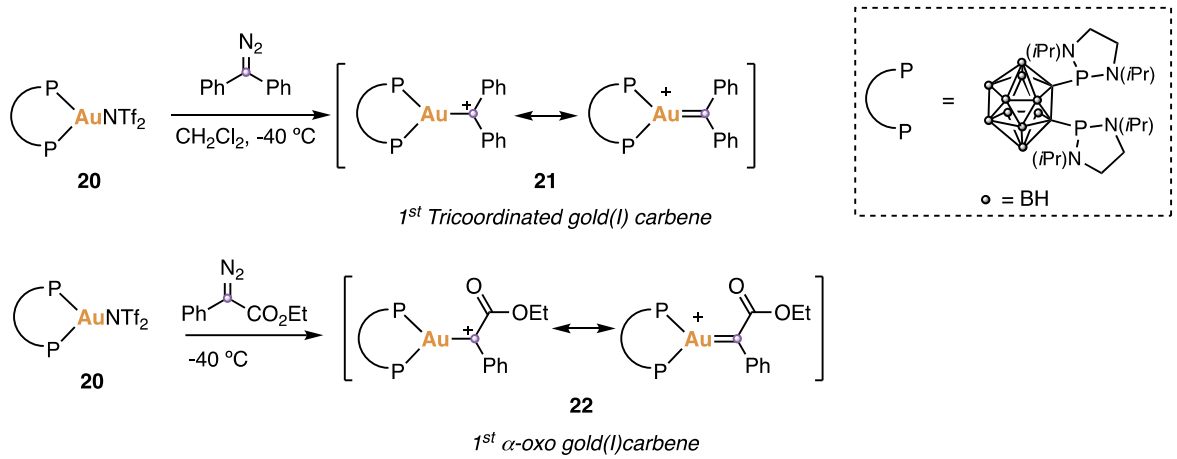

Scheme 11. Synthesis of tricoordinated gold(I) carbenes and gold(I) α-oxo carbenes.

Only one year later, our group generated and spectroscopically characterized the first monosubstituted aryl gold(I) carbene **24** in solution (Scheme 12). These species had been previously detected only in the gas phase, after fragmentation of its corresponding phosphonium ylide.[47] To synthesize gold(I) carbene **24**, a new strategy via halogen abstraction with $GaCl_3$ from the previously formed gold(I) carbenoid **23** was described.[48] These complexes shown to be unstable over –70ºC, but they could be characterized by low temperature NMR, showing C1 downfield resonances (≈ 285ppm) in accordance with the previous characterized gold(I) carbenes. Additionally, they present a characteristic ^{1}H NMR signal at extremely

44 Joost, M.; Estevez, L.; Mallet-Ladeira, S.; Miqueu, K.; Amgoune A.; Bourissou, D. *Angew. Chem., Int. Ed.*, **2014**, *53*, 14512–12516.

45 Zeineddine, A.; Rekhroukh, F.; Carrizo, E. D. S.; Mallet-Ladeira, S.; Miqueu, K.; Amgoune, A.; Bourissou, D. *Angew. Chem. Int. Ed*. **2018**, *57*, 1306 –1310.

46 For reviews in this topic: (a) Qian, D.; Zhang, J. *Chem. Soc. Rev.* **2015**, *44*, 677–698; (b) Liu, L.; Zhang, J. *Chem. Soc. Rev.* **2016**, *45*, 506 – 516; (c) Fructos, M. R.; Diaz-Requejo, M. M.; Pérez, P. J. *Chem. Commun.* **2016**, *52*, 7326–7335.

47 (a) Federov, A.; Moret, M.-E.; Chen, P. *J. Am. Chem. Soc.* **2008**, *130*, 8880–8881. (b) Federov, A.; Chen, P. *Organometallics* **2009**, *28*, 1278–1281. (c) Fedorov, A.; Chen, P. *Organometallics* **2009**, *29*, 2994–3000. (d) Fedorov, A.; Batiste, L.; Bach, A.; Birney, D. M.; Chen, P. *J. Am. Chem. Soc.* **2011**, *133*, 12162–1217. (e) Ringger, D. H.; Kobylianskii, I. J.; Serra, D.; Chen, P. *Chem. –Eur. J.* **2014**, *20*, 14270–14281.

48 García-Morales, C; Pei, X-L; Sarria Toro, J.M.; Echavarren. A.M. *Angew. Chem. Int. Ed.* **2019**, *58*, 3957–3961.

downfield (11.7–12.7 ppm) corresponding to the H attached to C1 (grey). NBO analysis showed that most of the stabilization stems from the C1–C_{Aryl} π-bonding, although small π-backdonation from gold was detected. Finally, Gold(I) carbene **24** displayed the broadest reactivity reported so far for isolated gold(I) carbenes, undergoing cyclopropanations, oxidations, dimerization and C–H insertion reactions.

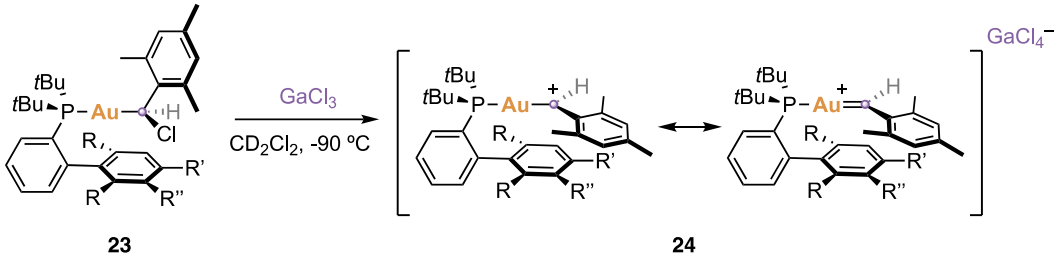

Scheme 12. Generation of the first monosubstituted gold(I) carbene.

As it has been shown in this section, gold(I) carbenes have been broadly studied in the last 10 years, according to their high involvement in gold(I)-catalyzed reactions. In this section the main discoveries and synthetic routes to access them have been explained, although other routes and examples have been proposed.[49] Despite the broad research in the field of gold(I) carbenes, the study of other carbene related species experimented a slower development, such as gold(I) difluorocarbenes,[50] gold(I) cumulenes[51] or gold(I) vinylidenes[52]. The latter will be deeply discussed in Chapter III.

49 (a) Ung, G.; Bertrand, G. *Angew. Chem. Int. Ed.* **2013**, *52*, 11388–11391. (b) Ciancaleoni, G.; Biasiolo, L.; Bistoni, G.; Macchioni, A.; Tarantelli, F.; Zuccaccia, D.; Belpassi, L. *Chem. Eur. J.* **2015**, *21*, 2467–2473. (c) Tskhovrebov, A. G.; Goddard, R.; Fürstner, A. *Angew. Chem. Int. Ed*. **2018**, *57*, 8089–8094.

50 Tskhovreboc, A.G.; Lingnau, J.B.; Fürstner, A. *Angew. Chem. Int. Ed.* **2019**, *58*, 8834–8838.

51 (a) Hansmann, M. M.; Rominger, F.; Hashmi, A. S. K. *Chem.Sci*., **2013**, 4, 1552–1559. (b) Xiao, X.-S.; Kwong, W.-L.; Guan, X.; Yang, C.; Lu, W.; Che, C.-M. *Chem. Eur. J.*, **2013**, *19*, 9457–9462.

52 Harris, R. J.; Widenhoefer, R. A. *Angew. Chem., Int. Ed*., **2015**, *54*, 6867–6869.

Chapter I

Chapter II: *Expanding the Pyrrolidinyl-Biaryl Phosphine Gold(I) Complexes Family*

Chapter II

Introduction

Enantioselectivity in Gold(I) Catalysis

The use of gold(I) in catalysis has grown exponentially in the last twenty years, however, the enantioselective versions of these catalytic transformations has suffered a slower development.[1]

The first occasion in which gold(I) participated in an enantioselective reaction was reported by Hayashi, Ito and Sawamura in 1986.[2] In this work, they described an aldol-type reaction between aldehydes and isocyanoacetates, using gold(I) as a Lewis acid to activate the carbonyl group and a chiral bis(diphenylphosphino)ferrocenylamine ligand as the source of enantioselectivity.

In 2005 our group presented gold(I) as the main character of an enantioselective transformation. The approach presented the use of chiral bis(gold(I)) complex with atropoisomeric Tol–BINAP ligands in the enantioselective alkoxycyclization of 1,6–enynes **1** (Scheme 1).[3]

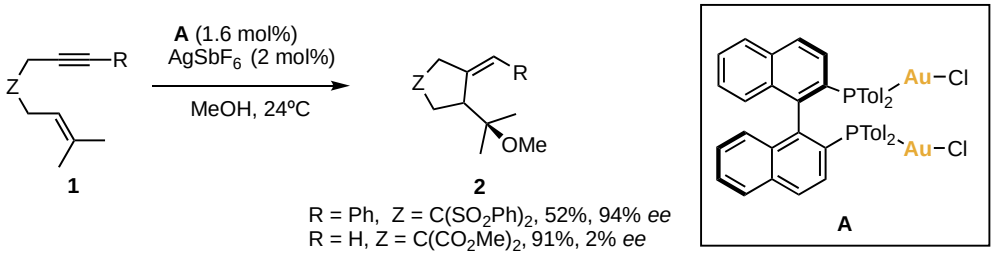

Scheme 1. First example of gold(I)-catalyzed enantioselective alkoxycyclization of 1,6-enynes.

This was a hit in the asymmetric chemistry of gold(I) and it inspired many subsequent studies on this topic, however it turned out to be highly substrate-dependent, as evidenced the drop of enantiomeric excess in the products when the tethered group was changed from a sulfone to a malonate. These results demonstrated the need for a deeper study in this field of gold(I) chemistry.

The sluggish development of enantioselective strategies in gold(I) catalysis is mainly due to important restrictions derived from the linear dicoordination of gold(I) (Figure 1). This coordination geometry sets the chiral ancillary ligand opposite to the reactive center, providing poor enantio-induction. Moreover, gold(I)-catalyzed reactions take place through an outer-sphere mechanism, setting even

1 (a) Fairlamb, I. J. S. *Angew. Chem. Int. Ed*. **2004**, *43*, 1048–1052. (b) Bongers, N; Krause, N. *Angew. Chem. Int. Ed.* **2008**, *47*, 2178–2181. (c) Widenhoefer, R. A. *Chem Eur J*. **2008**, *14*, 5382–5391. d) Escofet, I.; Zuccarello, G.; Echavarren, A. M. *Adv. Organomet. Chem.* **2022**, *77*, 1–42.

2 Ito, Y.; Sawamura, M.; Hayashi, T. *J Am Chem Soc*. **1986**, *108*, 6405–6406.

3 Muñoz, M. P.; Adrio, J; Carretero, J. C.; Echavarren, A. M. *Organometallics* **2005**, *24*, 1293–1300.

further the chiral information from the reaction. Finally, the relatively easy rotation of the substrate–Au bond and the ligand–Au bond makes difficult the fixation of the substrate in the chiral environment.

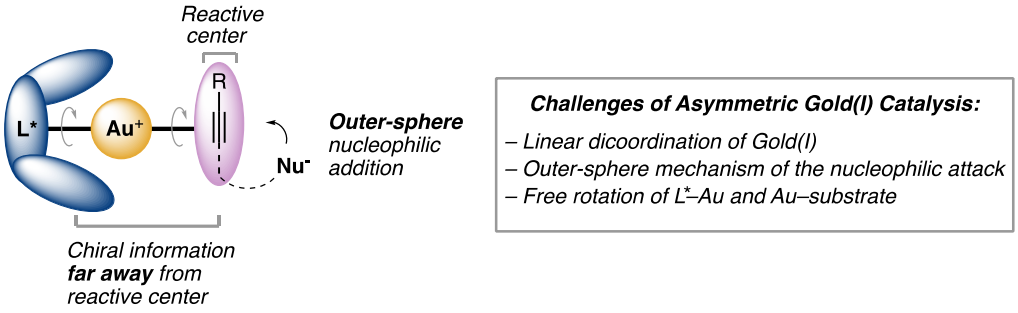

Figure 1. Challenges in asymmetric gold(I) catalysis.

To face the challenges of asymmetric gold(I) catalysis, several methodologies have been applied. Based on the example reported by our group,[3] many strategies using bimetallic gold(I) complexes bearing atropoisomeric bisphosphines, such as BINAP, SEGPHOS or BIHEP, were disclosed (Figure 2).[4] This approach showed to be effective in inter- and intramolecular transformations, however, the actual mode of activation is ambiguous, since it became clear that the second gold plays a crucial role for the chiral environment but the origin of enantioselectivity is not properly identified.

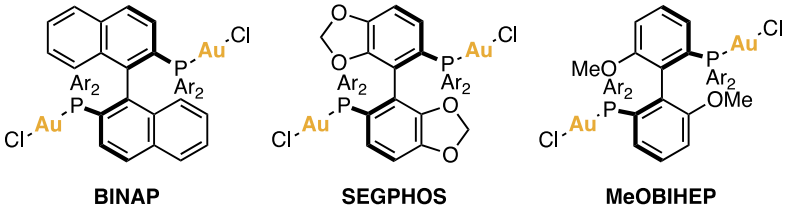

Figure 2. Typical bimetallic gold(I) complexes bearing atropoisomeric bisphosphines.

In 2007, the group of Toste demonstrated the crucial role of the counterions in the asymmetric hydroamination of allenes catalyzed by chiral dinuclear gold(I)–atropoisomeric bisphosphines.[5] In 2010, they reported the synergistic use of chiral and nonchiral gold(I) complexes with chiral counteranions in the enantioselective hydroaminations and hydroalkoxylations of allenes **3** with

4 (a) Zhang, Z.; Liu, C.; Kinder, R. E.; Han, X.; Qian, H.; Widenhoefer, R. A. *J. Am. Chem. Soc.* **2006**, *128*, 9066–9073. (b) Tarselli, M. A.; Chianese, A. R.; Lee, S. L.; Gagné, M. R. *Angew. Chem. Int. Ed.* **2007**, *46*, 6670–6673. (c) Luzung, M. R.; Mauleón, P.; Toste, F. D. *J. Am. Chem. Soc.* **2007**, *129*, 12402–12403. (d) Zhang, Z.; Widenhoefer, R. A. *Angew. Chem. Int. Ed.* **2007**, *46*, 283–285. (e) Zhang, Z.; Bender, C. F.; Widenhoefer, R. A. *Org. Lett.* **2007**, *9*, 2887–2889. (f) LaLonde, R. L.; Sherry, B. D.; Kang, E. J.; Toste, F. D. *J. Am. Chem. Soc.* **2007**, 129, 2452–2453.

5 Hamilton, G. L.; Kang, E. J.; Mba, M.; Toste, F. D. *Science* **2007**, *317*, 496–499.

hydroxylamines and hydrazines (Scheme 2).[6] This strategy allows the efficient transmission of the chiral information from the counterion via tight ion pairs.

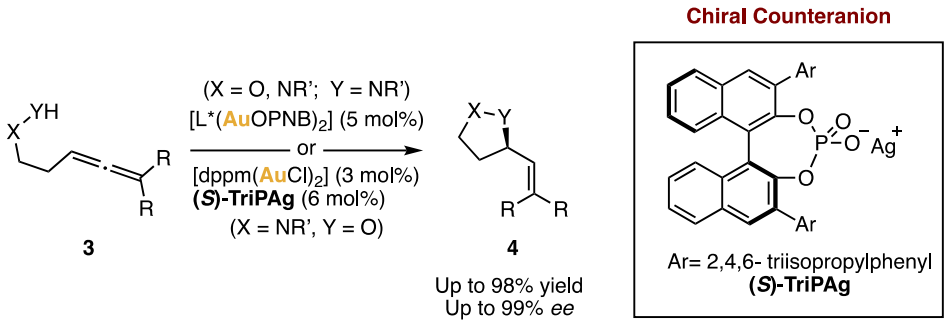

Scheme 2. Enantioselective hydroaminations and hydroalkoxylations of allenes catalyzed by the synergistic use of a nonchiral gold(I) complex and a chiral counteranion.

Alternatively, Fürstner,[7] Mascareñas,[8] and Toste[9] proposed gold(I) complexes based on monodentate phosphoramidites as suitable candidates for different enantioselective gold(I)-catalyzed reactions. In this approach, the chiral amine moiety was proved to be fundamental to provide a chiral environment around the reactive center (Figure 3).

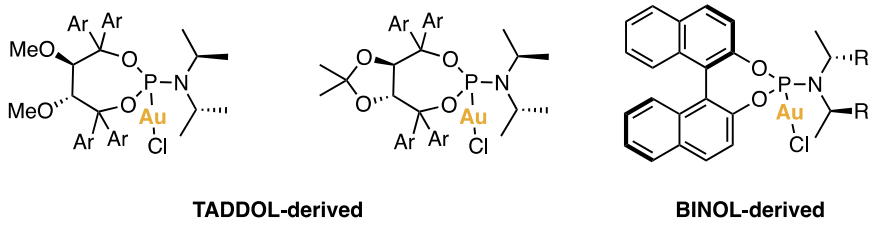

Figure 3. Commonly used monogold complexes based on monodentate phosphoramidite.

Latest advances have addressed strategies that provide enantio-induction based on substrate fixation or preorientation of the substrate via non-covalent interactions (Figure 4). Thus, the use of helically chiral phosphine ligands attached to gold(I) proved to be effective in the enantioselective cyclization of nitrogen-tethered 1,6-enynes.[10] Junliang Zhang reported systems incorporating chiral sulfonamides in phosphine ligands such as Xiang-Phos and Ming-Phos which, taking advantage of non-covalent H–

6 LaLonde, R. L.; Wang, Z. J.; Mba, M.; Lackner, A. D.; Toste F. D. *Angew. Chem. Int. Ed.* **2010**, *49*, 598–601.

7 Teller, H.; Corbet, M.; Mantilli, L.; Gopakumar, G.; Goddard, R.; Thiel, W.; Fürstner, A. *J. Am. Chem. Soc*. **2012**, *134*, 15331–15342.

8 Alonso, I.; Trillo, B.; López, F.; Montserrat, S.; Ujaque, G.; Castedo, L.; Lledós, A.; Mascareñas, J. L. *J. Am. Chem. Soc*. **2009,** *131*,13020–13030.

9 Wang, Y.; Lackner, A. D.; Toste F. D. *Acc. Chem. Res*. **2014**, *47*, 889–901.

10 (a) Yavari, K.; Aillard, P.; Zhang, Y.; Nuter, F.; Retailleau, P.; Voituriez, A.; Marinetti, A. *Angew. Chem., Int. Ed.* **2014**, *53*, 861−865. (b) Aillard, P.; Dova, D.; Magne, V.; Retailleau, P.; Cauteruccio, S.; Licandro, E.; Voituriez, A.; Marinetti, A. *Chem. Commun.* **2016**, *52*, 10984−10987.

bonding with the substrates, resulted in efficient enantio-induction in inter- and intramolecular cycloadditions. The use of Xiang-Phos ligand in gold(I) complexes provided enantio-induction in the enantioselective cyclopropanation of indenes and trisubstituted alkenes while Ming-Phos gold(I) complexes were effective in the intermolecular (3+2) cycloaddition of 2-(1-alkynyl)-2-alken-1-ones with 3-styrylindoles.[11] A similar strategy was used by Liming Zhang for the cyclization of 4-allene-1-ols using an axially chiral binaphthyl phosphine–supported gold(I) complex with a remote basic amide group.[12]

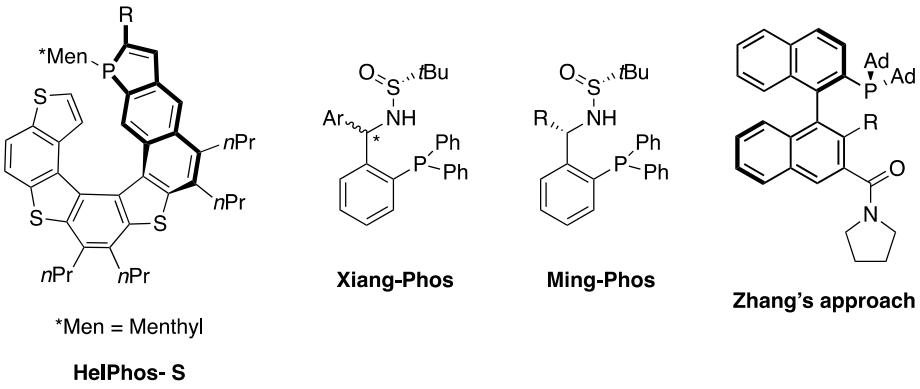

Figure 4. Ligands used for the different recent approaches in asymmetric gold(I) catalysis.

Other approaches are based on the use of chiral NHC-ligands attached to gold(I)[13] or supramolecular structures such as gold(I) cavitands, which efficiently encapsulate the substrates.[14]

Gold(I) Catalysts with a Remote C_2-Chiral Element

Recently, our group introduced a new class of mononuclear gold(I) complexes bearing chiral modified JohnPhos ligands containing C_2-symmetric *trans*-2,5-diaryl pyrrolidines at the 4' position.[15] This pioneer design aims to overcome the linear diccordination of gold(I) by encapsulating the substrate in a chiral pocket (Figure 5). The bulkiness of the disubstituted phosphine blocks the rotation around the C_{aryl}–P bond directing the P–Au–Cl axis towards the rigid biphenyl scaffold, which holds the pyrrolidine

11 (a) Zhang, Z. M.; Chen, P.; Li, W.; Niu, Y.; Zhao, X. L.; Zhang, J. *Angew. Chem. Int. Ed.* **2014**, *53*, 4350–4354. (b) Wang, Y.; Zhang, P.; Di, X.; Dai, Q.; Zhang, Z.–M.; Zhang, J. *Angew. Chem., Int. Ed.* **2017**, *56*, 15905−15909. (c) Wang, Y.; Zhang, Z.–M.; Liu, F.; He, Y.; Zhang, J. *Org. Lett.* **2018**, *20*, 6403−6406. (d) Zhang, P.–C.; Wang, Y.; Zhang, Z.–M.; Zhang, J. *Org. Lett.* **2018**, *20*, 7049−7052.

12 Wang, Z.; Nicolini, C.; Hervieu, C.; Wong, Y. F.; Zanoni, G.; Zhang, L. *J. Am. Chem. Soc*. **2017**, *139*, 16064–16067.

13 (a) Bohan, P. T.; Toste, F. D. *J. Am. Chem. Soc*. **2017**, *139*, 11016–11019. (b) Wu, C. Y.; Horibe, T.; Jacobsen, C. B.; Toste, F. D. *Nature* **2015**, *517*, 449–454.

14 Martin–Torres, I.; Ogalla, G.; Yang, J.–M.; Rinaldi, A.; Echavarren, A. M. *Angew. Chem. Int. Ed.* **2021**, *60*, 9339–9344.

15 Zuccarello, G.; Mayans, J. G.; Escofet, I.; Scharnagel, D.; Kirillova, M. S.; Pérez-Jimeno, A. H.; Calleja, P.; Boothe, J. R.; Echavarren, A. M. *J. Am. Chem. Soc.* **2019**, *141*, 11858–11863.

with the chiral information. This distribution assures the proximity of the substrate to the ligand providing the desired facial discrimination during the reaction.

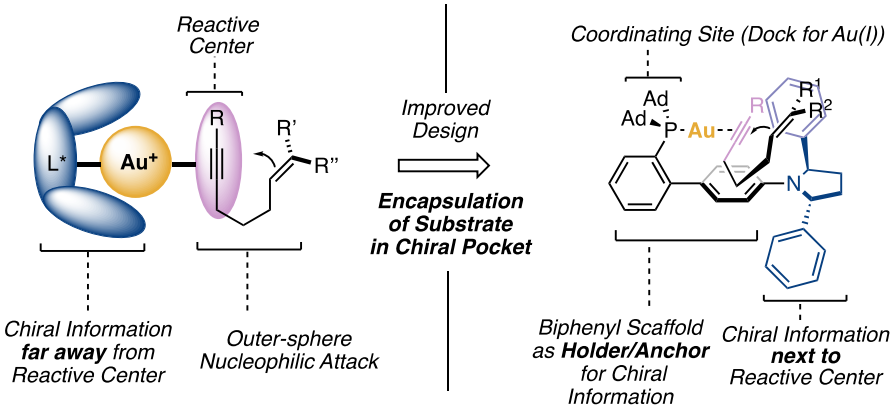

Figure 5. New catalyst design to overcome the challenges of asymmetric gold(I) catalysis.

Based on this new design, a family of gold(I) complexes was developed modifying the phosphine ligands, the pyrrolidine aryl substituents and the pyrrolidine position in the aryl of the biphenyl scaffold. The complexes resulted to be especially successful in the intramolecular [4+2] cycloaddition of 1,6-enynes **5** leading to the formation of cycloadducts **6**. A screening of all the members of the family of catalysts in this reaction evidenced that (*R*,*R*)-**B** gave the best results (Scheme 3a). The success of this catalyst was extended to the asymmetric synthesis of 1,2-dihydronaphthalenes **8** from their corresponding 1,6-arylenynes **7**, applied on the enantioselective total synthesis of the carexane family of natural products (Scheme 3b).

Additionally, the performance of (*R*,*R*)-**B** was tested in the 6-*endo*-dig cyclization of *N*-tethered-1,6-arylenyne **9** catalyzed by gold(I), showing moderate to good yields and excellent enantioselectivities (Scheme 3c). The mode of action of these complexes was studied by experimental and theoretical approaches, which indicated the importance of attractive non-covalent π–π interactions between stereo-directing aromatic elements of the substrates and the pyrrolidine–biphenyl scaffold. These interactions determine the preferred binding orientation of the substrate and, consequently, the enantioselective folding in the chiral pocket towards the products.

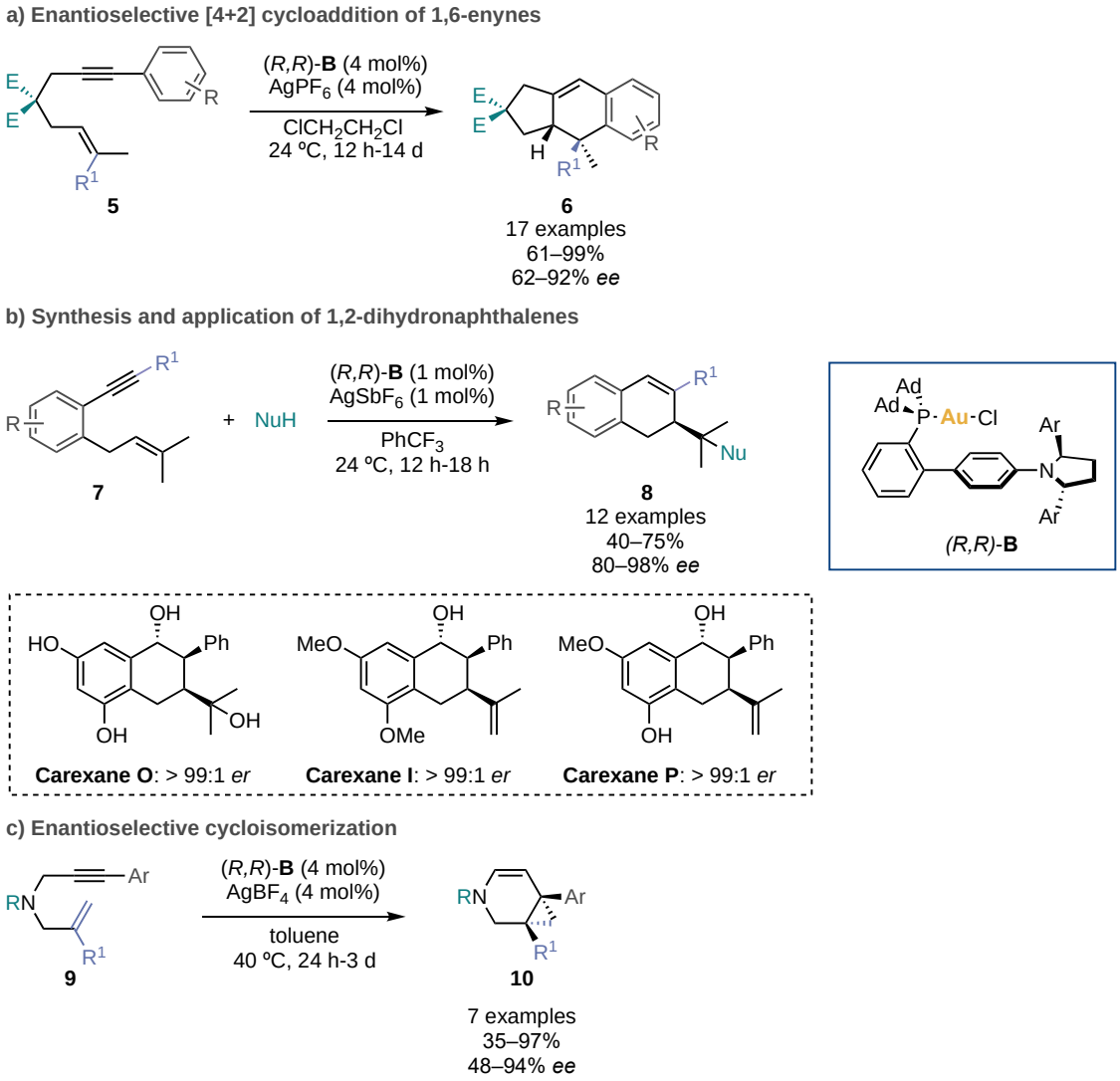

Scheme 3. Applications of chiral complex (*R*,*R*)-**B**.

Objectives

In view of the successful performance of the family of chiral pyrrolidinyl-biaryl phosphine gold(I) complexes presented in the introduction of this chapter,[15] it seems natural to apply further modifications to the molecular skeleton of these gold(I) complexes. This would give us more insights about their mode of action and would allow us to expand their usefulness in other enantioselective transformations.

We envisioned that a more crowded central ring would allow us to tighten the chiral pocket of the catalysts, enhancing the enantioselectivity of different reactions and presumably allowing us to access smaller enantiopure molecules. Therefore, the first objective of this Doctoral Thesis will be the design, synthesis and reactivity study of new members of the family of chiral pyrrolidinyl-biaryl phosphine gold(I) complexes amplifying the central ring of their structure (Figure 6).

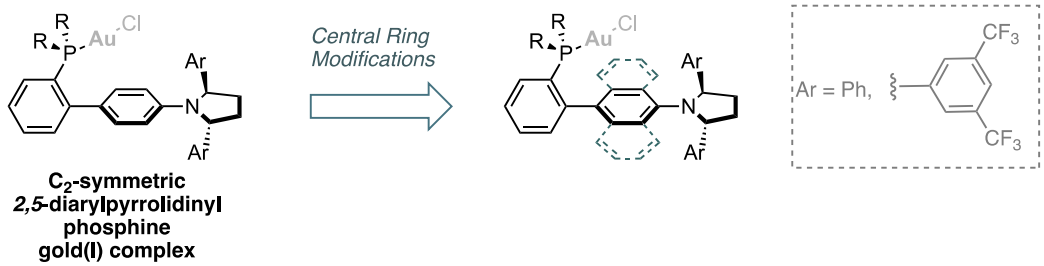

Figure 6. Envisioned modifications in chiral diarylphosphine pyrrolidine gold(I) complexes.

Results and Discussion

Design and Synthetic Approach

To obtain a full picture on how the modification of the central ring affects the properties of these catalysts, we decided to amplify the central ring adding one or two additional rings to the central core of the structure. Hence, our aim was to set a naphthyl or an anthracenyl moiety as the central ring of these diaryl pyrrolidine complexes. Additionally, focusing our efforts on reproducing the best results obtained with (*R*,*R*)-**B** gold(I) complex in the previous generation of this family of catalysts, we decided to use 3,5-$(CF_3)_2C_6H_3$ as the aryl substituent, since it showed to be the most effective in terms of enantio-induction (Figure 7).[15]

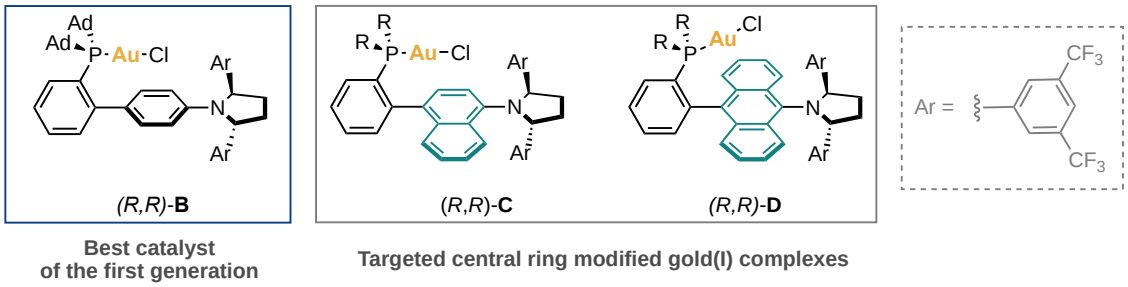

Figure 7. Previous and targeted chiral diarylphosphine pyrrolidine gold(I) complexes.

The synthetic route for the new complexes (*R*,*R*)-**C** and (*R*,*R*)-**D** was inspired by the one developed in the group for the synthesis of the first generation of this family of catalysts ((*R*,*R*)-**B**) which follows a modular approach.[15] It consists on the parallel synthesis of enantiopure (*S*,*S*)-1,4-diaryl-1,4-diols and the biaryl aniline, followed by cyclization of the diol to form a biaryl pyrrolidine, which after phosphine coupling and gold(I) complexation would lead to our desired complexes (Figure 8).

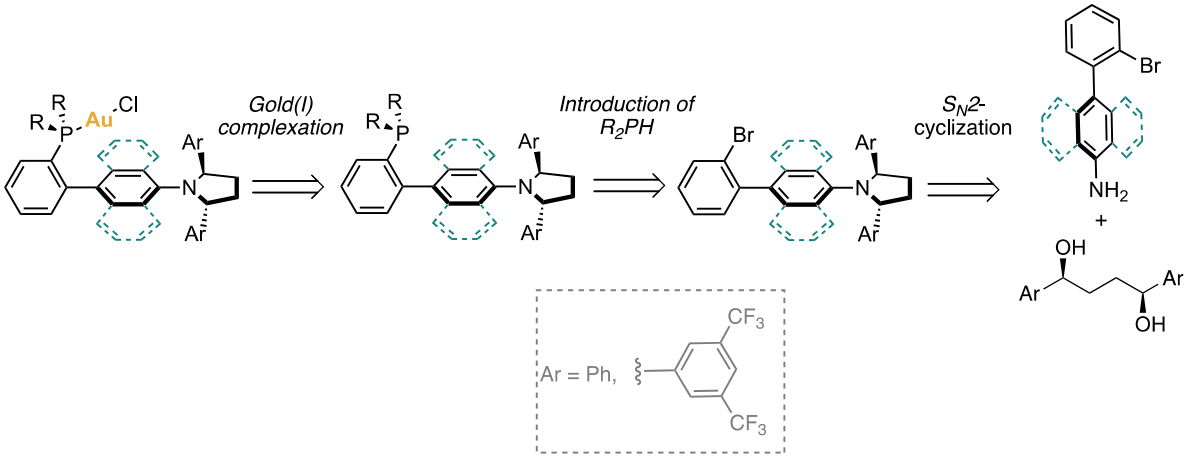

Figure 8. Modular synthesis developed for the first generation of C_2–symmetric 2,5–diarylphopshine pyrrolidine gold(I) complex.

Synthesis of Gold(I) Complexes (*R*,*R*)-C and (*R*,*R*)-D

The first synthetic attempt started by the parallel synthesis of enantiopure (*S*,*S*)-1,4-diaryl-1,4-diol **16** and the corresponding aniline needed for each complex. The synthetic route to access substituted benzylic 1,4-diols was developed in our group with the aim of finding an uniform synthetic route for the different members of the family of pyrrolidine complexes.[15] To afford the enantiopure diol **16**, benzaldehyde **11** was treated with vinyl magnesium bromide forming the racemic mixture of allylic alcohol **12** in good yield. This racemic mixture was submitted to enzymatic kinetic resolution with Novozyme 435 and isopropenyl acetate leading to the enantiopure allylic alcohol **14** in excellent yield. With the enantiopure allylic alcohol in hand, alkene metathesis using Grubbs 2nd generation catalyst was performed to obtain allylic 1,4-diol **15** in good yield. Finally, hydrogenation in presence of catalytic amounts of Adams' precatalyst allowed us to access (*S*,*S*)-1,4-diaryl-1,4-diol **16** in quantitative yield (Scheme 4).

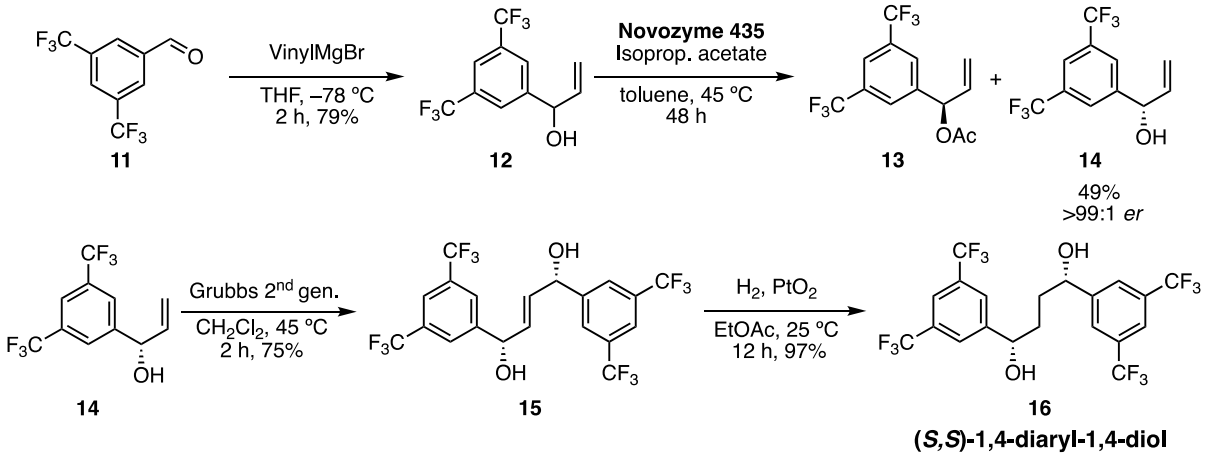

Scheme 4. Synthesis of (*S*,*S*)-1,4-diaryl-1,4-diol **16**.

With the chiral diol in hand, we set as our second target to synthesize the naphthylamine which will give us access to (*R*,*R*)-**C** complex. The synthesis of naphthyl amine **20** was performed following the procedure reported in the literature for the analogous compounds of the first generation of catalysts.[15] Starting from 1,4-iodonitronaphthalene **18,** Suzuki–Miyaura coupling with 2-bromophenylboronic acid **17** led to nitro compound **19,** which was directly used without further purification to form the naphthylamine **20** after reduction with iron powder, in moderate yield over two steps (Scheme 5).

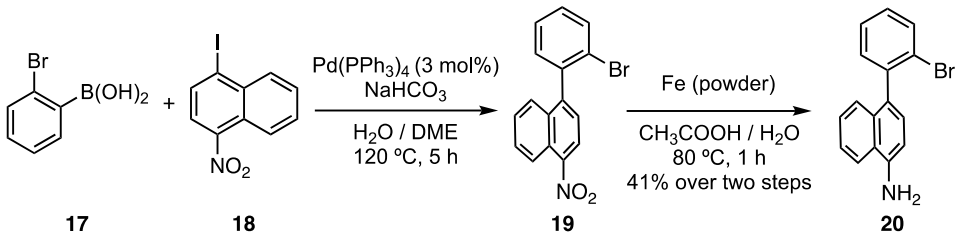

Scheme 5. Synthesis of naphthyl amine **20**.

The synthesis of (*R*,*R*)-**C** complex was continued performing the *in situ* mesylation of 1,4-diol **16** followed by double S_N2 reaction with naphthylamine **20** to afford pyrrolidine **21** in moderate yield (Scheme 6). At this point, the crowded environment between the aryl substituents and the naphthyl moiety causes the restricted rotation around the C_{aryl}–N bond, as it proves the splitting of the signals in the ^{1}H NMR of **21** at low temperature.

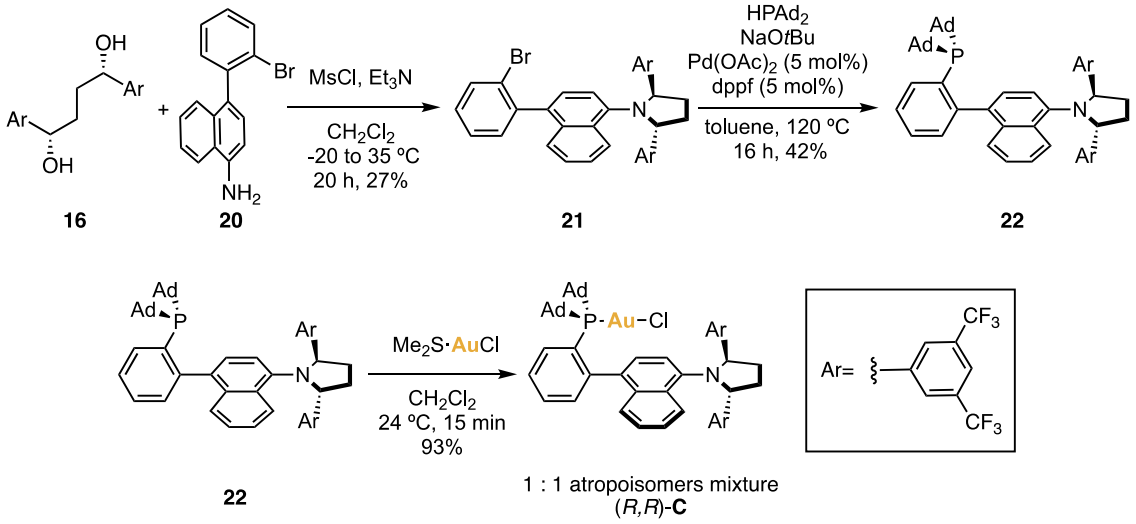

Scheme 6. Final steps of the synthesis of (*R*,*R*)-**C** complex.

Next, we decided to introduce di-1-adamanthylphosphine in the *ipso* position of the bromine of pyrrolidine **21**, since it has been shown before that it gave better results than other less bulky phosphines. To our delight, the Pd-catalyzed cross-coupling conditions used in the reported synthetic route[15] were suitable for our system and phosphine **22** was obtained in moderate yield. Further complexation with dimethylsulfide gold(I) chloride gave complex (*R*,*R*)-**C** in excellent yield (*Scheme 6*). The introduction of gold(I) blocked the rotation of the molecule, causing the formation of a mixture of atropoisomers in 1:1 ratio as it can be observed in the ^{31}P{H} NMR of the complex.[16] Unfortunately, we were not able to separate the mixture of atropoisomers via column chromatography. The formation of this mixture is

16 Zhang, J.-Q.; Liu, Y.; Wang, X.-W.; Zhang L. *Organometallics* **2019**, *38*, 3931–3938.

due to the chiral axis derived from the central naphthyl moiety in these molecules, in contrast with the C_2- symmetric complexes of this family previously synthesized.

Encouraged by the successful synthesis of (*R*,*R*)-**C** gold(I) complex and with the aim of preventing the presence of atropoisomers, we decided to introduce a third aromatic ring in the structure, building the anthracenyl derivative (*R*,*R*)-**D** complex (Figure 7).

The first approach considered to synthesize (*R*,*R*)-**D** complex was to follow the modular synthetic route previously used for complex (*R*,*R*)-**C**, coupling anthracenyl aniline **23** with (*S*,*S*)-1,4-diaryl-1,4-diol **16**, however, this cyclization reaction was not suitable for the anthracenyl substrate, due to the bulkiness of the anthracenyl amine (Scheme 7).

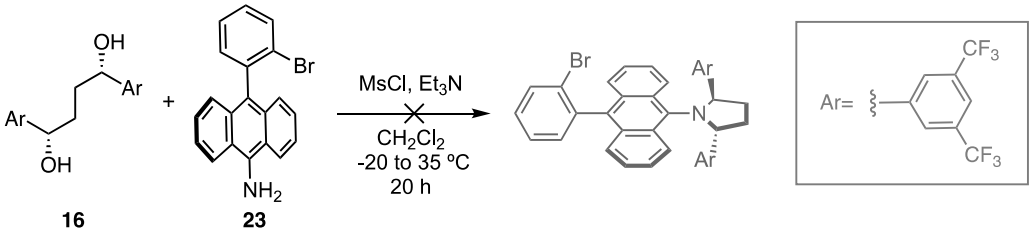

Scheme 7. Unsuccessful first approach of (*R*,*R*)-**D** synthesis.

To overcome this challenge, we decided to develop a different strategy based on the initial formation of the chiral pyrrolidine and subsequent construction of the arylpyrrolidine by using a Chan-Lam type coupling. The conditions of this step were reported by Lalic and co-workers and consist on a copper(I) catalyzed coupling between the corresponding boronic ester and a benzoylated hydroxylamine giving access to sterically hindered anilines.[17] It is worth mentioning that this methodology presents a general strategy for the synthesis of highly sterically hindered amines, difficult to access with traditional C–N coupling methods. Encouraged by their results, we decided to apply this methodology as one of the central steps of our synthesis, followed by the phosphine coupling and subsequent complexation with gold(I) to achieve our goal (Figure 9).

17 Mailig, M.; Rucker, R. P.; Lalic, G. *Chem. Commun.,* **2015**, *51*, 11048–11051.

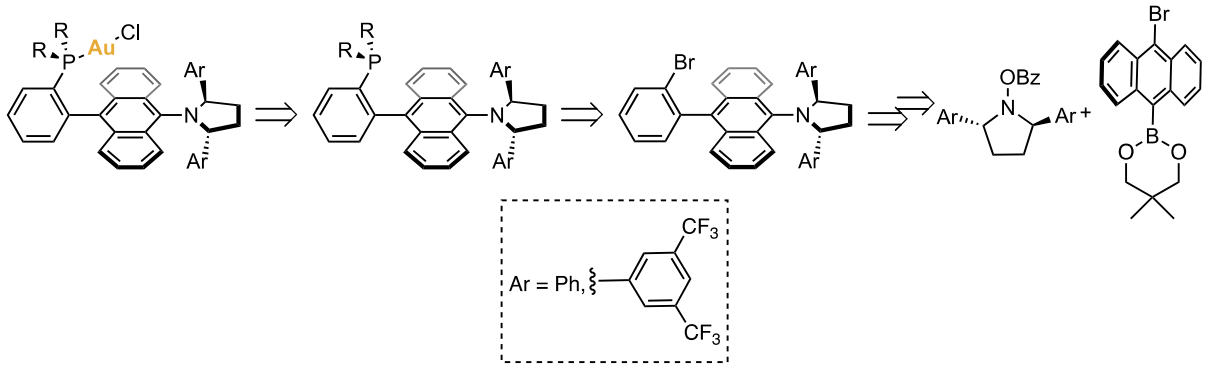

Figure 9. New approach for (*R*,*R*)-**D** synthesis.

Our first step was to develop a synthetic route to achieve benzoylated hydroxylamine **27** (Scheme 8).[18] The synthesis of the benzoylated hydroxylamine required the use of pyrrolidine **26** as the starting material. To achieve this pyrrolidine, *in situ* mesylation of 1,4-diol **24** followed by S_N2 reaction with allylamine afforded allylpyrrolidine **25** in good yield. Subsequent deallylation with Wilkinson's catalyst gave us access to pyrrolidine **26** in good yield.

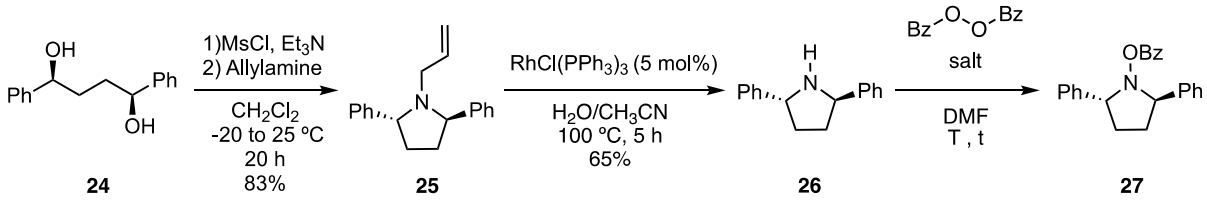

Scheme 8. Synthetic route to achieve benzamide **27**.

Parallelly to the formation of the pyrrolidine, the optimization of the benzoylation reaction was performed, using (*S*,*S*)-1,4-dyphenyl pyrrolidine as the model substrate (Table 1).

18 In collaboration with Dr. Marc Montesinos.

Table 1. Optimization of the benzoylation reaction of pyrrolidine **26.**

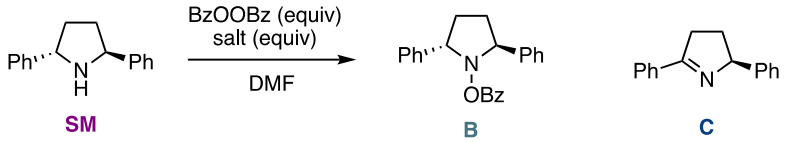

Entry	Salt	BzOOBz (equiv)	Salt (equiv)	T (°C)	Time (h)	SM : B : C[a]
1	K_2HPO_4	1.5	3.0	25	5	0.6 : 1.0 : 0.5
2	K_2HPO_4	1.5	3.0	25	16	0.0 : 1.0 : 1.5
3	K_2HPO_4	0.8	3.0	25	16	0.5 : 1.0 : 0.5
4	K_2HPO_4	3.0	3.0	25	16	0.0 : 1.0 : 0.8
5	K_2HPO_4	1.5	3.0	0	16	0.6 : 1.0 : 0.4
6	K_2HPO_4	1.5	3.0	–20	16	0.3 : 1.0 : 3.5
7	K_2HPO_4	5.0	2.0	–20	16	— : 1.0 : 2.8
8	K_2HPO_4	10.0	2.0	–20	16	— : 1.0 : 1.6
9	**K_2HPO_4**	**3.0**	**1.5**	**25**	**16**	**0.2 : 1.0 : 0.1**
10	KH_2PO_4	3.0	1.5	25	16	0.1 : 1.0 : —*
11	Et_3N	3.0	1.5	25	16	9.5 : 1.0 : —

[a] Ratios were determined by ^{1}H NMR spectroscopy. *Different side product.

Irreversible formation of the imine byproduct **C** evidenced the need of tunning the reaction looking for the best conditions. Following the reaction by ^{1}H NMR we observed total consumption of the starting material after 16 hours at 25 ºC (entry 2). Keeping constant the reaction time,the optimal amount of the reagents was tested: the variation of the number of equivalents of benzoyl peroxide indicated that 3 equivalents of this reagent was the most convenient option (entry 4). Parallelly, temperature tests were performed, showing the need of a higher excess of the benzoyl peroxide in the reaction to be completed when lower temperatures were used (entries 5 and 6). However, this increase only led to a major formation of the imine product **C** (entries 7 and 8). Additionally, the equivalents of salt used were halved, which resulted in a decrease in the formation of byproduct **C** (entry 9). As a last trial, a different potassium salt was tested, but the reaction showed the formation of other byproducts (entry 10). Et_3N was also tried as base, however the reaction turned to become extremely slow (entry 11). Hence, according to the results shown, the optimal conditions were obtained running the reaction at 25 ºC, using 0.5 excess of K_2HPO_4 as base and 3.0 equivalents of benzoic anhydride (entry 9). Moreover, the reaction monitoring by NMR helped us to determine that running the reaction over 18 hours allows the total consumption of the starting material without any increase of the byproduct formed. With the conditions previously mentioned, benzoyl hydroxylamine **27** was obtained in 66% yield (Scheme 9).

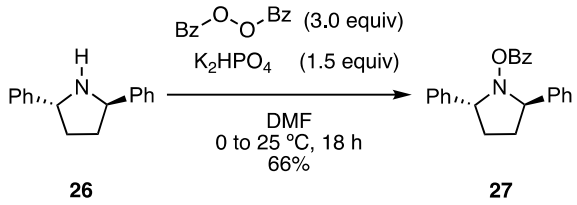

Scheme 9. Benzoylation reaction of pyrrolidine **26**.

These conditions were also tested for the synthesis of the (*R*,*R*)-1,4-diaryl-benzoylpyrrolidine **30** (Scheme 10), however the only product observed was imine **31**, so we decided to go on with the development of the synthetic route using the diphenyl substituted precursor.

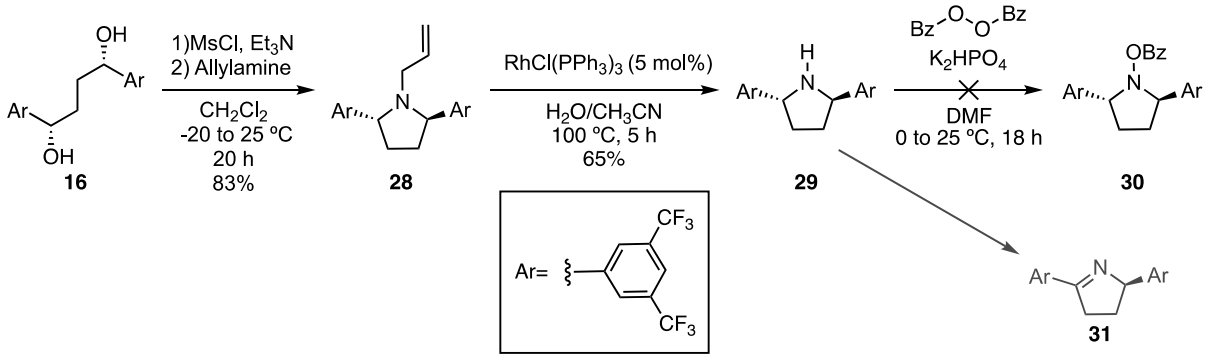

Scheme 10. Unsuccessful synthesis of benzoylpyrrolidine **30**.

The synthesis of boronic ester **32** was performed from commercially available 9,10-bromoanthracenyl boronic acid following a previously reported procedure.[19] The treatment of benzoylpyrrolidine **27** with boronic ester **32** applying Lalic's strategy[17] gave anthracenyl pyrrolidine precursor **33** in a moderate yield. At this point, the most direct step for the synthesis of our ligand was expected to be the introduction of a bromo substituted aryl on the *ipso* position of the bromo via Suzuki-Miyaura coupling, however, not full conversion could be achieved in this reaction (even when tunning the conditions) so an alternative approach was found. A phenol group was coupled instead, obtaining anthracenylphenol **34** in good yield. The triflation of **34**, provided us with anthracenyl triflate **35**, which presented an accessible group for the phosphine coupling (Scheme 11).

19 Ikawa, T.; Yamamoto, R.; Takagi, A.; Ito, T.; Shimizu, K.; Goto, M.; Hamashima, Y.; Akai, S. *Adv. Synth. Catal.* **2015**, *357*, 2287– 2300.

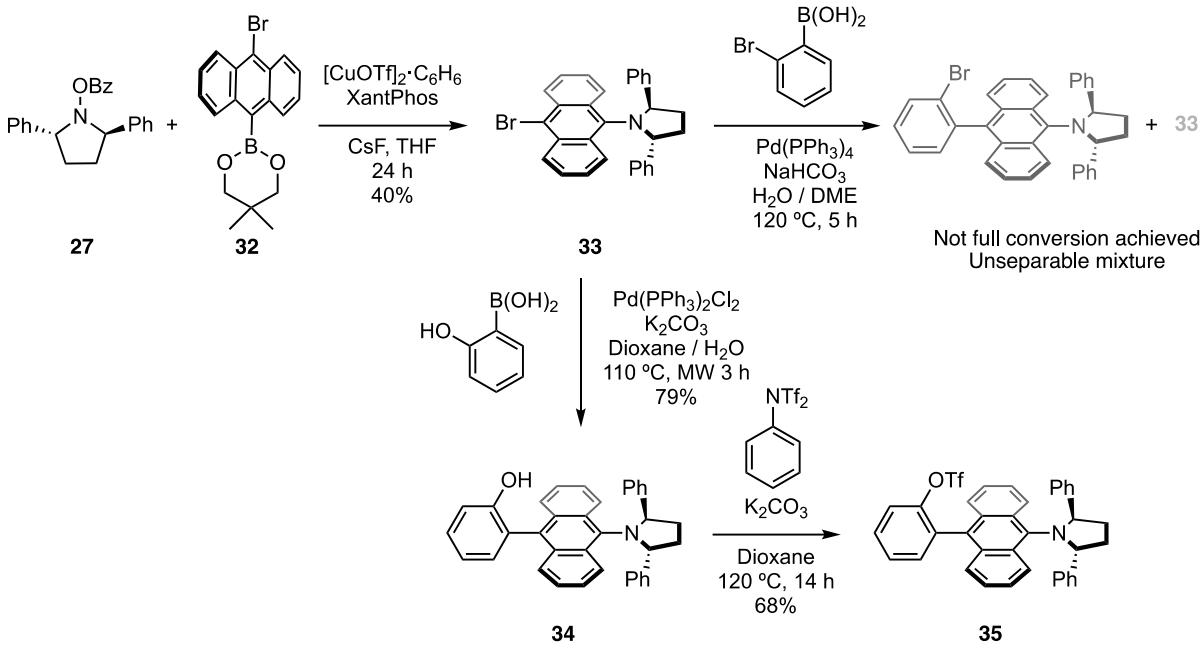

Scheme 11. Next steps through (R,R)-**D** synthesis.

Phosphine coupling reaction showed to be challenging due to the bulkiness of precursor **35** so, as a first approach, we decided to start introducing di-*tert*-butylphosphine, more compact than di–adamanthylphosphine used in other members of the first generation of this family of complexes.[15,20] To find the best conditions for the phosphine coupling, we performed a screening of conditions (Table 2).

20 In collaboration with Dr. Inma Martín.

Table 2. Screening of conditions for the anthracenyl phosphine coupling reaction.

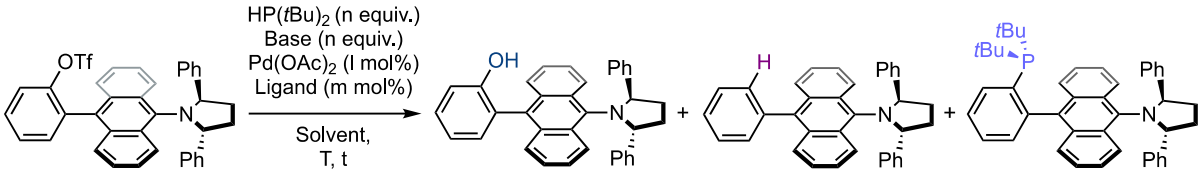

SM **A** **B** **C**

Entry	Ligand	Base	$Pd(OAc)_2$ (mol%)	Ligand (mol%)	$HP(tBu)_2$ and Base (equiv)	Solvent	T (ºC)	Time	SM : A : B : C[a]
1	dppf	NaO*t*Bu	5	6	1.2	toluene	120	12 h	**63** : 35 : 0 : 2
2	dppf	NaO*t*Bu	5	6	1.2	toluene	120	60 h	**63** : 35 : 0 : 2
3	dppf	NaO*t*Bu	7.5	9	1.8	toluene	120	3 d	**33** : 58 : 0 : 9
4	diipf	K_3PO_4	5	6	1.1	toluene	120	24 h	**80** : 0 : 0 : 20
5	diipf	K_3PO_4	10	12	2.2	toluene	150 (MW)	4 h	**62** : 12 : 2 : 25
6	diipf	K_2HPO_4	10	12	1.1	1,4–dioxane	130	20 h	**75** : 0 : 7 : 17
7	diipf	K_2HPO_4	20	24	2.2	1,4–dioxane	130	36 h	**49** : 0 : 17 : 35
8	diipf	K_2HPO_4	10	12	1.5	1,4–dioxane	150 (MW)	4 h	**83** : 0 : 3 : **15**
9	**diipf**	**K_2HPO_4**	**20**	**24**	**3**	**1,4–dioxane**	**150 (MW)**	**8 h**	**47** : 0 : 11 : 42

[a] Ratios were determined by UHPLC–MS.

The results obtained following the reaction by UHPLC–MS disclosed that the conditions previously used in the synthesis of phosphine **36** (**C**), resulted in an extremely slow and unsuccessful reaction (entry 1) with phenol **A** as the major product and just traces of the desired phosphine. To find out if the reaction could reach completion under these conditions, we ran the reaction for 48 additional hours, however no significant changes were observed (entry 2). At this point, we considered a possible poisoning of the catalyst, so we added extra amounts of catalyst, ligand and base (2.5 mol%, 3 mol% and 0.6 equivalent respectively), however we observed just a small increase in the ratio of the product formed and phenol **A** as the main product (entry 3). After these results, we contemplated that the base used was too strong for this system, so we decided to change the conditions, testing different bases and solvents.

Milder conditions previously used in the group[21] were tried, choosing a potassium base and diipf. With this, we avoided the formation of the phenol **A** as a byproduct, although still low conversion was observed after 24 hours (entry 4). To accelerate the reaction, we set it under MW conditions, observing a slightly higher conversion after 4 hours of irradiation, however, in this case, phenol **A** and the

[21] Franchino, A.; Martí, À.; Echavarren, A. M. *J. Am. Chem. Soc* **2022**, *144*, 3497–3509.

detriflated product **B** were observed as byproducts (entry 5). Once known that potassium salt prevents the major formation of phenol byproduct, we decided to test K_2HPO_4 as the base and dioxane as the solvent as an alternative to increase the reaction yield (entries 6 – 9), based on previous conditions proved in our group. The use of a 10 mol% of catalyst loading resulted in a 25% of conversion that stopped after 20 hours (entry 6), indicating a possible poisoning of the catalyst. To solve this potential deactivation of the catalyst, we made a second addition of all the reagents, and we stirred the reaction for additional 20 hours, observing an increase of the product ratio to 35% (entry 7). To shorten the reaction time, we decided to run the reaction under MW heating, and the results showed that after 8 hours and performing a second addition of the reagents, it was possible to obtain up to 42 ratio of product **C** formed, with the only formation of a small amount of the detriflated species **B** as a byproduct (entry 9).

Finally, the optimized conditions allowed us to obtain phosphine **36** in a modest yield, which was treated with [Me_2SAuCl] to give complex (*R,R*)-**D** (Scheme 12). The structure and configuration of gold(I) complex (*R,R*)-**D** was confirmed by X-Ray diffraction (Figure 10).

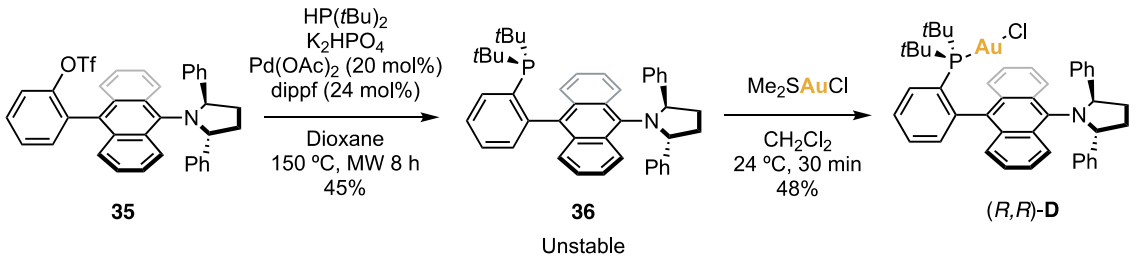

Scheme 12. Phosphine coupling and final gold(I) complexation in (R,R)-**D** synthesis.

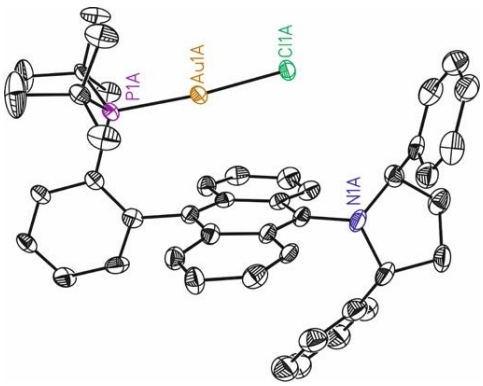

Figure 10. X–Ray structure of Gold(I) complex (R,R)-**D**.

Study of the Performance of Complexes (*R*,*R*)-C and (*R*,*R*)-D in Catalysis

The study of the performance of the new synthesized gold(I) complexes (*R*,*R*)-**C** and (*R*,*R*)-**D** was tested in different reactions, comparing it with the reactivity and enantioselectivity of (*R*,*R*)-**B** with the aim of studying the influence of the central ring modifications in this kind of structures (Figure 11).

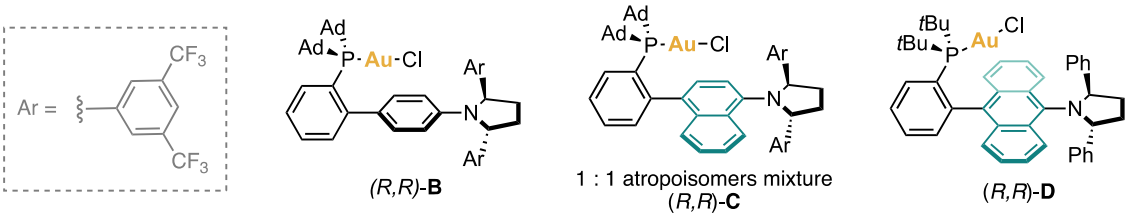

Figure 11. Gold(I) complexes considered for comparison.

The activity of the catalysts was tested in five different enantioselective reactions, three of which were enyne cyclizations that gave excellent results with the (*R*,*R*)-**B** gold(I) complex, thanks to the proper encapsulation of the substrates by the catalyst. To test if our structure preferably fits other kind of substrates, we also applied central ring modified complexes in an atroposelective reaction and a retro-Buchner reaction.

To begin with, the complexes were tested in the formal [4+2] cycloaddition of 1,6-arylenyne **37** with the optimized conditions for the first generation of these catalysts.[15] The results showed a good reactivity of the complexes with good to excellent yields using both new catalysts, and a faster reaction time compared with the model catalyst (*R*,*R*)-**B**. However, to our surprise, the enantioselectivity observed using the central ring modified catalysts (*R*,*R*)-**C** and (*R*,*R*)-**D** was almost inexistant (Table *3*).

Table 3. Test of gold(I) complexes in the formal [4+2] cycloaddition of **37**.

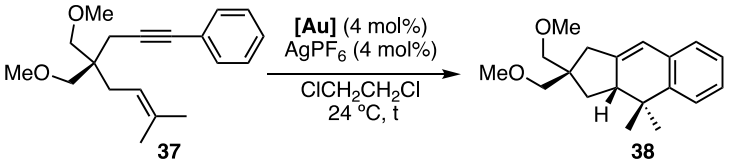

[Au]	t (h)	Yield (%)[a]	*er* (%)[b]
(*R*,*R*)-**B**	16	92	94 : 6
(*R*,*R*)-**C**	3	>99	49 : 51
(*R*,*R*)-**D**	6	83	44 : 56

[a] Yields determined by ^{1}H NMR using Ph_2CH_2 as internal standard.

[b] Enantiomeric ratios determined by HPLC.

Our second trial involved the study of the developed catalysts on the 6-*endo*-dig cyclization of aryl-tethered 1,6-enyne **39** in presence of water as an external nucleophile to form 2,3-substituted 1,2-dihydronaphthalene **40**, also proved to be successfully catalyzed by (*R*,*R*)-**B**. In this case, we observed an increase of the yield together with a moderate enantioselectivity when (*R*,*R*)-**C** was used, what suggested us a possible good performance of the more hindered anthracenyl gold(I) complex (R,R)-**D** where the competition between the rotamers did not exist, however, the reaction outcome showed disappointing results with almost racemic product obtained (Table 4).

Table 4. Evaluation of gold(I) complexes in the formation of 1,2–dihydronaphthalene **40**.

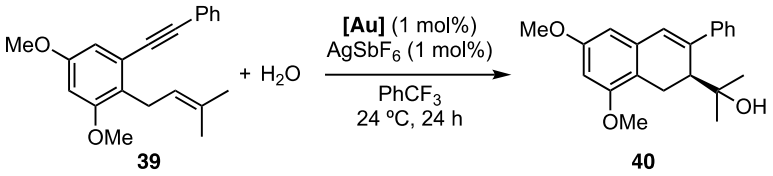

39 **40**

[Au]	Yield (%)[a]	*er (%)*[b]
(*R*,*R*)-**B**	60	99 : 1
(*R*,*R*)-**C**	76	71 : 29
(*R*,*R*)-**D**	57	57 : 43

[a] Isolated yield. [b] Enantiomeric ratios determined by HPLC.

As our next approach, we applied (*R*,*R*)-**C** and (*R*,*R*)-**D** in the cyclization of nitrogen-tethered 1,6-arylenyne **41**. These nitrogen-tethered 1,6-arylenyne compounds have successfully undergone 6-*endo*-dig cyclization under Au(I) and $PtCl_2$-catalyzed reactions, forming azabicyclic compounds.[22] Moreover, the asymmetric version of this reaction can be performed with (*R*,*R*)-**B** with good results.[15] In this case, although the performance of (*R*,*R*)-**C** complex was promising, with better yields than the one observed with (*R*,*R*)-**B** and moderate enantio-induction, our expectations with (*R*,*R*)-**D** were in vain, since there was no reaction when this complex was used as the catalyst in this transformation (Table 5).

22 (a) Fürstner, A.; Szillat, H.; Stelzer, F. *J. Am. Chem. Soc.* **2000**, *122*, 6785–6786. (b) Fürstner, A.; Stelzer, F.; Szillat, H. *J. Am. Chem. Soc.* **2001**, *123*, 11863–11869.

Table 5. Test of (R,R)-**C** and (R,R)-**D** in the enantioselective formation of azabicyclic compound **42**.

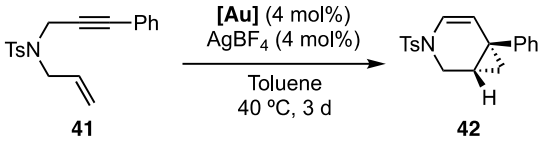

41 42

[Au]	Yield (%)[a]	*er (%)*[b]
(*R*,*R*)–**B**	35	95 : 5
(*R*,*R*)–**C**	61	76 : 24
(*R*,*R*)–**D**	–	–

[a] Isolated yield. [b] Enantiomeric ratios determined by SFC.

Once concluded that enynes were not the optimal substrates to fit in the chiral pocket of our new catalysts, we tested them in completely different reactions. We started by the atroposelective cyclization of naphthyl derivatives to give enantioenriched indoles, previously optimized in the group and tested with several members of the family of chiral diarylphosphine pyrrolidine gold(I) complexes.[23] In this case, we newly observed a good reactivity of (*R*,*R*)-**C** and (*R*,*R*)-**D** gold(I) complexes providing good yields but not enantio-induction at all (Table 6).

Table 6. Evaluation of the performance of (R,R)-**C** and (R,R)-**D** in the the atroposelective cyclization of naphthyl derivative **43**.

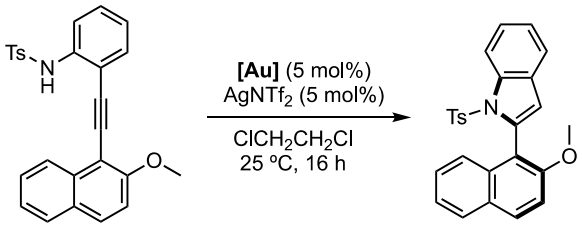

43 44

[Au]	Yield (%)[a]	*er (%)*[b]
(*R*,*R*)-**B**	>99	87 : 13
(*R*,*R*)-**C**	82	52 : 48
(*R*,*R*)-**D**	71	55 : 45

[a] Yields determined by ^{1}H NMR using Ph_2CH_2 as internal standard.

[b] Enantiomeric ratios determined by SFC.

Finally, to diversify the reactivity tests of our catalysts, we decided to apply the central ring modified gold(I) catalysts in the retro-Buchner reaction. This reaction was developed in the group, however an

23 Zucarello, G. Doctoral Thesis, *Chiral Pyrrolidinyl–Biphenyl Phosphine Ligands in Gold(I) Catalysis* (2020).

asymmetric version of it is still pending.[24] We thought that since we were passing by a less bulky intermediate, a tighter chiral pocket would favor a good enantio-induction. Unfortunately, the results obtained were discouraging, what can be derived from the fact that these reactions need relatively high temperatures to work, which will be a negative factor for the generation of enantio-induction (Table 7).

Table 7. Test of gold(I) catalysts in the retro-Buchner reaction of cycloheptatriene **45**.

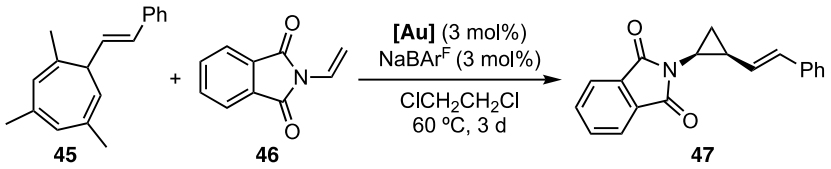

45 **46** **47**

[Au]	Yield (%)[a]	*er (%)*[b]
(*R*,*R*)-**B**	45	35 : 65
(*R*,*R*)-**C**	20	53 : 47
(*R*,*R*)-**D**	43	48 : 52

[a] Isolated yields. [b] Enantiomeric ratios determined by SFC.

24 Mato, M.; Herlé, B.; Echavarren, A. M. *Org. Lett.* **2018**, *20*, 4341–4345.

Conclusions

Two new members of the family of chiral biaryl-pyrrolidinyl phosphine gold(I) complexes have been designed and synthesized, successfully enlarging the central ring of their structure. Additionally, a different type of modular synthesis has been disclosed, paving the way for other modifications of these structures (Figure 12).

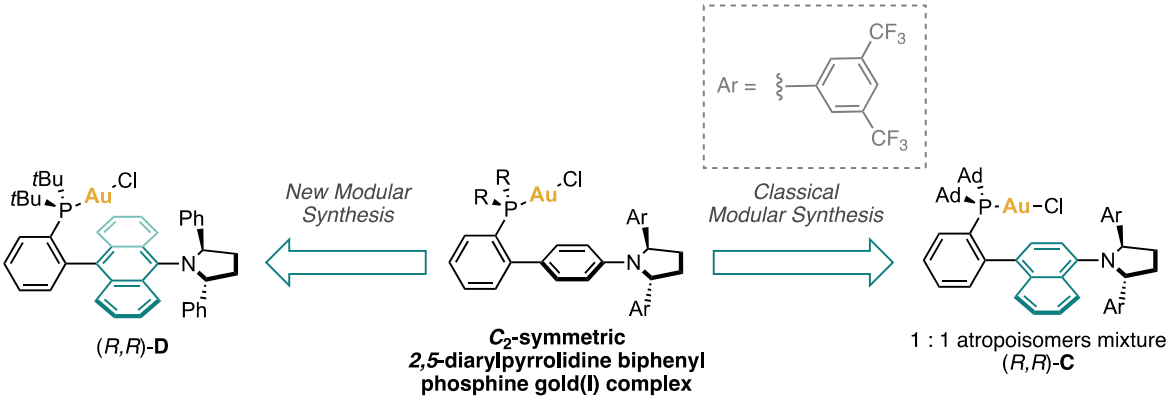

Figure 12. Expansion of the family of chiral biaryl-pyrrolidinyl phosphine gold(I) complexes via central ring modifications.

Although the modification in the central ring of the complexes envisioned a tighter chiral pocket, the structures do not correctly fit the substrates in a favorable position to provide enantio-induction, as it has been shown in the performance of the complexes in five different types of reactions. With this, we have gained more information about how modification in the structure of this family of complexes affects their performance, indicating that these modifications of the central ring are not a suitable option for expanding the application of these catalysts.

Experimental Section

General Information

Unless otherwise stated, all the reactions were performed under argon atmosphere. Unless otherwise stated, all reagents and solvents were purchased from commercial sources and used without further purification. All the dry solvents used were dried by passing through an activated alumina column on a PureSolv$_{TM}$ Solvent Purification System (SPS, Innovative Technologies, Inc., MA), or they were commercially available anhydrous solvents purchased from ACROS Organics. Reactions which were performed at temperatures higher than the boiling point of the employed solvents, were ran in sealed microwave vials using an aluminum heating block and must be done applying the appropriate precautions for working in such set up. The progress of the reactions was followed by GC–MS, UHPLC–MS (Agilent Technologies 1290 Infinity II, LC/MS with single–quad detector InfinityLab (APCI ionization source)), TLC (thin layer chromatography) or by NMR analysis. Analytical thin layer chromatography was carried out using TLC aluminum sheets coated with 0.2 mm of silica gel (Merck Gf234) using UV light as the visualizing agent and an acidic solution of vanillin in ethanol or basic solution of $KMnO_4$ in water as stain. Chromatographic purifications were carried out using flash grade silica gel (SDS Chromatogel 60 ACC, 40–60 μm) as the stationary phase manually,or using a CombiFlash®Rf instrument with normal phase disposable columns of different sizes (Teledyne Isco). Preparative thin layer chromatography was performed on TLC plates (Analtec Silica Gel GF UV254, 20×20 cm, 1000 μm or 2000 μm). NMR spectra were recorded at 298 K on BrukerAvance Ultrashield NMR spectrometers (300 MHz, 400 MHz, 500 MHz and 500 MHz with CryoProbe). Chemical shifts (δ) are reported in parts per million (ppm) and referenced to residual solvent (For ^{1}H NMR: $CDCl_3$ at 7.26 ppm, CD_2Cl_2 at 5.31 ppm, C_6D_6 at 7.16 ppm, for $^{13}C\{^{1}H\}$ NMR: $CDCl_3$ at 77.16 ppm, CD_2Cl_2 at 54.00 ppm, C_6D_6 at 128.06 ppm). The following abbreviations were used to explain multiplicities: s = singlet, d = doublet, t = triplet, q = quartet, p = pentet, m = multiplet, br s = broad singlet. Coupling constants (*J*) are reported in Hertz (Hz). Mass spectra were recorded on a Waters LCT Premier Spectrometer (ESI and APCI) or on an Autoflex Broker Daltonics (MALDI and LDI). Specific optical rotation measurements were carried out on a Jasco P–1030 model polarimeter equipped with a PMT detector using the sodium line at 589 nm, and 1 mL (10 mm pathlength) or 2 mL (100 mm pathlength) cells. Melting points were determined using a Mettler Toledo MP70 melting point apparatus. Chiral HPLC analyses were performed on an Agilent Technologies 1200 series. SFC analyses were performed on an Agilent Technologies 1260 Infinity II, a Waters ACQUITY UPC2 System with diode array detector and by Chiral Technologies Europe analytical service. X-ray diffraction data were collected at 100 K on a Rigaku MicroMax-007HF, Mo Kα rotating anode, equipped with a Pilatus 200 K detector or on a Bruker APEX DUO, Mo Kα Microfocus source E025 IuS anode, equipped with an APEX DUO detector using omega scans.

Synthetic Procedures and Analytical Data

Synthesis of Complex (*R,R*)-C

1-(2-Bromophenyl)-4-nitronaphthalene (19)

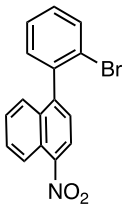

A 25 mL round bottom flask equipped with a stirring bar was charged with 1-iodo-4-nitronaphthalene (384.0 mg, 1.3 mmol, 1.0 equiv), (2-bromophenyl)boronic acid (323.0 mg, 1.6 mmol, 1.3 equiv), $Pd(PPh_3)_4$ (44.5 mg, 39.0 mmol, 3 mol%) and sodium bicarbonate (324.0 mg, 3.9 mmol, 3.0 equiv) in dimethoxyethane (3.7 mL, 0.35 M). The solution was stirred for 5 minutes, water (1.8 mL) was added and the solution was degassed under an argon flow during 15 minutes. The solution was sealed and stirred at 120 ºC for 5 hours. The reaction was monitored by TLC (cyclohexane/EtOAc, 3:1) and GC-MS. When no more starting material remained, the crude was extracted with Et_2O, dried over Na_2SO_4 and concentrated. Crude product was used in the next step without further purification.

4-(2-Bromophenyl)naphthalen-1-amine (20)

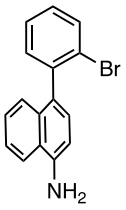

A 25 mL round bottom flask equipped with stirring bar was charged with approximately 330 mg of 1-(2-bromophenyl)-4-nitronaphthalene (crude product obtained in the previous step, expected 1.3 mmol), acetic acid (1.7 mL) and water (0.6 mL, 0.6 M). The solution was warmed up to 80 ºC and iron (562.0 mg, 10.1 mmol, 10.0 equiv) was added (attention foaming). The mixture was stirred for 1 h at 80 ºC and the solvent was removed under vacuum. A black mud was obtained. The residue was "dissolved" in CH_2Cl_2 (9.0 mL) and $NaHCO_3$ (6.0 mL), NaOH solution (10%) was added until basic pH was obtained and the two phases were separated. The aqueous phase was extracted with CH_2Cl_2 twice (2x). The organic phase was washed with brine (2x). The organic phase was dried over Na_2SO_4 and concentrated. Crude product was purified by flash SiO_2 column chromatography (cyclohexane/CH_2Cl_2, 1:1) and 4-(2-bromophenyl)naphthalen-1-amine (158.0 mg, 0.5 mmol, 41% yield over two steps) was obtained as a pink solid.

^{1}H NMR (400 MHz, $CDCl_3$) δ 7.90 (d, *J* = 8.2 Hz, 1H), 7.72 (dd, *J* = 8.0, 1.2 Hz, 1H), 7.50 – 7.34 (m, 5H), 7.30 – 7.25 (m, 1H), 7.18 (d, *J* = 7.6 Hz, 1H), 6.86 (d, *J* = 7.6 Hz, 1H). **^{13}C{^{1}H} NMR** (101 MHz, $CDCl_3$) δ 142.2, 141.9, 132.8, 132.7, 132.4, 130.5, 128.9, 127.7, 127.3, 126.8, 126.2, 125.4, 125.0, 123.6, 121.2, 109.3. **HRMS** (ESI+) calculated for $[C_{16}H_{13}BrN]^+$ 298.0226 *m/z*; found $[M + H]^+$ 298.0212 *m/z*. **M.p.** = 137–138 °C.

(2*R*,5*R*)-2,5-bis(3,5-Bis(trifluoromethyl)phenyl)-1-(4-(2-bromophenyl)naphthalen-1-yl) pyrrolidine (21)

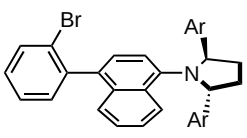

A 50 mL flamed and dried two-necked round bottom flask equipped with a stirring bar was charged with (1*S*,4*S*)-1,4-bis(3,5-bis(trifluoromethyl) phenyl) and butane-1,4-diol (400.0 mg, 778.0 µmol, 1.0 equiv) dissolved in CH_2Cl_2 (6.5

mL, 0.1 M). Solution was cooled down to –20 °C and triethylamine (236.0 mg, 325.0 µL, 2.3 mmol, 3.0 equiv) and methanesulfonyl chloride (232.0 mg, 156.0 µL, 2.0 mmol, 2.6 equiv) were added under argon atmosphere. The mixture was stirred for 4 h at –20 °C. Then, at –20 ºC, 4-(2-bromophenyl) naphthalen-1-amine (1.1 g, 3.8 mmol, 4.9 equiv) in 0.8 mL of CH_2Cl_2 was added. The reaction was left to warm up to room temperature and then stirred for 16 h at 25 ºC. The reaction was checked by TLC and ^{1}H NMR. As it had not finished, was heated at 40 ºC during 2 additional hours. The reaction was quenched with water, the product was extracted with EtOAc (3x), and the organic phase was washed with brine and $NaHCO_3$, dried over Na_2SO_4, filtered and concentrated. The crude product was purified by SiO_2 column chromatography (cyclohexane/CH_2Cl_2, 2:1) obtaining (2*R*,5*R*)-2,5-bis(3,5-bis(trifluoromethyl)phenyl)-1-(4-(2-bromophenyl)naphthalen-1-yl) pyrrolidine (165.0 mg, 0.2 mmol, 27% yield) as a brown foam. ^{1}H NMR at 243K evidenced restricted rotation around the C_{aryl}–N bond, showing splitting of the 1H signals (Figure 13).

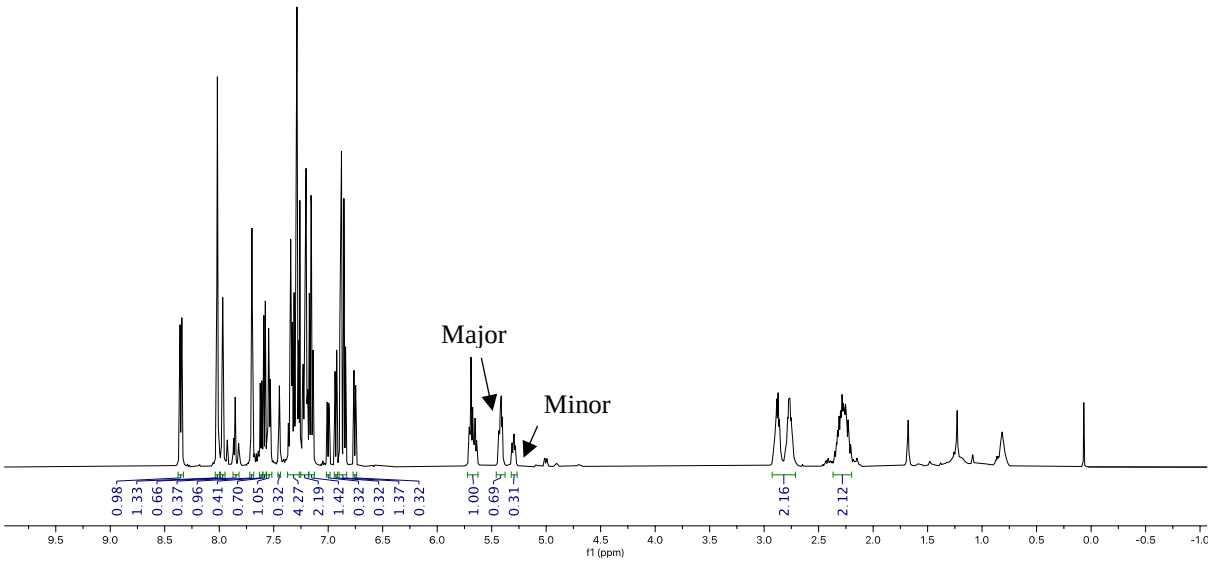

Figure 13. ^{1}H NMR at 243K of rotamers mixture of pyrrolidine **21**.

^{1}H NMR (500 MHz, $CDCl_3$, 243 K) **Major and Minor Rotamers** (significant signals specified): 8.35 (d, *J* = 8.4, Hz, 1H), 8.02 (s, 1.3H), 7.97 (major rotamer, s, 0.7H), 7.87 – 7.80 (minor rotamer, m, 0.4H), 7.70 (s, 1H), 7.62 (minor rotamer, dd, *J* = 8.1, 1.3Hz, 0.4H), 7.58 (major rotamer, dd, *J* = 8.0, 1.3 Hz, 0.7H), 7.56 – 7.51 (m, 1H), 7.45 (minor rotamer, s, 0.3H) 7.37 – 7.27 (m, 4.3H), 7.25 – 7.18 (m, 2H), 7.16 (td, *J* = 7.8, 1.4 Hz, 1.4H), 7.00 (minor rotamer, dd, *J* = 7.6, 1.7 Hz, 0.3H), 6.93 (minor rotamer, d, *J* = 7.8 Hz, 0.3H), 6.87 (dd, *J* = 20.8, 7.7 Hz, 1.3H), 6.76 (minor rotamer, d, *J* = 7.8 Hz, 0.3H) 5.72 – 5.63 (m, 1H), 5.42 (major rotamer, dd, *J* = 9.8, 5.3 Hz, 0.7H), 5.32 – 5.27 (minor rotamer, m, 0.3H) 2.93 – 2.71 (m, 2H), 2.37 – 2.20 (m, 2H). **^{13}C{^{1}H^{19}F} NMR** (126 MHz, $CDCl_3$, 243 K) **Major Rotamer:** δ 145.6, 144.6, 141.6, 140.9, 134.2, 132.5, 132.4, 132.2, 131.8, 131.6, 130.2, 128.9, 128.3, 128.2, 127.7, 127.2, 127.1, 126.8, 126.5, 126.1, 125.9, 125.2, 124.5, 124.0, 123.3, 123.0, 123.0, 121.8, 120.6, 116.3,

67.7, 64.2, 37.3, 35.5. **Minor Rotamer** (only significant signals) **:** δ 145.5, 144.1, 141.4, 134.4, 134.2, 132.1, 132.1, 130.1, 129.0, 128.4, 128.3, 126.5, 126.0, 125.4, 124.4, 121.7, 120.5, 116.6, 63.4, 36.6, 34.3. **^{19}F{^{1}H} NMR** (471 MHz, $CDCl_3$, 243 K) **Major and Minor Rotamer** δ –62.5 – –62.8 (m, 6F). **HRMS** (ESI+) calculated for $[C_{36}H_{22}BrF12NNa]^+$ 798.0636 *m/z*; found $[M + Na]^+$ 798.0656 *m/z*. **M.p.** = 71–72 °C $\boldsymbol{\alpha_D^{589}}$ = –2.5 deg.cm^2.g^{-1} (CH_2Cl_2, c 0.1, 302 K).

Ligand C (22)

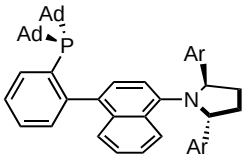

A MW vial equipped with a stirring bar was charged with (2*R*,5*R*)-2,5-bis(3,5-bis(trifluoromethyl)phenyl)-1-(4-(2-bromophenyl)naphthalen-1-yl) pyrrolidine (110.0 mg, 142.0 mmol, 1.0 equiv), $Pd(OAc)_2$ (1.6 mg, 7.1 μmol, 5 mol%), dppf (4.7 mg, 8.5 μmol, 6 mol%), NaO*t*Bu (16.3 mg, 0.2 mmol, 1.2 equiv) and toluene (0.7 mL, 0.2 M). Resulting suspension was stirred for 15 min at 24 ºC. Di(adamantan-1-yl)phosphane (47.1 mg, 156.0 mmol, 1.1 equiv) was added and the reaction mixture was stirred at 120 ºC for 16 h. Then, the reaction was allowed to cool to 24 ºC and the crude was purified by flash column chromatography (cyclohexane/CH_2Cl_2 10:1, then 100% EtOAc) to yield ligand **C** (60.0 mg, 60.0 mmol, 42% yield) as a yellow foam in a 55:45 rotamers mixture. In this case, a ^{1}H NMR T slope experiment was performed to separate the signals of the two rotamers, which coalesce around 298K (Figure 14). Since the product decomposes over time in $CDCl_3$, for the ^{13}C{H} NMR characterization the solvent used was CD_2Cl_2, however the rest of experiments where ran in $CDCl_3$ on behalf of the clarity of the signals.

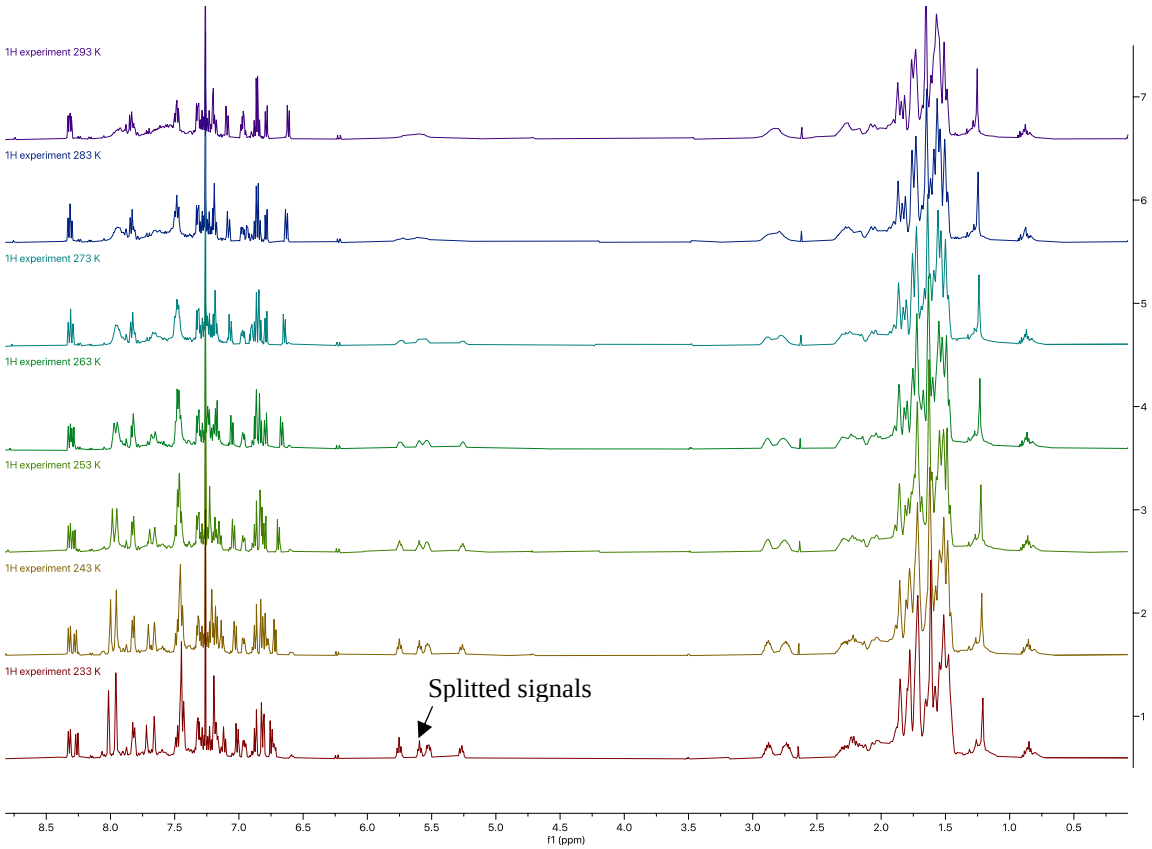

Figure 14. ^{1}H T slope to evidence the rotamers mixture of ligand **C**.

^{1}H NMR (500 MHz, $CDCl_3$) **1:1 mixture of rotamers, only some picks distinguishable** δ 8.32 (dd, *J* = 8.6, 3.5 Hz, 1H), 8.02 – 7.45 (m, 7H), 7.34 – 7.27 (m, 2H), 7.25 – 7.15 (m, 2.5H), 7.10 (dd, *J* = 8.6, 1.3 Hz, 0.5H), 6.99 – 6.95 (m, 1H), 6.88 – 6.83 (m, 1H), 6.79 (d, *J* = 7.1 Hz, 0.5H), 6.61 (d, *J* = 7.7 Hz, 0.5H), 5.81 – 5.18 (m, 2H), 3.0 – 2.71 (m, 2H), 2.42 – 2.21 (m, 2H), 2.21 – 1.80 (m, 6H), 1.75 (d, *J* = 15.6 Hz, 7H), 1.69 – 1.63 (m, 5H), 1.59 (d, *J* = 14.4 Hz, 7H), 1.53 – 1.47 (m, 5H). **^{13}C{^{1}H} NMR** (126 MHz, CD_2Cl_2) **mixture of rotamers, only some picks distinguishable** δ 149.9, 149.8, 149.6, 149.5, 140.8, 140.3, 137.6 (d, J =, 6.7 Hz), 137.4 (d, 7.3 Hz), 137.2 (d, J = 2.5 Hz), 137.1 (d, J = 2.5 Hz), 135.8, 135.6, 135.4, 135.2, 134.1, 134.0, 132.3, 132.2, 132.1, 132.1, 129.6, 129.3, 128.5, 128.4, 128.2, 128.0, 128.0, 127.9, 125.9, 125.8, 125.4, 125.3, 125.1, 124.9, 124.9, 124.0, 123.9, 122.7, 117.4, 117.3, 42.5 – 42.2 (m), 38.4 – 37.9 (m), 37.7 (d, *J* = 1.3 Hz), 37.6, 37.5, 37.3, 37.2, 37.1 – 36.8 (m), 30.1, 29.6 (dd, *J* = 12.0, 8.5) 28.8, 28.7, 28.6, 28.6, 28.5. **^{31}P{^{1}H} NMR** (162 MHz, $CDCl_3$) **Mixture of Rotamer** δ 26.4, 25.8. **^{19}F{^{1}H} NMR** (376 MHz, $CDCl_3$) **Mixture of Rotamer** δ -62.2 – -63.4 (m, 6F). **HRMS** (ESI+) calculated for $[C_{56}H_{53}F_{12}NP]^+$ 998.3719 *m/z*; found $[M + H]^+$ 998.3695 *m/z*. **M.p.** = 113–115 °C. $\boldsymbol{\alpha_D^{589}}$ = +3.62 deg.cm^2.g^{-1} (CH_2Cl_2, c 0.1, 301 K).

Complex (*R*,*R*)-C

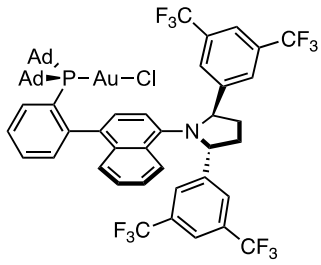

Me_2SAuCl (12.1 mg, 41.1 mmol, 1.0 equiv) and ligand **C** (41.0 mg, 41.1 mmol, 1.0 equiv) were dissolved in dry CH_2Cl_2 (0.4 mL, 0.1 M) under an atmosphere of argon. The reaction mixture was stirred at 24 ºC for 15 min. The mixture was filtered through a syringe filter and concentrated. The residue was dissolved in CH_2Cl_2, filtered through a path of neutral Al_2O_3 and concentrated to yield complex *(R,R)*-**C** (47.0 mg, 38.0 mmol, 93% yield) as a light yellow solid in 1:1 mixture of atropoisomers. The signals of the two atropoisomers were not easily distinguishable via ^1H NMR even performing the experiment at different temperatures (Figure 15). However, $^{31}P\{H\}$ NMR revealed two singlets corresponding to each one of the atropoisomers (Figure 16). Although the atropoisomer mixture was not separable via column chromatography, (nOe) irradiation NMR experiments were performed applying a selective pulse to two ^1H identified signals of the two atropoisomers to confirm that not interconversion of ^1H was observed (Figure 17).[25]

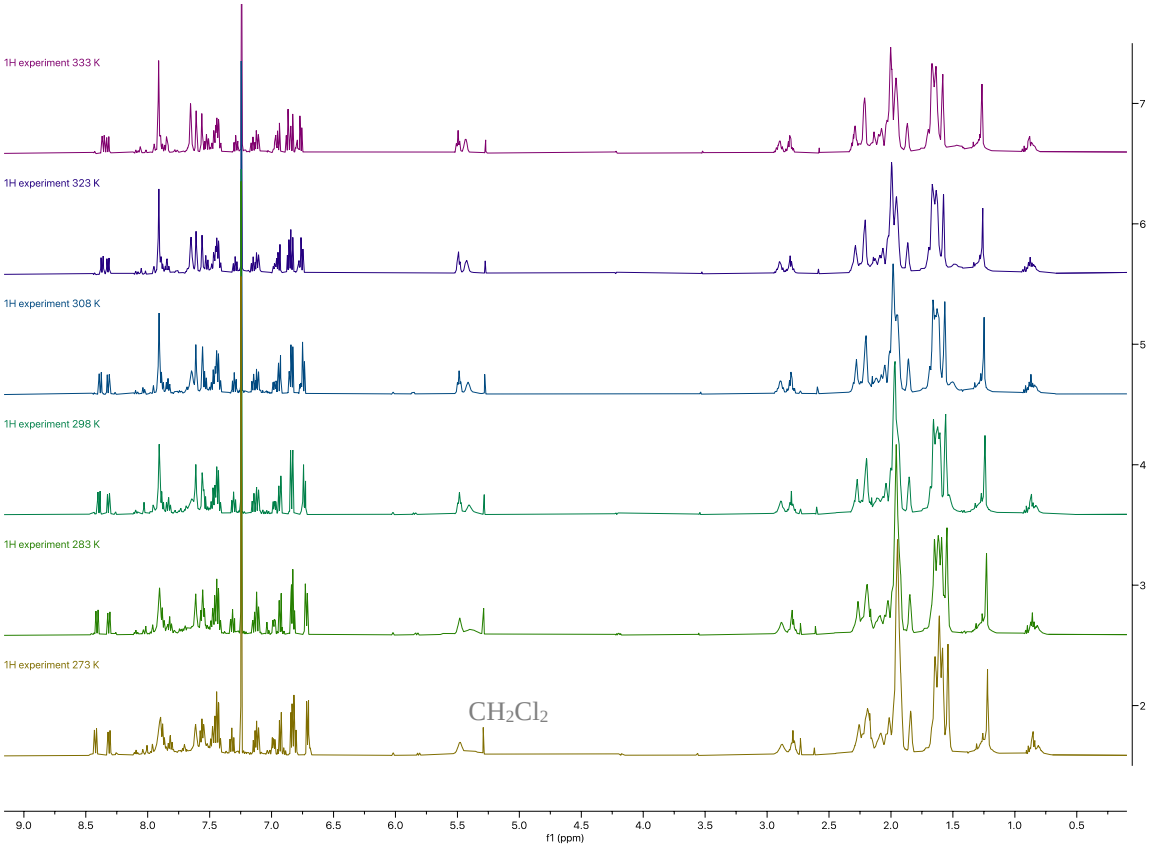

Figure 15. ^1H T slope to evidence the mixture of atropoisomers of complex (*R*,*R*)-**C.**

25 Hu, D. X.; Grice, P.; Ley S. V. J. *Org. Chem.* **2012**, *77*, 5198−5202.

$^{31}P\{^{1}H\}$ CD_2Cl_2

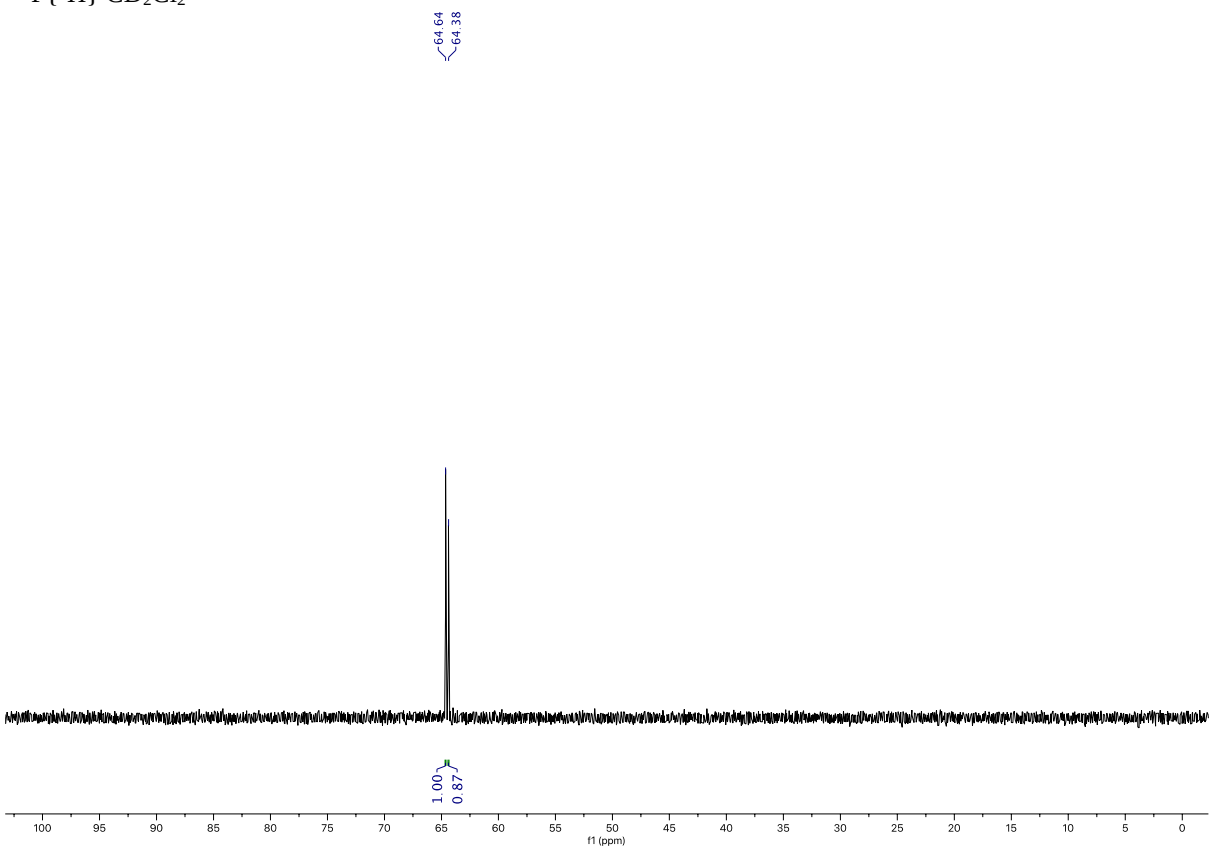

Figure 16. $^{31}P\{^{1}H\}$ NMRs of (*R,R*)-**C** mixture of atropoisomers.

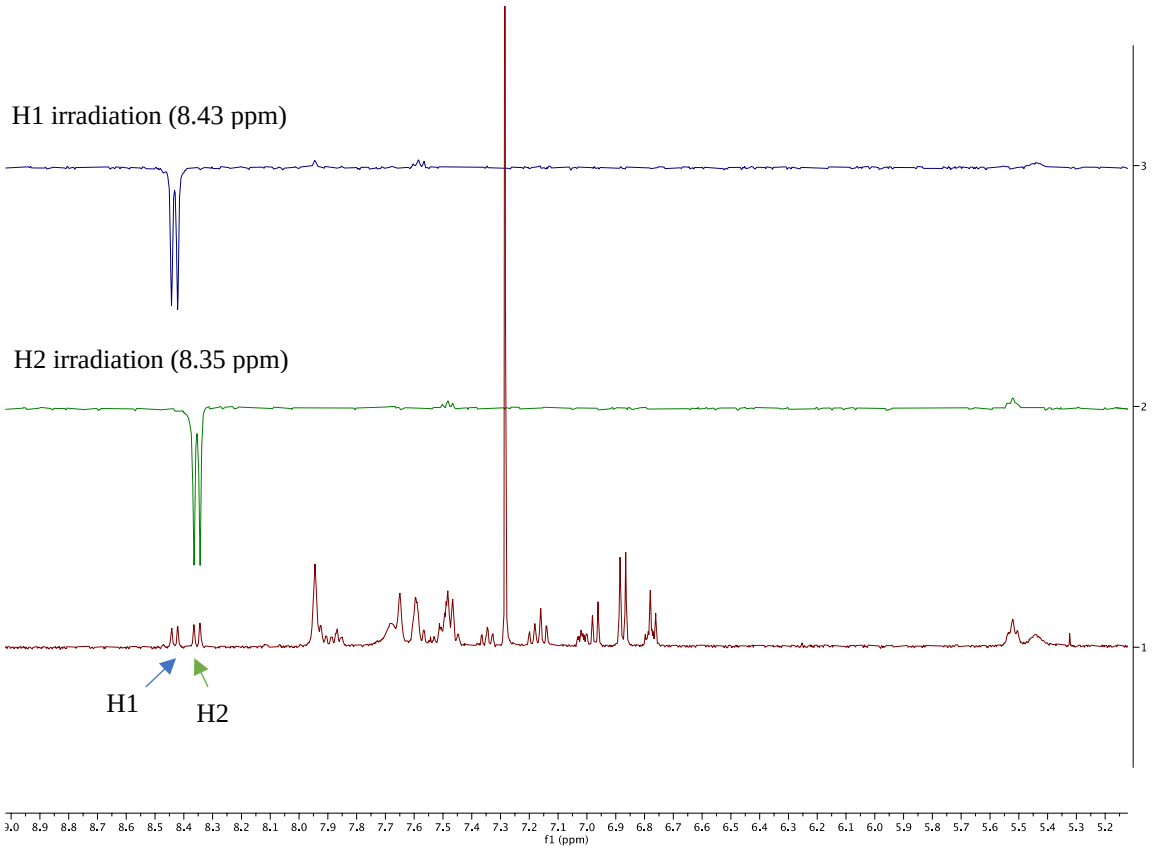

Figure 17. GOESY (nOe) Irradiation on H1 (8.43 ppm) and H2 (8.35 ppm).

^{1}H NMR (500 MHz, CD_2Cl_2) **Mixture of atropoisomers** (identified signals specified). δ 8.44 (d, *J* = 8.8 Hz, 0.5 H), 8.37 (d, *J* = 8.3 Hz, 0.5 H), 7.98 – 7.86 (m, 3H), 7.78 – 7.63 (m, 2.5 H), 7.60 – 7.54 (m, 1.5 H), 7.53 – 7.40 (m, 3H), 7.35 (ddd, *J* = 8.2, 6.7, 1.2 Hz, 0.5H), 7.22 – 7.18 (ddd, *J* = 8.3, 6.7, 1.2 Hz, 0.5H), 7.17 – 7.13 (d, *J*= 9.1 Hz, 0.5H), (6.99 – 6.93 (m, 1H), 6.88 – 6.83 (m, 1.5H), 6.80 (d, *J* = 7.6 Hz, 0.5H), 6.65 (ddd, *J* = 7.6, 4.2, 1.6 Hz, 0.5H), 5.58 – 5.51 (m, 1 H), 5.42 (m, 1 H), 2.98 – 2.73 (m, 2H), 2.31 – 2.17 (m, 5H), 2.13 – 1.87 (m, 16H), 1.72 – 1.57 (m, 12H). **^{13}C{^{1}H} NMR** (126 MHz, CD_2Cl_2) **Mixture of Atropoisomers** δ 149.1, 149.0, 148.8, 146.8, 145.8, 144.1, 141.5, 137.1, 137.0, 135.2, 135.1, 135.0, 134.9, 134.8, 134.7, 134.2, 133.1, 131.3, 131.0, 130.9 (d, *J* = 2.3 Hz), 130.5 (d, *J* = 2.3 Hz), 129.6, 128.5, 128.3, 127.8, 127.6, 127.6, 127.1, 127.0, 126.9, 126.8, 126.7, 126.3, 126.1, 126.0, 125.9, 125.7, 125.6, 125.5, 125.3, 125.2, 125.1, 125.0, 124.5, 122.9, 122.8, 121.9, 121.4 – 120.9 (m), 116.5, 43.9, 43.7, 43.2, 43.2, 42.8, 42.7, 42.7, 42.6, 42.5, 42.5, 42.2, 42.2, 42.0, 41.7, 41.7, 36.7, 36.6, 36.6, 30.5, 30.1, 29.4, 29.4, 29.2, 29.2, 29.1, 29.0, 29.0. **^{31}P{^{1}H} NMR** (202 MHz, CD_2Cl_2**)** δ 64.6, 64.4. **^{19}F{^{1}H} NMR** (376MHz, CD_2Cl_2) δ –63.0. **HRMS** (ESI+) calculated for $[C_{56}H_{53}AuClF_{12}NP]^+$ 1230.3073 *m/z*; found $[M + H]^+$ 1230.3075 *m/z*. **M.p. =** >137 °C (decomposition). **α_D^{589}** = +11.8 deg.cm^2.g^{-1} (CH_2Cl_2, c 0.09, 301 K).

Synthesis of Complex (*R*,*R*)-D

Synthetic route for (1*S*,4*S*)-1,4-diphenylbutane-1,4-diol

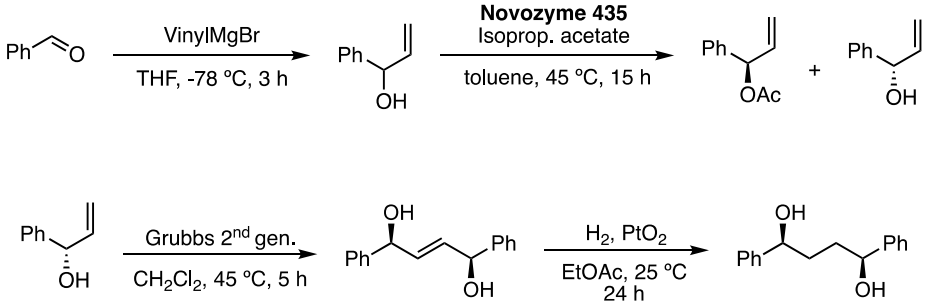

1-Phenylprop-2-en-1-ol

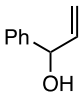

1-phenylprop-2-en-1-ol was synthesized according to the reported procedure.[26] Vinylmagnesium bromide (1.0 M in THF, 56.5 mL, 56.5 mmol, 1.2 equiv) was added dropwise to a solution of benzaldehyde (4.8 mL, 47.1 mmol, 1.0 equiv) at –78 °C. The mixture was stirred at –78 °C for 10 min, then at 24 °C for 3 h. Sat. Aq. NH_4Cl (100 mL) was added to the mixture and the aqueous phase was extracted with EtOAc (3x). The combined organic layers were washed with brine, dried over $MgSO_4$ and concentrated in vacuo. The crude material was flash chromatographed over silica gel eluting with cyclohexane and EtOAc (0–40%) to provide the title compound as a clear oil (5.3 g, 39.6 mmol, 84% yield).

^{1}H NMR (300 MHz, $CDCl_3$) δ 7.42 – 7.27 (m, 5H), 6.06 (ddd, *J* = 17.2, 10.2, 6.0 Hz, 1H), 5.36 (dt, *J* = 17.2, 1.4 Hz, 1H), 5.26 – 5.16 (m, 2H), 1.91 (br s, 1H).

The characterization data were fully consistent with those previously reported.[25]

(*S*)-1-Phenylprop-2-en-1-ol

The synthesis of (*S*)-1-phenylprop-2-en-1-ol was performed following an analogous procedure to the one previously reported for other enantioenriched aryl substituted allylic alcohols.[15] A 250 mL two-necked round bottom flask equipped with a stirring bar was charged with powdered 4 Å molecular sieves (8.3 g) and heated to 200 ºC under high vacuum (ca 0.1 mbar) during 40 min. The flask was allowed to cool to 24 ºC under argon and Novozyme 435 resin (1.82 g, >5000 U/g) was added. The solids were suspended in 700 mL of anhydrous toluene. Isopropenyl acetate (47.5 mL, 436.4 mmol, 4.6 equiv) was added followed by 1-phenylprop-2-en-1-ol (12.9 g, 95.9 mmol, 1.0 equiv) added by cannula to the mixture as a 100.0 mL solution in toluene, and the mixture was stirred at 44 °C for 15 h. The reaction progress was tracked by chiral HPLC and upon completion, was cooled to 23 ºC then filtered through celite, and concentrated under reduced pressure. The crude material was

26 Yung–Son, H.; Ying–Chieh, W.; Kuo–Jui, W. *J. Chin. Chem. Soc*., **2008,** *55*, 896–914.

purified by silica gel flash column chromatography eluting with cyclohexane and EtOAc (0–30%) to provide the title compound as a light yellow oil (5.6 g, 41.7 mmol, 43% yield, > 99:1 *er*).

^{1}H NMR (300 MHz, $CDCl_3$) δ 7.41 – 7.26 (m, 5H), 6.13 – 5.99 (m, 1H), 5.36 (dt, *J* = 17.2, 1.4 Hz, 1H), 5.24 – 5.17 (m, 2H), 1.94 (dd, *J* = 3.9, 1.8 Hz, 1H). **α_D^{589}** = +163.7 deg.cm^2.g^{-1} ($CHCl_3$, c 0.089, 301 K).

HPLC Chiracel OJ–H (250 x 4.6 mm, 5 µm) at 25 ºC, flow 1.0 mL/min, isocratic hexane/iPrOH 98:2, 220 nm; t_{R1}= 28.6 min, t_{R2}= 35.8 min.

All other experimental data were in agreement with the literature.[27]

(1*S*,4*S*)-1,4-Diphenylbut-2-ene-1,4-diol

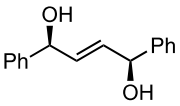

The synthesis of (1*S*,4*S*)-1,4-diphenylbut-2-ene-1,4-diol was performed following an analogous procedure to the one previously reported for other enantioenriched aryl substituted allylic diols.[15] Grubbs gen. 2 catalyst (65.0 mg, 79.0 mmol, 5 mol%) was added to a solution of (*S*)-1-phenylprop-2-en-1-ol (2.0 g, 15.2 mmol, 1.0 equiv) in dichloromethane (3.0 mL, 5.0M). The mixture was stirred for 5 h at 40 °C. The crude material was purified by silica gel chromatography using Combiflash eluting with cyclohexane and Et_2O (0–70%) to provide the title compound (831.0 mg, 4.6 mmol, 45% yield) as a beige solid.

^{1}H NMR (500 MHz, $CDCl_3$) δ 7.39 – 7.27 (m, 10H), 6.03 (dd, *J* = 3.3, 1.5 Hz, 2H), 5.26 (td, *J* = 3.5, 1.5 Hz, 2H), 1.92 (d, *J* = 3.8 Hz, 2H). **^{13}C{^{1}H} NMR** (126 MHz, $CDCl_3$) δ 142.7, 133.3, 128.8, 127.9, 126.4, 74.5. **M.p. =** > 70 °C (decomposition). **α_D^{589}** = +12.5 deg.cm^2.g^{-1} ($CHCl_3$, c 0.1, 296 K).

(1*S*,4*S*)-1,4-Diphenylbutane-1,4-diol (24)

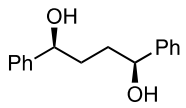

The synthesis of (1*S*,4*S*)-1,4-diphenylbutane-1,4-diol was performed following an analogous procedure to the one previously reported for other enantioenriched aryl substituted diols.[15] A 20 mL microwave vial was charged with PtO_2 (39.3 mg, 173.0 mmol, 5 mol%), then evacuated and back-filled with argon three times. Then (1*S*,4*S*,E)-1,4-diphenylbut-2-ene-1,4-diol (831.0 mg, 3.5 mmol, 1.0 equiv) dissolved in 15.0 mL of EtOAc (0.2M) was added to the vial. Subsequently, the reaction mixture was evacuated and back-filled with hydrogen. The reaction was stirred at 24 °C for 24 h under hydrogen atmosphere (1 atm), then filtered over Celite, and concentrated in vacuo. The crude material was purified by silica gel flash column chromatography eluting with cyclohexane and Et_2O (30–70%) to provide the title compound **24** (1.4 g, 5.8 mmol, 97% yield) as a white solid.

^{1}H NMR (500 MHz, $CDCl_3$) δ 7.34 (d, *J* = 4.4 Hz, 8H), 7.29 – 7.26 (m, 2H), 4.76 – 4.69 (m, 2H), 2.52 (br s, 2H), 1.99 – 1.89 (m, 2H), 1.88 – 1.78 (m, 2H). **^{13}C{^{1}H} NMR** (126 MHz, $CDCl_3$) δ 144.75,

27 Lyothier, I.; Defieber, C.; Carreira, E. M. *Angew. Chem. Int. Ed*. **2006**, *45*, 6204–6207.

128.63, 127.71, 125.96, 74.80, 35.98. **M.p. =** 72–73 °C. α_D^{589} = –44.6 deg.cm^2.g^{-1} ($CHCl_3$, c 0.1, 302 K).

(2*R*,5*R*)-1-Allyl-2,5-diphenylpyrrolidine (25)

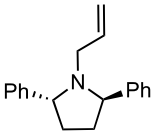

Flamed and dried 250 mL round-bottom flask equipped with a stirring bar was charged with (*1S,4S*)-1,4-diphenylbutane-1,4-diol (1.0 g, 4.1 mmol, 1.0 equiv) and dichloromethane (37.2 mL, 0.1 M). Solution was cooled down to –20 °C and triethylamine (1.3 g, 1.7 mL, 12.4 mmol, 3.0 equiv) and methanesulfonyl chloride (1.2 g, 798.0 µL, 10.3 mmol, 2.5 equiv) were added under argon atmosphere. The mixture was stirred for 3 h at –20 °C. Then, at –20 ºC, allylamine (23.6 g, 31.0 mL, 412.7 mmol, 100.0 equiv) was added. The reaction was left to warm up to room temperature and then stirred for 16 h at 25 ºC. The reaction was monitored by TLC and concentrated under reduced pressure. Residue was diluted with Et_2O, washed with a saturated solution of $NaHCO_3$ (3x), brine and dried over Na_2SO_4, filtered and concentrated. The crude product was purified by flash SiO_2 column chromatography (cyclohexane/CH_2Cl_2, 10:1 to 1:1) obtaining (2*R*,5*R*)-1-allyl-2,5-diphenylpyrrolidine (796.0 mg, 3.0 mmol, 73% yield) as a colorless oil.

^{1}H NMR (400 MHz, $CDCl_3$) δ 7.36 –7.22 (m, 10H), 5.64 (dddd, *J* = 17.0, 10.4, 7.4, 4.5 Hz, 1H), 4.97 – 4.87 (m, 2H), 4.33 (ddd, *J* = 7.4, 4.0, 1.5 Hz, 2H), 3.02 – 2.95 (m, 1H), 2.71 (dd, *J* = 14.7, 7.4 Hz, 1H), 2.59 – 2.47 (m, 2H), 1.97 – 1.86 (m, 2H).

The spectral data were fully consistent with those previously reported.[28]

(2*R*,5*R*)-2,5-Diphenylpyrrolidine (26)

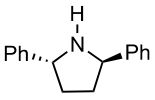

250 mL round bottom flask equipped with a stirring bar was evacuated and fulfilled with argon. Flask was charged with (2*R*,5*R*)-1-allyl-2,5-diphenylpyrrolidine (770.0 mg, 2.9 mmol, 1.0 equiv) and solid was dissolved in a 84:16 mixture of MeCN/H_2O (42.6 mL, 68.6 mM). Wilkinson's catalyst (135.2 mg, 146.2 µmol, 5 mol%) was added, solution was purged with argon for 10 minutes and reaction was heated to reflux over 4 hours. Reaction was checked by TLC (cyclohexane/EtOAc, 3:1),cooled down to room temperature and diluted with diethyl ether and brine. Aqueous phase was extracted with diethyl ether (3x), combined organic fractions were washed with brine (2x), dried over Na_2SO_4 and concentrated. Crude product was purified by flash SiO_2 column chromatography (cyclohexane/EtOAc, 4:1) to obtain (2*R*,5*R*)-2,5-diphenylpyrrolidine (425.0 mg, 2.9 mmol, 65% yield) as a white solid.

28 Chong, J. M.; Clarke, I. S.; Koch, I.; Olbach, P.C.; Taylor, N. J. *Tetrahedron: Asymmetry*, **1995**, 6, 2, 409–418.

^{1}H NMR (500 MHz, $CDCl_3$) δ 7.44 – 7.39 (m, 4H), 7.37 – 7.32 (m, 4H), 7.26 – 7.22 (m, 2H), 4.58 – 4.53 (m, 2H), 2.45 – 2.37 (m, 2H), 1.96 – 1.87 (m, 2H). $\boldsymbol{\alpha_D^{589}}$ = +138.7 deg.cm^2.g^{-1} ($CHCl_3$, c 0.1, 301K).

The characterization data were fully consistent with those previously reported.[27]

(2*R*,5*R*)-2,5-Diphenylpyrrolidin-1-yl benzoate (27)

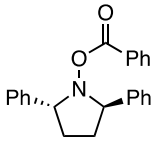

A 50 mL round bottom flask equipped with stirring bar was charged with K_2HPO_4 (480.0 mg, 2.8 mmol, 1.5 equiv) and benzoic peroxyanhydride (1.9 g, 70% Wt, 5.5 mmol, 3.0 equiv), the vial was purged with Ar and 12 mL of DMF were added. The vial was placed in an ice–water bath and a solution of (*2R,5R*)–2,5–diphenylpyrrolidine (410.0 mg, 1.8 mmol, 1.0 equiv) in 8 mL of DMF was added dropwise. The reaction was allowed to reach room temperature slowly, inside the ice–water bath. Reaction was stirred during 18 h at 25 ºC and followed by ^{1}H NMR. When starting material was consumed, reaction was quenched with deionized water and stirred vigorously over 5 minutes. The reaction mixture was extracted with dichloromethane (3x). The organic phase was collected and washed with brine, dried over anhydrous Na_2SO_4 and concentrated under vacuum. The residue was purified by SiO_2 column chromatography using Combiflash (0% to 75% DCM in cyclohexane), to obtain the desired product O-benzoyl hydroxylamine (360.0 mg, 1.1 mmol, 57% yield) as a colorless oil.

^{1}H NMR (500 MHz, $CDCl_3$) δ 7.56 – 7.51 (m, 2H), 7.48 – 7.44 (m, 4H), 7.43 – 7.38 (m, 1H), 7.31 (tt, *J* = 6.7, 0.9 Hz, 4H), 7.26 – 7.21 (m, 4H), 4.84 (t, *J* = 7.0 Hz, 2H), 2.64 – 2.54 (m, 2H), 2.33 – 2.21(m, 2H). **^{13}C{^{1}H} NMR** (126 MHz, $CDCl_3$) δ 165.3, 132.8, 130.3, 129.4, 129.3, 128.6, 128.4, 128.2, 128.1, 127.6, 126.7, 68.0, 28.8. **HRMS** (ESI+) calculated for $[C_{23}H_{21}NNaO_2]^+$ 366.1464 *m/z*; found $[M + Na]^+$ 366.1465 *m/z*. $\boldsymbol{\alpha_D^{589}}$ = +68.5 deg.cm^2.g^{-1}(CH_2Cl_2, c 0.10, 299 K).

2-(10-Bromoanthracen-9-yl)-5,5-dimethyl-1,3,2-dioxaborinane (32)

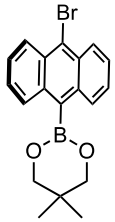

25 mL round bottom flask equipped with a stirring bar was charged with (10-bromoanthracen-9-yl)boronic acid (2.9 g, 9.7 mmol, 1.0 equiv) dissolved in dichloromethane (19.5 mL, 0.5 M). 2,2-Dimethylpropane-1,3-diol (1.2 g, 11.7 mmol, 1.2 equiv) was added to the solution and the yellow suspension was stirred for 4 hours at room temperature. After 3 hours the suspension becomes a solution. The reaction was quenched with H_2O and the mixture was extracted with CH_2Cl_2 (3x). The combined organic phases were washed with brine and dried over $MgSO_4$. The organic phase was filtered and concentrated. The residue was purified by SiO_2 column chromatography using Combiflash (0% to 50% EtOAc in cyclohexane) and 2-(10-bromoanthracen-9-yl)-5,5-dimethyl-1,3,2-dioxaborinane (2.7 g, 7.2 mmol, 74% yield) was obtained as a pink solid.

^{1}H NMR (500 MHz, $CDCl_3$) δ 8.57 (d, *J* = 8.8 Hz, 2H), 8.25 (d, *J* = 8.5 Hz, 2H), 7.58 (ddd, *J* = 8.9, 6.5, 1.2 Hz, 2H), 7.51 (ddd, *J* = 8.6, 6.5, 1.3 Hz, 2H), 4.03 (s, 4H), 1.28 (s, 6H). **^{13}C{^{1}H} NMR** (126 MHz, $CDCl_3$) δ 135.3, 130.3, 129.1, 128.4, 126.8, 125.7, 124.9, 72.9, 32.1, 22.6. **HRMS** (ESI+) calculated for $[C_{19}H_{18}BBrO_2]^+$ 368.0692 *m/z*; found $[M + H]^+$ 368.0685 *m/z*. **M.p. =** 129–130 °C.

(2*R*,5*R*)-1-(10-Bromoanthracen-9-yl)-2,5-diphenylpyrrolidine (33)

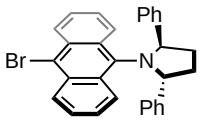

This reaction was performed following the procedure previously reported.[29] A MW vial was charged with a stirring bar, 2-(10-bromoanthracen-9-yl)-5,5-dimethyl-1,3,2-dioxaborinane (425.6 mg, 1.15 mmol, 1.2 equiv) and XantPhos (19.5 mg, 33.6 µmol, 3.5 mol%). The vial was introduced in the glovebox and cesium fluoride (437.9 mg, 2.9 mmol, 3.0 equiv) and $[Cu(OTf)]_2{\cdot}C_6H_6$ (6.1 mg, 12.0 µmol, 1.25 mol%) were added. Then, a solution of (2*R*,5*R*)-2,5-diphenylpyrrolidin-1-yl benzoate (330.0 mg, 960.9 µmol, 1.0 equiv) in THF (5.6 mL) was added and the vial was capped and taken out of the glovebox. The mixture was stirred at 66 °C for 24 h. Reaction was checked by TLC (cyclohexane/EtOAc, 30:1, Rf product: 0.4, yellow spot without stain).The mixture was filtered through silica gel, eluting with CH_2Cl_2/Et_2O (1:1, then 100% Et_2O). The crude product was purified by SiO_2 column chromatography using Combiflash (cyclohexane 100%) to obtain (2*R*,5*R*)-1-(10-bromoanthracen-9-yl)-2,5-diphenylpyrrolidine (184.0 mg, 384.6 mmol, 40% yield) as a yellow solid.

^{1}H NMR (400 MHz, $CDCl_3$) δ 8.36 (ddd, *J* = 8.8, 1.4, 0.7 Hz, 2H), 8.19 (d, *J* = 8.4 Hz, 2H), 7.42 (ddd, *J* = 8.8, 6.5, 1.3 Hz, 2H), 7.36 (ddd, *J* = 8.7, 6.5, 1.3 Hz, 2H), 7.11 – 7.05 (m, 4H), 6.94 – 6.89 (m, 6H), 5.55 – 5.50 (m, 2H), 2.98 – 2.85 (m, 2H), 2.64 – 2.49 (m, 2H). **^{13}C{^{1}H} NMR** (101 MHz, $CDCl_3$) δ 142.7, 139.0, 132.0, 130.9, 128.3, 128.0, 127.5, 127.1, 126.5, 126.0, 124.5, 119.7, 68.2, 34.9, 29.9. **HRMS** (ESI+) calculated for $[C_{30}H_{24}BrNNa]^+$ 500.0984 *m/z*; found $[M + Na]^+$ 500.0989 *m/z*. **M.p. =** >55°C (decomposition). $\boldsymbol{\alpha_D^{589}}$ = – 308.0 deg.cm^2.g^{-1}(CH_2Cl_2, c 0.1, 300 K).

2-(10-((2*R*,5*R*)-2,5-Diphenylpyrrolidin-1-yl)anthracen-9-yl)phenol (34)

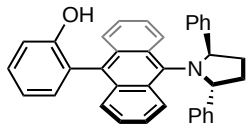

A MW vial equipped with a stirring bar was charged with (2*R*,5*R*)-1-(10-bromoanthracen-9-yl)-2,5-diphenylpyrrolidine (165.0 mg, 344.9 µmol, 1.0 equiv), potassium carbonate (143.0 mg, 1.0 mmol, 3.0 equiv), $Pd(PPh_3)_2Cl_2$ (15.2 mg, 34.5 µmol, 10 mol%) and (2-hydroxyphenyl)boronic acid (71.4 mg, 517.3 µmol, 1.5 equiv). Reagents were dissolved in a 6:1 mixture of dioxane/water (1.5:0.3 mL). Solution was degassed with argon during 15 minutes and sealed. Reaction was submitted to MW irradiation for 3 h at 110 ºC. Reaction completion was confirmed by TLC (cyclohexane/EtOAc, 98:2). Once finished, mixture was diluted with EtOAc, aqueous phase was extracted with EtOAc (3x) and resulting organic fractions were collected together and washed with water and brine. Organic fraction was dried over Na_2SO_4, filtered

29 Mailig, M.; Rucker, R. P.; Lalic G. *Chem. Commun.*, **2015**, *51*, 11048–11051.

and concentrated. Crude was purified by SiO_2 column chromatography using Combiflash (100% cyclohexane to 75:25 % cyclohexane/CH_2Cl_2). 2-(10-((2*R*,5*R*)-2,5-diphenylpyrrolidin-1-yl)anthracen-9-yl)phenol (134.5 mg, 273.6 mmol, 79% yield) was obtained as a yellow solid.

^{1}H NMR (400 MHz, $CDCl_3$) δ 8.36 (d, *J* = 8.9 Hz, 1H), 8.29 (d, *J* = 8.9 Hz, 1H), 7.45 (d *J* = 8.8, Hz, 2H), 7.42 – 7.34 (m, 3H), 7.25 (t, *J* = 1.4 Hz, 1H), 7.24 – 7.22 (m, 1H), 7.22 – 7.19 (m, 2H), 7.13 – 7.09 (m, 3H), 7.08 – 7.02 (m, 2H), 7.01 – 6.94 (m, 3H), 6.93 – 6.88 (m, 3H), 5.67 (t, *J* = 6.4 Hz, 1H), 5.60 (t, *J* = 6.6 Hz, 1H), 4.30 (s, 1H), 2.99 – 2.87 (m, 2H), 2.65 – 2.51 (m, 2H). **^{13}C{^{1}H} NMR** (101 MHz, $CDCl_3$) δ 154.0, 143.2, 143.0, 139.9, 132.4, 131.5 (d, *J* = 7.2 Hz), 131.0 (d, *J* = 8.3 Hz), 129.7, 128.1, 127.9, 127.5 (d, *J* = 8.8 Hz), 127.1 (d, *J* = 4.2 Hz), 126.6 (d, *J* = 3.4 Hz), 126.5, 126.0, 125.9, 125.6 (d, *J* = 7.9 Hz), 124.6, 124.4 (d, *J* = 4.2 Hz), 120.5, 115.6, 68.4 (d, *J* = 10.1 Hz), 35.2 (d, *J* = 5.9 Hz). **HRMS** (ESI+) calculated for $[C_{36}H_{30}NO]^+$ 492.2322 *m/z*; found $[M + H]^+$ 492.2320 *m/z*. **M.p. =** 160–161 ºC (cyclohexane). $\boldsymbol{\alpha_D^{589}}$ = – 435.8 deg.cm^2.g^{-1} (CH_2Cl_2, c 0.1, 301 K).

2-(10-((2*S*,5*S*)-2,5-Diphenylpyrrolidin-1-yl)anthracen-9-yl)phenyl trifluoromethanesulfonate (35)

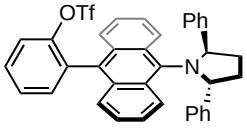

Microwave vial equipped with a stirring bar was charged with 1,1,1-trifluoro-N-phenyl-N-((trifluoromethyl)sulfonyl)methanesulfonamide (54.4 mg, 152.0 µmol, 1.1 equiv) and 2-(10-((2*R*,5*R*)-2,5-diphenylpyrrolidin-1-yl)anthracen-9-yl)phenol (68.0 mg, 138.0 µmol, 1.0 equiv). Mixture was dissolved in dry 1,4-dioxane (1.60 mL, 0.09 molar), and K_2CO_3 (68.8 mg, 498 µmol, 3.6 equiv) was added. Reaction was stirred at 120 ºC for 14 h and followed by LC-MS. When no starting material was detected, reaction was quenched with water and ethyl acetate. The aqueous phase was extracted with ethyl acetate (3x), the organic fractions were combined, washed with water and brine, dried over Na_2SO_4 and concentrated. Crude was purified by SiO_2 column chromatography (Pentane/Et_2O, 20:1 to 5:1) and 2-(10-((2*S*,5*S*)-2,5-diphenylpyrrolidin-1-yl)anthracen-9-yl)phenyl trifluoromethanesulfonate (59.0 mg, 94.6 µmol, 68% yield) was obtained as a yellow solid .

^{1}H NMR (500 MHz, $CDCl_3$) δ 8.33 (d, *J* = 8.9, 1H), 8.12 (d, *J* = 8.9, 1H), 7.56 (td, *J* = 7.7, 1.8 Hz, 1H), 7.51 – 7.46 (m, 2H), 7.42 – 7.35 (m, 2H), 7.33 (dt, *J* 8.8, 0.9, 1H), 7.31 – 7.27 (m, 2H), 7.25 – 7.17 (m, 4H), 7.09 – 7.04 (m, 2H), 7.00 – 6.93 (m, 3H), 6.92 – 6.88 (m, 3H), 5.61 (t, *J* = 6.4 Hz, 1H), 5.56 (t, *J* = 6.3 Hz, 1H), 2.99 – 2.89 (m, 2H), 2.66 – 2.50 (m, 2H). **^{13}C{^{1}H} NMR** (126 MHz, $CDCl_3$) 148.3, 143.5, 142.4, 139.8, 134.8, 132.7, 131.0 (d, *J* = 8.1 Hz), 130.8, 130.7, 129.7, 128.2, 128.0, 127.9, 127.5 (d, *J* = 9.9 Hz), 126.9 (d, *J* = 9.2 Hz), 126.6, 126.5, 126.4, 125.8, 125.7, 125.2 (d, *J* = 11.2 Hz), 124.2, 124.0, 122.1, 119.0, 116.4, 68.3, 68.0, 35.6, 34.2. **^{19}F{^{1}H} NMR** (471 MHz, $CDCl_3$) δ –75.0. **HRMS** (ESI+) calculated for $[C_{37}H_{29}F_3NO_3S]^+$ 624.1815 *m/z*; found $[M + H]^+$ 624.1823 *m/z*. **M.p. =** >186 ºC (decomposition). $\boldsymbol{\alpha_D^{589}}$ = –361.0 deg.cm^2.g^{-1} ($CHCl_3$, c 0.1, 301 K).

Ligand D (36)

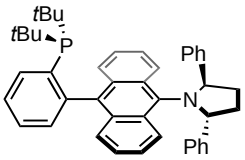

A microwave vial equipped with a stirring bar was charged with 2-(10-((2*R*,5*R*)-2,5-diphenylpyrrolidin-1-yl)anthracen-9-yl)phenyltrifluoromethane sulfonate (52.4 mg, 84.0 µmol, 1 equiv), potassium phosphate dibasic (16.1 mg, 92.4 µmol, 1.1 equiv), cyclopentyl(diisopropyl)phosphane iron (4.2 mg, 10.1 µmol, 12 mol%) and diacetoxypalladium (1.9 mg, 8.4 µmol, 10 mol%). The mixture was evacuated and fulfilled with argon (3x) and 1,4-dioxane (7.4 mg, 840.0 µL, 0.1 molar) was added. The solution was stirred during 5 minutes and di-*tert*-butylphosphane (18.4 mg, 23.0 µL, 126.0 µmol, 1.5 equiv) was added. Reaction was heated in the microwave at 150 ºC for 4 h, after which a second addition of potassium phosphate dibasic (16.1 mg, 92.4 µmol, 1.1 equiv), diacetoxypalladium (1.9 mg, 8.4 µmol, 10 mol%), cyclopentyl(diisopropyl)phosphane iron (4.2 mg, 10.1 µmol, 12 mol%) and di-*tert*-butylphosphane (18.4 mg, 23.0 µL, 126.0 µmol, 1.5 equiv) was done. Reaction was heated again under microwave irradiation for 4 more hours at 150 ºC and followed by LC-MS. When no more conversion was observed, the reaction was cooled down, diluted with dichloromethane, filtered through celite and washed with ethyl acetate. The crude was concentrated and purified by combiflash SiO_2 column chromatography (2.5% EtOAc, 97.5% cyclohexane). Ligand **D** (22.0 mg, 35 µmol, 42% yield) was obtained as a sticky yellow solid. The phosphine shown to be unstable under air and decomposes over time.

^{1}H NMR (500 MHz, CD_2Cl_2) δ 8.35 (dt, *J* = 8.8, 1.1 Hz, 1H), 8.13 (d, *J* = 8.9 Hz, 1H), 7.96 – 7.92(m, 1H), 7.50 – 7.42 (m, 2H), 7.38 – 7.27 (m, 6H), 7.21 (ddd, *J* = 9.0, 6.4, 1.3 Hz, 1H), 7.13 (ddd, *J* = 8.7, 6.4, 1.2 Hz, 1H), 7.07 – 6.97 (m, 6H), 6.95 – 6.76 (m, 3H), 5.68 (t, *J* = 6.5 Hz, 1H), 5.50 (t, *J* = 6.3 Hz, 1H), 2.98 – 2.83 (m, 2H), 2.67 – 2.46 (m, 2H), 0.85 (dd, *J* = 11.3, 8.6 Hz, 18H). **^{13}C{^{1}H} NMR** (126 MHz, CD_2Cl_2) δ 148.0, 147.7, 144.1, 143.0, 140.3, 140.0, 138.0, 136.6 (d, *J* = 2.6 Hz), δ 135.9 (d, *J* = 6.6 Hz), 132.7 (d, *J* = 6.3 Hz), 131.6 (d, *J* = 2.5 Hz), 131.4 (d, *J* = 2.5 Hz), 131.2, 130.4, 129.4, 129.2, 128.6, 128.2, 128.0, 127.9, 127.9, 127.2, 127.0, 126.6, 125.9, 125.5, 124.2, 123.9, 123.7, 123.7, 68.6, 68.1, 36.4, 34.1, 32.4 (d, *J* = 3.6 Hz), 32.2 (d, *J* = 3.4 Hz), 31.1 (dd, *J* = 15.9, 7.7 Hz). **^{31}P{H} NMR** (206 MHz, CD_2Cl_2) δ 24.2. **HRMS** (ESI+) calculated for $[C_{44}H_{47}NP]^+$ 620.3441 *m/z*; found $[M + H]^+$ 620.3442 *m/z*. $\boldsymbol{\alpha_D^{589}}$ = –295.0 deg.cm^2.g^{-1} (CH_2Cl_2, c 0.09, 301 K).

Complex (*R*,*R*)-D

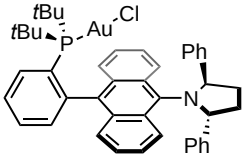

Dimethylsulfide gold(I) chloride (11.4 mg, 38.7 µmol, 1.0 equiv) and (2*R*,5*R*)-1-(10(2-(di-*tert*-butylphosphaneyl)phenyl)anthracen-9-yl)-2,5-diphenyl pyrrolidine (24.0 mg, 38.7 µmol, 1.0 equiv) were dissolved in dry CH_2Cl_2 (0.4 mL, 0.1 M) under argon atmosphere. The reaction mixture was stirred at 24 ºC for 30 min. The mixture was filtered through a syringe filter and concentrated. The residue was purified

by SiO_2 column chromatography combiflash (100% cyclohexane to 80% cyclohexane, 20% EtOAc). Complex (*R*,*R*)-**D**, (16.0 mg, 38.7 mmol, 46% yield) was obtained as a yellow solid.

^{1}H NMR (500 MHz, C_6D_6) δ 8.90 (d, *J* = 8.8 Hz, 1H), 7.83 (dt, *J* = 8.2, 1.6 Hz, 2H), 7.68 (d, *J* = 8.9 Hz, 1H), 7.65 – 7.55 (m, 2H), 7.44 (d, *J* = 8.6 Hz, 1H), 7.35 – 7.29 (m, 1H), 7.25 – 7.16(m, 4H), 7.10 (td, *J* = 7.2, 1.2 Hz, 1H), 7.02– 6.95 (m, 3H), 6.93 (d br., *J* = 8.8 Hz, 1H), 6.89– 6.82 (m, 1H), 6.70 (dd, *J* = 8.2, 7.0 Hz, 2H), 6.63 – 6.55(m, 2H), 6.12 – 6.08 (m, 1H), 5.44 (dd, *J* = 7.7, 5.9 Hz, 1H), 2.94 – 2.78 (m, 2H), 2.46 – 2.36 (m, 2H), 1.08 (d, *J* = 15.1 Hz, 9H), 0.81 (d, *J* = 15.4 Hz, 9H). **^{13}C{^{1}H} NMR** (126 MHz, C_6D_6) δ 148.0 (d, *J* = 13.3 Hz), 143.9, 143.3, 140.9, 136.0 (d, *J* = 7.9 Hz), 134.4 (d, *J* = 2.7 Hz), 133.3, 132.6, 132.4 (d, *J* = 5.4 Hz), 132.2, 131.7, 130.8 (d, *J* = 2.6 Hz), 129.9, 129.5, 129.0, 127.5, 127.5, 127.3, 127.2, 127.0, 126.7, 126.5 (d, *J* = 6.6 Hz), 125.6, 125.5, 124.2, 123.0, 68.7, 65.9, 38.6, 38.4, 36.8, 36.6, 31.6 (d, *J* = 6.7 Hz), 30.4, 30.4 (d, *J* = 6.8 Hz). **^{31}P{H} NMR** (206 MHz, C_6D_6) δ 62.7. **HRMS** (ESI+) calculated for $[C_{44}H_{46}AuClNNaP]^+$ 874.2614 *m/z*; found $[M + Na]^+$ 874.2587 *m/z*. **M.p.** = >98 ºC (decomposition). $\boldsymbol{\alpha_D^{589}}$ = –165.6 deg.cm^2.g^{-1} (CH_2Cl_2, c 0.1, 301 K).

Reactions tested with (*R*,*R*)-C and (*R*,*R*)-D complexes

Formal [4+2] cycloaddition of 1,6-arylenyne 37

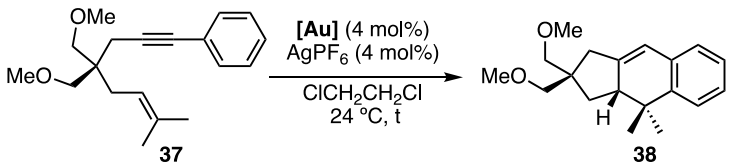

37 **38**

The procedure for this reaction was previously optimized in the group.[15] 1,6-Enyne **37** (1.0 equiv) and (*R*,*R*)-gold(I) catalyst (4 mol%) were dissolved in dry 1,2-dichloroethane and a solution of $AgPF_6$ (4 mol%) in 1,2-dichloroethane (total concentration 0.05M) was added dropwise. The reaction was stirred for the given time at 24 ºC in the dark, quenched by addition of 3 drops of NEt_3 and concentrated. Yield was determined by ^{1}H NMR using Ph_2CH_2 as internal standard.

Enantioselective formation of 1,2-dihydronaphthalene 40

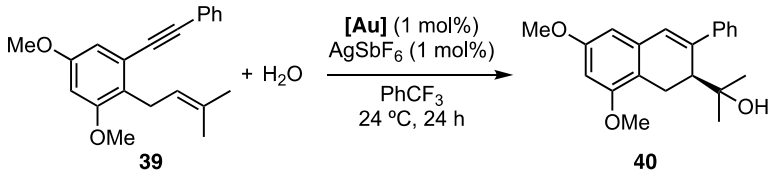

39 **40**

The procedure for this reaction was previously optimized in the group.[15] 1,6-Enyne **39** (1.0 equiv) and H_2O (5.0 equiv) were dissolved in dry α,α,α-trifluorotoluene (0.2 M). This solution was added to a vial containing (*R*,*R*)-gold(I) catalyst (1 mol%) and $AgSbF_6$ (1 mol%) and the reaction was stirred for 24 h at 24 ºC. The reaction was quenched by addition of 1 drop of NEt_3 and concentrated. The crude was purified by SiO_2 flash column chromatography (pentane/CH_2Cl_2 2:1, pentane/Et_2O 1:1).

Enantioselective synthesis of azabicyclo[4.1.0]hept-4-ene 42

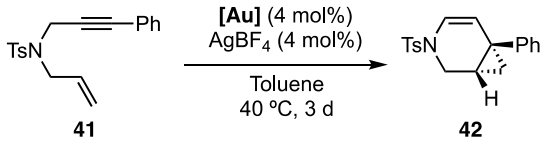

The procedure for this reaction was previously optimized in the group.[15] 1,6-Enyne **41** (1.0 equiv) and (*R*,*R*)-gold(I) catalyst (4 mol%) were dissolved in dry toluene. A solution of AgBF4 (4 mol%) in toluene (total concentration 0.05M) was added dropwise and the reaction was stirred for 3 days at 40 ºC in the dark. The reaction was quenched by addition of 3 drops of NEt_3 and concentrated. The crude was purified by SiO_2 flash column chromatography (toluene/CH_2Cl_2 1:1) to afford azabicyclo[4.1.0]hept-4-ene **42**.

Atroposelective synthesis of biaryl 44

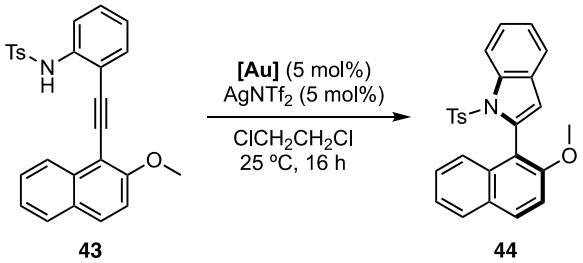

Ts-protected aniline **43** (1.0 equiv) and (*R*,*R*)-gold(I) catalyst (5 mol%) were dissolved in 1,2-dichloroethane. A solution of $AgNTf_2$ (5 mol%) in 1,2-dichloroethane (total concentration 0.05 M) was added dropwise and the reaction was stirred at 25 ºC for 16 h. The reaction was quenched by addition of 3 drops of NEt_3 and concentrated. Yield was determined by ^1H NMR using Ph_2CH_2 as internal standard.

Gold(I) retro Büchner reaction of cycloheptatriene 45

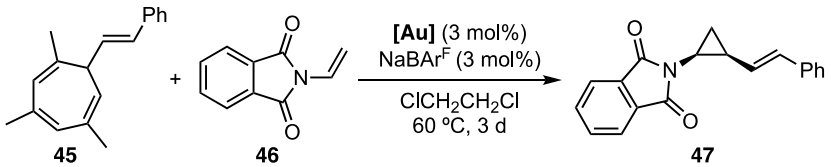

(*E*)-1,3,5-trimethyl-7-styrylcyclohepta-1,3,5-triene **44** (1.0 equiv), N-vinylphtalimide **46** (1.5 equiv) and (*R*,*R*)-gold(I) catalyst (3 mol%) were dissolved in dry 1,2-dichloroethane. Sodiumtetrakis[3,5-bis(trifluoromethyl)phenyl]borate (3 mol%) dissolved in 1,2-dichloroethane was added (total concentration 0.2 M), and the reaction was stirred at 60 ºC for 3 days. The crude was purified by flash SiO_2 column chromatography (pentane/Et_2O 8:2 to 7:3).

Crystallographic Data

Complex (*R*,*R*)-D

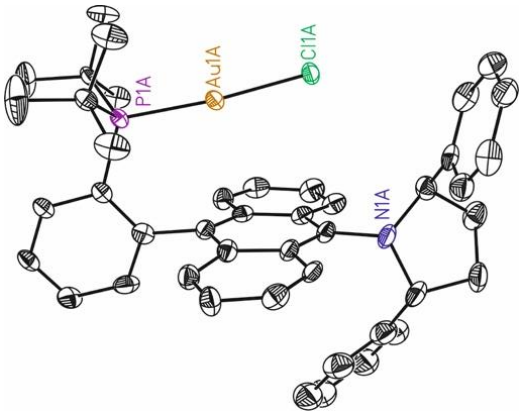

Table 8. Crystal data and structure refinement for Complex (R,R)-**D**.

Identification code	cu_AHP04305-b_0m	
Empirical formula	C143 H163 Au3 Cl5 N3 P3	
Formula weight	2784.81	
Temperature	100(2)K	
Wavelength	1.54178 Å	
Crystal system	orthorhombic	
Space group	P 21 21 21	
Unit cell dimensions	a = 14.3179(5)Å	a= 90°.
	b = 15.2523(6)Å	b = 90°.
	c = 56.637(2)Å	g = 90°.
Volume	12368.4(8) $Å^3$	
Z	4	
Density (calculated)	1.496 Mg/m^3	
Absorption coefficient	8.312 mm^{-1}	
F(000)	5636	
Crystal size	0.400 x 0.150 x 0.010 mm^3	
Theta range for data collection	3.000 to 68.302°.	
Index ranges	-16<=h<=15,-16<=k<=18,-64<=l<=68	

Reflections collected	123397
Independent reflections	21945[R(int) = 0.0540]
Completeness to theta =68.302°	98.2%
Absorption correction	Multi-scan
Max. and min. transmission	0.74 and 0.49
Refinement method	Full-matrix least-squares on F^2
Data / restraints / parameters	21945/ 1370/ 1722
Goodness-of-fit on F^2	1.017
Final R indices [I>2sigma(I)]	R1 = 0.0360, wR2 = 0.0829
R indices (all data)	R1 = 0.0410, wR2 = 0.0850
Flack parameter	x =-0.014(3)
Largest diff. peak and hole	0.804 and -1.349 e.$Å^{-3}$

Chapter II

Chapter III: *On the Nature of Gold(I) Vinylidenes*

Chapter III

Introduction

Vinylidenes

Vinylidenes or alkenylidenes are reactive intermediates where the carbenic carbon (C1) is attached to an unsaturated carbon (C2) through a π-bond.[1] They exist in a singlet state, with the electron pair occupying an *sp*-hybridized non-bonding orbital (HOMO) perpendicular to an empty *p* orbital (LUMO). As it was done in chapter I with the description of carbenes, to facilitate the reading of this section, the terminology C1 and C2 abovementioned will be used to refer to the two main carbons in the vinylidene structures.

Due to their high reactivity, free vinylidenes need to be generated *in situ* when used in organic reactions, being their tautomerization to the corresponding alkyne their preferred transformation.[2] This 1,2-migration is specially favored when the substituents of the alkene are hydrogens or aromatic rings and can be slowed down stabilizing the vinylidenes by adding alkyl substituents in the alkene[3] or using metal vinylidenes instead.[4] The increase of stability of the vinylidene structure allows its participation in the insertion to C–H,[5] O–H[6] and N–H[7] bonds or its addition to π-bonds (Figure 1).[8]

The most typical strategies to access free vinylidenes are the thermolysis of diazoalkenes[9], and the 1,1-elimination of 1-metallo-1-halo-alkenes,[10] although other methods have been developed.[11] In the last strategy mentioned, although vinylidenes have been historically represented as free vinylidenes, the

1 Taber, D. F.; Meagley, R. P.; Doren, D. J. *J. Org. Chem.* **1996**, *61*, 5723–5728.

2 Habrant, D.; Rauhala, V.; Koskinen, A. M. P. *Chem. Soc. Rev.* **2010**, *39*, 2007−2017.

3 (a)Stang, P. J.; Mangum, M. G.; Fox, D. P.; Haak, P. *J.Am.Chem Soc.* **1974**, *96*, 4562−4569.(b) Colvin, E. W.; Hamill, B. J. *J. Chem. Soc., Perkin Trans. 1* **1977**, 869−874. (c) Gilbert, J. C.; Weerasooriya, *J. Org. Chem.* **1982**, *47*, 1837−1845.

4 Roh, S. W.; Choi, K.; Lee, C. *Chem. Rev.* **2019**, *119*, 4293–4356.

5 (a) Karpf, M.; Dreiding, A. S. Thermische *Helv. Chim. Acta* **1979**, *62*, 852− 865. (b) Gilbert, J. C.; Giamalva, D. H.; Baze, M. E. *J. Org. Chem.* **1985**, *50*, 2557–2563. (c) Wardrop, D. J.; Zhang, W. M. *Tetrahedron Lett.* **2002**, *43*, 5389–5391.

6 Miwa, K.; Aoyama, T.; Shioiri, T. *Synlett* **1994**, 461–462.

7 Yagi, T.; Aoyama, T.; Shioiri, T. *Synlett* **1997**, 1063–1064.

8 (a) Ogawa, H.; Aoyama, T.; Shioiri, T. *Synlett* **1994**, 757–758. (b) Feldman, K. S.; Bruendl, M. M.; Schildknegt, K.; Bohnstedt, A. C. *J. Org. Chem.* **1996**, *61*, 5440–5452; (c) Hari, Y.; Tanaka, S.; Takuma, Y.; Aoyama, T. *Synlett* **2003**, 2151–2154.

9 Boutagy, J.; Thomas, R. *Chem. Rev.* **1974**, *74*, 87–99. (b) Ohira, S.; Okai, K.; Moritani, T. J. *Chem. Soc., Chem. Commun.* **1992**, 721–722.

10 (a) Kirmse, W. *Angew. Chem., Int. Ed. Engl.* **1965**, 4, 1–10. (b) Braun, M. *Angew. Chem., Int. Ed.* **1998**, *37*, 430−451. (c) Satoh, T. *Chem. Soc. Rev.* **2007**, *36*, 1561–1572. (d) Satoh, T. *Heterocycles* **2012**, *85*, 1–33.

11 Grainger, R.S.; Munro K.R. *Tetrahedron* **2015**, *71*, 7795–7835.

complete dissociation of the metal salt from the vinylidene is not confirmed, hence, the contribution of the metal to the vinylidene stability remains unclear.[11] Studies on the reactivity of 1-metallo-1-halo-alkenes proved the same reactivity of free vinylidenes, undergoing 1,2-migration and insertion reactions.[10b,12] Even more, DFT studies of the structure of these precursors have confirmed their partial vinylidene character.[13] Moreover, metal vinylidenes have been extensively studied in the last years, proven to significantly stabilize the vinylidene structure.[4] This could support the participation of metal vinylidenes instead of free vinylidenes in the cases in which 1-metallo-1-halo-alkenes are used as the vinylidenes source.

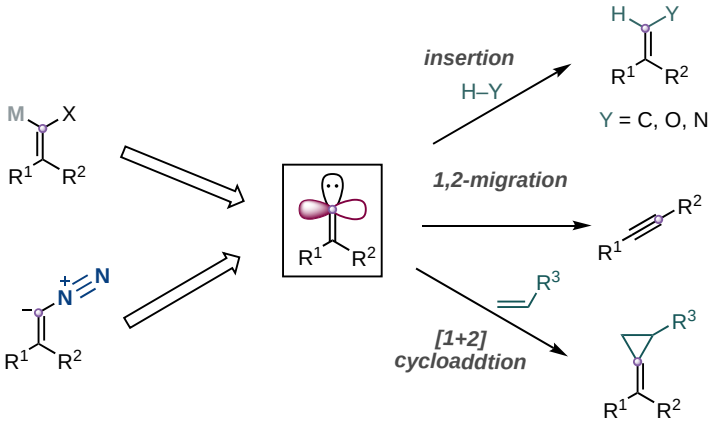

Figure 1. Structure, generation and reactivity of vinylidenes.

Transition Metal Vinylidenes

Contrary to the difficult access to free vinylidenes, transition metal vinylidenes can be easily generated from their corresponding η^2-alkynes.[14] This generation strategy is possible because transition metal vinylidenes usually are more stable than their corresponding metal η^2-alkyne tautomers. Therefore, computational studies show how the simplest vinylidene is 44 kcal/mol less stable than its acetylene tautomer, with a minimum energy barrier for the interconversion from the vinylidene (Figure 2a).[15] In contrast, the study of the alkyne/vinylidene interconversion of $RuCl_2(PH_3)_2(\eta^2\text{-}HC{\equiv}CH)$ to $RuCl_2(PH_3)_2(=C=CH_2)$ discloses a 19 kcal/mol higher stability of the Ru vinylidene over the coordinated alkyne (Figure 2b).[16]

12 Knorr, R. *Chem. Rev.* **2004**, *104*, 3795–3849.

13 (a) Kimura, T.; Satoh, T. *J. Organomet. Chem.* **2012**, *715*, 1–4. (b) Kimura, T.; Satoh, T. *Tetrahedron* **2013**, *69*, 6371–6374.

14 Wakatsuki, Y. *J. Organomet. Chem.* **2004**, *689*, 4092−4109.

15 Gallo, M. M.; Hamilton, T. P.; Schaefer, H. F., *J. Am. Chem. Soc.* **1990**, *112*, 8714−8719.

16 Wakatsuki, Y.; Koga, N.; Yamazaki, H.; Morokuma, K. *J. Am. Chem. Soc.* **1994**, *116*, 8105−8111.

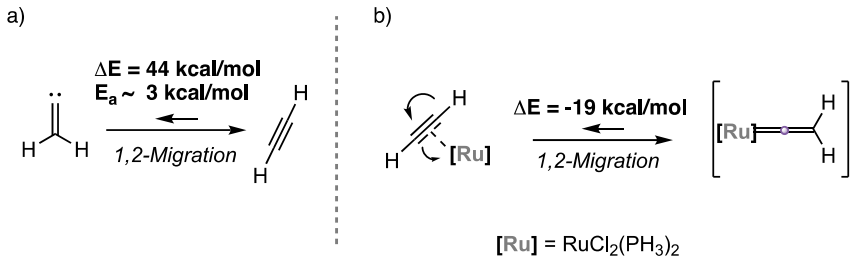

Figure 2. Favored stability in the vinylidene–alkyne tautomerization in free and ruthenium vinylidenes.

Other examples of Ru vinylidenes, bearing different ligands and alkene substituents have given similar results,[17] supporting the higher stability of metal vinylidenes. The same situation has been observed in other transition metals such as Mn,[18] W,[19] and the d^7-group metals,[20] among others.[21] This has allowed the development of a wide scope of isolated transition metal vinylidenes which structural features and reactivity have been extensively studied.[4, 22]

The coordination of transition metals to the vinylidene body usually stabilizes these intermediate species, preventing 1,2-migration. However, it also results in a modification of the electronic properties of the vinylidene, derived from the two π-systems between the C–C and the C–M double bonds. According to the molecular orbital model for d^8-metal vinylidene complexes proposed by Fenske in 1982, 25% of the HOMO is localized in C2, while 60% of the π antibonding orbital (LUMO) is localized on C1. This would account an electrophilic character of C1 and a nucleophilic character of C2, broadening the reactivity of metal vinylidenes to free vinylidenes. Thus, nucleophilic addition to the C1 of metal vinylidenes has been observed in different systems. Examples of this reactivity has been shown in the addition of water to $[CpRu(PPh_3)_2(=C=CHPh)]PF_6$ **1**, which through the acyl ruthenium intermediate **2** leads to the formation of ruthenium carbonyl **3** (Scheme 1a),[23] or the addition of an

17 (a) De Angelis, F.; Sgamellotti, A.; Re, N. *Organometallics* **2002**, *21*, 5944–5950. (b) De Angelis, F.; Sgamellotti, A.; Re, N. *Dalton Trans* **2004**, 3225−3230.

18 Silvestre, J.; Hoffmann, R. *Helv. Chim. Acta* **1985**, *68*, 1461−1506.

19 (a) Birdwhistell, K. R.; Nieter Burmayer, S. J.; Templeton, J. L. *J. Am. Chem. Soc.* **1983**,*105*, 7789–7790. (b) Birdwhistell, K. R.; Tonker, T. L.; Templeton, J. L. *J. Am. Chem. Soc.* **1987**,*109*, 1401–1407.

20 (a)Wolf, J.; Werner, H.; Serhadli, O.; Ziegler, M. L. *Angew. Chem., Int. Ed. Engl.* **1983**, *22*, 414−416. (b) Wakatsuki, Y.; Koga, N.; Werner, H.; Morokuma, K. *J. Am. Chem. Soc.* **1997**, *119*, 360−366. (c) Höhn, A.; Otto, H.; Dziallas, M.; Werner, H. *J. Chem. Soc., Chem. Commun.* **1987**, 852−854. (d) Bianchini, C.; Peruzzini, M.; Vacca, A.; Zanobini, F. *Organometallics* **1991**, *10*, 3697−3707.

21 Bruce, M.I. *Chem. Rev.* **1991**, *91*, 197-257.

22 For a review on this topic: (a) Bruce, M. I.; Swincer, A. G. *Adv. Organomet. Chem.* **1983**, *22*, 59−128. (b) Werner, H. *Coord. Chem. Rev.* **2004**, *248*, 1693−1702. (c) Bruneau, C.; Dixneuf, P. H. *Acc. Chem. Res.* **1999**, *32*, 311−323. (d) Trost, B. M.; McClory, A. *Chem. Asian J.* **2008**, *3*, 164−194.

23 Bruce, M. I.; Swincer, A. G.; Wallis, R. C. *J. Organomet. Chem.* **1979**, *171*, C5−C8.

allylic alcohol to iron vinylidene **4** to form its Fischer carbene **5**, which can undergo further reactions (Scheme 1b).[24]

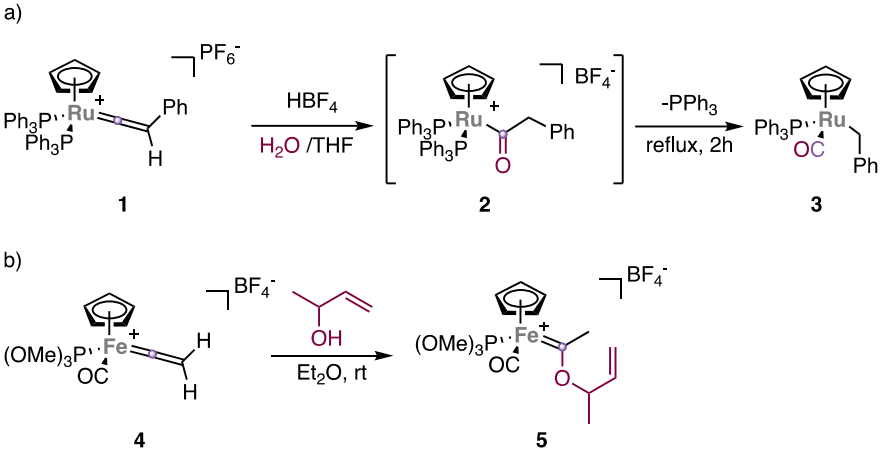

Scheme 1. Examples of nucleophilic addition reactivity in transition metal vinylidenes.

In parallel, the nucleophilic character of C2 has allowed the synthesis of ruthenium carbynes **7** through electrophilic addition of H to ruthenium vinylidenes **6** (Scheme 2).[25]

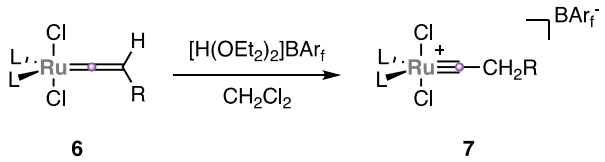

Scheme 2. Electrophilic addition of H^+ to C2 in Ru vinylidenes to form Ru carbynes.

Additionally, the electronic perturbation of the metal coordination in transition metal vinylidenes allows their participation in [2+2] cycloadditions processes,[26] a type of reactivity not observed in free vinylidenes.

The simple access and the broad reactivity of transition metal vinylidenes has derived in a great expansion of the study of its chemistry, considering not only their stoichiometric transformations, but also their participation in catalytic processes.[4, 27]

24 Barrett, A. G. M.; Carpenter, N. E. *Organometallics* **1987**, *6*, 2249−2250.

25 González-Herrero, P.; Weberndörfer, B.; Ilg, K.; Wolf, J.; Werner, H. *Organometallics* **2001**, *20*, 3672–3685.

26 Alvarez, P.; Lastra, E.; Gimeno, J.; Bassetti, M.; Falvello, L. R. *J. Am. Chem. Soc.* **2003**, *125*, 2386−2387.

27 For a review on this topic: Trost, B. M.; McClory, A. *Chem. Asian J.* **2008**, *3*, 164–194.

Gold(I) Vinylidenes

Within the world of gold(I) carbenes, gold(I) vinylidenes are a specially intriguing type. Despite the extensive efforts made for the synthesis and characterization of gold(I) carbenes, discussed in chapter I, and the wide study of transition metal vinylidenes, the knowledge about gold(I) vinylidenes is quite limited. This lack of understanding is due to the difficult access to these intermediates. Contrary to many other transition metal vinylidenes, gold(I) vinylidenes cannot be generated from their η^2-alkyne tautomers, since, equally to free vinylidenes, the vinylidene-alkyne equilibrium in the presence of gold(I) is shifted to the gold(I) coordinated η^2-alkyne species. This can be ascribed to the high electrophilicity of gold(I), which causes a lower π-backdonation of gold(I) to the electron deficient C1, reducing the metal stabilization of the vinylidene tautomer (Figure 3).[28]

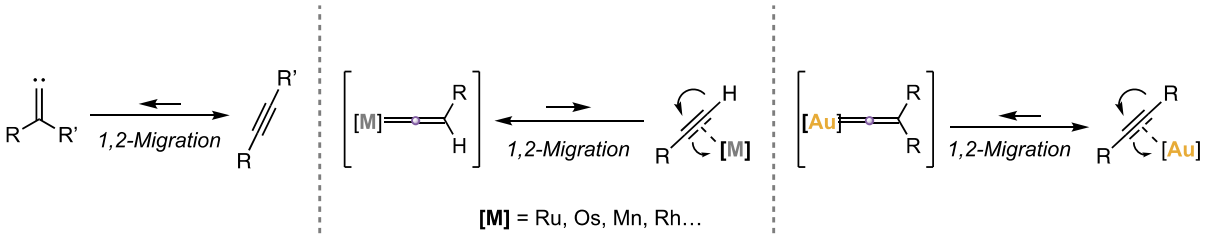

Figure 3. Tautomeric equilibrium of free, transition metal and gold(I) vinylidenes with η^2-alkynes.

Thus, although the popularity gold(I) of vinylidenes as intermediates in gold(I)-catalyzed reactions has increased in the last 10 years,[29] evidence of their existence is scarce.

The debut of gold(I) vinylidenes took place in 2004, when Fürstner proposed them as potential intermediates in the gold(I)-catalyzed polycyclization of *o*-alkynyl arenes.[30] The study of the synthesis of substituted phenanthrenes from the cyclization of *o*-alkynyl arenes **8** catalyzed by $InCl_3$ or AuCl, evidenced different results depending on the catalyst used (Scheme 3). While the use of $InCl_3$ resulted in the expected 10-halophenanthrene products **9**, the gold(I)-catalyzed reaction selectively caused an unexpected rearrangement of the halogen tethered to the alkyne leading to 9-halophenanthrenes **12**. To justify this outcome, gold(I) vinylidenes **10** were proposed as intermediates of the reaction, comparing these results to the ones previously obtained via ruthenium vinylidenes in which halide walk phenomena was observed.[31] The participation of gold(I) vinylidene as the main intermediate of this transformation was further supported via DFT studies by Soriano and Marco-Contelles.[32] Their studies proposed the

28 Pickup, O. J. S.; Khazal, I.; Smith, E. J.; Whitwood, A. C.; Lynam J. M. *Organometallics* **2014**, *33*, 1751−1761.

29 Praveen, C.; Dupeux, A.; Michelet, V. *Chemistry – A European Journal*. **2021**; 10495–10532.

30 Mamane, V.; Hannen, P.; Fürstner, A. *Chem. Eur. J.* **2004**, *10*, 4556–4575.

31 Shen, H.-C.; Pal, S.; Lian, J.-J.; Liu, R.-S. *J. Am. Chem. Soc.* **2003**, *125*, 15762 –15763.

32 Soriano, E.; Marco-Contelles, J. *Organometallics* **2006**, *25*, 4542–4553.

formation of gold(I) carbene **11** after trapping of gold(I) vinylidene **10** by the substituted aryl, followed by protodeauration and release of the observed product **12**.

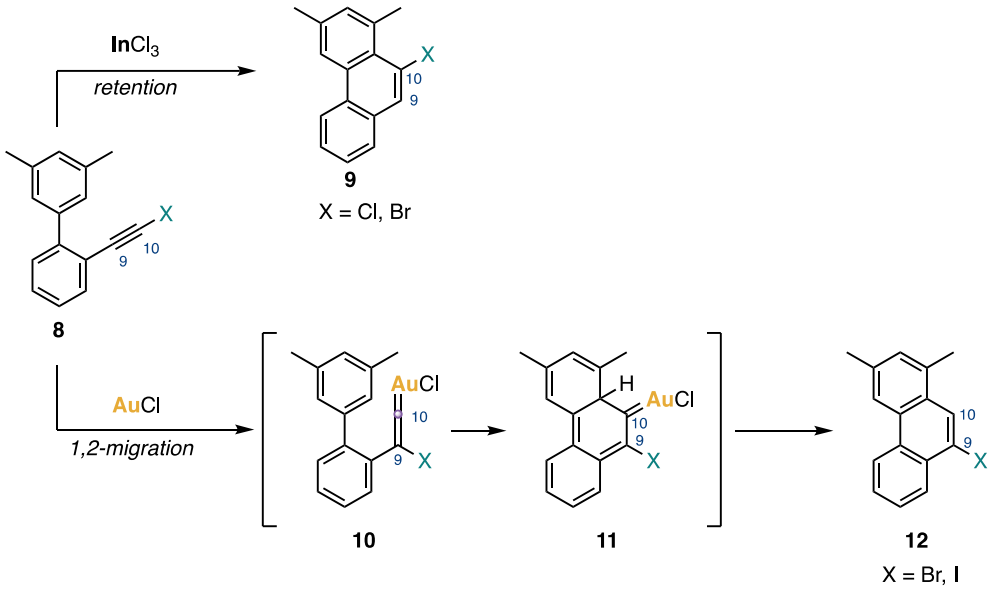

Scheme 3. First proposal of gold(I) vinylidenes as intermediates of an organic reaction.

The application of this strategy for the selective synthesis of dehydroiodoquinolines and 3-iodo-2H-chromenes showed a high influence of the substrate and of the structure of the gold(I) complex in the reaction outcome.[33,34] Hence, the product formed after 1,2-iodine migration is favored when electron-donating NHC ligands are tethered to gold, which stabilize the vinylidene intermediates. Parallelly, the use of electron-withdrawing aryl substituents also favors the formation of the vinylidene intermediate, preventing the direct cyclization.

The regioselectivity provided by the formation of gold(I) vinylidenes after activation of halogen substituted alkynes was also applied in the selective synthesis of iodoindenes[35] and in the formation of 1,3-diiodonaphathalenes from 1,2-bis(iodoethyl)arenes.[36] Going a step further, 1,2-silylmigration was also postulated as a possible reaction of gold(I) vinylidenes, upon activation of silylalkynes.[37] More

33 Morán-Poladura, P.; Suárez-Pantiga, S.; Piedrafita, M.; Rubio, E.; González, J. M. J. *Organomet. Chem.* **2011**, *696*, 12–15.

34 Morán-Poladura, P.; Rubio, E.; González, J. M. *Beilstein J. Org. Chem.* **2013**, *9*, 2120–2128.

35 Morán-Poladura, P.; Rubio, E.; González, J. M. *Angew. Chem. Int. Ed.* **2015**, *54*, 3052–3055.

36 Nösel, P.; Müller, V.; Mader, S.; Moghimi, S.; Rudolph, M.; Braun, I.; Rominger, F.; Hashmi, A. S. K. *Adv. Synth. Catal*. **2015**, *357*, 500–506.

37 (a) Seregin, I. V.; Gevorgyan, V. *J. Am. Chem. Soc.* **2006**, *128*, 12050–12051. (b) McGee, P.; Bellavance, G.; Korobkov, I.; Tarasewicz, A.; Barriault, L. *Chem. Eur. J.* **2015**, *21*, 9662–9665.

recently, González and co-workers also applied this strategy in the oxacyclization of iodoalkynes to form benzofurans.[38]

Despite the examples above mentioned, the research on gold(I) vinylidenes experimented a slow development until 2012, when Hashmi and Zhang independently reported effective C–H insertion via dual gold catalysis (Scheme 4).[39]

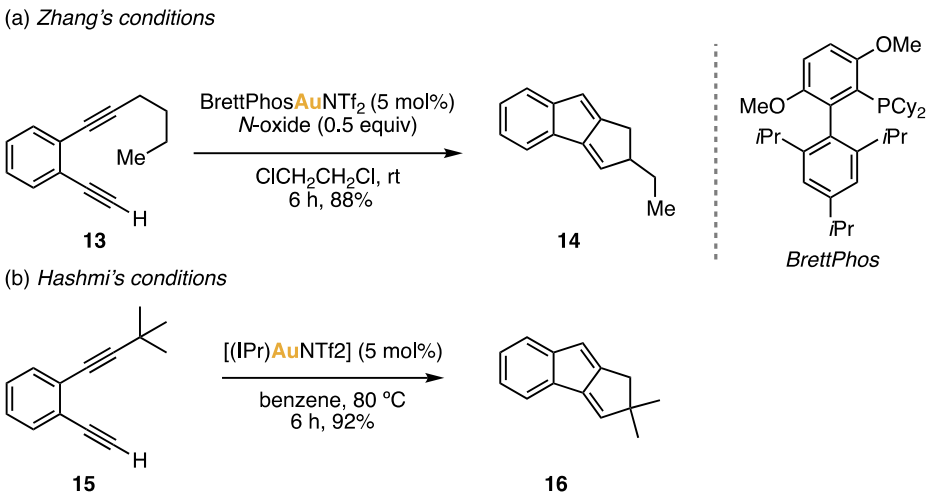

Scheme 4. Concurrent reports of dual gold catalyzed synthesis of tricyclic indenes.

The investigation of the mechanism of the cycloisomerization of (2-ethynylphenyl) alkynes to form tricyclic indenes revealed the key participation of gold(I) vinylidenes in an effective manner to perform C–H activation of unactivated alkyl groups (Scheme 5).

Both groups discovered that the reaction happens through a dual Gold(I) catalysis process in which the first gold(I) complex forms gold acetylide **I**, after removal of the H from the terminal alkyne **15** (with or without base assistance) while the second molecule of catalyst activates the other triple bond forming the η^2-alkyne gold complex **II**. At this point, dual σ–π activation takes place, forming the reactive gold(I) vinylidene **III** via 5-*endo*-dig cyclization. In the next step, the group of Zang suggested a concerted C–H insertion to directly form intermediate **V**, while Hashmi proposed a 1,5-hydride shift, prior to the second cyclization to form intermediate **V**. This intermediate **V** undergoes monodeauration, forming alkenyl gold(I) complex **VI**, which, in accordance with the mechanistic experiments, should be in equilibrium with *gem*-diaurated complex **VII**. The reaction finishes with the release of the indene

38 Fernández-Canelas, P.; Rubio, E.; González J.M. *Org. Lett.* **2019**, *21*, 6566–6569.

39 (a) Ye, L.; Wang, Y.; Aue, D. H.; Zhang, L. *J. Am. Chem. Soc.* **2012**, *134*, 31−34. (b)Hashmi, A. S. K.; Braun, I.; Rudolph, M.; Rominger, F. *Organometallics* **2012**, *31*, 644–661.(c) Hashmi, A. S. K.; Braun, I.; Nösel, P.; Schädlich, J.; Wieteck, M.; Rudolph, M.; Rominger, F. *Angew. Chem. Int. Ed.* **2012**, *51*, 4456−4460.

product **15** after the catalyst exchange to form a new molecule of gold acetylide **I**. Both proposals of the mechanism of the reaction were supported with control experiments which confirmed the formation of intermediates **VI** and **VII** during the reaction and the equilibrium between them. Additionally, Zhang's group performed DFT experiments which supported the proposed pathway as the most energetically favored.

Further experiments performed by Zhang and co-workers proved the applicability of this methodology to the insertion into O–H and N–H bonds. Additionally, Hashmi successfully demonstrated that this reactivity was not limited to terminal alkyne substrates, reporting the effective cycloisomerization of iodoalkynes into iodofulvenes.[40]

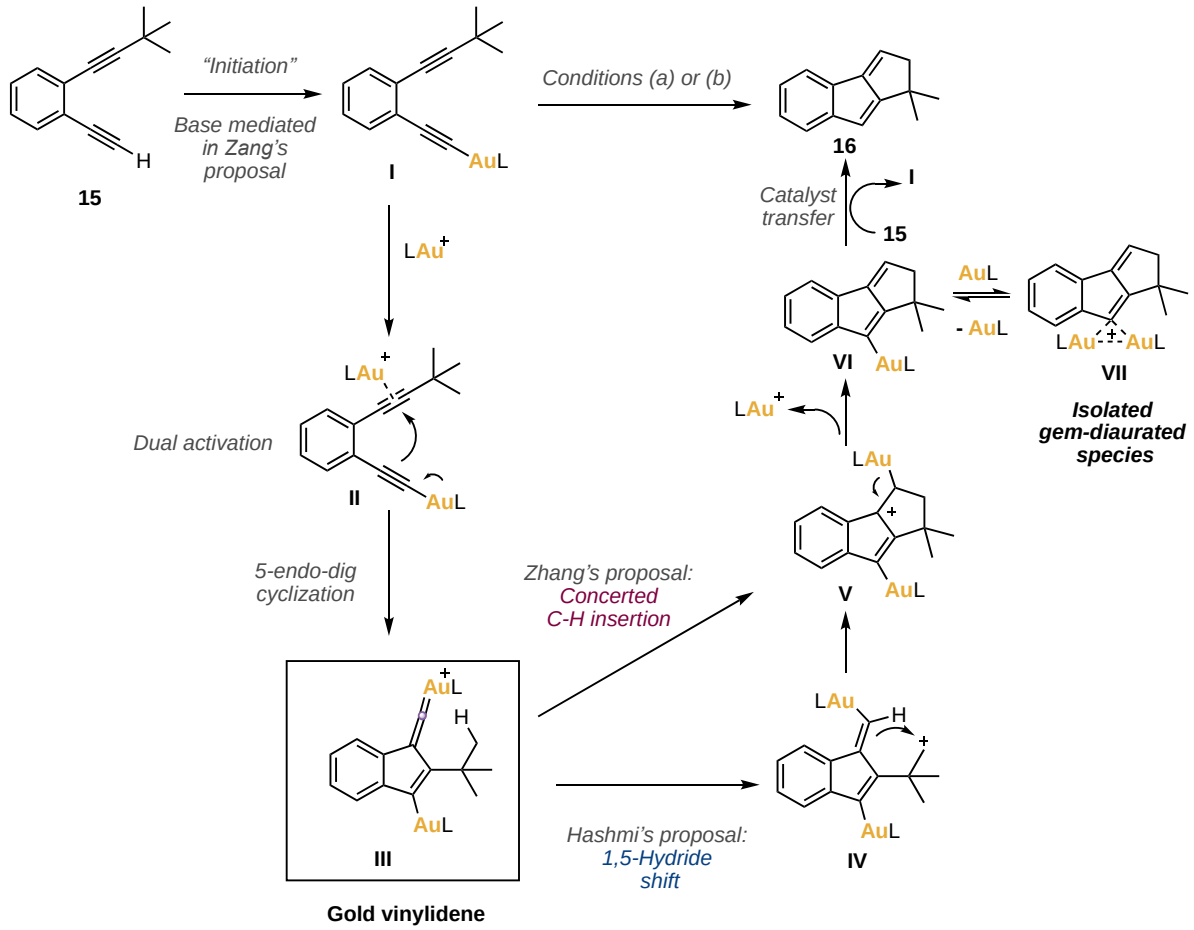

Scheme 5. Proposed mechanism of the dual gold catalysis.

Prior to the synthesis of tricyclic indenes, the group of Hashmi had already proposed the formation of gold(I) vinylidenes via dual gold catalysis in the synthesis of naphthyl benzene adducts **18** from

40 Nösel, P.; Lauterbach, T.; Rudolph, M.; Rominger, F.; Hashmi, A. S. K. *Chem. Eur. J.* **2013**, *19*, 8634−8641.

arenediynes **17**.[41] The first two steps of the suggested mechanism of this reaction (Scheme 6) are the same of the one reported above (Scheme 5), however, changes are observed after the formation of gold vinylidene **X**. In this case, gold vinylidene **X**, instead of undergoing C–H insertion, experienced a nucleophilic trapping by benzene, used as the solvent in the reaction. Subsequent hydrogen transfer formed gold(I) carbene **XII** which after ring expansion and deauration led to arylgold(I) complex **XIV**, in equilibrium with *gem*-diaurated species **XV**. Finally, catalyst transfer regenerated gold acetylide **VIII** and released the reaction product **18**.

The application of this methodology in an intramolecular fashion allowed the formation of dibenzopentalenes from phenyldiyene derivatives via the nucleophilic trapping of the pendant benzene to the vinylidene intermediate formed. [42] Subsequent computational analysis supported the formation of gold(I) vinylidenes during these transformations.[43] Additionally, this methodology proved to be effective when the pendant benzene was substituted by an allyl or benzyl group, leading to the formation of fluorenes and benzofluorenes.[44]

41 Hashmi, A. S. K.; Braun, I.; Rudolph, M.; Rominger, F. *Organometallics* **2012**, *31*, 644 – 661.

42 Hashmi, A. S. K.; Wieteck, M.; Braun, I.; Nösel, P.; Jongbloed, L.; Rudolph, M.; Rominger, F. *Adv. Synth. Catal.* **2012**, *354*, 555–562.

43 (a) Højer Vilhelmsen, M.; Hashmi, A. S. K. *Chem. Eur. J*. **2014**, *20*, 1901–1908. (b) Højer Larsen, M.; Houk, K. N.; Hashmi, A. S. K. *J. Am. Chem. Soc*. **2015**, *137*, 10668–10676. (c) Villegas-Escobar, N.; Højer Larsen, M.; Gutiérrez-Oliva, S.; Hashmi, A. S. K.; Toro-Labbé, A. *Chem. Eur. J*. **2017**, *23*, 13360–13368.

44 Bucher, J.; Wurm, T.; Taschinski, S.; Sachs, E.; Ascough, D.; Rudolph, M.; Rominger, F.; Hashmi, A. S. K. *Adv. Synth. Catal.* **2017**, *359*, 225–233.

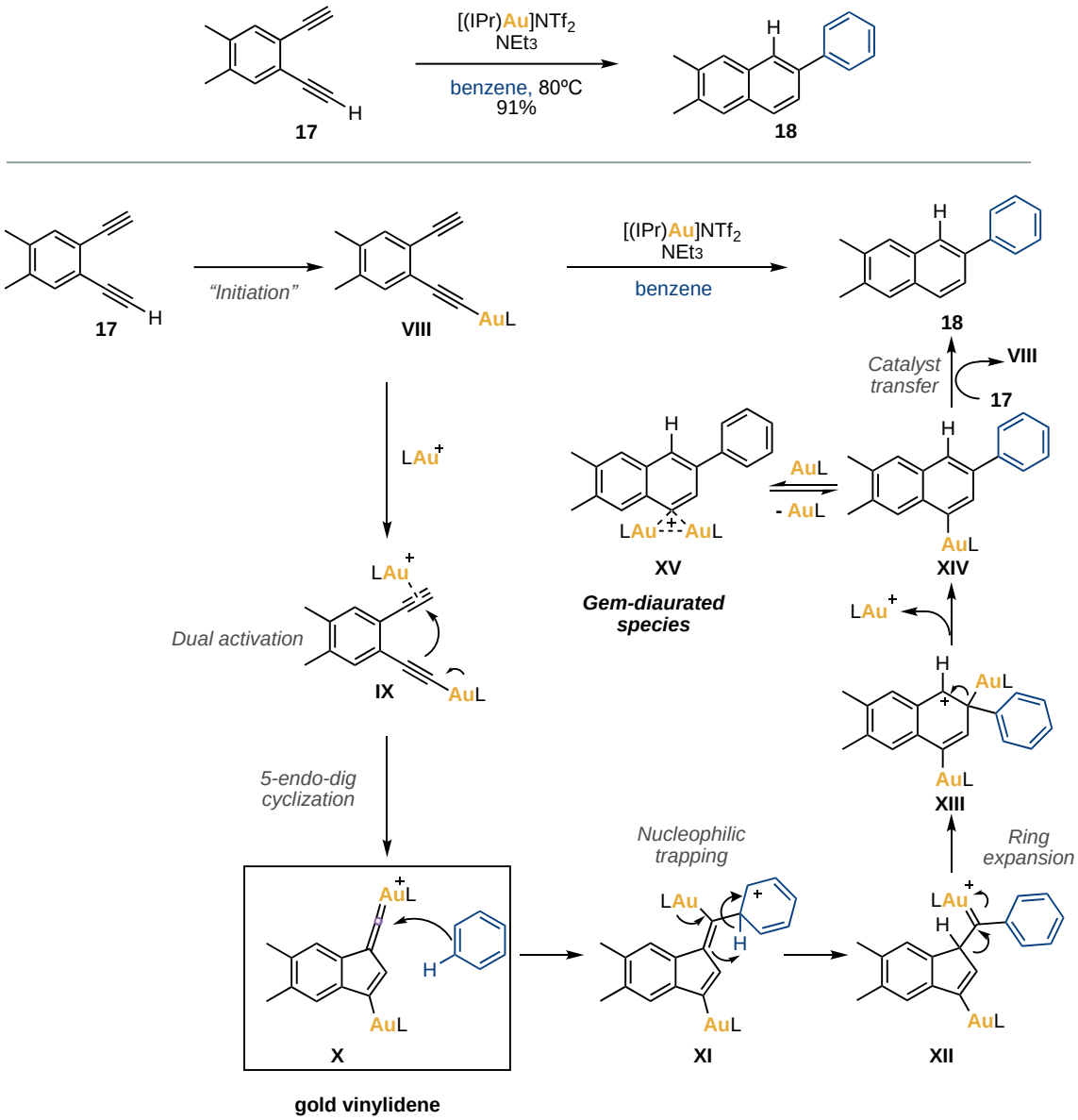

Scheme 6. Proposed mechanism for the hydroarylating-aromatization of arenediynes.

The work of Zhang and Hashmi opened a new field of study, causing a burst of investigation on the possibilities offered by dual gold catalysis. Thus, plenty of modifications were applied on the previous

systems, allowing the cyclizations of diyenes lacking an arene tether,[45] the use of allenynes as substrates,[46] or the synthesis of molecules containing heterocycles motifs.[47]

Additionally, further outcomes derived from the nucleophilic trapping of gold(I) vinylidenes were explored. In this way, the use of water for trapping the gold(I) vinylidene generated during the diyne cyclization allows the access to indenes via decarbonylative carbocyclization (Scheme 7).[48] Following the same principle, the direct trapping of a gold(I) vinylidene with sulfonate anion was performed by Hashmi in the gold-catalyzed cycloisomerization of tosylates.[49]

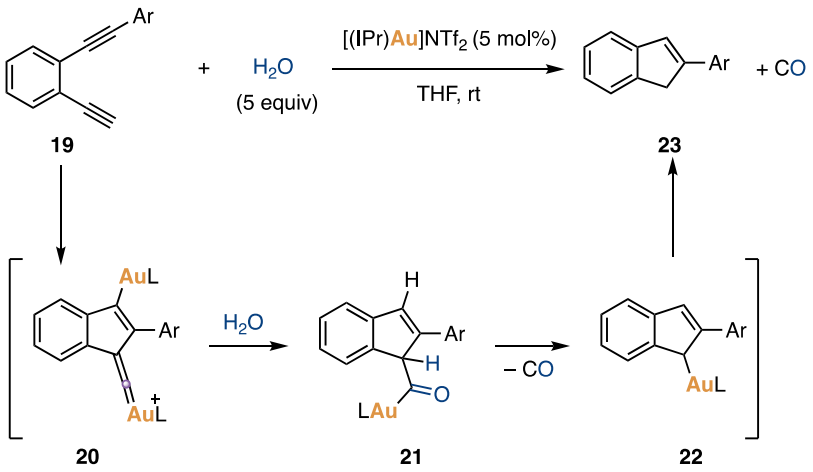

Scheme 7.Formation of indenes via decarbonylative carbocyclization.

Finally, in addition to C–H insertion or nucleophilic attack, gold(I) vinylidenes have been demonstrated to display other typical reactivity from vinylidenes, such as [1+2]-addition to alkenes to afford alkylidenecyclopropanes.[50]

45 (a) Vachhani, D. D.; Galli, M.; Jacobs, J.; Van Meervelt, L.; Van der Eycken, E. V. *Chem. Commun.* **2013**, *49*, 7171−7173. (b) Wieteck, M.; Tokimizu, Y.; Rudolph, M.; Rominger, F.; Ohno, H.; Fujii, N.; Hashmi, A. S. K. *Chem. Eur. J.* **2014**, *20*, 16331–16336.

46 Jaroschik, F.; Simonneau, A.; Lemière, G.; Cariou, K.; Agenet, N.; Amouri, H.; Aubert, C.; Goddard, J.-P.; Lesage, D.; Malacria, M.; Gimbert, Y.; Gandon, V.; Fensterbank, L. *ACS Catal.* **2016**, *6*, 5146−5160.

47 (a) Tšupova, S.; Cadu, A.; Stuck, F.; Rominger, F.; Rudolph, M.; Samec, J. S. M.; Hashmi, A. S. K. *ChemCatChem* **2017**, *9*, 1915–1920. (b) Tokimizu, Y.; Wieteck, M.; Rudolph, M.; Oishi, S.; Fujii, N.; Hashmi, A. S. K.; Ohno, H. *Org. Lett.* **2015**, *17*, 604–607. (c) Zhao, Q.; León Rayo, D. F.; Campeau, D.; Daenen, M.; Gagosz, F. *Angew. Chem. Int. Ed.* **2018**, *57*, 13603–13607. (d) Wang H.-F., Wang S.-Y., Qin T.-Z., Zi W. *Chem. Eur. J.* **2018**, *24*, 17911–17914.

48 Bucher, J.; Stöβer, T.; Rudolph, M.; Rominger, F.; Hashmi, A. S. K. *Angew. Chem., Int. Ed.* **2015**, *54*, 1666−1670.

49 Bucher, J.; Wurm, T.; Nalivela, K. S.; Rudolph, M.; Rominger, F.; Hashmi, A. S. K. *Angew. Chem., Int. Ed.* **2014**, *53*, 3854−3858.

50 Hashmi, A. S. K.; Wieteck, M.; Braun, I.; Rudolph, M.; Rominger, F. *Angew. Chem. Int. Ed.* **2012**, *51*, 10633–10637.

Despite the wide variety of reactions in which gold(I) vinylidenes has been proposed as key intermediates,[51] direct proofs of their existence are very limited. In 2015 the group of Widenhoefer reported the first synthesis and characterization of a gold(I) vinylidene, taking advantage of the stabilization of alkyl and vinyl carbenium ions provided by β-Si–C hyperconjugation (Scheme 8).[52]

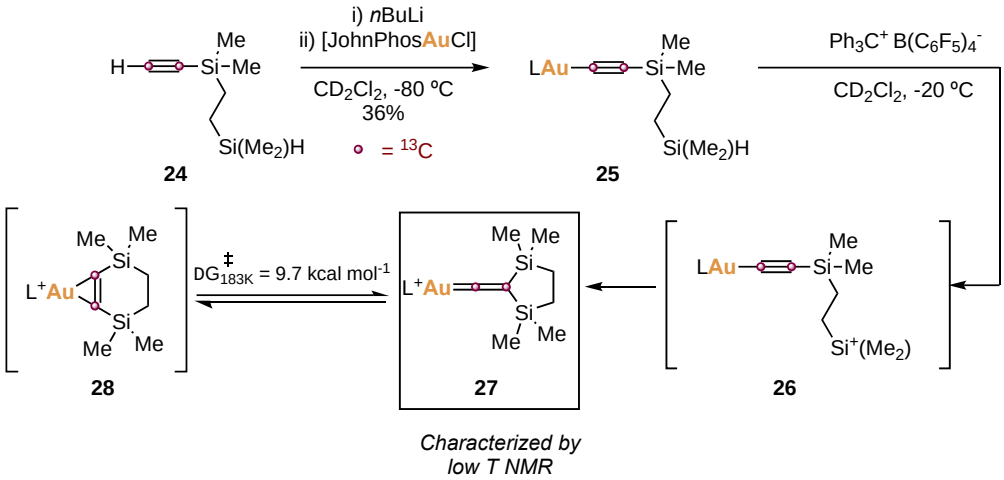

Scheme 8. First synthesis and characterization of a gold(I) vinylidene.

(β,β-Disilyl)-vinylidene **27** was synthesized from gold(I) acetylide complex **25**, via hydride abstraction/cyclization. Due to its thermal instability, the isolation of this intermediate in solid state was not possible, however, they managed to successfully characterize it by using low temperature NMR and synthesizing the doubly labelled ^{13}C isotopomer of the product. The cyclic and symmetric structure of the compound was confirmed by ^{1}H NMR. Additionally, ^{13}C NMR spectrum displayed broad multiplets at 206 and 122 ppm corresponding to C1 and C2 of the gold vinylidene. Surprisingly, ^{13}C-Spin saturation transfer analysis experiments disclose the interconversion of C1 and C2 with an energy barrier of ΔG_{183K}=9.7 kcal/mol. This interconversion was attributed to the equilibrium of the vinylidene with the unobserved product of the 1,2–silyl migration **28**.

Finally, analysis of the ^{29}Si NMR showed a significant downfield with respect to the C(sp)-Si resonance of the neutral acetylide precursor **25**, indicating the accumulation of the positive charge on the β-silicon atoms. Prior studies made by Müller stablished a correlation between the deshielding of the ^{29}Si NMR resonances of α-aryl-β,β-disilyl vinyl cations relative to their neutral arylacetylenes and the electron donor ability of the α-substituents of the compounds.[53] The comparison of the results obtained in the (β,β-disilyl)vinylidene with α-*tert*-butyl-β,β-disilyl vinyl cation indicated a higher electron donor

51 For a review on this topic: Gagosz. F, *Synthesis* **2019**, *51*, 1087–1099.
52 Harris, R.J.; Widenhoefer, R.A. *Angew. Chem. Int. Ed.* **2015**, *54*, 6867–6869.
53 Müller, T.; Margraf, D.; Syha, Y. *J. Am. Chem. Soc*. **2005**, *127*, 10852–10860.

ability of the L–Au fragment over the one provided from the *tert*-butyl groups. This would indicate a delocalization of the positive charge in both, the β-silyl groups and the gold fragment.

The above-described work can be considered the only direct experimental evidence on the existence of gold(I) vinylidenes. However, the need of the two silyl groups to stabilize the vinylidene unit, pushes far away this species from the genuine intermediates proposed in gold(I)-catalyzed reactions.

Recent studies continue to propose gold(I) vinylidenes as reaction intermediates, suggesting new generation pathways as their generation from 1,1-halometalated alkenes after halogen migration, [54] however studies on their nature seem stacked.

In this chapter we propose a new methodology for accessing gold(I) vinylidenes. Based on previous findings published by our group on the analogy to the relationship between gold(I) carbenes and their gold(I) carbenoids (Figure 4a),[55] we envisioned a possible way of accessing gold(I) vinylidenes from their carbenoid like species, from now on called gold(I) vinylidenoids in this manuscript (Figure 4b). This terminology has been previously used for naming analogous nickel species.[56]

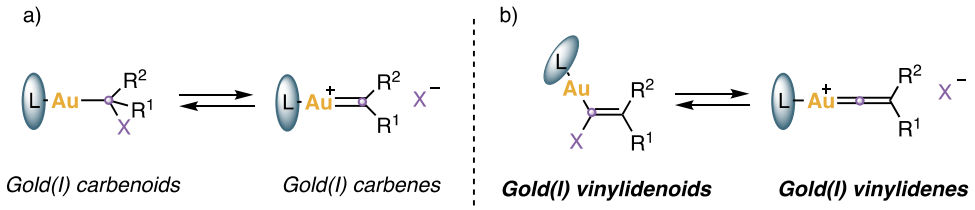

Figure 4. Relationship between gold(I) vinylidenes/ vinylidenoids in analogy to gold(I) carbenes/carbenoids.

In this way, we have synthesized a family of gold(I) vinylidenoids and their reactivity has been explored. The outcome of the experimental results has been studied by DFT, which has given us insights about the gold(I) vinylidenes nature.

54 (a) de Orbe, M. E.; Zanini, M.; Quinonero, O.; Echavarren, A. M. *ACS Catal.* 2019, *9*, 7817–7822. (b) Kreuzahler, M.; Haberhauer, G. *Chem. Eur. J.* **2022**, *28*, e202103046.

55 García-Morales, C; Pei, X-L; Sarria Toro, J.M.; Echavarren A. M. *Angew. Chem. Int. Ed.* **2019**, *58*, 3957–3961.

56 Pal, S.; Zhou, Y; Uyeda, C. *J. Am. Chem. Soc.* **2017**, *139*, 11686−11689.

Objectives

As it was explained in the introduction, evidence on the existence of gold(I) vinylidenes is still scarce. The proof of their existence is based on indirect experimental and computational studies. In addition, the structure of the only gold(I) vinylidene experimentally detected is electronically far away from the expected species in catalysis.[52]

Hence, our main goal in this chapter is to gain understanding on the structural and electronic nature of gold(I) vinylidenes and their reactivity. In 2019, our group reported an efficient methodology to generate gold(I) carbenes from gold(I) carbenoids.[55] Based on this methodology, we envisioned a synthetic strategy relying on the relationship between gold(I) vinylidenoids and vinylidenes and on including stabilizing substituents (Figure 5). Our aim is to synthesize a family of gold(I) vinylidenoids to study its connection to gold(I) vinylidenes, their reactivity and its structural features. DFT will be used to support our findings and gain further insights about gold(I) vinylidenes.

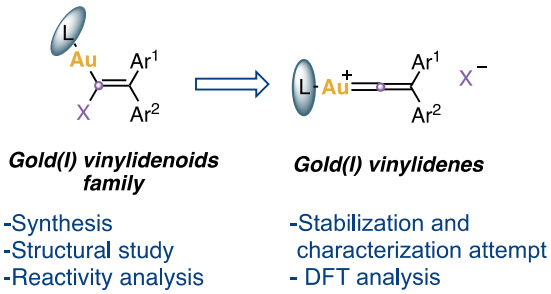

Figure 5. Strategy for the study of gold(I) vinylidenes.

Results and Discussions

Strategy and Proof of Concept

As it has been remarked in the introduction of this chapter, the number of synthetic protocols to access gold(I) vinylidenes is quite limited.[51,52] Hence, our first task was to find a convenient way to generate our target species. Considering the previous work on the generation of gold(I) carbenes performed in our group (Scheme 9, left),[55] we decided to exploit this strategy, using $GaCl_3$ as the chloride scavenger to generate gold(I) vinylidenes from their corresponding gold(I) vinylidenoids (Scheme 9, right).

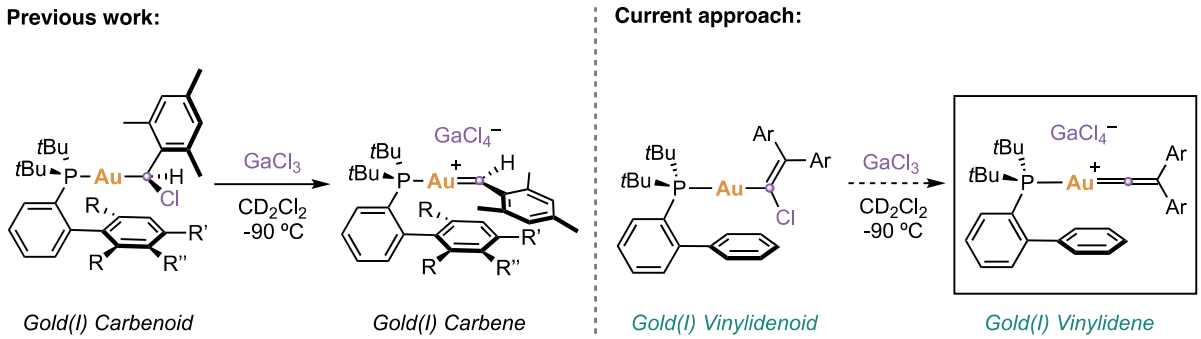

Scheme 9. Strategy for the generation of gold(I) vinylidenes.

To initiate our investigations, we applied our strategy on the synthesis of a gold(I) vinylidenoid bearing JohnPhos as the ligand tethered to gold (Scheme 10). JohnPhos was chosen since it is commercially available, it allows us to follow the reactivity via $^{31}P\{^{1}H\}$ NMR and it has been proved to favor the stability of the only example of characterized gold(I) vinylidenes.[52] Additionally, we set two phenyl groups as the olefin organic substituents expecting them to stabilize electronically the vinylidene center. Using our envisioned approach, gold(I) vinylidenoid **30** was achieved with a moderate yield in just two steps. First, 1-diphenylethene was chlorinated using N-chlorosuccinimide. Then, vinyl chloride **29** was treated with *n*-BuLi at –90ºC to achieve lithium-hydrogen exchange. At the same low temperature, lithium intermediate was treated with JohnPhos Gold(I) chloride to achieve via transmetalation the desired gold(I) vinylidenoid **30**. Gold(I) vinylidenoid **30** demonstrated to be stable enough to be purified by nitrogen flashed column chromatography on neutral aluminum oxide and can be stored indefinitely in the fridge when protected from air. The stability of this compound allows the measurement of its molecular structure by X–Ray diffraction (Figure 6).

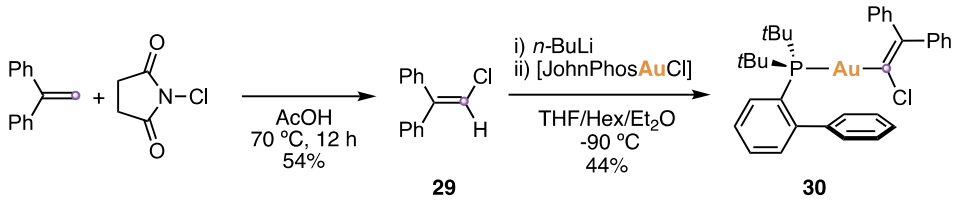

Scheme 10. Synthesis of gold(I) vinylidenoid **30**.

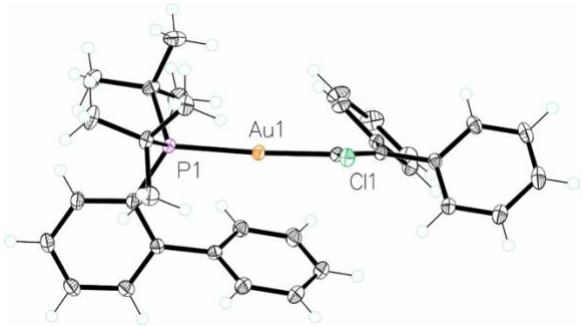

Figure 6. X–Ray structure of gold(I) vinylidenoid **30**.

With gold(I) vinylidenoid **30** in hand, the generation of the corresponding gold(I) vinylidene **31** was attempted by the treatment of gold(I) vinylidenoid **30** with $GaCl_3$ at –90 ºC under inert atmosphere following the reaction by $^{31}P\{^1H\}$ NMR (Scheme 11).

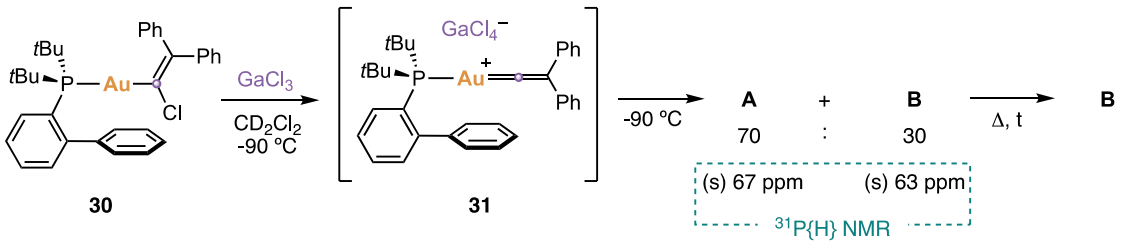

Scheme 11. Treatment of gold(I) vinylidenoid **30** with $GaCl_3$.

The $^{31}P\{^1H\}$ NMR experiment at –90ºC showed the immediate evolution of starting material **30** into two ^{31}P containing products **A** and **B**. The products observed displayed in the $^{31}P\{^1H\}$ spectrum a singlet signal at 67 (major product, **A**) and a singlet signal at 63 (minor product, **B**) ppm. The increase of the temperature showed the progressive decomposition of product **A** into product **B**, achieving full conversion into **B** above 0 ºC. The GC-MS analysis of the crude product of the reaction indicated the formation of diphenylacetylene as the main organic product. In parallel, product **B** could be isolated and characterized by X-Ray diffraction, exposing the structure of the chloride bridge formed from $GaCl_3$ and two units of JohnPhos gold(I)$^+$ (Figure 7).

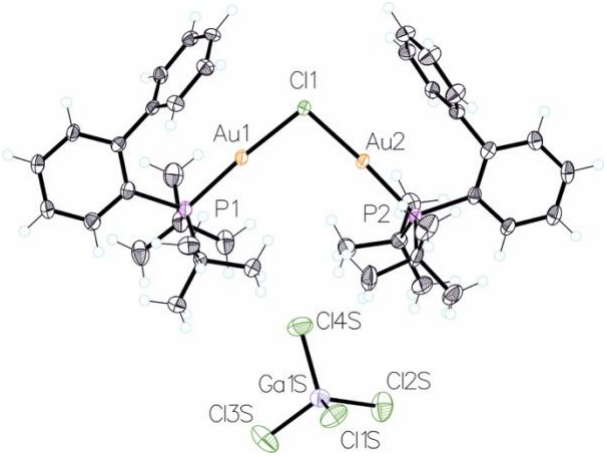

Figure 7. X-Ray structure of product **B**.

To elucidate the structure of intermediate **A**, reaction was repeated and monitored via $^{13}C\{^{1}H\}$ NMR. Parallelly, $^{13}C\{1H\}$ NMR signals of gold(I) vinylidene **31** were computed using DFT. The mismatching between the computed NMR shifts and the experimentally observed $^{13}C\{^{1}H\}$ signals discarded **A** as gold(I) vinylidene **31**. However, the $^{13}C\{^{1}H\}$ spectra presented matching signals to the ones computed for the product of the 1,2-aryl shift reaction: (η^2-diphenylacetylene)gold(I) complex **32** (or **A**), which were also consistent with the resonances of similar compounds previously reported.[57] (η^2-diphenylacetylene)gold(I) complex **32** showed to be thermally unstable, decomposing in the chloride bridge **33** (or **B**) and diphenylacetylene when the temperature was increased (Scheme 12).

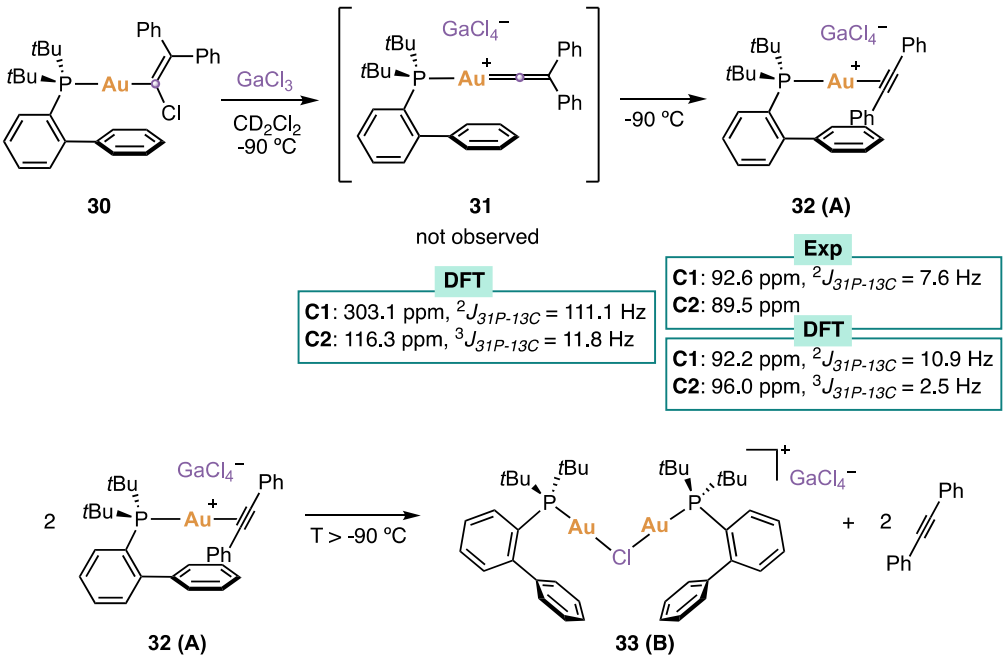

Scheme 12. Identified products from the treatment of Gold(I) vinylidenoid **30** with $GaCl_3$.

57 Brown, T.J.; Widenhoefer, R.A. *Journal of Organometallic Chemistry* **2011**, *696*, 1216–1220.

To further confirm that this reaction goes through (η^2-diphenylacetylene)gold(I) complex **32**, this species was directly synthesized from JohnPhos gold(I) chloride **34** and diphenylacetylene (Scheme 13). The comparison of both $^{31}P\{H\}$ NMR and ^{1}H NMR spectra confirmed that complex **32** was the major product in both reactions.

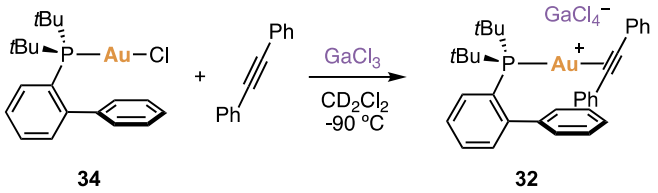

34 **32**

Scheme 13. Alternative generation of (η^2-diphenylacetylene)gold(I) complex **32**.

Although we did not observe any signal corresponding to gold(I) vinylidene **31** by NMR, the formation of (η^2-diphenylacetylene)gold(I) complex **32** indicates a typical reactivity of our targeted intermediates. As it was explained in the introduction of this chapter, 1,2-migration is known as the preferred reactivity of free vinylidenes, resulting in the formation of the thermodynamically much more stable corresponding alkynes.[2] This tautomer interconversion is also typical of metal vinylidenes, although in this case, the vinylidene form is more stable (not when gold is involved).[14, 28] In the case of gold vinylidenes, 1,2-shift has been reported as a way of generation of gold(I) vinylidenes during the formation of phenanthrenes from *o*-alkynyl arenes and related transformations.[51] However aryl migration have never been observed before in gold(I)-catalyzed transformations.

In addition to the previous experiments, preliminary DFT studies on gold(I) vinylidene **31** reactivity were performed by Dr. Cristina García-Morales (Scheme 14).

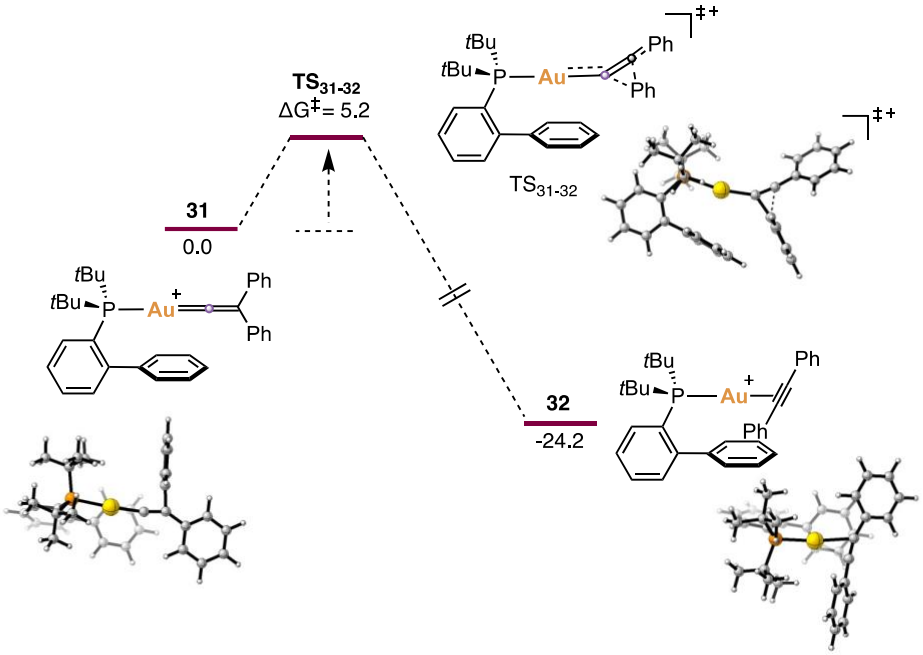

Scheme 14. Free energy profile of 1,2-aryl migration from gold(I) vinylidene **31**. The energy differences are given in kcal/mol and represent the relative free energies. DFT calculation performed with 6-31G(d,p) (C, H, P) and SDD (Au) in CH_2Cl_2 (SMD).

The outcome of these studies supported that gold(I) vinylidene **31** undergoes 1,2-aryl migration with an energy activation barrier of just 5.2 kcal/mol. This low energy barrier explains the high speed of this transformation even at low temperatures, shifting the equilibrium from the highly unstable gold(I) vinylidene **31** to its η^2-diphenylacetylene gold tautomer **32**, 24.2 kcal/mol more stable.

Once confirmed that our approach can give us insights about the relationship between gold(I) vinylidenoids and gold(I) vinylidenes, we focused on introducing modifications in the aryl substituents of the gold(I) vinylidenoids and on studying how these could affect their stability and reactivity. To do so, a family of gold(I) diarylvinylidenoids was synthesized and its behaviour was compared to the one reported for other metal vinylidenoids and for free and transition metal vinylidenes. Finally, gold(I) vinylidenes were studied by DFT to get a complete picture of the mechanisms of gold(I) vinylidene reactivity.

Synthesis of a Family of Diaryl Gold(I) Vinylidenoids

Recently, the group of Lloyd-Jones reported a complete study on the evaluation of the 1,2-aryl migration trends in free vinylidenes.[58] We envisioned that a family of gold(I) vinylidenoids with different electronics on the aryl substituents for C2 could provide enough insight on the 1,2-migration

58 Dale, H. J. A.; Nottingham, C.; Poree, C.; Lloyd-Jones, G.C. *J. Am. Chem. Soc.* **2021**, *143*, 2097−2107.

to compare the behavior of gold(I) vinylidenes with free vinylidenes. Additionally, studies on the diarylalkyne-vinylidene isomerization of Ru compounds have also been reported, providing us information about the behavior of transition metal vinylidenes in these transformations.[59] The analysis of these migration reactions requires the ^{13}C isotopic labelling of one of the alkenyl carbons and for synthetic reasons we chose to label C1 in our compounds. On this basis, we synthesized four ^{13}C labelled gold(I) vinylidenoids modifying one of the aryl rings of the alkene unit by adding four different groups with diverse electronic properties: –Me,–F,–OMe and $–CF_3$. Thus, we were able to compare the migration trends of the five different substituents (including phenyl) and to check if any of the structures could stabilize enough gold(I) vinylidenes to characterize them by low temperature NMR. For the comparison of the migration trends, we decided to use exclusively one of the diastereomers of the olefins, to mitigate the influence of prior chloride abstraction in the comparison (Scheme 15).

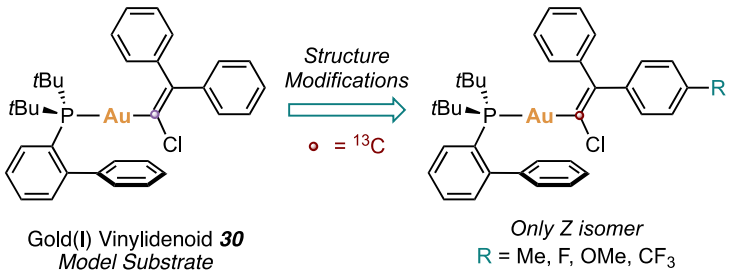

Scheme 15. Structure modifications to synthesize the different gold(I) vinylidenoid substrates.

Our first synthetic approach involved the diastereoselective formation of the alkenyl precursors followed by derivatization and subsequent JohnPhos Gold(I) insertion by lithiation and subsequent transmetalation (Scheme 16), reproducing the strategy optimized for the model substrate.

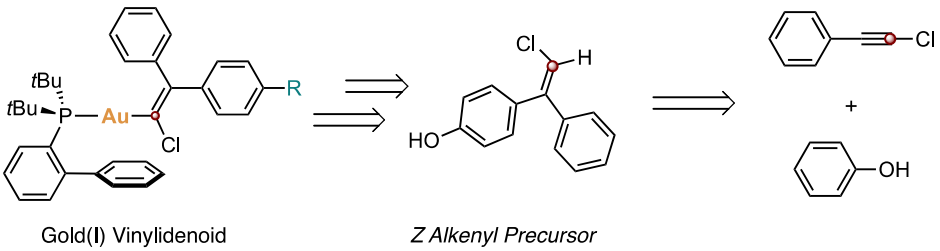

Scheme 16. Synthetic approach for the formation of the Z gold(I) vinylidenoids.

Once stablished the modifications to be included and the synthetic approach to follow, we started by synthesizing the *Z* alkenyl chloride precursors.^{13}C-chlorophenylacetylene **36** was used as the isotopic labelled source, since it could be easily prepared by chlorination of the commercially available ^{13}C-

59 (a) Mutoh, Y.; Ikeda, Y.; Kimura, Y.; Ishii, Y. *Chem. Lett.* **2009**, *38*, 534−535. (b) Otsuka, M.; Tsuchida, N.; Ikeda, Y.; Kimura,Y.; Mutoh, Y.; Ishii, Y.; Takano, K. *J. Am. Chem. Soc.* **2012**, *134*, 17746−17756.

phenylacetylene **35** with excellent yield.[60]A procedure reported by F. Yang and co-workers paved our way to synthesize diastereoselectively *Z* alkenyl chlorides **37** and **38**, via a gold(I)-catalyzed addition of nucleophiles to chloro alkynes,[61] obtaining the desired products with moderate yields (Scheme 17).

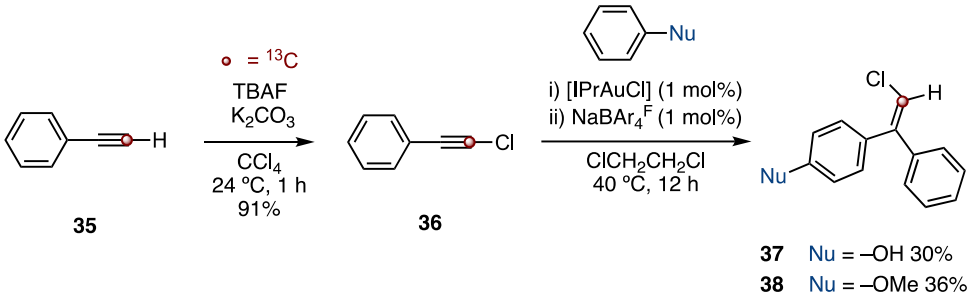

Scheme 17. Synthesis of Z alkenyl chlorides **37** and **38**.

Alkenyl precursor **38** was used directly for the synthesis of its corresponding gold(I) vinylidenoid, while alkenyl precursor **37** was synthesized envisioning a subsequent derivatization of the alcohol group. Before continuing the synthesis, we tested that the treatment with *n*-BuLi in next steps would not cause a loss of stereochemistry. To do so, we trapped the lithiated species formed with water, confirming by NMR that only *Z* isomer could be identified (Scheme 18).

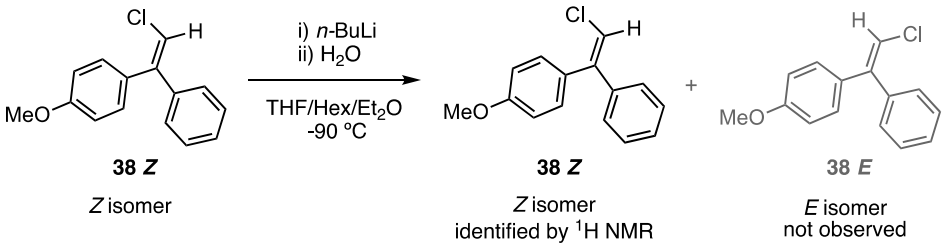

Scheme 18. Test of preservation of stereochemistry.

Once the preservation of stereochemistry was confirmed, we sought the best way of introducing a –Me and a –F in alkenyl precursor **37**. Although we tested several options, the best one came by triflation of the phenol group and subsequent functionalization of aryl triflate **39**. For the synthesis of tolyl alkenyl chloride **40**, the use of a Stille coupling of the aryl triflate with tetramethyl tin catalyzed by $PdCl_2(PPh_3)_2$ led us to our desired product **40** in good yield. In the case of flurophenyl alkenyl chloride **41** a procedure of deoxyfluorination of aryl fluorosulfonates with tetramethylammonium fluoride, developed by Sanford and co-workers,[62] provided us our desired product **41** in good yield (Scheme 19).

60 Sasson, Y.; Webster, O. W. ***J. Chem. Soc., Chem. Commun.***, **1992**, 1200–1201.

61 Liu, C.; Xue, Y.; Ding, L.; Zhang, H.; Yang, F. *Eur. J. Org. Chem*. **2018**, 6537–6540.

62 Schimler, S. D.; Froese, R. D. J.; Bland, D.C.; Sanford, M. S. *J. Org. Chem.* **2018**, *83*, 11178−11190.

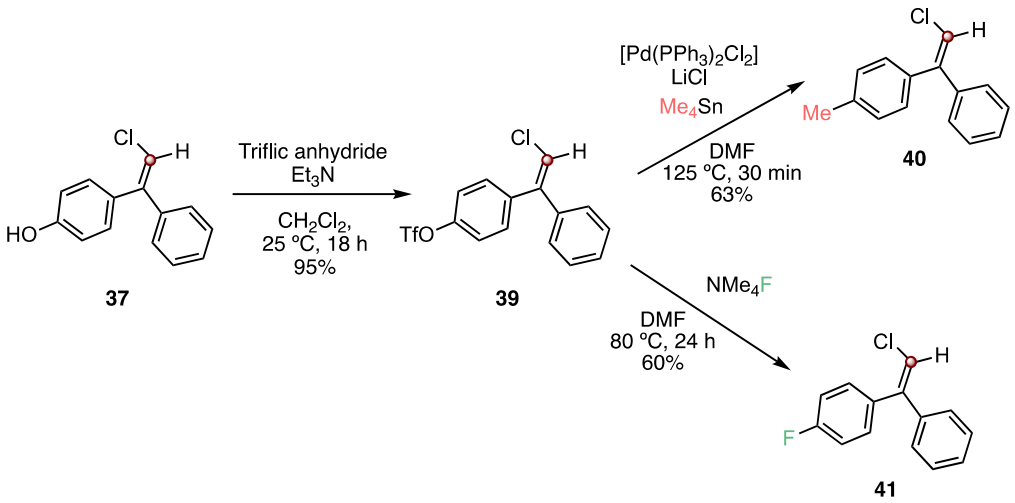

Scheme 19. Synthesis of chloro alkenylderivatives **40** and **41**.

With these three different olefin precursors in hand, the introduction of the JohnPhos gold(I) moiety was performed following the procedure used in the model substrate, obtaining gold(I) vinylidenoids **42**, **43** and **44** in moderate to good yields (Scheme 20). The structure of gold(I) vinylidenoid **42** and **43** was confirmed by X–Ray diffraction (Figure 8).

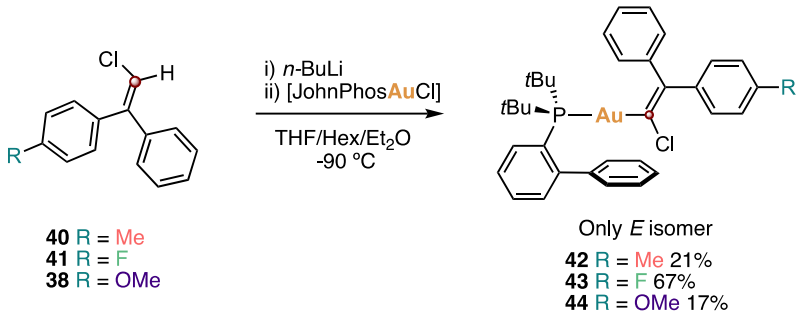

Scheme 20. Synthesis of gold(I) vinylidenoids **42**, **43** and **44**.

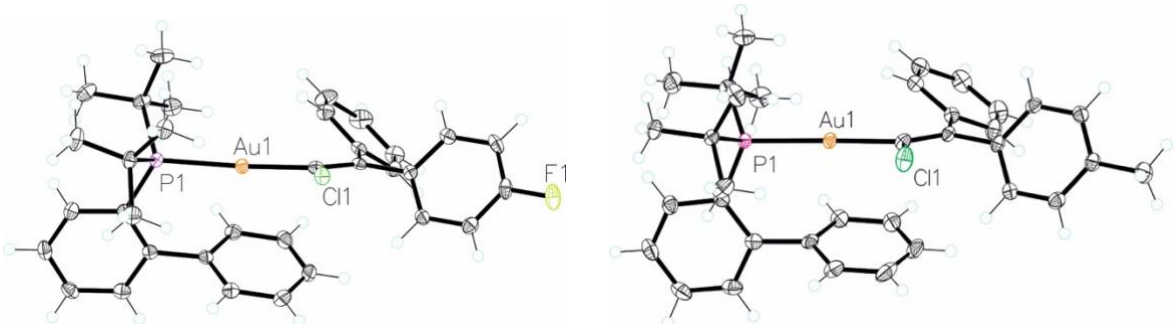

Figure 8. X-Ray structures of gold(I) vinylidenoid **42** (left) and gold(I) vinylidenoid **43** (right).

At this point, we considered to synthesize the opposite diastereoisomer *Z* of one of the gold(I) vinylidenoids to test the influence of the chloride abstraction in their reactivity. Considering the electronic properties of the synthesized vinylidenoids, –OMe aryl vinylidenoid **44** is the one which presents higher differences in terms of electronics between both aryl substituents (phenyl and anisyl group), which results in a more different migration trend.[58, 59] This would make easier to distinguish the influence of the chloride abstraction step on the migration process, so we decided to synthesize *Z* gold(I) vinylidenoid **44**.

To that end, we developed a non-diastereoselective synthetic route using $^{13}CH_3I$ as the ^{13}C isotopic labelled source. The use of this reagent allowed us to synthesize a ^{13}C labelled phosphonium salt which via a Wittig reaction conduct us directly to a labelled olefin. The chlorination of this olefin gave us access to both diastereoisomers of the alkenyl chloride precursors, which could be subsequently separated by preparative HPLC and complexed to form gold(I) vinylidenoids **44** ***E*** and **44** ***Z*** (Scheme 21).

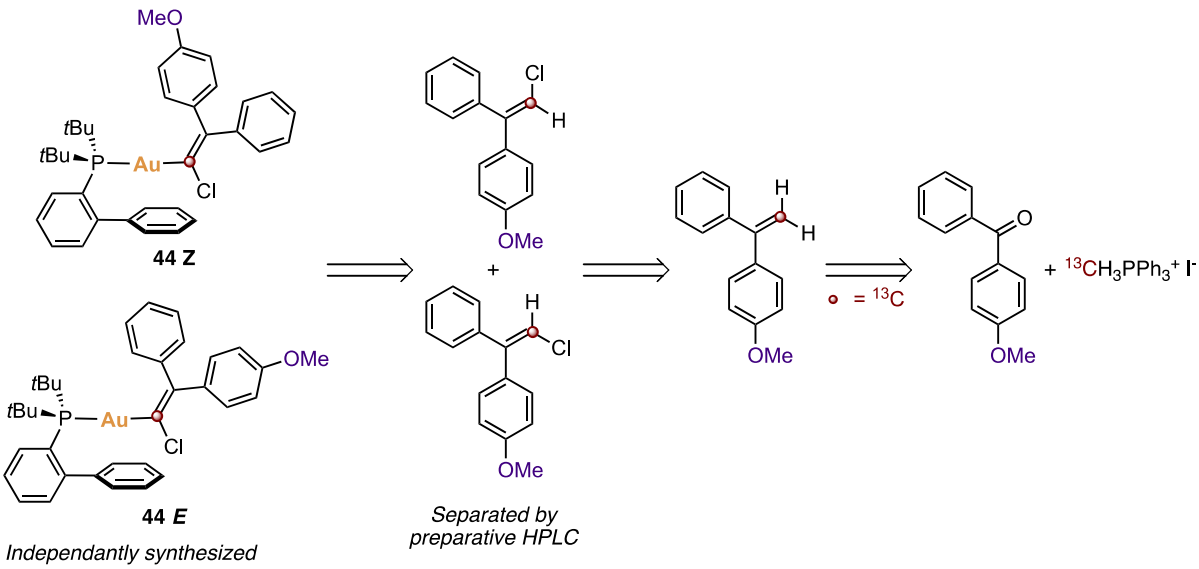

Scheme 21. Synthetic strategy of both diastereoisomers of vinylidenoid **44**.

With the planned synthetic strategy in mind, phosphonium salt **45** was synthesized with excellent yield by treating PPh_3 with $^{13}CH_3I$.[63] Next, 4-methoxybenzophenone reacted with previously formed isotopic labelled phosphonium salt in a Wittig reaction producing diarylakene **46** in good yield. Diaryl alkene **46** was subsequently chlorinated with N–chlorosuccinimide to obtain a 3:2 mixture of *E:Z* alkenyl chloride **38**, which were subsequently separated via HPLC. Once separated, both isomers were independently treated with *n*-BuLi at low temperature and directly complexed with JohnPhos gold(I)

63 Ikeda, S.; Shintani, R. *Angew. Chem. Int. Ed.* **2019**, *58*, 5734–5738.

chloride to obtain *E* and *Z* vinylidenoids **44** in moderate yields (Scheme 22). The structure of gold(I) vinyldienoid **44 *Z*** was further confirmed by X-Ray diffraction (Figure 9).

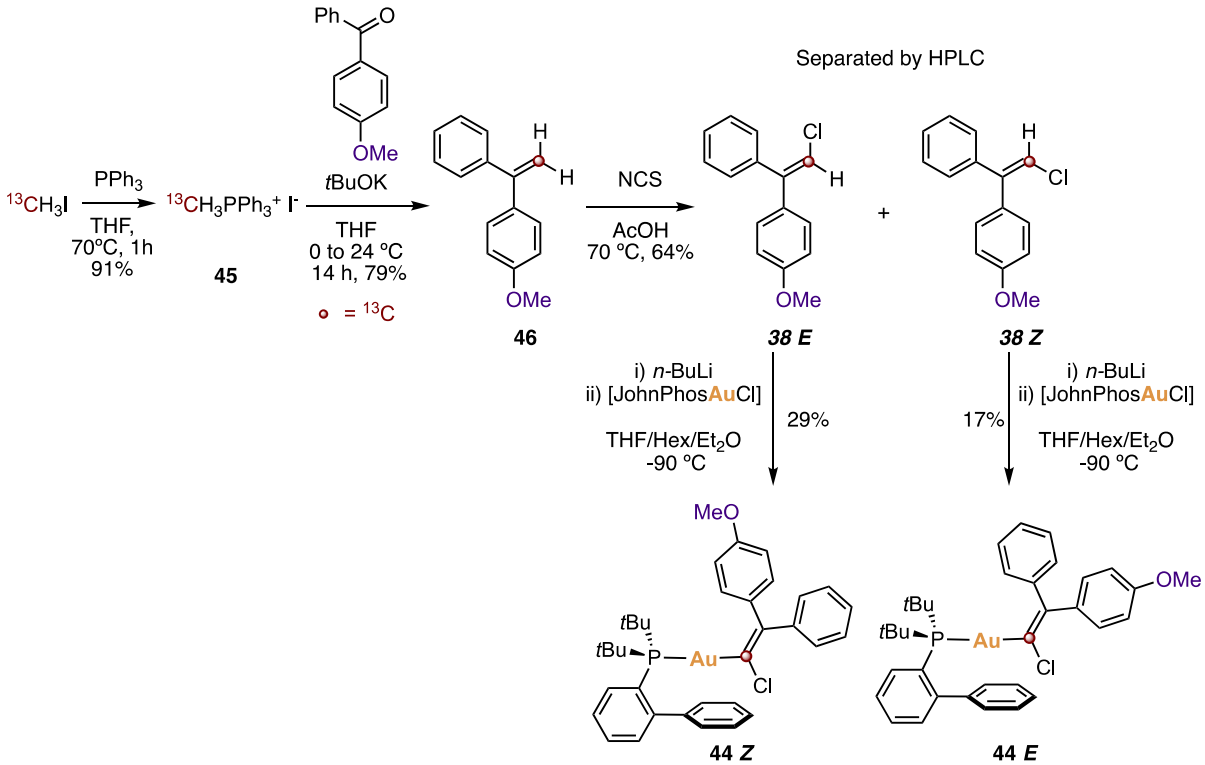

Scheme 22. Synthethic route of gold(I) vinylidenoids **44 *E*** and **44 *Z***.

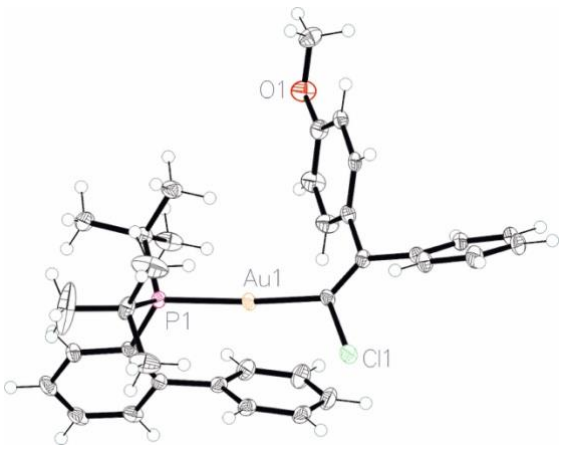

Figure 9. X-Ray structure of gold(I) vinylidenoid **44 *Z***.

We decided to apply the same synthetic route for the synthesis of trifluoromethyl aryl substituted gold(I) vinylidenoid **50**. However, in this case we only managed to isolate a significant amount of the ***Z*** alkenyl chloride after the separation of the isomers via HPLC. This ***Z*** alkenyl chloride **49**, gave us access to the last of our studied substrates, gold(I) vinylidenoid **50 *E*** (Scheme 23).

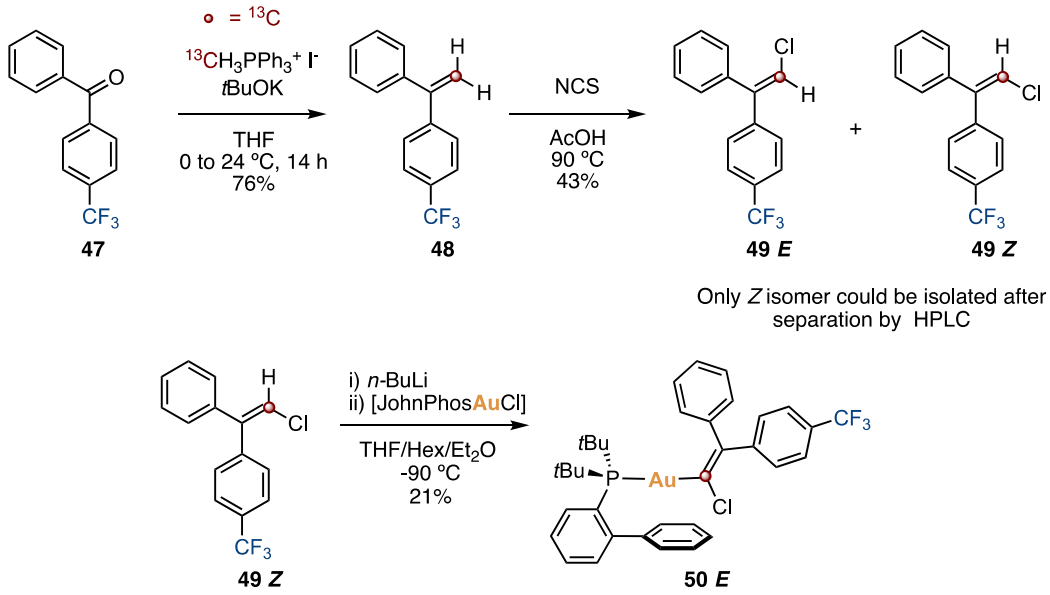

Scheme 23. Synthesis of Gold(I) vinylidenoid **50** ***E***.

All gold(I) vinylidenoids (**42**–**44** and **50**) showed to be stable enough to be purified by nitrogen flushed column chromatography using neutral aluminum oxide. Additionally, they can be storage indefinitely in the fridge protected from air, what facilitates their subsequent use on their reactivity studies.

Reactivity Studies of Gold(I) Diaryl Vinylidenoids

The reactivity of the family of gold(I) vinylidenoids synthesized was tested by treating them with $GaCl_3$ at –90ºC under inert atmosphere. Reactions were monitored by ^{1}H and ^{13}C NMR using DEPTq–135 experiments, since they offer more information about the hybridization state of the carbons together with higher sensitivity in less time. Immediately after adding $GaCl_3$ the formation of each corresponding (η^2-diarylacetylene) gold(I) complexes were observed, together with variable amounts of the corresponding byproduct derived from protodeauration. This byproduct was detected to rapidly be formed with minimum amounts of HCl derived from the exposure of $GaCl_3$ to air, even when $GaCl_3$ is stored in the glovebox. None of the reactions showed characteristic ^{13}C signals of gold(I) vinylidenes at extremely downfield (≈ 300 ppm, according to DFT), indicating that, if we are passing through these intermediates, the chosen substituents do not stabilize them. However, the use of isotopic labelling allowed us to study the migration aptitude of the different aryl substituents in the considered gold(I) vinylidenoids (Scheme 24).

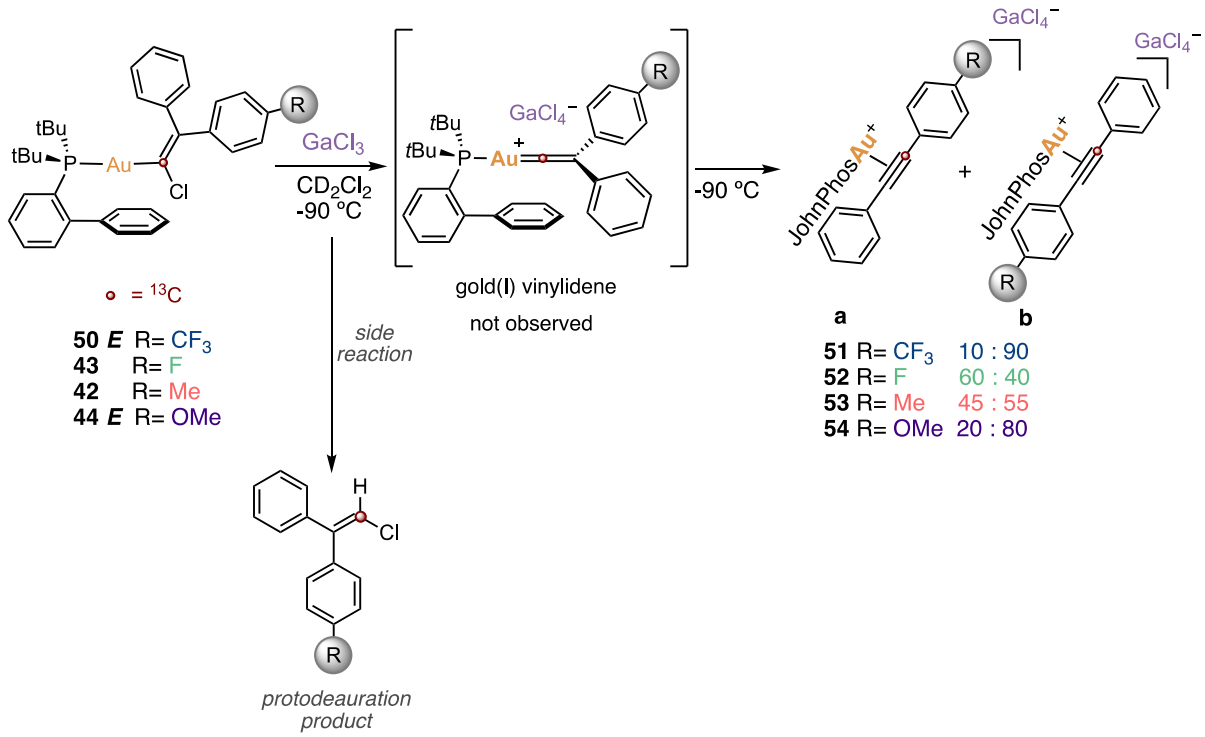

Scheme 24. Reactivity study of *Z* gold(I) vinylidenoids.

The migration ratio was kept constant after the increase of the temperature caused decomposition of (η^2-diarylacetylene) gold(I) complexes into the corresponding free diarylacetylenes and chloride bridge **33** (Scheme 25), the small differences observed can be ascribed to the manual integration error.

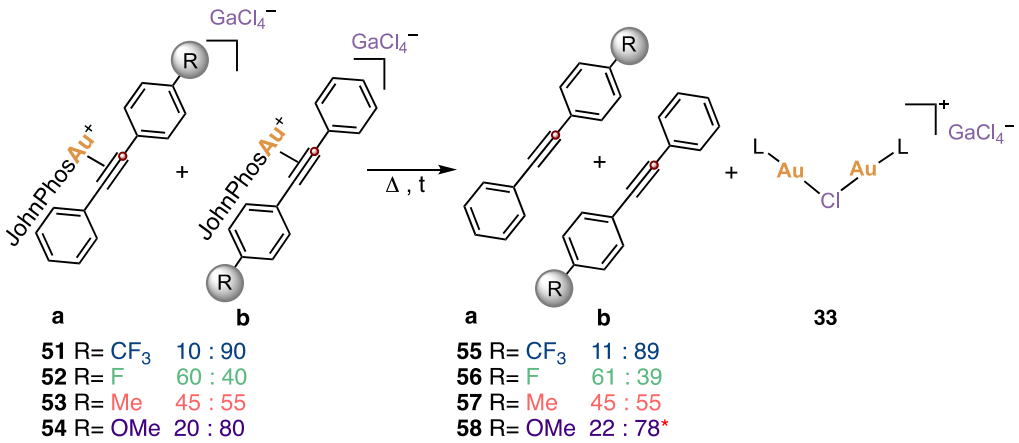

Scheme 25. Thermal decomposition of (η^2-diarylacetylene) gold(I) complexes **51** to **54**.

The only case in which this situation changes is the one of gold(I) vinylidenoid **44** ***E*** (marked with a red star in Scheme 25). Surprisingly, the ratio of the alkynes seems to be inverted with the loss of coordination when the temperature was increased. Even more, the shifts of the free alkynes do not match with the ones previously reported.[58] This made us consider other species involved in the

transformation.[64] To elucidate this question, we synthesized (η^2-diarylacetylene)Gold(I) complex **54** ^{12}C isotopologue from alkyne **58** ^{12}C isotopologue and JohnPhos gold(I) chloride and we confirmed that the coordinated alkyne **54** was being formed. We observed that, instead of decomposing in the free alkyne and the chloride bridge, a different species was being formed. We considered the possibility of a coordination between gold(I) and the oxygen of the methoxy group, however we did not manage to isolate this species **59**. Additionally, the broadening of the signals observed indicated a possible equilibrium between **54** and **59**. However, we verified that by adding an olefin (such as norbornene) diarylacetylene is released, shifting the gold coordination (Scheme 26).

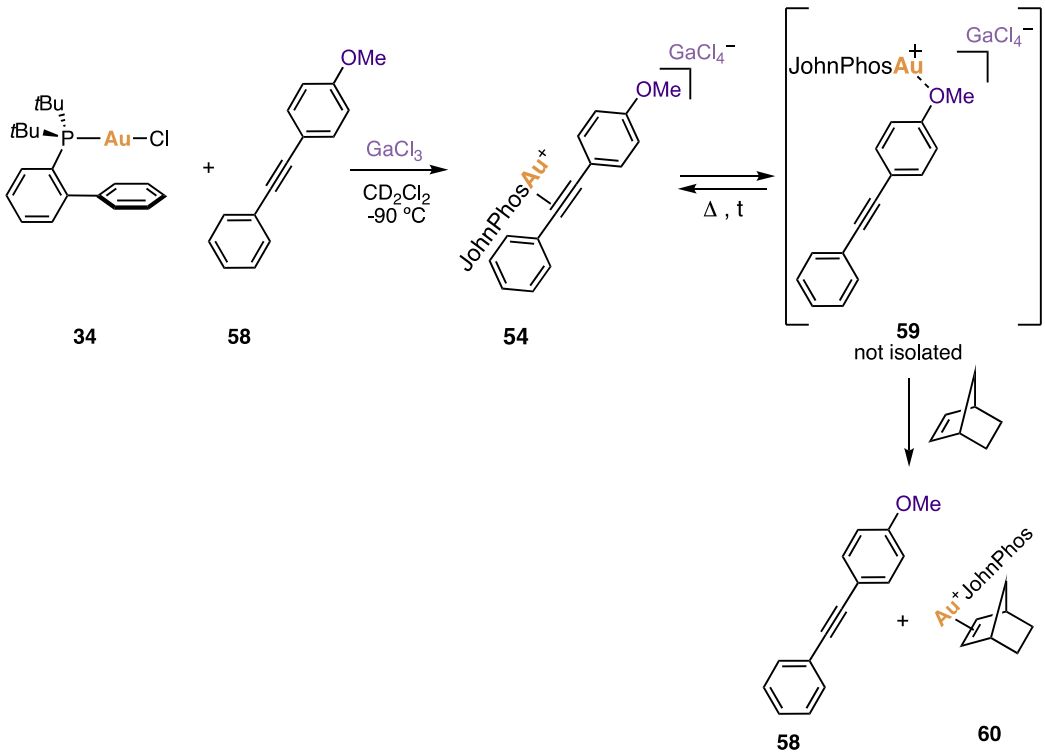

Scheme 26. Control experiment to elucidate the reactivity of gold(I) vinylidenoid **44** ***E***.

Thus, the addition of 3.0 equivalents of norbornene to the reaction of gold(I) vinylidenoid **44** ***E*** with $GaCl_3$, allowed us to confirm the preservation of the migration ratio after decomposition of (η^2-diarylacetylene)Gold(I) complex **54** into the free alkynes.

The integration of the isotopic ^{13}C labelled signals of the alkynes formed after the 1,2-arylmigrations (Scheme 24), allowed the measurement of the migration ratio of the aryl substituents in each case of study. The outcomes of the reactions are explained in ascending order of electron-donation of the aryl substituents (Table 1).

64 See experimental section.

Gold(I) vinylidenoid **50** ***E*** disclose a highly preferred migration trend of the phenyl ring over the trifluoromethylphenyl ring, with 10 to 90 ratio (Table 1, entry 1). This indicates a highly preferred migration of the most electron-rich aryl ring (phenyl), situated in the *trans* position to the chloride in the starting material.

Gold(I) vinylidenoid **43** presents a migration ratio of 60 to 40 (Table 1, entry 2)., with a preferred migration of the fluorophenyl substituent, although with a low difference over the migration of the phenyl substituent. In this case, we found a higher migration of the less electron-rich aryl substituent, however, this could be due to the special nature of the *p*-fluorine substituent. Despite being an electron-withdrawing group, fluorine has the ability of stabilizing aromatic systems through the interactions of its nonbonding electrons with the π system of the ring.[65] This situation can cause the preferred migration of the *p*-fluoro substituted ring to stabilize the positive charge of the gold(I) vinylidene, in case it is formed. Additionally, it is worth mentioning that the preferred migrating aryl group is the one in *cis* to the chlorine in the starting material **43**.

Gold(I) vinylidenoid **42** undergoes 1,2-aryl migration with a migration ratio of 45 to 55 of the tolyl group with respect to the phenyl group (Table 1, entry 3). This indicates a practically equal migration of both substituents, with a slightly preference for the migration of the less electron-rich group. Equally to the case of vinylidenoids **50** ***E***, the preferred migrating group from gold(I) vinylidenoids **42** is in *trans* to the chloride in the starting material.

Finally, gold(I) vinylidenoid **44** ***E***, presents a migration ratio of 20 to 80 (Table 1, entry 4)., with a high preference of migration of the phenyl ring, situated in the *trans* position to the chloride in the starting material. In this case, we were highly surprised of the migration of the clearly more electron-deficient substituent over the anisyl one. It is unclear if this 1,2-migration is influenced by any coordination of gold(I) to the OMe substituent.

65 Fuhrer, T. J.; Houck, M.; Iacono, S. T. *ACS Omega* **2021**, *6*, 32607−32617.

Table 1. Results of the migration experiments

Entry	Vinylidenoid	R	Migration ratio Ar : Ph	*cis/trans* mig. to Cl	Comment
1	50 *E*	CF_3	10 : 90	*trans*	Mig. of most electron-rich aryl
2	43	F	60 : 40	*cis*	Similar mig. trend
3	42	Me	45 : 55	*trans*	Similar mig. trend
4	44 *E*	OMe	20 : 80	*trans*	Mig. of less electron-rich aryl
5	44 *Z*	OMe	45 : 55	*cis*	Similar mig. trend

The substrates present a non-linear migration trend, with a clear preference of the phenyl migration in the case of the –OMe and $–CF_3$ phenyl substitution (vinylidenoids **44** ***E*** and **50** ***E***). This is consistent with the fact that in other metal vinylidenoids, there is a preferred migration of the group opposite to the halogen group,[66] indicating a clear influence of the chloride abstraction in the reactivity of gold(I) vinylidenoids. However, when the Hammett σ constants of the substituents are similar, –F *vs* –H and –Me *vs* –H, we observe a very similar migration trend, even with a preferred migration of the substituent in *cis* to the halogen in the case of vinylidenoid **43**. This would indicate an extremely dependency on the migration aptitude of the substituent more than on the position of this one, supporting the existence of the elusive gold(I) vinylidene intermediates. These results are in accordance with the ones observed in free vinylidenes generated from their diazo precursors, showing a very similar migration trend for substituents with similar electronics and bulkiness.[58]

In contrast, according to previous results reported from the migration of free vinylidenes generated from their diazo precursors, free vinylidenes always show a preferred migration of the more electron-rich substituent,[58] while in our case, the migration seems not to follow this trend for most of the cases (vinylidenoids **42**, **43** and **44** ***E***) indicating a high influence of the chloride abstraction.

To clarify this aspect, gold(I) vinylidenoid **44** ***Z*** was treated with $GaCl_3$ at low temperature, confirming a change in the ratio of the migration products formed. In this case, the formation of the coordinated product with the –OMe group was even faster, so the ratio of products was studied directly in the free diarylacetylenes **58** after the addition of the olefin (Scheme 27).

66 (a) Bothner-By, A. A. *J. Am. Chem. Soc.* **1955**, *77*, 3293–3296. (b) Curtin, D. Y.; Flynn, E. W.; Nystrom, R. F. *J. Am. Chem. Soc.* **1958**, *80*, 4599–4601. (c) Kobrich G. *Angew. Chem. Int. Ed.* **1967,** *6*, 41–52.

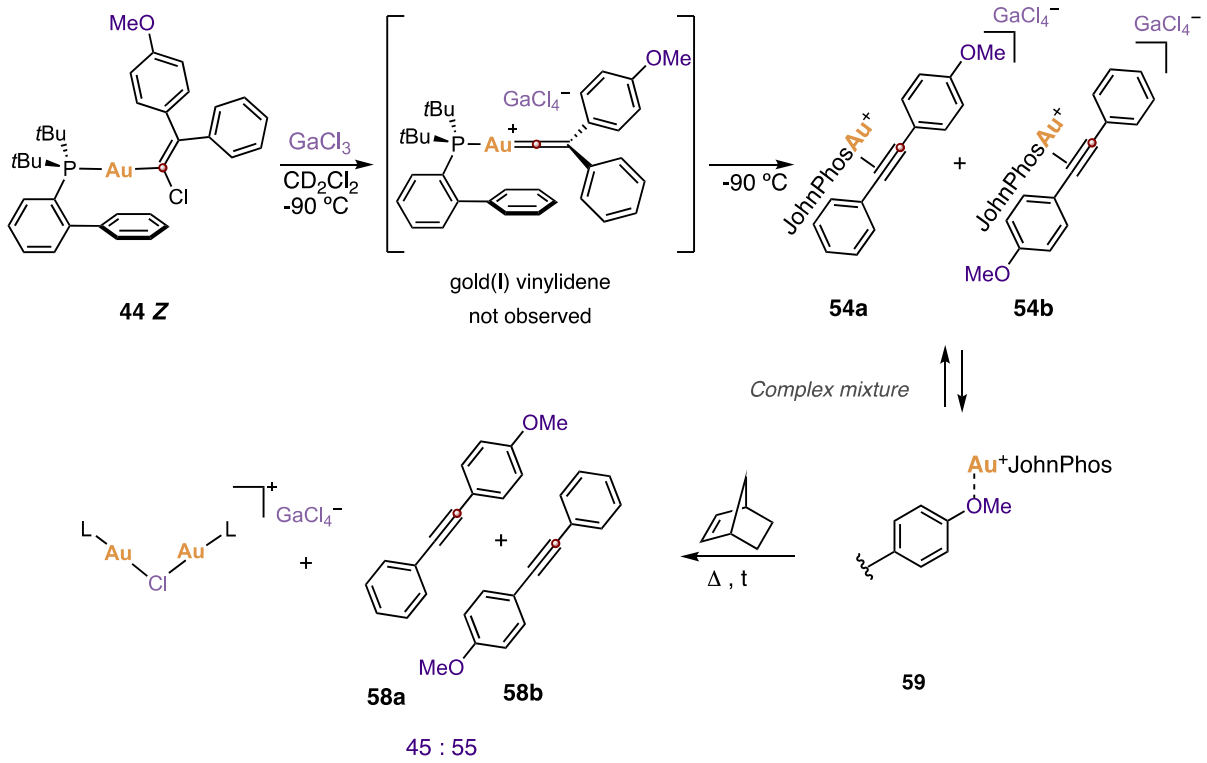

Scheme 27. Reactivity of gold(I) vinylidenoid **44 Z** with $GaCl_3$.

The ratio observed this time was of 45 to 55 with a preferred migration of the phenyl group (Table 1, entry 5). This could indicate a competition between two reaction pathways, one favouring the migration of the aryl in *trans* to the chloride in starting material vinylidenoid **44 *Z***, and other one which favours the stabilization of an intermediate species. This experiment confirms the high influence of the chloride abstraction, at least in the case of vinylidenoids **44**.

To confirm that $GaCl_3$ did not affect the reactivity of the substrates, we performed a control experiment treating alkenylchloride **38** ^{12}C isotopologue with $GaCl_3$ (Scheme 28). The test showed no reaction at all, confirming that $GaCl_3$ does not promote the 1,2-shift migration.

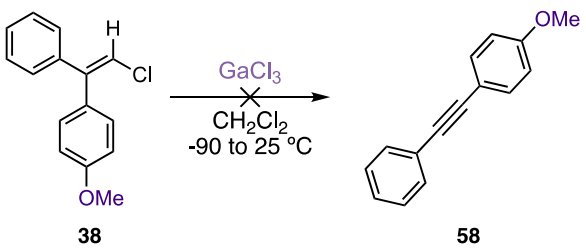

Scheme 28. Control experiment with $GaCl_3$.

To go a step further and with the aim of confirming the strong influence of gold(I) in these transformations, we studied the Fritsch-Buttenberg-Wiechell (FBW) rearrangement of the alkenyl chlorides **38** (Scheme 29).

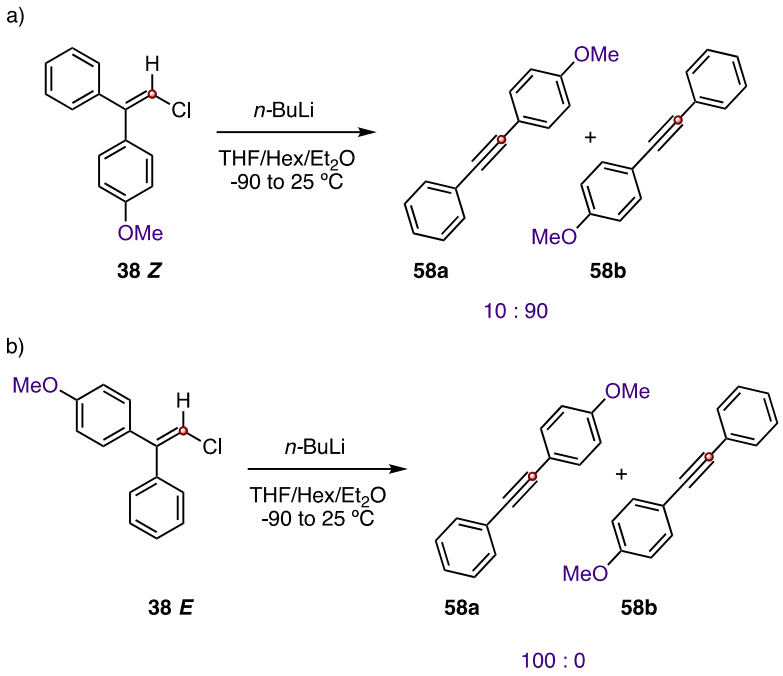

Scheme 29. FBW rearrangement of alkenyl chlorides **38**.

The experiments showed a clear preferred migration of the aryl in *trans* to the halogen, and the ratios of the products greatly differ from the experiments starting from gold(I) vinylidenoids **44**. According to FBW rearrangement, alkynes are formed from metal vinylidenoids via free vinylidenes after halodemetallation. If the vinylidenoids would not have vinylidene character, 1,2-migration wouldn´t take place, and a heteroatom substituted alkene would be obtained.[67] The different results in the presence or absence of gold(I) indicates that we are passing through different intermediates (Table 2), however according to FBW rearrangement we would be passing through (gold or free) vinylidenes in both cases. This could give us insights about the presence of a gold(I) vinylidene as an intermediate of the studied reactions, however, more evidence will be needed to confirm the existence of these species.

67 Kimura, T.; Sekiguchi, K.; Ando, A.; Imafuji A. *Beilstein J. Org. Chem.* **2021**, *17*, 1352–1359.

Table 2. Summary of migration trend results.

Entry	Substrate	Migration ratio Ar : Ph	*cis/trans* mig. to Cl	Comment
1	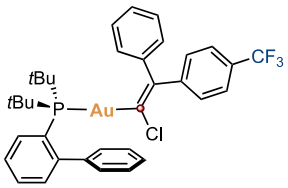 **50 *E***	10 : 90	*trans*	Mig. of most electron-rich aryl
2	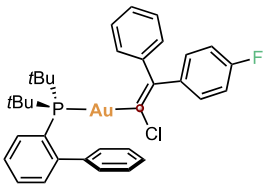 **43**	60 : 40	*cis*	Similar mig. trend
3	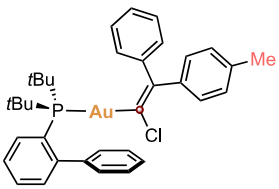 **42**	45 : 55	*trans*	Similar mig. trend
4	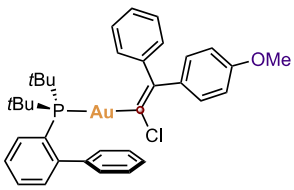 **44 *E***	20 : 80	*trans*	Mig. of less electron-rich aryl
5	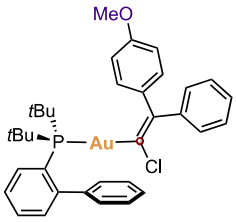 **44 *Z***	45 : 55	*cis*	Similar mig. trend
6	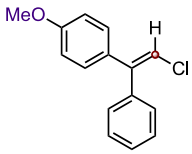 **38 *E***	100 : 0	*trans*	Mig. of most electron-rich aryl
7	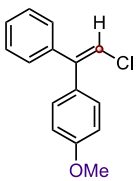 **38 *Z***	10 : 90	*trans*	Mig. of less electron-rich aryl

Stabilization Studies of Gold(I) Vinylidenes

Based on the observed reactivity of the synthesized gold(I) vinylidenoids, the stabilization of gold(I) vinylidenes was tested from two different approaches: blocking completely the migration or setting two substituents reluctant to migrate in the alkene unit (Scheme 30).

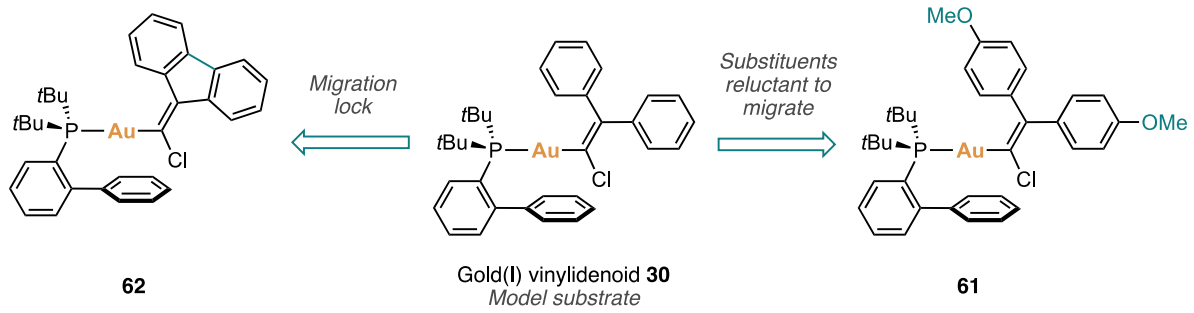

Scheme 30. Strategies for the stabilization of gold(I) vinylidenes.

Both gold(I) vinylidenoids were synthesized in just two steps starting from the structurally corresponding ketones, following a similar procedure to the one used for vinylidenoids **44** and **50**.[68] In these cases no isotopic labelling was needed, since migration studies were not done. Additionally, since the organic moiety of the vinylidenoids was symmetric, there was no need of forming a trisubstituted olefin, so the Wittig reaction was directly performed using PPh_3 and CCl_4 to obtain alkenyldichlorides precursors **64** and **66** in moderate and good yields. The subsequent Li-halogen exchange with *n*-BuLi paved the way for the introduction of JohnPhos gold(I) via a transmetalation process, obtaining gold(I) vinylidenoids **61** and **62** in moderate yields (Scheme 31). The structure of gold(I) vinylidenoid **62** was confirmed by X-Ray diffraction (Figure 10).

68 Rezaei, H.; Normant J. F. *Synthesis* **2000**, *1*, 109–112.

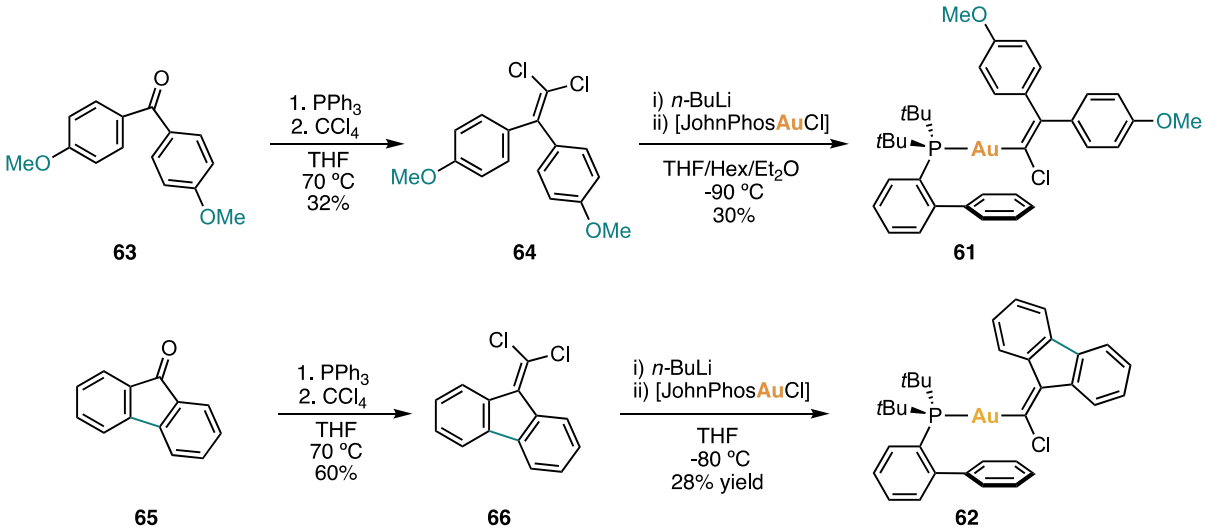

Scheme 31. Synthesis of gold(I) vinylidenoids **61** and **62**.

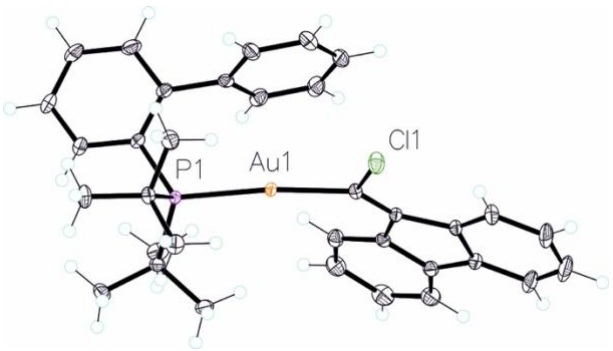

Figure 10. X-Ray structure of gold(I) vinylidenoid **62**.

The treatment of gold(I) vinylidenoid **61** with $GaCl_3$ at –90ºC revealed once more 1,2-aryl migration but, again, signals corresponding to gold(I) vinylidene **67** intermediate were not identified (Scheme 32).

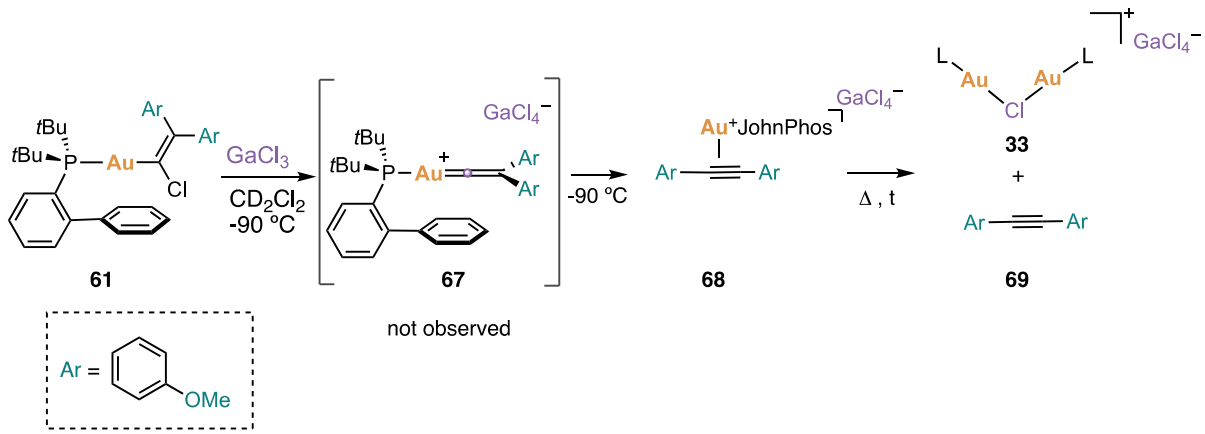

Scheme 32. Treatment of gold(I) vinylidenoid **61** with $GaCl_3$.

Finally, fluorenyl gold(I) vinylidenoid **62** was submitted to the usual chloride abstraction with $GaCl_3$ at low temperature, however, to our disappointment, the block of the migration did not stabilize the gold(I) vinylidene **70**. By the contrary, gold(I) vinylidenoid **62** was too stable to migrate and it favored the protodeauration as the only reaction taking place (Scheme 33).

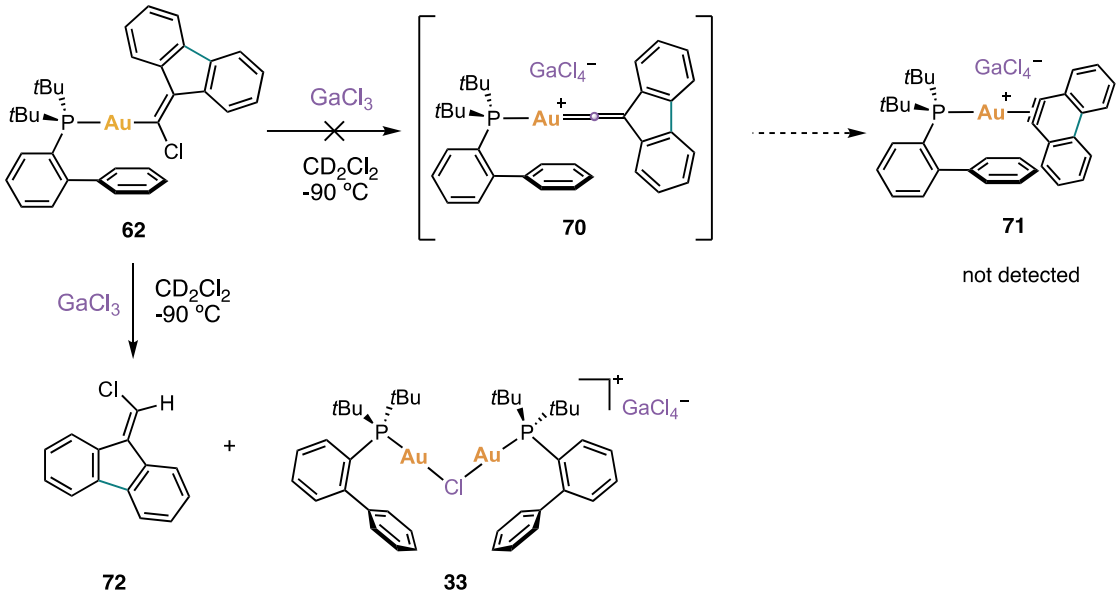

Scheme 33. Treatment of gold(I) vinylidenoid **62** with $GaCl_3$.

Structural Analysis of Gold(I) Vinylidenoids

The molecular structures of gold(I) vinylidenoids **30**, **42**, **43**, **44** ***Z*** and **62** provided us the opportunity of analyzing their features (Figure 11). They confirmed the space disposition of the atoms in the complexes and allowed us to measure key distances and angles, comparing them with the one reported for other metal vinylidenoids (Table 3). Additionally, C**1**–Au distances were compared to the ones known for gold(I) carbenoids.

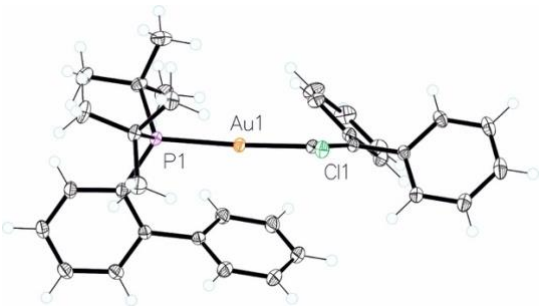

Gold(I) vinylidenoid **30**

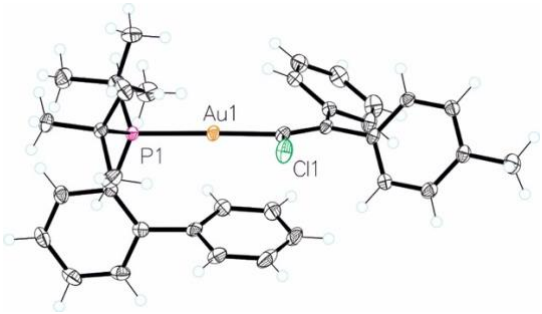

Gold(I) vinylidenoid **42**

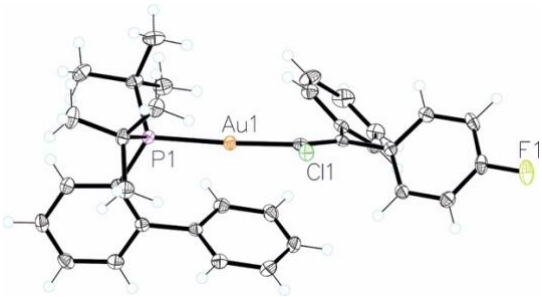

Gold(I) vinylidenoid **43**

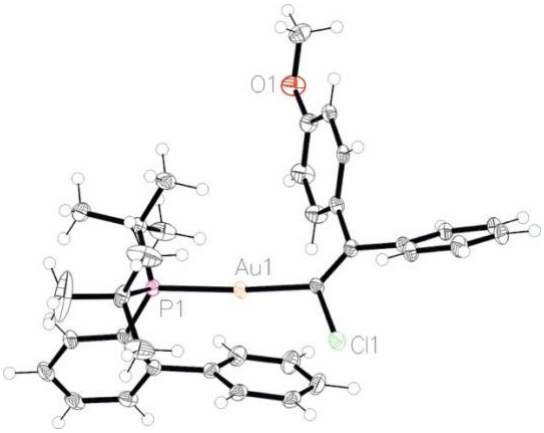

Gold(I) vinylidenoid **44** ***Z***

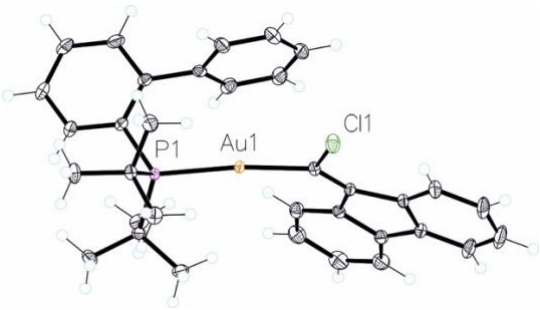

Gold(I) vinylidenoid **62**

Figure 11. X-ray crystal structures of some of the gold(I) vinylidenoids synthesized.

Measured Au–C1 distances are within the range of 2.037–2.047 Å (Table 3, column 2), even shorter than in previous gold(I) carbenoids reported.[69] Additionally, this bond lengths are shorter than the expected M–C1 distances for Mg and Li vinylidenoids (2.071–2.140 Å).[70]

69 (a) Steinborn, D.; Becke, S.; Herzog, R.; Günther, M.; Kircheisen, R.; Stoeckli-Evans, H.; Bruhn, C. *Z. Anorg. Allg. Chem.* **1998**, *624*, 1303–1307. (b) Sarria Toro, J. M.; García-Morales, C.; Raducan, M.; Smirnova, E. S.; Echavarren, A. M. *Angew. Chem. Int. Ed.* **2017**, *56*, 1859–1863.

70 Kimura, T.; Satoh, T. *Tetrahedron* **2013**, *69*, 6371–6374.

By the contrary, the elongation of C1–Cl distances is more evident in the case of lithium or magnesium vinylidenoids.[71] However, in the case of the synthesized gold(I) vinylidenoids, the C1–Cl bond distances (1.779–1.807 Å, Table 3, column 3) are still slightly longer than the average for C_{sp}–Cl bonds (1.735 Å). [70, 71a] The lengths of the alkene bond C1–C2 (1.343–1.353 Å, Table 3, column 4) are in agreement with the one measured in a similar lithium vinylidenoid (1.344 Å). [71b]

Table 3. Selected parameters from X-ray crystal structures and chemical shifts of some of the gold(I) synthesized vinylidenoids.

Structure	**Au-C1** (Å)	**C1-Cl** (Å)	**C1-C2** (Å)	**Cl-C1-C2** (º)	**Au-C1-C2** (º)	**C1** (ppm)
30	2.038	1.799	1.352	115.79	134.03	174.1
42	2.042	1.798	1.344	115.69	135.33	173.9
43	2.037	1.807	1.353	115.35	134.5	174.6
44 *Z*	2.046	1.788	1.343	117.56	129.75	172.9
62	2.047	1.779	1.349	117.77	130.34	190.9

As we can observe, all the structures showed angles that move away from the expected sp^2–hybridized geometry of the C1. The Au–C1–C2 angle of all the structures (Table 3, column 6) is broader than 120, with values from 129.8 to 135.3º, whereas the Cl–C1–C2 angles (Table 3, column 5) are also smaller than the expected 120º. This indicates a high s character of the C1–Au bond, and a higher p content on the C1–Cl bond, in accordance to the structural characteristics of other Li arylvinylidenoids.[71b,c] Additionally, the strong downfield shift of the ^{13}C NMR shift of the C1 atom (Table 3, column 7), evidences the strong electrophilic character of these species. All the above-mentioned features would indicate the suitability of the synthesized gold(I) vinylidenoids for the generation of gold(I) vinylidenes after chloride abstraction.

71 (a) Maercker, A. *Angew. Chem. Int. Ed. Engl.* **1993**, *32*, 1023–1025. (b) Boche, G.; Marsch, M; Müller, A.; Harms, K. *Angew. Chem. Int. Ed. Engl.* **1993**, *32*, 1032–1033. (c) Boche, G.; Harms, K.; Marsch, M.; Müller, A. *J. Chem. Soc. Chem. Commun.* **1994**, 1393–1394.

Computational Studies of Gold(I) Vinylidenes

As it was showed in the second section of this chapter, preliminary DFT studies supported the tendency of gold(I) vinylidenes to undergo 1,2-aryl migration. For this reason, to get a complete picture of the mechanism of the transformations exposed in this chapter, we decided to study them by DFT. B3LYP-D3/6-31G(d,p) + SDD(Au) level of theory representing CH_2Cl_2 with the PCM was used, considering its efficiency proved in other studies of gold(I) related complexes.[55]

1,2-Aryl migration of the gold(I) vinylidenes presumably formed after the chloride abstraction was evaluated. With that aim, the reaction pathway for the 1,2-aryl migration of gold(I) vinylidenes **IV**, **V** and **VI** was depicted (Scheme 34), simplifying the system by omitting the counterion ($GaCl_4^-$).

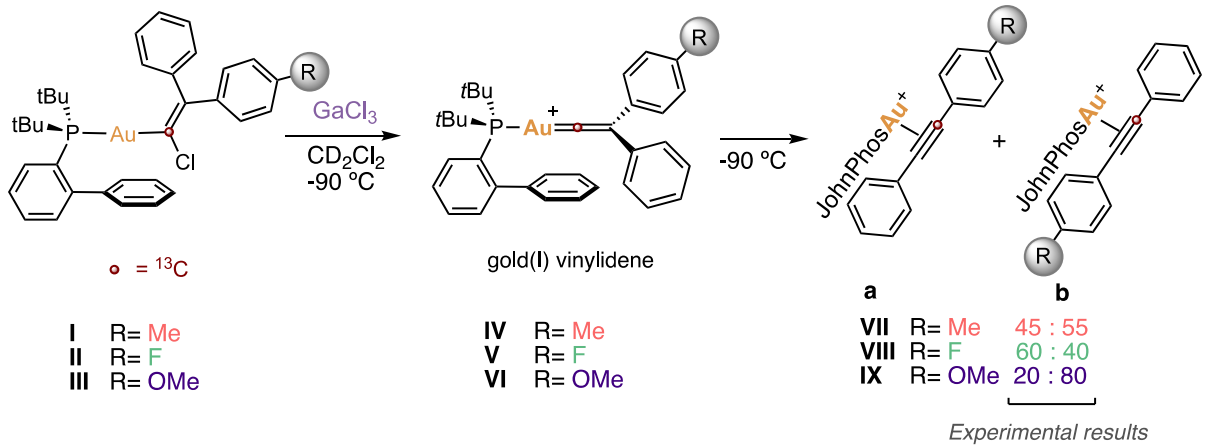

Scheme 34. 1,2-Aryl migration transformations studied by DFT.

To connect gold(I) vinylidenoids with their corresponding gold(I) vinylidenes, the chloride abstraction step needs to be considered, even more after the experimental results indicated a high influence of the chloride abstraction in the reaction outcome (Table 2). However, the study of this phase showed to be problematic. To solve this situation, we equated this step for the gold(I) vinylidenoid **III** with the nitrogen extrusion of a gold(I) vinylidene generated from its diazo precursor **III'** (Scheme 35). Thus, both isomers ***E*** and ***Z*** of gold(I) vinylidenoid **III'** were optimized and subsequently studied via a scan calculation which evaluates the nitrogen extrusion.

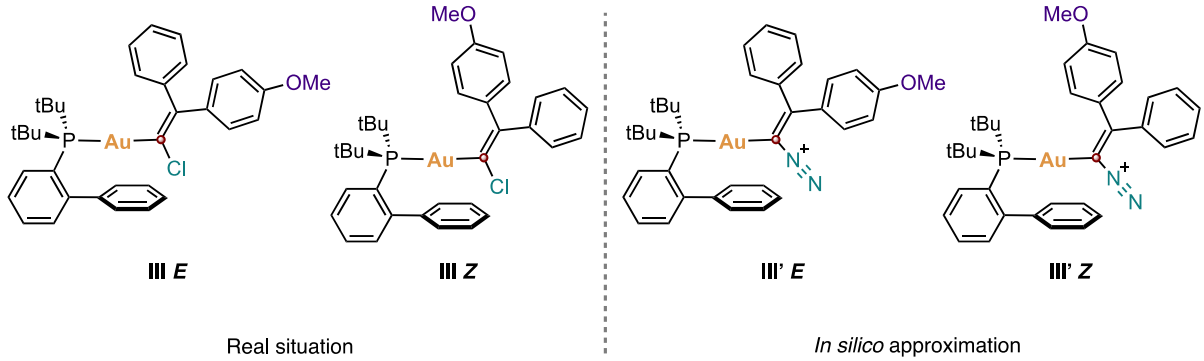

Scheme 35. Approximation of the gold(I) vinylidenoid structure to study the chloride abstraction step.

The scan calculations led to two conformational isomers of gold(I) vinylidene **VI** (Scheme 36). Gold(I) vinylidene **VIa** presented the anisyl ring perpendicular to the molecular plane, while vinylidene **VIb** presented the opposite disposition, with the phenyl ring in perpendicular to the plane. This disposition could seem surprising, since free vinylidenes were originally proposed as symmetric structures. The studies performed on this issue indicate that both isomers are interconvertible via a very low interconversion barrier and that each one of the conformational isomers leads to a different product of the 1,2-shift reaction.

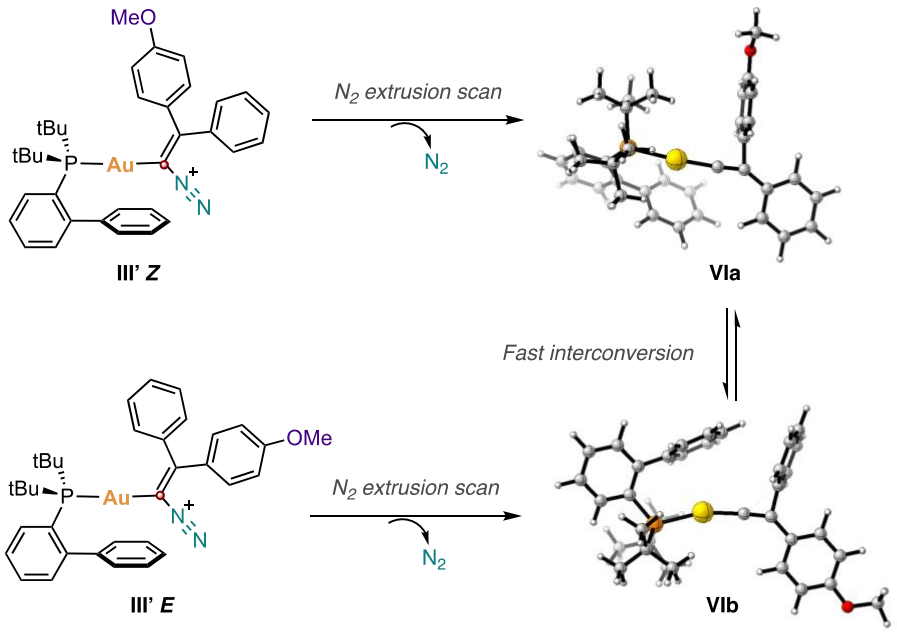

Scheme 36. Nitrogen extrusion scan of **III' *Z*** and **III' *E***.

Once elucidated the connection between gold(I) vinylidenoids and gold(I) vinylidenes, the 1,2-aryl migration reaction pathway was studied for the three different vinylidenes **IV**, **V** and **VI** (Schemes 37,

38 and 39). In all cases, a different reaction pathway was elucidated for each conformational isomer of the vinylidenes (**IVa** and **IVb**, **Va** and **Vb** and **VIa** and **VIb**). The disposition of the conformational isomers determines the preferred aryl migration, leading to the formation of η^2-alkynes **a** or **b**. Our calculations and previous studies indicate that both vinylidene isomers are interconvertible,[58] however the energy barrier was too low to be found.

In all the cases low activation barriers ($\Delta G^{\ddagger}$ = 4.0–6.4 kcal/mol) of the 1,2-aryl shift from gold(I) vinylidenes to form (η^2-diarylacetylene)gold(I) complexes are observed. This would explain the impossibility of observing the gold(I) vinylidenes during the reaction, even when it is run at –90ºC.

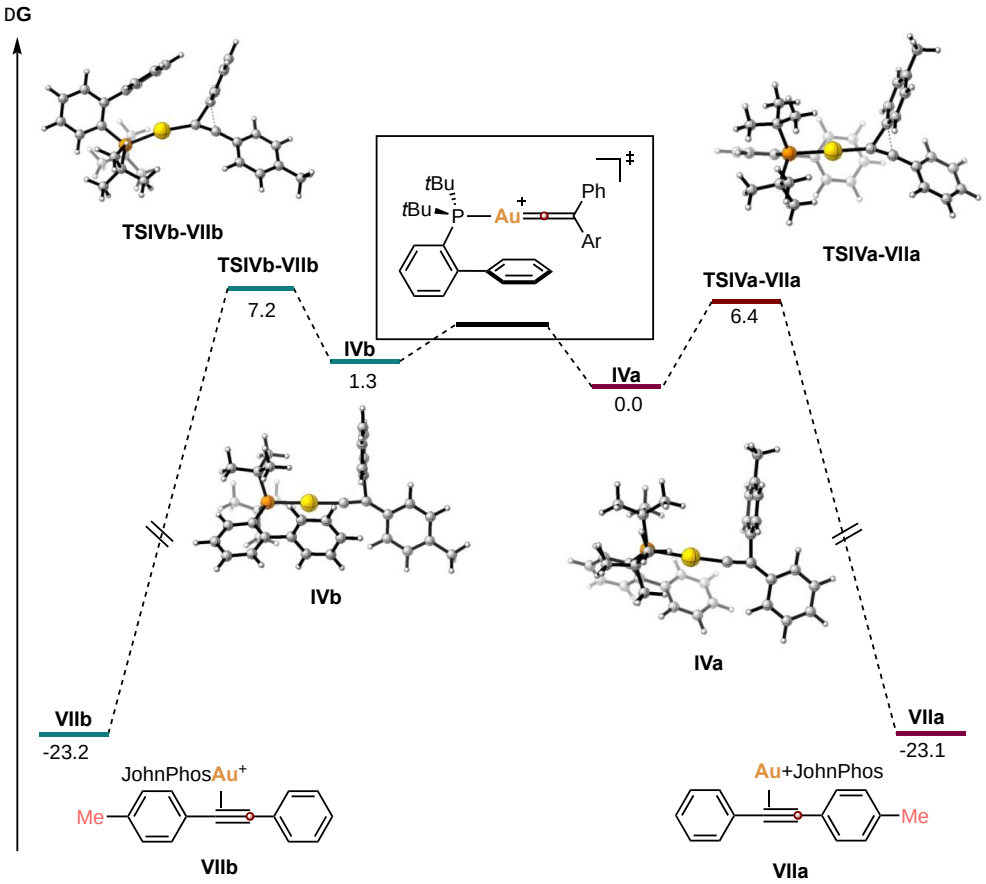

Scheme 37. Free energy profiles for the 1,2-aryl shift of gold(I) vinylidene **IV**. The energy values are given in kcal/mol at 25 ºC and 1 atm and represent the relative free energies.

Free energy profile of gold(I) vinylidene **IV** (Scheme 37) predicts a very similar stability of both conformational isomers of the vinylidene, with a slightly higher stability of gold(I) vinylidene **IVa**. The stability of $\mathbf{TS_{IVa\text{-}VIIa}}$ and $\mathbf{TS_{IVb\text{-}VIIb}}$ is also alike, indicating a comparable migration trend. This agrees with the experimental results observed.

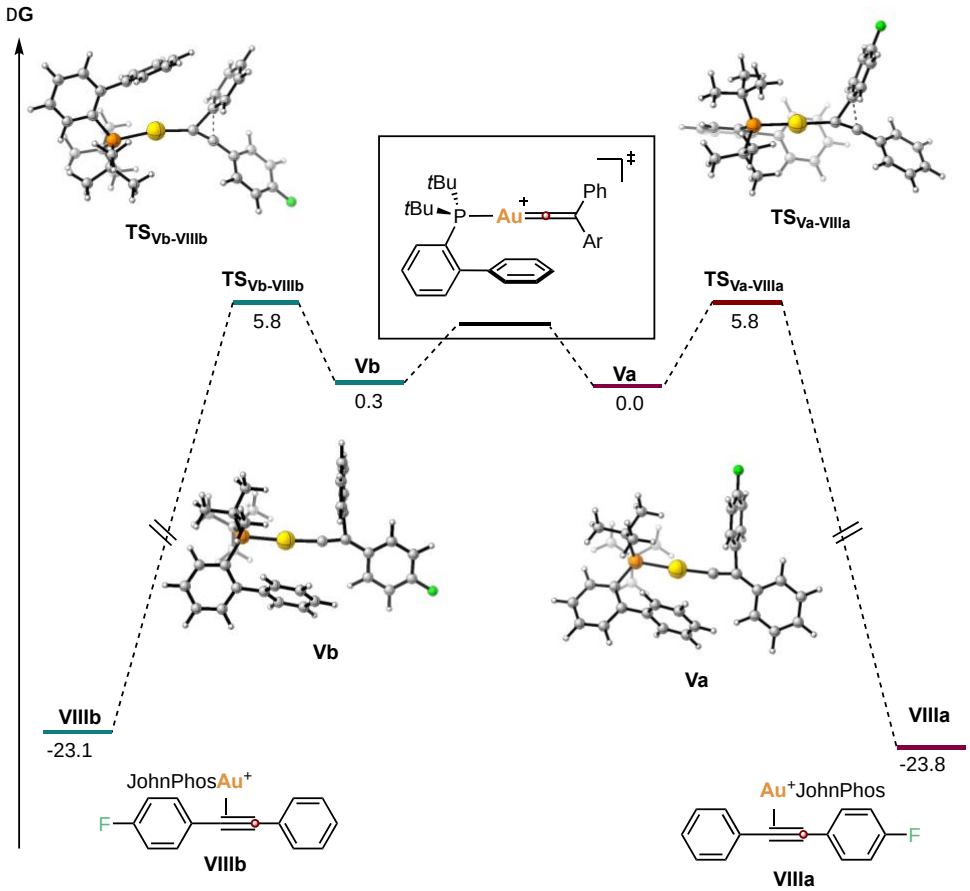

Scheme 38. Free energy profiles for the 1,2-aryl shift of gold(I) vinylidene **V**. The energy values are given in kcal/mol at 25 ºC and 1 atm and represent the relative free energies.

This situation is repeated for the free energy profile of gold(I) vinylidene **V**, in which the difference in stability between the two conformational isomers of vinylidene **Va** and **b** is even smaller, with a neglectable difference in energy (Scheme 38), Additionally, both conformational isomers display the same energy barrier towards the 1,2-aryl migration. In this case, the DFT results does not match the experimental outcome, which shows a small preference for the migration of the phenyl substituent.

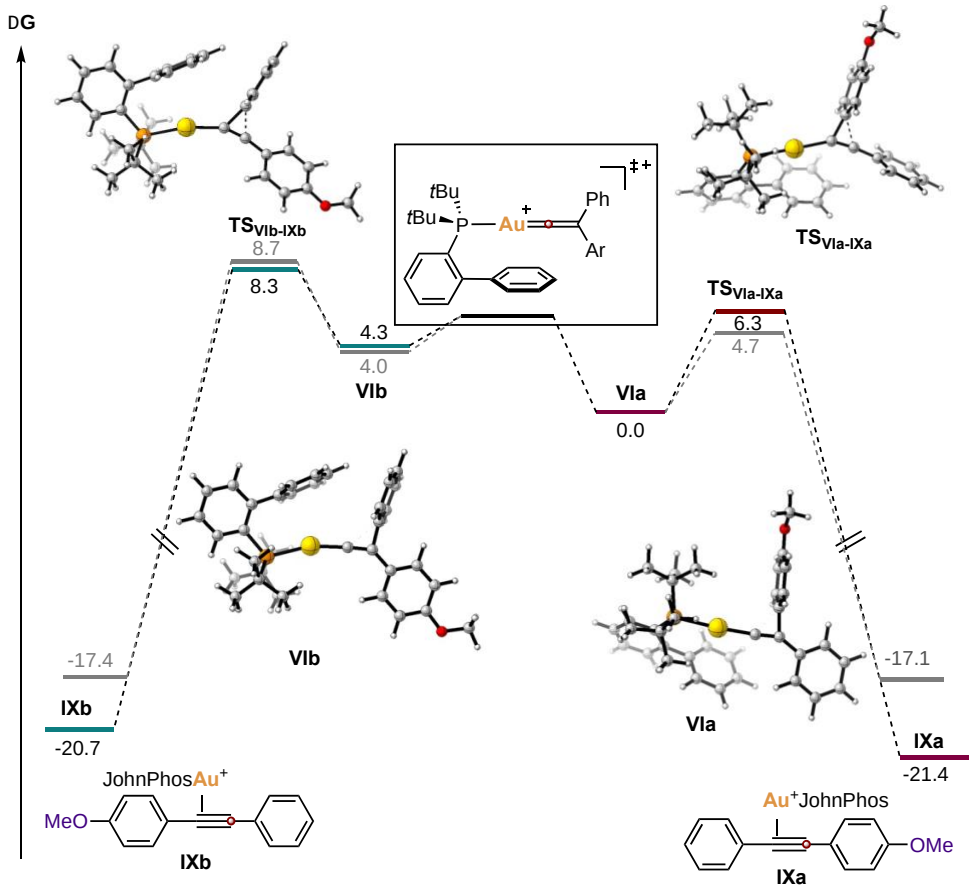

Scheme 39. Free energy profiles for the 1,2-aryl shift of gold(I) vinylidene **VI**. The energy values are given in kcal/mol at 25 ºC and 1 atm and represent the relative free energies (green and red). Energy values were also calculated at –90 ºC (grey).

The discordance between experimental and computational results increases when we analyze the free energy profile of gold(I) vinylidene **VI** (Scheme 39, green and red). According to the computational analysis, gold(I) vinylidene conformer **VIa** is 4.3 kcal/mol more stable than gold(I) vinylidene **VIb**. Additionally, the transition state between gold(I) vinylidene **VIa** and (η^2-diarylacetylene)gold(I) complex **IXa**, is also more stable than **TS$_{VIb-IXb}$**. This would result in a preferred migration of the anisyl group over the phenyl group, however, experimental results reflected the opposite situation.

To discard the influence of the temperature in the observed mismatching results, DFT frequency calculations for the 1,2-aryl shift of gold(I) vinylidene **VI** were performed considering a temperature of –90 ºC(Scheme 39, grey). However, the outcome of these calculations was very similar to the one observed at 25ºC.

Once discarded the influence of the temperature, the mismatch between the experimental and the theoretical results (Table 4*)* could be due to two main reasons: either the methodology used for studying our systems was not the appropriated one, or we were omitting an important step in the reaction. To

elucidate this issue, we performed a benchmark of DFT functionals using gold(I) vinylidene **VI** as the model substrate to discard any artifact associated to the DFT method of choice (Table 5).

Table 4. Comparison between DFT and experimental results.

Entry	Vinylidenoid	R	Experimental Migration ratio Ar : Ph	DFT predicted Mig	Agreement between DFT and experimental results?
1	**I**	Me	45 : 55	Similar mig. trend	Yes
2	**II**	F	60 : 40	Equal mig. trend	No
3	**III *E***	OMe	20 : 80	OMePh– preferred mig.	No
4	**III *Z***	OMe	45 : 55	OMePh– preferred mig.	No

The benchmark was performed choosing a combination of pure functional methods (**BP86, B97D, TPSS, PBE)** and hybrid functional methods (**B3LYP, B3PW91, BMK, M06**) to calculate the single points that were afterwards compared to the optimized minima previously computed using **B3LYP** (highlighted in blue). Additionally, we used domain pair natural orbital method, **DLPNO-CCSD(T),** that allow us to obtain high accurate energies in the faster and easier way, as a calibration method for the benchmark (highlighted in yellow).

Although the relative energies changed depending on the method used, no dramatical effect was detected with the change of the method: in all cases (including **ORCA**) gold(I) vinylidene **VIa** is more stable than gold(I) vinylidene **VIb**, and this situation is maintained in the case of the **TS**. Comparing the results of the single points energy to the ones obtained with **ORCA**, we could define **M06** as the most accurate method for this system (highlighted in green).

The benchmark results elucidated that, although **B3LYP** was not the most accurate method for studying our system, it provides consistent data to the one obtained with more accurate methods. Therefore, the mismatching with the experimental results was derived from a misinterpretation of the reaction mechanism.

Table 5. DFT functional benchmark regarding **VIa**, **VIb**, **$TS_{VIa-IXa}$** **$TS_{VIb-IXb}$**, **IXa** and **IXb.**

	VIa	VIb	$TS_{VIa-IXa}$	$TS_{VIb-IXb}$	IXa	IXb
B3LYP	0.0	4.3	6.3	8.3	-21.4	-20.7
B3LYP	0.0	3.8	6.2	7.9	-21.7	-21.4
B3PW91	0.0	4.9	6.1	7.4	-21.1	-20.8
B97D	0.0	3.6	5.9	7.6	-20.0	-19.7
BMK	0.0	5.3	6.8	6.9	-19.2	-18.3
BP86	0.0	4.1	6.1	7.4	-19.7	-19.3
M062X	0.0	6.2	4.7	5.3	-24.4	-24.7
M06HF	0.0	7.4	6.2	8.0	-24.0	-24.4
M06L	0.0	4.7	5.1	5.6	-22.6	-22.5
M06	0.0	5.4	5.2	5.6	-23.0	-23.2
PBE1PBE	0.0	5.5	6.0	7.5	-20.6	-20.3
PBEPBE	0.0	4.9	5.7	7.6	-19.1	-18.9
TPSSTPSS	0.0	4.7	6.0	7.6	-19.2	-18.9
DLPNO-CCSD(T) -ORCA	0.0	5.7	5.4	6.6	-23.8	-23.9

Dispersion GD3 was included in all the cases. Energies of single points related to **VI a** in kcal/mol, (6-31G**) basis set and SDD (Au) level in CH_2Cl_2 (PCM). Single points calculations in DLPNO-CCSD(T) for B3LYP optimized calculation.

To obtain a more accurate picture of the mechanism of the 1,2-aryl migration in gold(I) vinylidenes, we introduce the counteranion $GaCl_4^-$ in the DFT calculations. The stabilization provided by $GaCl_4^-$ allow us to optimize the transition state which connects the two possible conformers of the vinylidenes after chloride abstraction. This conformational equilibrium influences the outcome of the reaction and it is different in each substrate, since not all the cases are in a Curtin–Hammett situation. Because of this, we studied by DFT the four different 1,2-aryl migration reactions which has been previously experimentally monitored and all the situations were independently examined (Scheme 40).

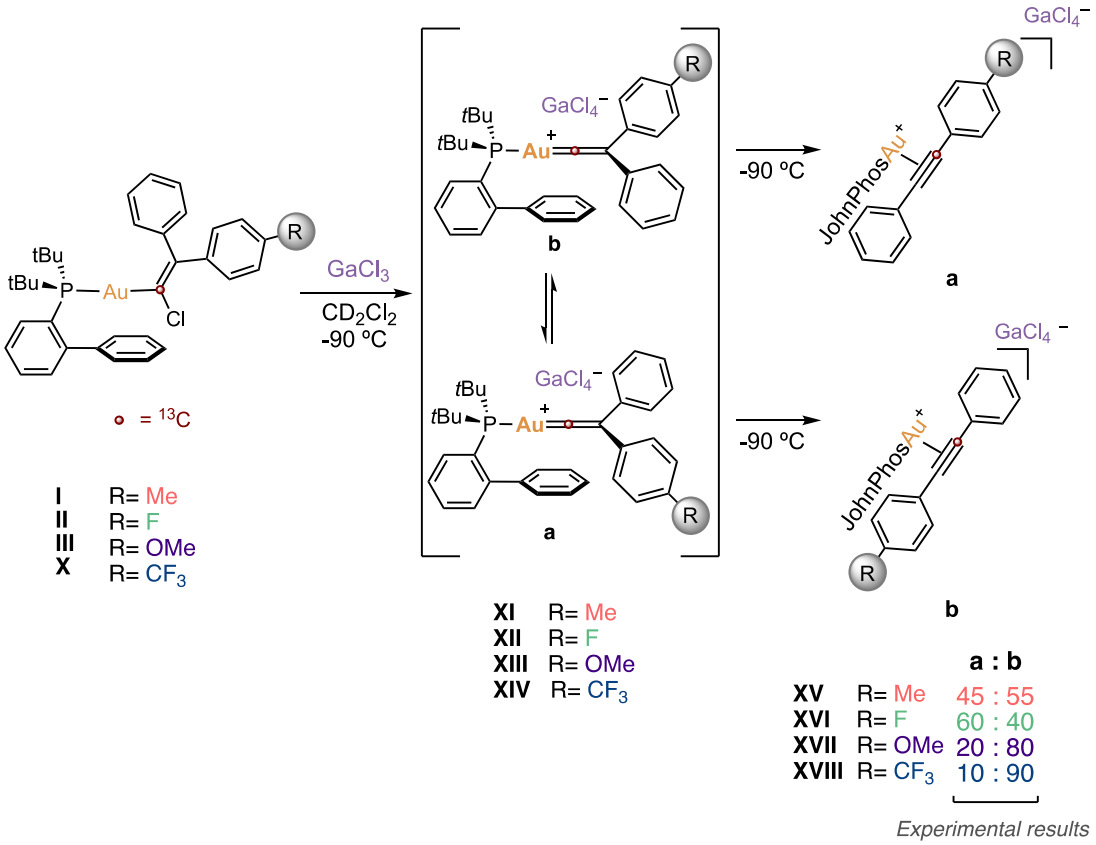

Scheme 40. 1,2-Aryl migration reactions experimentally and DFT studied.

Prior to analyze the results obtained by the DFT analysis, it is important to consider some aspects of the Curtin-Hammett principle. The Curtin–Hammett principle states that when equilibrium of conformers take place in the starting material of a reaction, the ratio of the products "depends only on the relative energy levels of the transition states by which the products are formed, provided that the activation energy for product formation is large compared to the activation energy for the interconversion of the isomeric starting materials".[72] To apply this principle, the Winstein-Holness equation was designed. Winstein-Holness equation uses the kinetic method of conformational analysis to calculate conformer equilibrium distributions. Thus, it has been stablished that a system is under Curtin-Hammett conditions when the rate of interconversion between the two conformers is 10 times higher than the rate of the reaction.[73] To elucidate if our systems are under Curtin–Hammett conditions, we needed to relate the rate constants of the reactions to the calculated energies, Eyring equation is the one commonly used to relate both parameters (eq 1). The application of this equation to the comparison between the two processes of our systems led us to equation 2,[58] where k_{mig} is referred to the rate constant

72 Eliel, E. L.; Allinger, N. L.; Angyal, S. J.; Morrison, G. A "Conformational Analysis", *Interscience, New York*, N.Y., **1965**, P. 28.

73 (a) Seeman, J. I.; Farone, W. A. *J. Org. Chem.* **1978**, *43*, 1854–1864. (b) (a) Seeman, J. I. *Chemical Reviews*, **1983**, *83*, 83–134. (c) Seeman, J. I. *J. Chem. Educ.* **1986**, *63*, 42–48.

of the aryl migration reaction while k_{conf} refers to the rate constant of the interconversion between the vinylidene conformers. The energies are the relative free energies calculated for each process and are considered in kJ/mol and finally the temperature considered is 183K.

$$k = A \exp(-E_0 / RT) \qquad \text{(Eq 1)}$$

$$\frac{k_{conf}}{k_{mig}} = \exp\left(\frac{\Delta^{\ddagger}E_{mig} - \Delta^{\ddagger}E_{conf}}{RT}\right) \qquad \text{(Eq 2)}$$

The theoretical study was performed optimizing the structures using **B3LYP**/6–31G** (C, H, P, O, F, Ga), **SDD** (Au) level of theory. However, to discard any artifact associated to the DFT method of choice, we performed a benchmark of eight different levels of theory, using 4 different functionals and changing the basis set from 6-31G** to the larger 6-311+G**. The functionals used for this comparative were **B3LYP**, **PBE0**, **M06**, **B97D**. The choice of this functionals follows the explained bellow reasoning. **B3LYP** was used to be consistent with the previous calculations performed for this system, its use allowed us to compare our results to the previously one obtained. **M06** is the DFT method which showed to be more accurate in the benchmark (Table 5). Finally, **PBE0** and **B97D** had been previously used in theoretical studies of free vinylidenes systems.[59] In this analysis we will follow the same order as the one stablished for the analysis without the counter anion.

The first case of study covers the reactivity of gold(I) vinylidenoid **I** after its treatment with $GaCl_3$ (Scheme 41). In this system, the two vinylidene conformers **XIa** and **XIb** are very similar in terms of stability. The competition between the interconversion ($\Delta G^{\ddagger}_{\mathbf{XIb\text{-}XIa}}$= 3.0 kcal/mol, $\Delta G^{\ddagger}_{\mathbf{XIa\text{-}XIb}}$= 2.0 kcal/mol) and the migration pathways ($\Delta G^{\ddagger}_{\mathbf{XIa\text{-}XVa}}$= 4.7 kcal/mol and $\Delta G^{\ddagger}_{\mathbf{XIb\text{-}XVb}}$ = 5.1 kcal/mol) is balanced through the migration process, justifying the formation of the η^2–alkyne gold(I) complexes **XVa** and **XVb** in almost 1:1 ratio (Scheme 40). Moreover, the activation barriers of both migration processes are very similar, allowing the migration of both aryl substituents.

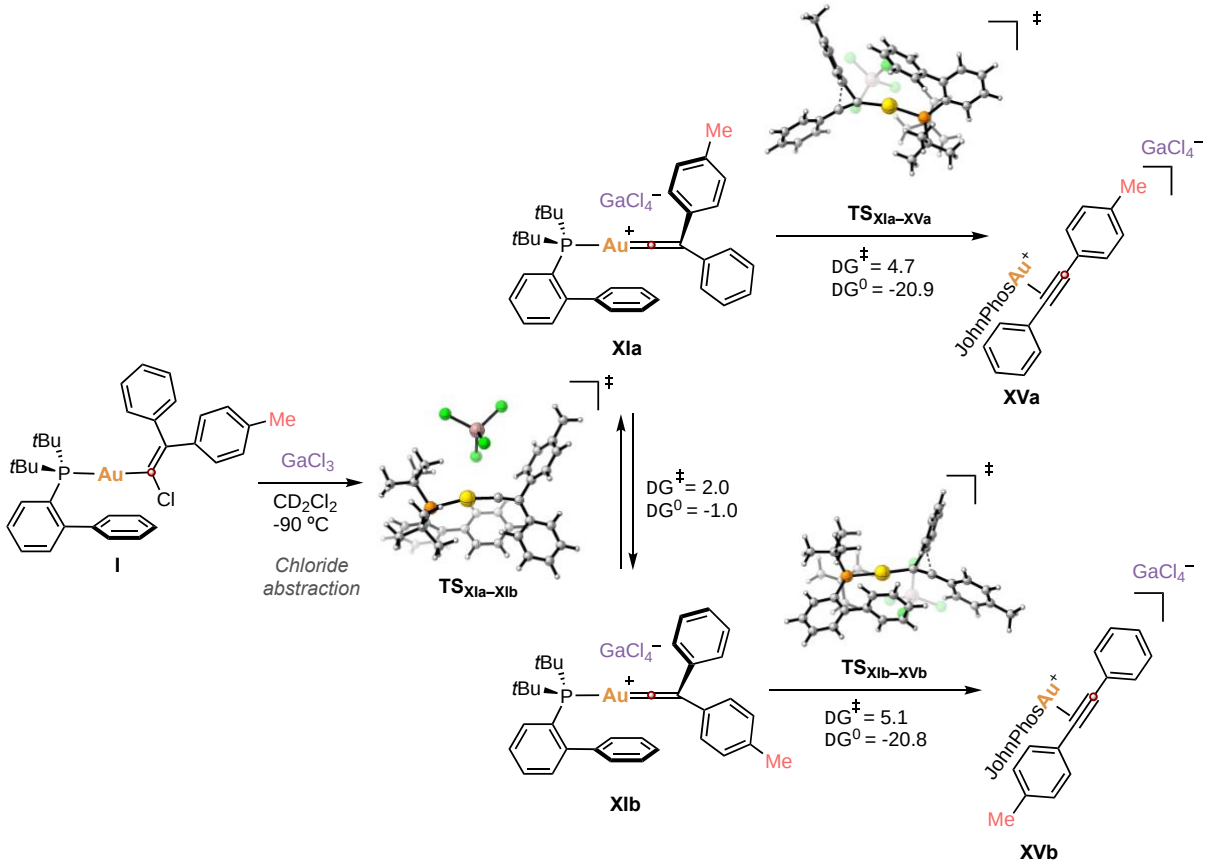

Scheme 41. Calculated Gibbs free energies of the competing processes after treatment of gold(I) vinylidenoid **I** with $GaCl_3$.

Single points calculations of the system at different levels of theory were performed obtaining the results collected in table 6 and 7. In this first case, both, absolute and relative energies values are presented, to give a full picture of the theoretical work. The values collected in table 6 show a broad dispersion of the potential energies calculated for each species with each level of theory. This is common when benchmarks are performed, whereby benchmark results are usually reported by only showing the relative energies.[74] The results of table 6 are represented in figure 12, which shows the high dispersion previously mentioned. Additionally, figure 12 shows the reaction profile calculated with each of the levels of theory, however, the wide range of the y axis and the small differences in energy of the species make difficult a correct interpretation of the data. Moreover, in this first benchmark (Table 6), the DFT level of theory is presented in the first column describing both the method and the basis

74 (a) Dale, H. J. A.; Nottingham, C.; Poree, C.; Lloyd-Jones, G. C. *J. Am. Chem. Soc.* **2021**, *143*, 2097−2107. Supporting information, pp 65–67. (b) Oeschger, R.J.; Bissig, R.; Chen P. *J. Am. Chem. Soc.* **2022**, *144*, 10330–10343. Supporting information p 29.

used. However, for facilitating the reading, in the next tables only the larger base 6-311+G** will be specified. Additionally, in the rest of the cases only relative energies will be discussed.

Table 6. Benchmark of absolute calculated energy values of 1,2-aryl migration process from gold(I) vinylidene **XI**.

	XVa	**TS $_{XIa-XVa}$**	**XIa**	**TS $_{XIa-XIb}$**	**XIb**	**TS $_{XIb-XVb}$**	**XVb**
B3LYP 6-31G**	-3513052.1	-3513024.6	-3513029.8	-3513028.7	-3513030.6	-3513024.9	-3513052
PBE0 6-31G**	-3511283.5	-3511257.7	-3511260.9	-3511259	-3511261.9	-3511258.3	-3511283.6
M06 6-31G**	-3512136.3	-3512109.5	-3512111.8	-3512110.2	-3512111.6	-3512109.5	-3512136.3
B97D 6-31G**	-3513110.4	-3513085.3	-3513089.9	-3513088.5	-3513090.6	-3513085.3	-3513110.3
B3LYP 6-311+G**	-3514639.9	-3514611.6	-3514616.9	-3514615.8	-3514617.6	-3514611.9	-3514640
PBE0 6-311+G**	-3512843	-3512816.5	-3512820	-3512818	-3512820.7	-3512817	-3512843.3
M06 6-311+G**	-3513728	-3513699.7	-3513702.3	-3513700.7	-3513701.5	-3513699.4	-3513728.1
B97D 6-311+G**	-3514692.1	-3514666	-3514671.2	-3514669.8	-3514671.7	-3514666.5	-3514692.2

All the energies are given in kcal/mol.

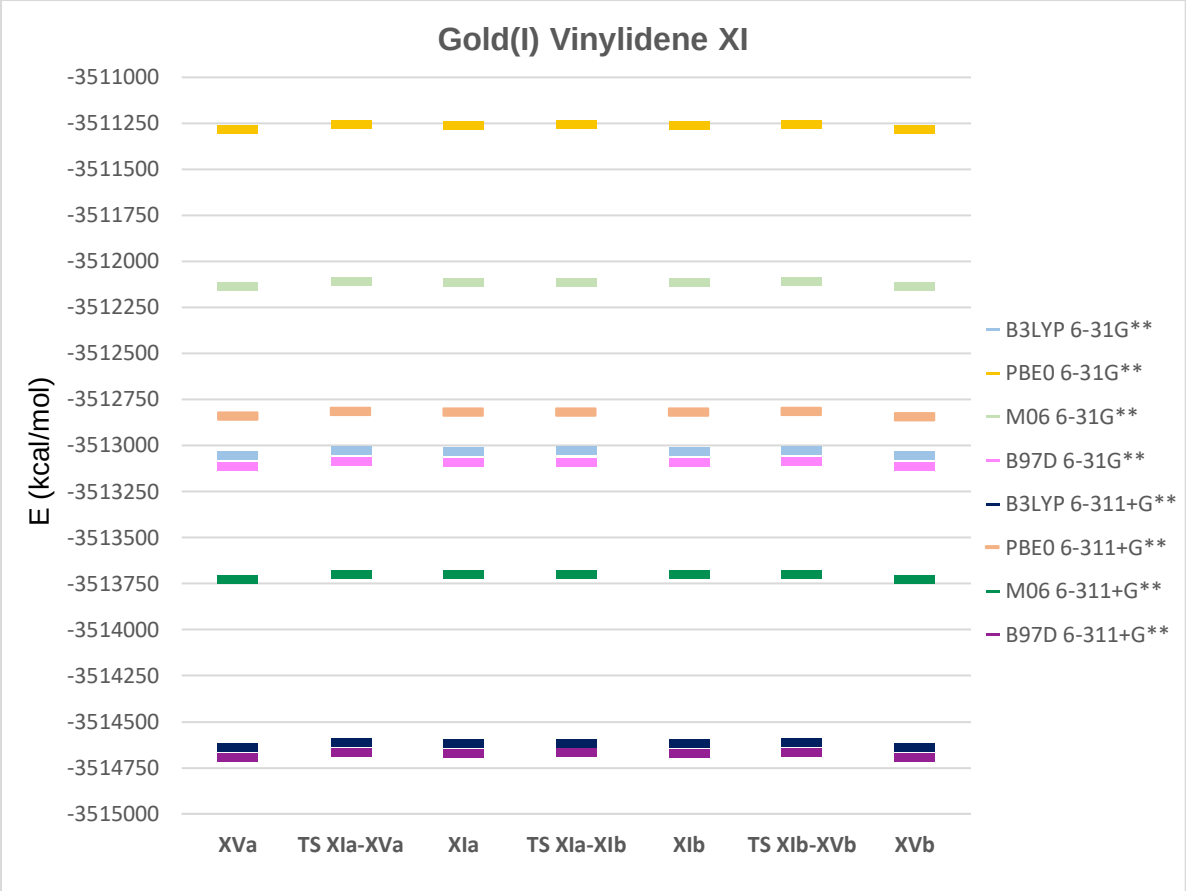

Figure 12. Representation of the absolute potential energies of the species in scheme 41 calculated at different levels of theory.

The relative energies of the competing processes of the aryl migration in gold(I) vinylidenes **XI** are collected in table 7. The results obtained are represented in figure 13. The benchmarking calculations illustrates very similar results to the ones observed in the free energies (Table 7 and Figure 13), with small differences in the stability between the two gold(I) vinylidenes conformers **XIa** and **XIb**. Additionally, the faster rate of interconversion process (**TS** $_{\mathbf{XIa\text{-}XIb}}$) in relation to the migration pathway (**TS**$_{\mathbf{XIb\text{-}XVb}}$ and **TS**$_{\mathbf{XIa\text{-}XVa}}$) is also shown in all the levels of theory used.

Table 7. Benchmark of relative potential energies of 1,2– aryl migration process from gold(I) vinylidene IV.

	XVa	TS $_{XIa-XVa}$	XIa	TS $_{XIa-XIb}$	XIb	TS $_{XIb-XVb}$	XVb
B3LYP	-21.5	6.0	0.8	1.9	0.0	5.7	-21.4
PBE0	-21.6	4.2	1.0	3.0	0.0	3.6	-21.7
M06	-24.5	2.3	0.0	1.6	0.2	2.4	-24.4
B97D	-19.7	5.7	0.8	2.1	0.0	5.3	-19.6
B3LYP 6-311+G**	-22.3	6.0	0.6	1.7	0.0	5.6	-22.4
PBE0 6-311+G**	-22.3	4.3	0.7	2.7	0.0	3.7	-22.6
M06 6-311G**	-25.7	2.6	0.0	1.6	0.8	2.9	-25.8
B97D 6-311G**	-20.4	5.7	0.6	1.9	0.0	5.3	-20.5

All the energies are given in kcal/mol.

Although the visual data indicates a Curtin–Hammett situation (Figure 13), equation 2 was applied to confirm it. The results disclose a $k_{conf}/k_{mig} \approx 1677$ for gold(I) vinylidene conformer **XIa** and a $k_{conf}/k_{mig} \approx 322$ for gold(I) vinylidene conformer **XIb**, confirming a Curtin–Hammett behavior of this process.

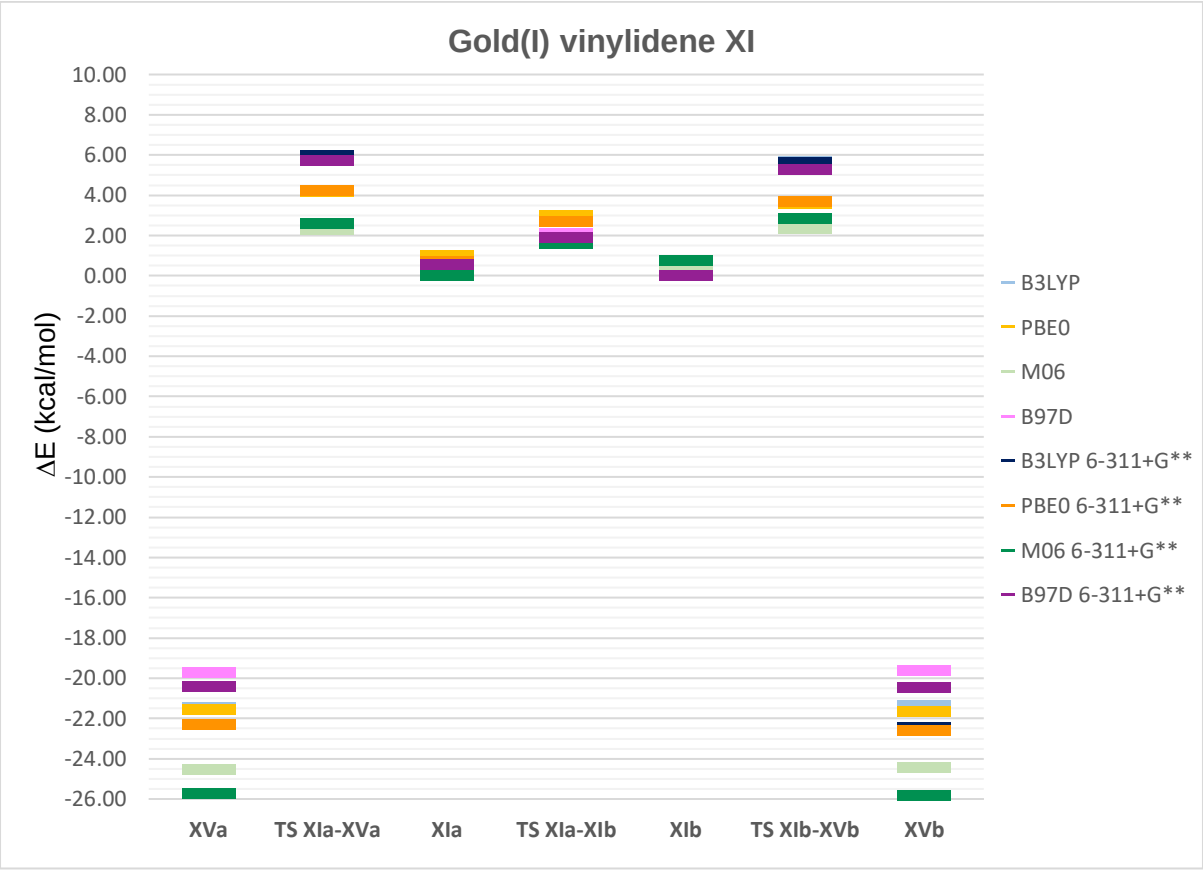

Figure 13. Representation of the relative potential energy values collected in Table 7.

Next, we studied the transformation derived from the treatment of gold(I) vinylidenoid **II** with $GaCl_3$ (Scheme 42). Gold(I) vinylidene conformer **XIIb** is 1.5 kcal/mol more stable than **XIIa** what could indicate a slightly favored migration of the phenyl substituent. However, the equilibrium energy barrier ($\Delta G^{\ddagger}_{\mathbf{XIIa\text{-}XIIb}}$ = 3.2 kcal/mol) is lower than the migration activation energies. Again, in this case the very similar migration ratio can be ascribed to the equilibrium between the two conformers. The slightly favored migration of the less electron-rich substituent observed in the experimental data (Scheme 40) can be justified by the smaller energy migration barrier of the fluorophenyl substituent ($\mathbf{TS_{XIIa\text{-}XVIa}}$, $\Delta G^{\ddagger}$= 6.6 kcal/mol).

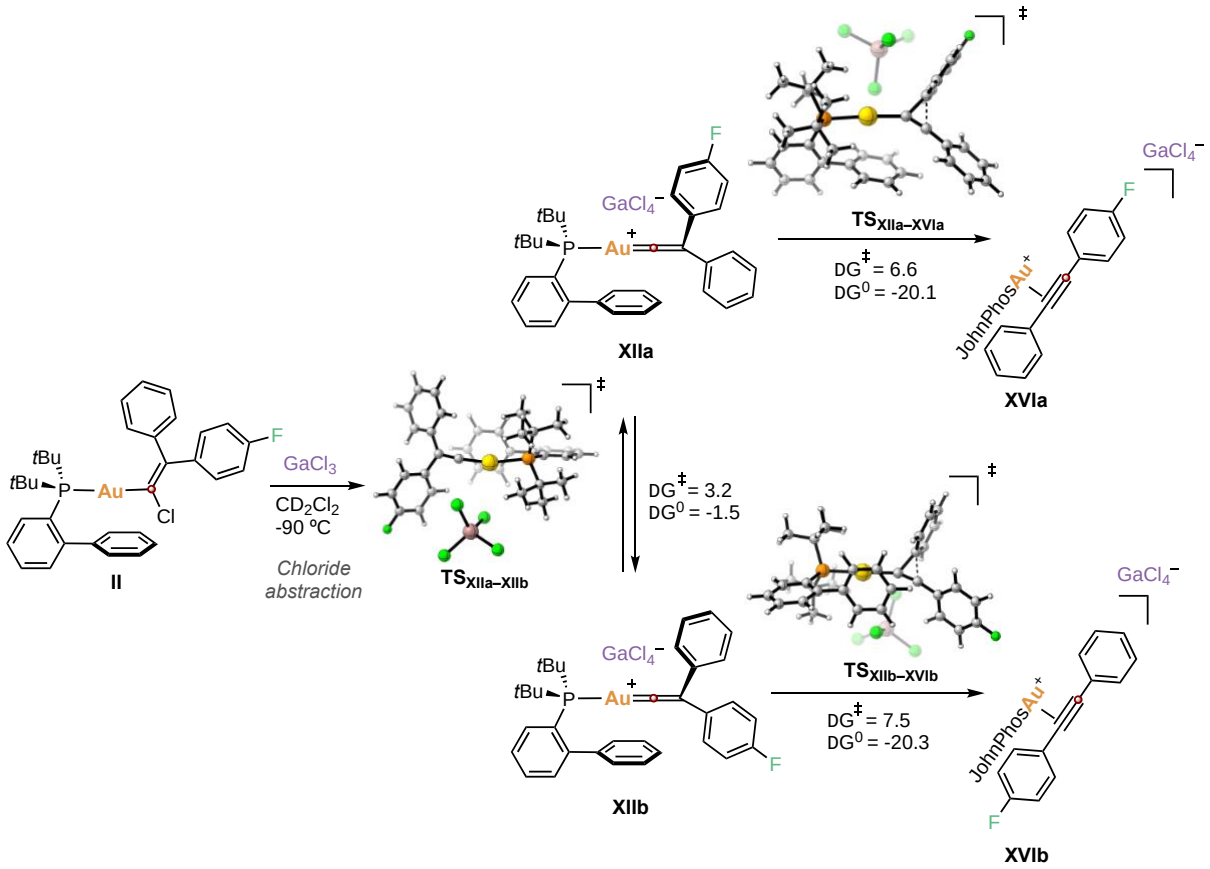

Scheme 42. Calculated Gibbs free energies of the competing processes after treatment of gold(I) vinylidenoid **II** with $GaCl_3$.

The benchmarking calculations present similar results (Table 8 and Figure 14), with differences between 1.3 and 3 kcal/mol between the interconversion and the migration processes, supporting the higher rate of the interconversion over the migration. The relationship between the rate constants of the two processes was calculated. k_{conf}/k_{mig} ≈ 11498 for gold(I) vinylidene for conformer **XIIa**, while k_{conf}/k_{mig} ≈ 2208 for gold(I) vinylidene conformer **XIIb**, confirming again that we are under Curtin-Hammett conditions.

Table 8. Benchmark of relative potential energies of aryl migration process of gold(I) vinylidenoid **II**.

	XVIa	TS $_{XIIa-XVIa}$	XIIa	TS $_{XIIa-XIIb}$	XIIb	TS $_{XIIb-XVIb}$	XVIb
B3LYP	-20.4	6.4	1.6	2.3	0.0	5.9	-21.1
PBE0	-20.5	5.3	1.3	3.8	0.0	4.4	-21.1
M06	-23.8	3.8	0.6	2.6	0.0	3.0	-24.1
B97D	-18.9	6.1	1.5	2.6	0.0	5.7	-19.4
B3LYP 6-311+G**	-22.1	6.3	1.9	2.2	0.0	6.2	-22.0
PBE0 6-311+G**	-22.0	5.0	1.4	3.6	0.0	4.7	-21.9
M06 6-311G**	-26.6	3.2	0.4	1.9	0.0	3.0	-26.0
B97D 6-311G**	-20.3	5.9	2.0	2.4	0.0	5.9	-20.2

All the energies are given in kcal/mol.

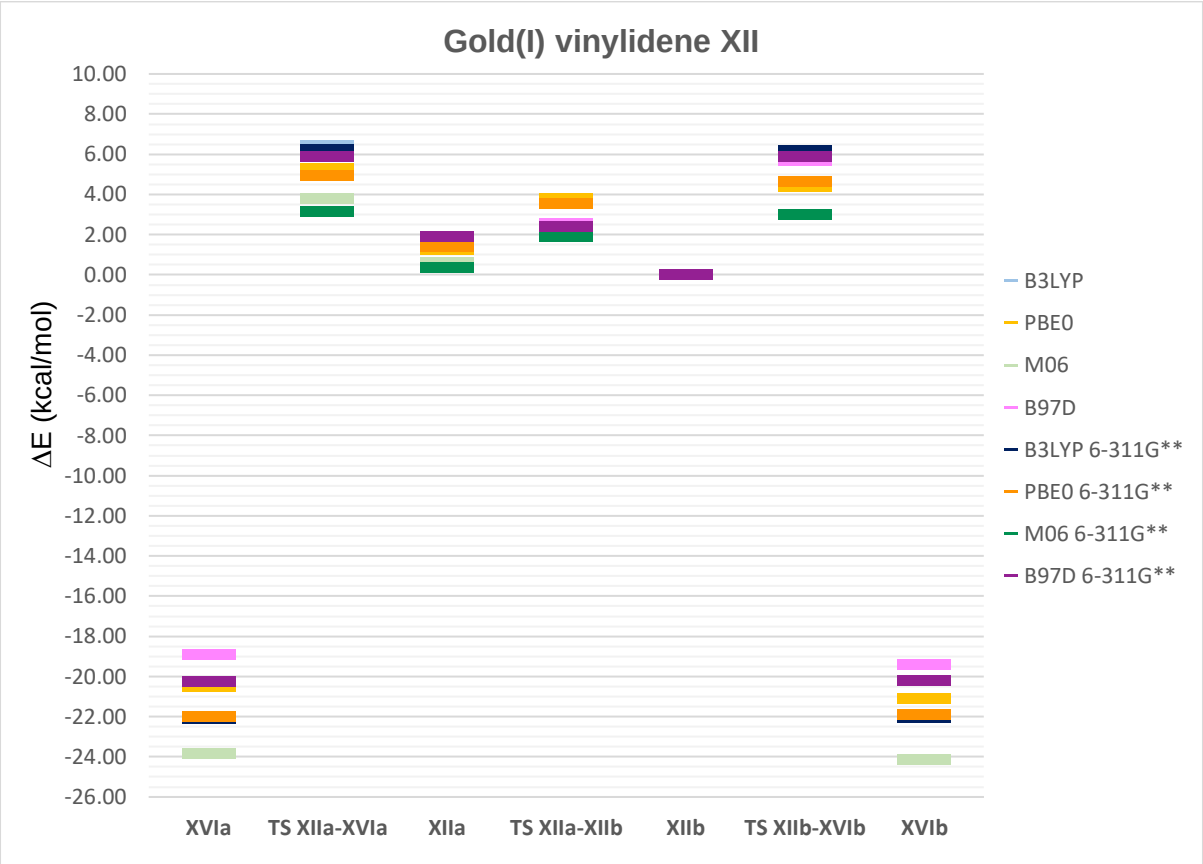

Figure 14. Representation of the relative potential energy values collected in Table 8.

The study of the 1,2-aryl migration of gold(I) vinylidene **XIII** shows equal stabilization of the two vinylidene conformers **XIIIa** and **XIIIb** (Scheme 43). The interconversion of **XIIIa** and **XIIIb** ($\Delta G^{\ddagger}_{\mathbf{XIIIa\text{-}XIIIb}}$ = 4.5 kcal/mol) competes with the aryl migration, especially in the case of the MeO-Phenyl migration (**TS$_{XIIIa\text{-}XVIIa}$**, $\Delta G^{\ddagger}_{\mathbf{XIIIa\text{-}XVIIa}}$ = 4.5 kcal/mol). In the case of the Ph migration (**TS$_{XIIIb\text{-}}$**

XVIIb) the migration barrier is slightly higher with an activation barrier of 6.0 kcal/mol. Thus, according to DFT, the preferentially product formed would be η^2–diarylacetylene gold(I) **XVIIa**, independently of the starting material. These results disagree from the experimental ones (Scheme 40), which confirms the high influence of the starting material used in the ratio of products **XVIIa** and **XVIIb** formed. Additionally, η^2–diarylacetylene Gold(I) **XVII a** is described as ≈ 3 kcal/mol more stable than η^2–diarylacetylene gold(I) **XVIIb**, from which only defers in the position of the ^{13}C isotopically labeled. All these facts make us consider the presence of artefacts derived from the theoretical method used.

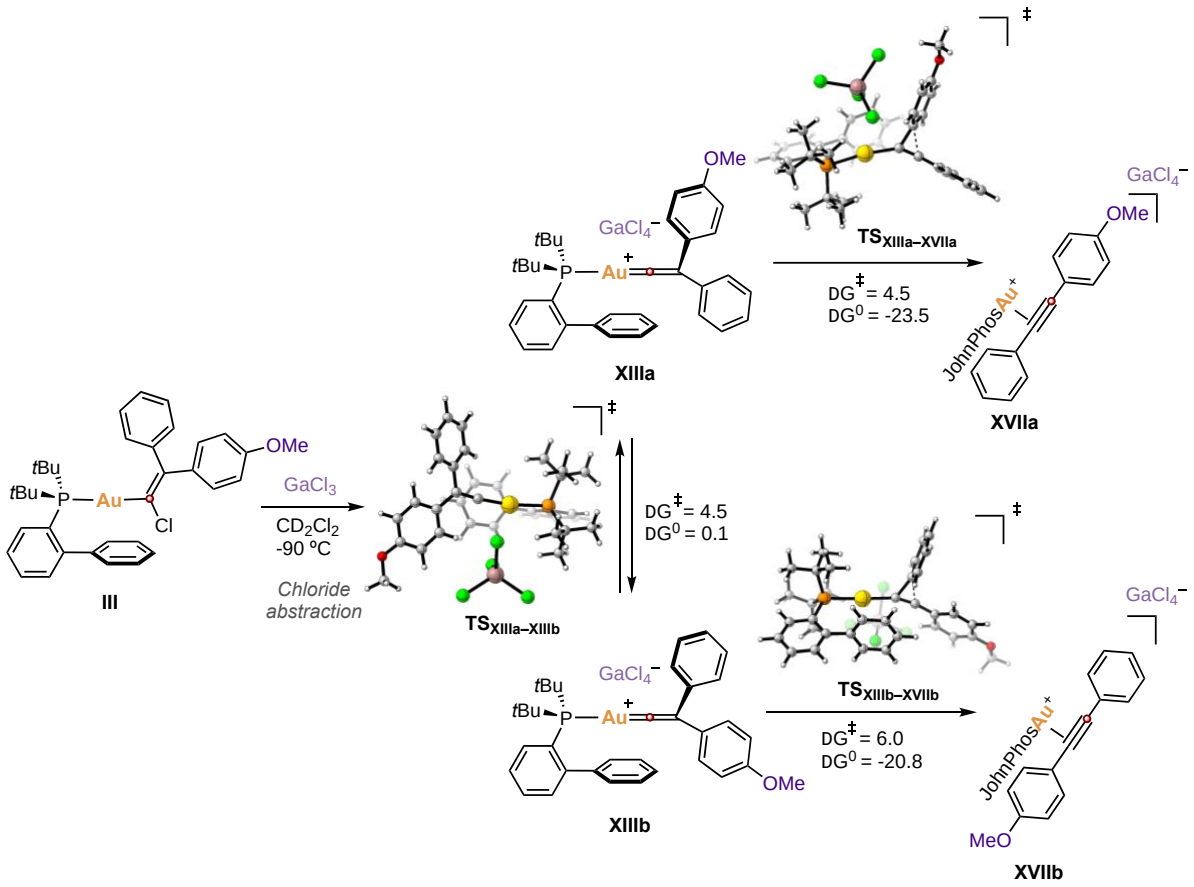

Scheme 43. Calculated Gibbs free energies of the competing processes after treatment of gold(I) vinylidenoid **III** with $GaCl_3$.

The variation of the DFT method shows methods which seems a better adjust to the experimental results observed, being PBE0 and M06 the ones which better describes this system. Thus, **M06/6-31G**** (highlighted in green in table 9, light green in figure 15) shows a more realistic similar stability of η^2–diarylacetylene gold(I) **XVIIa** and **XVIIb**. Additionally, this method shows an activation barrier for the interconversion of gold(I) vinylidene conformers **XIIIa** and **XIIIb** ($\Delta E^{\ddagger}_{\mathbf{XIIIa\text{-}XIIIb}}$ = 6.0 kcal/mol, $\Delta E^{\ddagger}_{\mathbf{XIIIb\text{-}XIIIa}}$ = 2.6 kcal/mol) which competes with the migration of the aryl substituents ($\Delta E^{\ddagger}_{\mathbf{XIIIa\text{-}XVIIa}}$ = 5.3 kcal/mol, $\Delta E^{\ddagger}_{\mathbf{XIIIb\text{-}XVIIb}}$ = 1.7 kcal/mol). This would explain the high influence of the gold(I)

vinylidenoid **III** diastereoisomer used in this reaction in the product ratio observed (Table 4). Additionally, the gently lower value of the activation energy of the phenyl migration over the interconversion of conformers, justifies the preferred formation of η^2–diarylacetylene Gold(I) **XVIIb** when the starting material is gold(I) vinylidenoid **III** (Scheme 40). To check if this situation remains at the low temperature at which the experiments were run, we performed frequency calculations at –90ºC which confirmed that temperature effect did not change the reaction mechanism described for this system.[75] Considering the higher accuracy of **M06/6-31G**** in this system, equation 2 was applied to the potential energies calculated with this method instead of to the free energies. The results displayed, as expected, that $k_{conf}/k_{mig} \approx 0.1$ for both gold(I) vinylidene conformers **XIIIa** and **XIIIb**, confirming that this process is not under Curtin–Hammett conditions.

Table 9. Benchmark of relative potential energies of aryl migration process of gold(I) vinylidenoid **III**.

	XVIIa	**TS $_{XIIIa\text{-}XVIIa}$**	**XIIIa**	**TS $_{XIIIa\text{-}XIIIb}$**	**XIIIb**	**TS $_{XIIIb\text{-}XVIIb}$**	**XVIIb**
B3LYP	-21.0	6.0	0.0	3.6	1.2	6.5	-20.6
PBE0	-20.5	6.2	0.0	6.0	2.7	5.9	-19.0
M06	-22.5	5.3	0.0	6.0	3.4	5.1	-21.8
B97D	-19.5	5.6	0.0	3.9	1.2	6.3	-18.9
B3LYP 6-311G**	-22.6	5.6	0.0	3.4	1.1	6.4	-21.8
PBE0 6-311G**	-21.7	5.9	0.0	5.9	2.7	5.9	-19.9
M06 6-311G**	-24.9	4.8	0.0	6.1	3.6	5.2	-23.6
B97D 6-311G**	-20.8	5.3	0.0	3.8	1.1	6.1	-19.8

All the energies are given in kcal/mol.

75 See experimental section table 22.

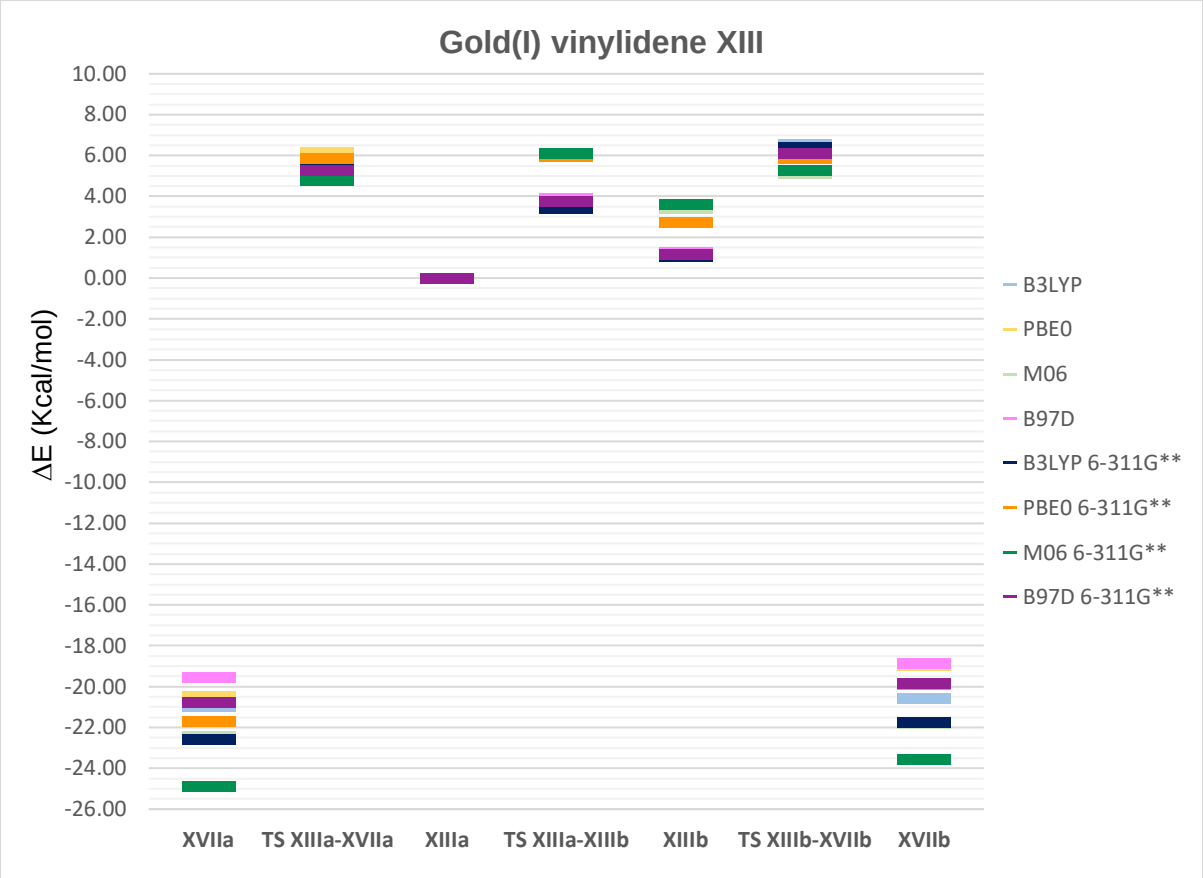

Figure 15. Representation of the relative potential energy values collected in Table 9.

The case of the reactivity calculated for gold(I) vinylidenoid **XIV** strongly differs from the previous cases studied (Scheme 44). Gold(I) vinylidene conformer **XIVb** is sharply more stable than **XIVa**. This difference in stability would shift the equilibrium to **XIVb**, resulting in the preferred formation of η^2–alkyne gold(I) complex **XVIIIb**, in accordance with the experimental results (Scheme 40). By the other side, if conformer **XIVa** would be preferentially formed after chloride abstraction from the *Z* isomer of **X**, the low difference between the activation energy of the migration (**TS** $_{\mathbf{XIVa\text{-}XVIIIa}}$, $\Delta G^{\ddagger}_{\mathbf{XIVa\text{-}XVIIIa}}$ = 4.6 kcal/mol) and the interconversion process (**TS**$_{\mathbf{XIVa\text{-}XIVb}}$, $\Delta G^{\ddagger}_{\mathbf{XIVa\text{-}XIVb}}$= 3.3 kcal/mol), could cause an equal formation of the η^2–alkyne gold(I) complexes formed. However, this could not be demonstrated experimentally. In this case we observe again a meaningless difference in the stability of the two η^2–alkyne gold(I) complexes **XVIIIa** and **XVIIIb**, so we looked for a better DFT method for our system performing a benchmark (Table 10).

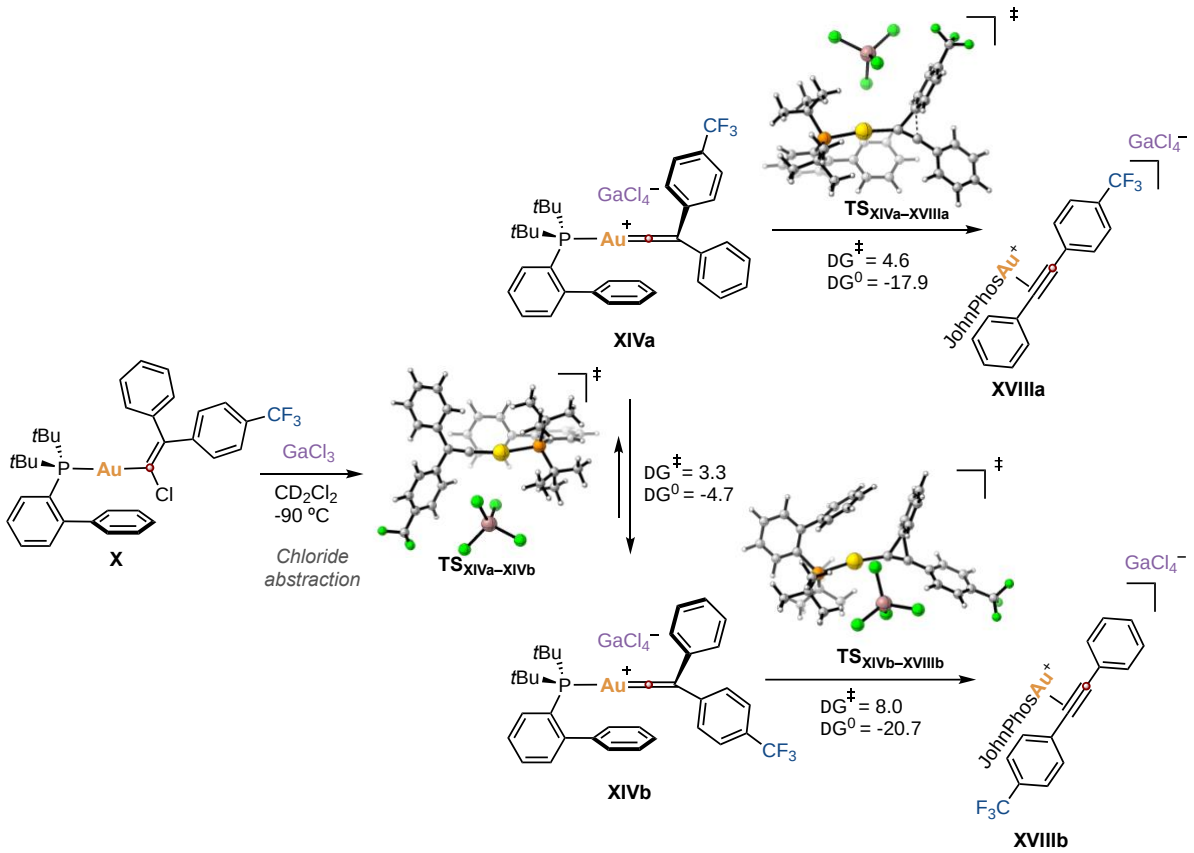

Scheme 44. Calculated Gibbs free energies of the competing processes after treatment of gold(I) vinylidenoid **X** with $GaCl_3$.

All the methods used in the benchmark supports the equilibrium shift towards **XIVb** gold(I) vinylidene (Table 10). However, similar stability of products **XVIIIa** and **XVIIIb** is only observed with the **M06** functional (highlighted in green in table 10, light green in figure 16). Using this functional, the energy barrier values of all the transformations decrease, although the reaction picture is the same.

Table 10. Benchmark of relative potential energies of aryl migration process of gold(I) vinylidenoid **X**.

	XVIIIa	**TS $_{XIVa-XVIIIa}$**	**XIVa**	**TS $_{XIVa-XIVb}$**	**XIVb**	**TS $_{XIVb-XVIIIb}$**	**XVIIIb**
B3LYP	-20.1	7.7	2.0	2.1	0.0	7.5	-22.5
PBE0	-20.0	6.3	2.8	3.2	0.0	5.6	-22.9
M06	-24.5	3.6	1.1	1.3	0.0	2.6	-24.5
B97D	-18.1	7.5	2.4	2.6	0.0	7.5	-20.8
B3LYP 6-311+G**	-21.1	8.1	2.6	2.3	0.0	7.7	-24.1
PBE0 6-311G**	-21.1	6.4	3.1	3.2	0.0	5.8	-24.3
M06 6-311G**	-26.6	3.3	1.0	0.9	0.0	2.6	-27.1
B97D 6-311G**	-18.8	7.9	3.1	2.9	0.0	7.6	-22.2

All the energies are given in kcal/mol.

The most striking event is the high instability of gold(I) vinylidene **XIVa**, which is almost isoenergetic with **TS$_{XIVa-XIVb}$** ($\Delta G^{\ddagger}$ $_{XIVa-XIVb}$ = 0.2 kcal/mol). Even more, the expansion of the basis set (**M06/6-311+G****, highlighted in yellow**)**, depicts **TS $_{XIVa-XIVb}$** 0.1 kcal/mol more stable than **XIVa**. This situation is also observed in the single points calculated using **B97D/6-311+G**** and **B3LYP 6-311+G****. Although the difference in energy between the two species is negligible and it could be due to an artifact of the DFT method, it can also indicate the high instability of gold(I) vinylidene **XIVa**, conceiving it as a TS more than a minimum in the reaction. This is in accordance with the experimentally observed main formation of η^2–alkyne gold(I) complex **XVIIIb** (Scheme 40). In this occasion, kinetic constants were not calculated, since the existence of gold(I) vinylidene **XIVa** as minimum is unlikely, whereby there will not be any conformers equilibrium.

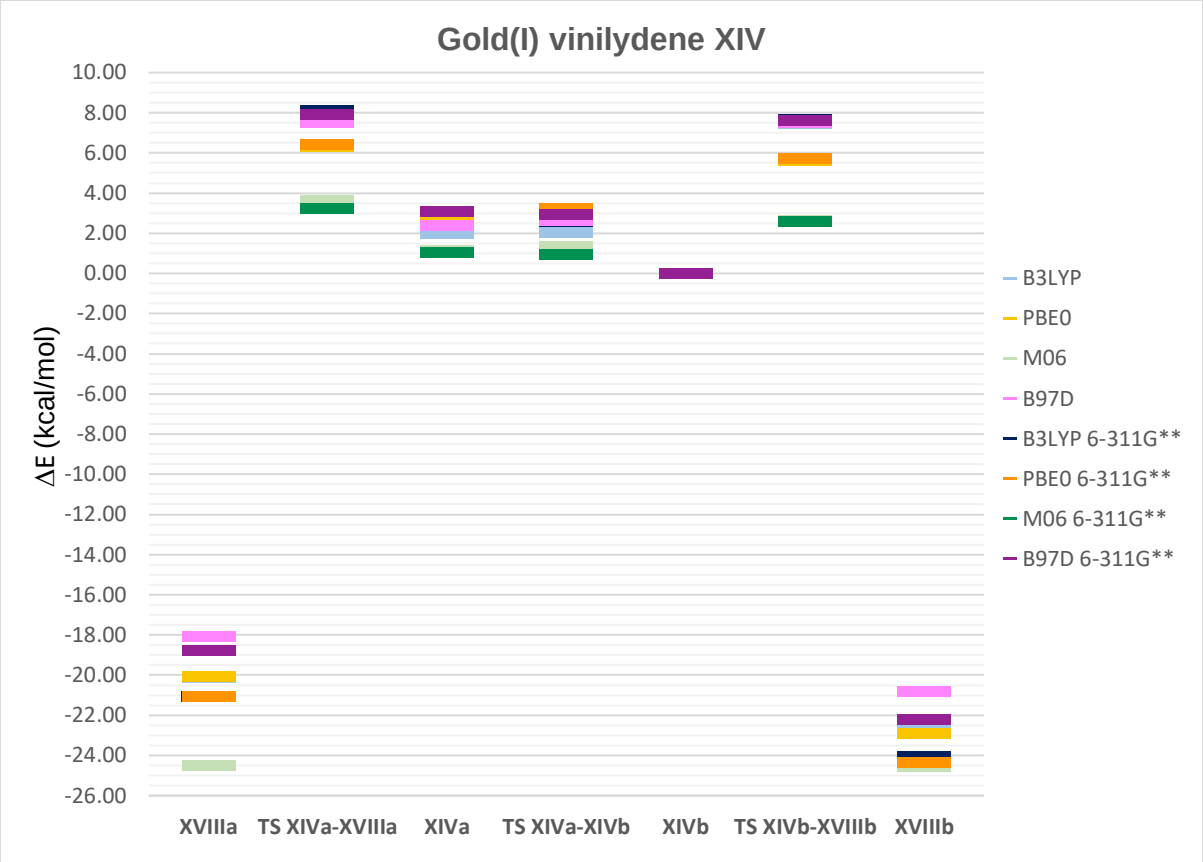

Figure 16. Representation of the relative potential energy values collected in Table 7.

Finally, all the results and analysis made in this section has been summarized in table 11.

Table 11. Summary of experimental and DFT results obtained.

Entry	Vinylidenoid	R	Experimental migration ratio Ar : Ph	DFT predicted mig.	DFT method	k_{mig}/k_{conf}	Curtin-Hammett situation?
1	**I**	Me	45 : 55	Similar mig. trend	B3LYP 6-31G**	>10	Yes
2	**II**	F	60 : 40	Preferred FPh–Mig.	B3LYP 6-31G**	>10	Yes
3	**III *E***	OMe	20 : 80	Preferred OMePh–mig.	M06 6-31G**	<10	No
4	**III *Z***	OMe	45 : 55	Preferred OMePh–mig.	M06 6-31G**	<10	No
5	**X**	CF_3	10 : 90	Preferred CF_3Ph–mig.	M06 6-31G**	–	No

Structural Analysis of Gold(I) Vinylidenes

The analysis of the optimized structures of gold(I) vinylidenes **XI–XIV,** depicted in figure 17, show the elongation of the Au–C1 (Table 12, column 2) bond with respect to the one observed in the X-Ray structures of gold(I) vinylidenoids (Table 1). The C1–C2 bond appears shorter than in gold(I) vinylidenoids, indicating a higher stabilization from the organic unit than from the gold(I) moiety (Table 12, column 3). Additionally, the comparison between the two bonds of the aryl substituents and C2 (C2–C3 and C2–C4), indicates a higher stabilization of the structure from the aryl situated in the plane of the molecule (C2–C4 bond, column 5, Table 12). The values of C1–C2–C3 angle, support the preferred migration observed in most of the cases. The slightly steeper angle in gold(I) vinylidene **XIb** with respect with **XIa**, indicates a preferred migration of the phenyl substituents. This situation is sharper in the case of gold(I) vinylidene **XIb** in which the C1–C2–C3 angle is almost 7 º smaller, in accordance with the markedly preferred migration of the phenyl group experimentally observed (Scheme 40). In the case of gold(I) vinylidene **XIIa**, the C1–C2–C3 angle is steeper than in **XIIb**, justifying the preferred migration of the *p*-fluorophenyl substituent. The only case that does not match with the experimental results observed is gold(I) vinylidene **XIII**. In this case, the structure data predicts the preferred migration of the anisyl substituent, although we have observed experimentally the preferred migration of the phenyl substituent. The computed structure showed π–π interactions between

the ligand and the anisyl substituent in vinylidene **XIIIa**, which were not present in vinylidene **XIIIb**. This π–π interactions could justify the major stabilization of gold(I) vinylidene **XIIIa** observed with this method and they probably are the responsible of the artefact found when **B3LYP**/6-31G** was used to study the reaction pathway of gold(I) vinylidenes **XIII**.

Table 12. Selected parameters from the optimized structures of gold(I) vinylidenes **XI–XIV**.

	Au-C1 (Å)	**C1-C2** (Å)	**C2-C3** (Å)	**C2-C4** (Å)	**C1-C2-C3** (º)	**C1-C2-C4** (º)
XIa	1.970	1.295	1.519	1.464	96.37	136.87
XIb	1.972	1.295	1.527	1.461	95.84	138.17
XIIa	1.984	1.289	1.527	1.458	90.52	142.01
XIIb	1.977	1.292	1.531	1.458	93.07	140.90
XIIIa	2.004	1.286	1.529	1.452	82.08	147.95
XIIIb	1.972	1.297	1.527	1.458	95.79	138.33
XIVa	1.956	1.299	1.516	1.471	102.24	132.84
XIVb	1.971	1.294	1.527	1.462	95.62	138.13

Gold(I) vinylidene XIa

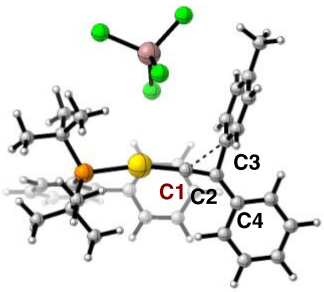

Gold(I) vinylidene XIb

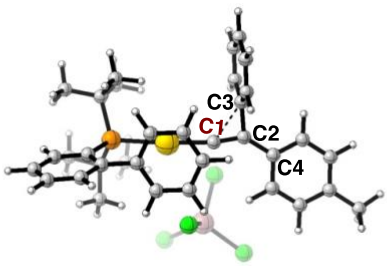

Gold(I) vinylidene XIIa

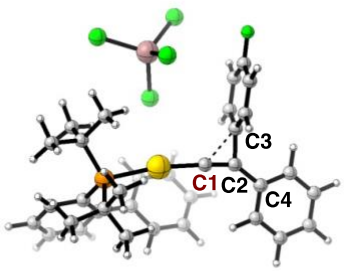

Gold(I) vinylidene XIIb

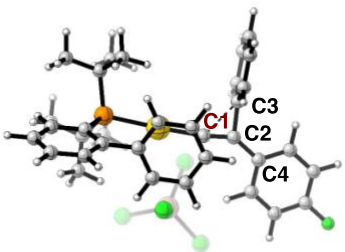

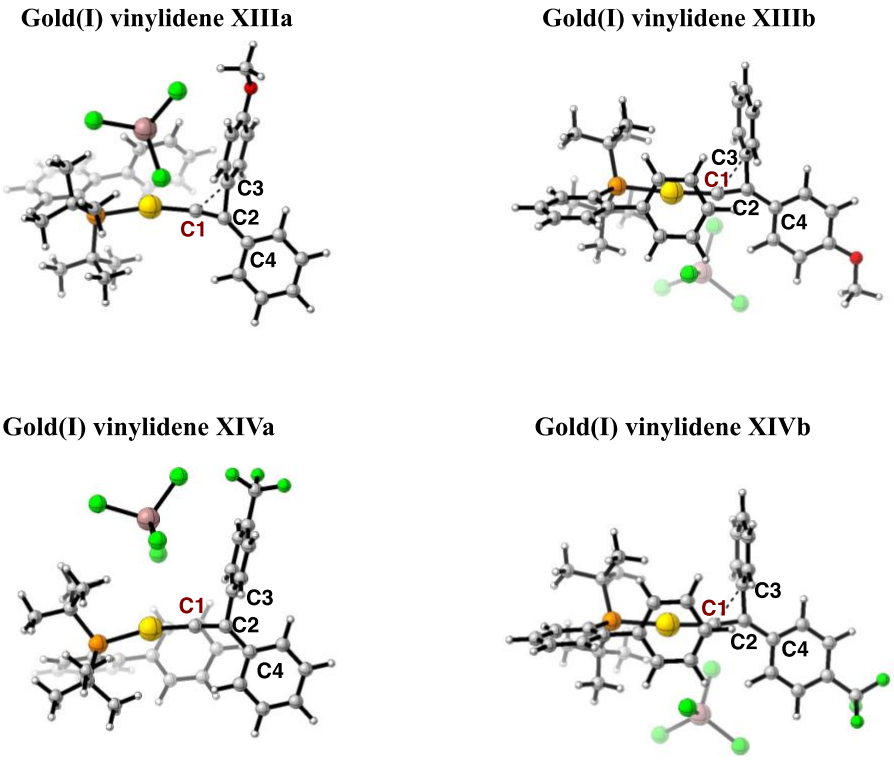

Figure 17. Optimized structures of gold(I) vinylidenes **XI-XIV**. The DFT method used for the optimization was B3LYP/6-31G**.

Conclusions

This chapter summarizes the work performed on the understanding of gold(I) vinylidenes (Scheme 45). A family of gold(I) vinylidenoids has been synthesized. The analysis of the structure of these gold(I) vinylidenoids has evidenced the vinylidene character of these species, potentially disclosing a new methodology for the generation of gold(I) vinylidenes.

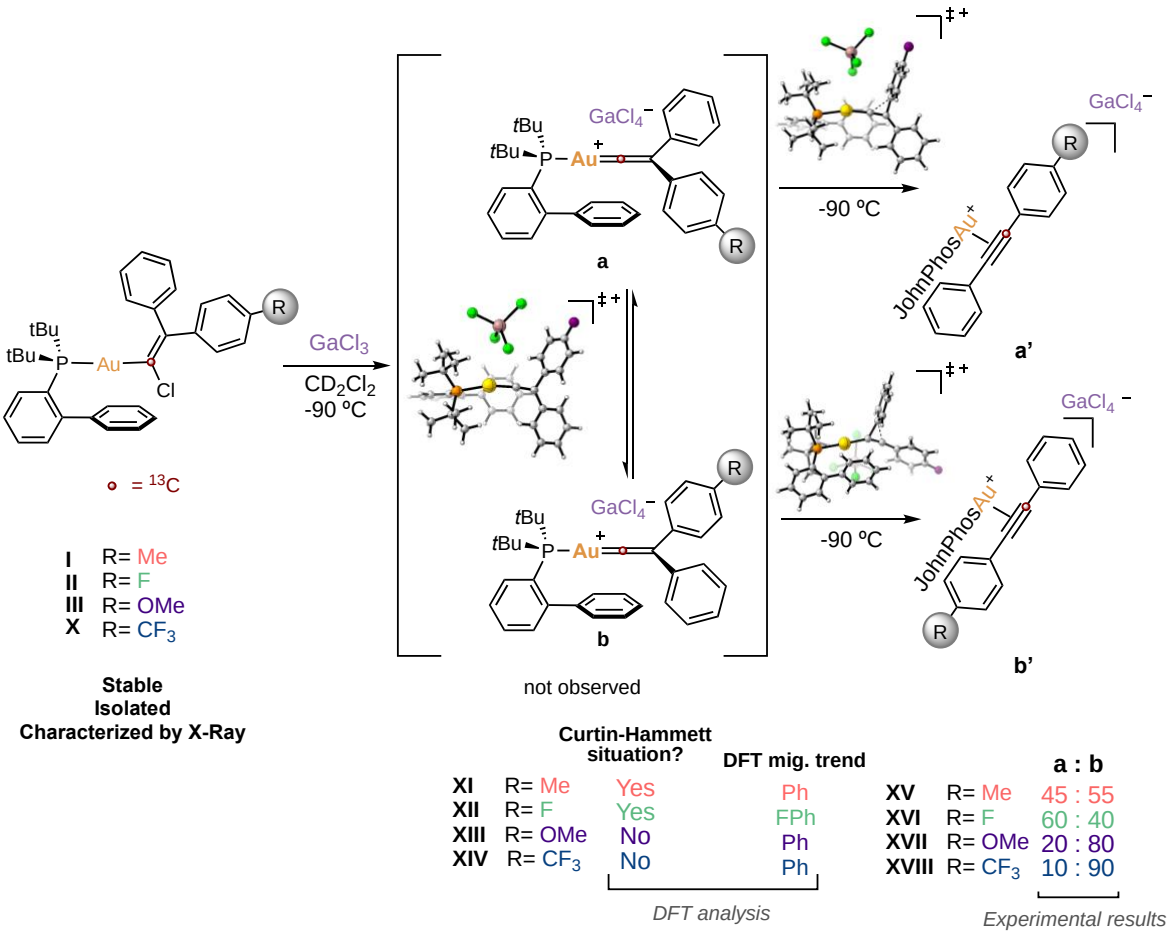

Scheme 45. Study on gold(I) vinylidenoids and gold(I) vinylidenes.

The reactivity of the synthesized gold(I) vinylidenoids has been studied, showing typical vinylidene reactivity. To the best of our knowledge, this would be the first time in which aryl migration through gold(I) vinylidenes has been reported, since this reactivity was limited to the migration of halogen or silyl substituents. Additionally, the migration trend of the aryl substituents in the synthesized gold(I) vinylidenoids has been studied via ^{13}C isotopic labelling.

DFT experiments has been performed to fully understand the mechanism of this reaction. The introduction of the counteranion $GaCl_3$ in the calculation showed to be crucial to get a real modelling of these systems that supports the experimental observations. 1,2-aryl migration showed to happen through two different interconvertible conformational isomers a and b of the corresponding gold(I)

vinylidenes. The stability of the gold(I) vinylidene conformers a and b and the rate of their interconversion determines the ratio of the ^{13}C labelled η^2–diarylacetylene gold(I) complexes a' and b' obtained. Additionally, the chloride abstraction of the gold(I) vinylidenoid plays an important role in the reaction outcome, since not all the vinylidene conformers are under Curtin-Hammett conditions.

Finally, the optimized structures of the gold(I) vinylidenes proposed as intermediates of this reaction were simulated by DFT. The features of this structures indicated a higher stabilization from the organic unit than the one provided from gold(I).

Experimental Section

General Methods

All reactions under an Ar atmosphere were conducted after preparation in the glovebox or using standard Schlenk techniques. Anhydrous solvents for synthesis were obtained by passing them through an activated alumina column on a PureSolvTM solvent purification system (Innovative Technologies, Inc., MA) or they were commercially available anhydrous solvents purchased from ACROS Organics. Deuterated solvents were purchased from Sigma-Aldrich. CD_2Cl_2 was dried over activated 4 Å molecular sieves and stored under Ar before use. Analytical TLC was performed on precoated neutral aluminum oxide plates (0.2 mm thick, Gf234, Merck, Germany) using UV light as the visualizing agent and an acidic solution of vanillin in ethanol or basic solution of $KMnO_4$ in water as stain. Column chromatography was performed on neutral aluminum oxide Carlo Erba or using flash grade silica gel (SDS Chromatogel 60 ACC, 40–60 μm) as the stationary phase. NMR spectra were recorded either on a BrukerAvance Ultrashield NMR spectrometer (300 MHz, 400 MHz, 500 MHz and 500 MHz with CryoProbe). Chemical shifts (δ) are reported in parts per million (ppm) and referenced to residual solvent (For ^{1}H NMR: $CDCl_3$ at 7.26 ppm, CD_2Cl_2 at 5.31 ppm, C_6D_6 at 7.16 ppm, for $^{13}C\{^1H\}$ NMR: $CDCl_3$ at 77.16 ppm, CD_2Cl_2 at 54.00 ppm, C_6D_6 at 128.06 ppm). The following abbreviations were used to explain multiplicities: s = singlet, d = doublet, t = triplet, q = quartet, p = pentet, m = multiplet, br s = broad singlet. Coupling constants (*J*) are reported in Hertz (Hz). Mass spectra were recorded on a Waters LCT Premier Spectrometer (ESI and APCI) or on an Autoflex Broker Daltonics (MALDI and LDI). or on an AgilentMSD-5975B (GC-MS). Melting points were determined using a Mettler Toledo MP70 melting point apparatus. X-ray diffraction data were collected at 100 K on a Rigaku MicroMax-007HF, Mo Kα rotating anode, equipped with a Pilatus 200 K detector or on a Bruker APEX DUO, Mo Kα Microfocus source E025 IuS anode, equipped with an APEX DUO detector using omega scans.

Unless otherwise stated, all other reagents were purchased from commercial sources and used without further purification.

Synthesis and Characterization of Gold(I) Vinylidenoids

(*Z*)-4-(2-Chloro-1-phenylvinyl-2-^{13}C) phenol (37)

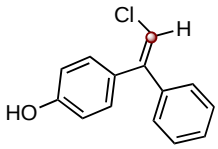

Formation of phenol **37** was performed inspired by previous work on selective synthesis of vinyl chlorides.[61] 10 mL Schlenk flask equipped with a stirring bar was evacuated and fulfilled with argon. Phenol (162.9 mg, 1.7 mmol, 1.2 equiv) was dissolved in dry dichloroethane (3.6 mL, 400.7 mM) and 1-chloro-2-phenyl-alkyne-1-^{13}C (197.0 mg, 1.4 mmol, 1.0 equiv) was added. iPrAuCl (9.0 mg, 14.0 μmol, 1 mol%) and $NaBAr^F$ (12.8 mg, 14.0 μmol, 1 mol%) were added subsequently. The resulting mixture was stirred at 40 °C for 16 h. Once not starting material was detected by TLC, mixture was cooled down to room temperature and concentrated. Crude product was purified by flash silica gel column chromatography, (Pentane/Et_2O, 10:1) to give (*Z*)-4-(2-chloro-1-phenylvinyl-2-^{13}C) **37** (99.0 mg, 0.43 mmol, 30% yield) as a white-greenish solid.

^{1}H NMR (500 MHz, $CDCl_3$) δ 7.32 – 7.28 (m, 3H), 7.25 – 7.18 (m, 4H), 6.85 (dt, *J* = 8.8, 2.6 Hz, 2H), 6.51 (d, $J_{H-^{13}C}$= 195.6 Hz, 1H), 4.77(br s, 1H). **^{13}C{^{1}H} NMR** (126 MHz, $CDCl_3$) 115.3 (^{13}C-labelled). **HRMS** (ESI –) calculated for $[C_{13}H_{10}ClO\text{^}^{13}C]^-$ 230.0459 *m/z*; found $[M - H]^-$ 230.0462. **M.p.** = 72–73 ºC. Matching known analytical data for the ^{12}C-isotopologue.[76]

(*Z*)-4-(2-Chloro-1-phenylvinyl-2-*^{13}C*) phenyl 4-triflate (39)

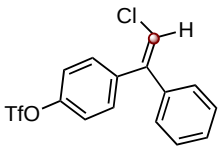

10 mL flamed and dried schlenk flask equipped with a stirring bar was charged under Ar atmosphere with phenol **37** (85.7 mg, 369.9 mmol, 1.0 equiv), pyridine (58.5 mg, 59.9 mL, 739.8 mmol, 2.0 equiv), and dichloromethane (1.2 mL, 0.3 M). The mixture was stirred during 10 minutes at 25 ºC and cooled down to 0 ºC in an ice bath. At this temperature, triflic anhydride (443.9 mL of a 1M in CH_2Cl_2 solution, 443.9 mmol, 1.2 equiv) was added dropwise. The reaction was allowed to warm to room temperature and stirred for 18 h. The reaction mixture was filtered through a plug of silica gel and subsequently washed with a mixture of cyclohexane/EtOAc (4:1). The resulting solution was concentrated under vacuum obtaining product (*Z*)-4-(2-chloro-1-phenylvinyl-2-^{13}C) phenyl 4-triflate (127.7 mg, 351.1 μmol, 95% yield) as a colorless oil without any further purification. The ^{12}C-isotopologue was parallelly synthesized to facilitate the characterization of the compound.

^{1}H NMR (400 MHz, $CDCl_3$) δ 7.45 – 7.40 (m, 2H), 7.35 – 7.29 (m, 5H), 7.20 – 7.15 (m, 2H), 6.64 (d, $J_{H-^{13}C}$ = 194.0 Hz, 1H). **^{13}C{^{1}H} NMR** (126 MHz, $CDCl_3$) δ 149.1, 142.4, 139.5, 138.1, 132.1, 128.8, 128.7, 127.8 (d, $J_{C-^{13}C}$ = 3.7 Hz), 121.4, 118.9 (d, J_{C-F} = 321 Hz), 117.2 (^{13}C-labelled). **^{19}F{^{1}H} NMR**

76 Adak, T.; Schulmeister, J.; Dietl, M. C.; Rudolph, M.; Rominger, F.; Hashmi, A. S. K. *Eur. J. Org. Chem.* **2019**, 3867–3876.

(376 MHz, $CDCl_3$) δ –72.9 (s, 3F). **HRMS** (ESI+) calculated for $[C_{14}H_{10}ClF_3NaO_3S^{\wedge 13}C]^+$ 385.9917 *m/z*; found $[M + Na]^+$ 385.9922.

(*Z*)-4-(2-Chloro-1-phenylvinyl-2-*^{13}C*) phenyl 4-methyl (40)

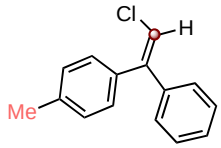

This compound was synthesized according to the procedure reported for other Stille coupling reactions of triflate compounds.[77] 10 mL Schlenk flask equipped with a stirring bar was charged with LiCl (50.2 mg, 1.2 mmol, 10.0 equiv) activated by heating under high vacuum for 30 min. After this time, Schlenk flask was refilled with argon and dry DMF (845.5 µl, 0.14 M) was added to the reaction vessel. Then (*Z*)-4-(2-chloro-1-phenylvinyl)phenyl trifluoromethanesulfonate (60.0 mg, 118.4 µmol, 1.0 equiv) and Me_4Sn (24.6 µL, 177.6 µmol, 1.5 equiv) were added to the reaction mixture. The mixture was stirred for 15 min at 25ºC and then $(PPh_3)_2PdCl_2$ (16.6 mg, 23.7 µmol, 20 mol%) was added. Reaction mixture was stirred at 125 °C for 30 min. Upon completion of the reaction, it was quenched with H_2O and diluted with EtOAc. The reaction mixture was partitioned between H_2O and EtOAc. The organic fraction was then washed with 10% KF solution and dried over anhydrous sodium sulfate, filtered, and concentrated. The crude product was purified by flash silica gel column chromatography (pentane) to afford **(***Z***)**-4-(2-chloro-1-phenylvinyl-2-^{13}C) phenyl 4-methyl (28.0 mg, 118.4 mmol, 63% yield) as a light yellow solid.

^{1}H NMR (400 MHz, CD_2Cl_2) δ 7.33 – 7.28 (m, 3H), 7.25 – 7.17 (m, 6H), 6.58 (d, $J_{H-^{13}C}$ = 195.5, 1H), 2.39 (s, 3H). **^{13}C{^{1}H} NMR** (101 MHz, CD_2Cl_2) δ 140.7 (d, *J*= 5.6 Hz), 138.4, 135.1, 130.1 (*J* = 2.9 Hz), 129.3, 128.8, 128.4, 128.4, 128.1 (*J* = 4.2 Hz), 115.8, 21.4. **HRMS** (APCI+) calculated for $[C_{14}H_{14}Cl^{\wedge 13}C]^+$ 230.0812 *m/z*; found $[M + H]^+$ 230.0806. **M.p.** = 76–77 ºC.

(*Z*)-1-(2-Chloro-1-phenylvinyl-2-*^{13}C*)-4-fluorobenzene (41)

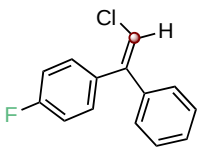

(*Z*)-1-(2-chloro-1-phenylvinyl-2-^{13}C)-4-fluorobenzene was synthesized following a procedure developed by the group of Sanford for similar compounds.[62] An owen dried MW vial equipped with a stirring bar, was charged inside the glovebox with tetramethylammonium fluoride (25.2 mg, 270.2 µmol, 2.0 equiv) and (*Z*)-4-(2-chloro-1-phenylvinyl)phenyl trifluoromethanesulfonate (49.0 mg, 135.1 µmol, 1.0 equiv) previously dried overnight over P_2O_5 under high vacuum. Anhydrous *N*,*N*-dimethylformamide (675.4 µL, 0.2 M) was added, the vial was sealed and taken out of the glovebox. Outside the glovebox, the reaction mixture was stirred at 80 ºC for 24 h. After this time, the resulting solution was diluted with diethyl ether and the two phases were separated. Aqueous phase was extracted with diethyl ether (2x) and the combined organic phases were washed with water (10x), collected, dried over magnesium sulfate, and

77 Toledo, H.; Amar, M.; Bar, S.; Iron, M. A.; Fridman, N.; Tumanskii, B.; Shimon, L. J. W.; Botoshanskya, M.; Szpilman A. M. *Org. Biomol. Chem.* **2015**, *13*, 10726–10733.

concentrated under vacuum. The crude reaction mixture was purified by flash column chromatography on silica gel with pentane and (*Z*)-1-(2-chloro-1-phenylvinyl)-4-fluorobenzene (19.0 mg, 82.0 µmol, 60% yield) was obtained as a colorless oil. The ^{12}C-isotopologue was parallelly synthesized to facilitate the characterization of the compound.

^{1}H NMR (400 MHz, CD_2Cl_2) δ 7.35 – 7.28 (m, 5H), 7.23 – 7.17 (m, 2H), 7.15 – 7.08 (m, 2H), 6.62 (d, $J_{H-^{13}C}$ = 195.8 Hz, 1H). **^{13}C{^{1}H} NMR (**126 MHz, $CDCl_3$), reported from the ^{12}C-isotopologue for clarity. δ 162.5 (d, J_{C-F} = 247.5 Hz), 143.1, 140.1, 133.6 (d, J_{C-F} = 3.3 Hz), 131.8 d, J_{C-F} = 7.8 Hz), 128.7, 128.4, 127.9, 116.2, 115.4 (d, J_{C-F} = 20.1 Hz). **^{13}C{^{1}H} NMR** (101 MHz, CD_2Cl_2) δ 116.5 (^{13}C-labelled). **^{19}F{^{1}H} NMR** (376 MHz, CD_2Cl_2) δ –114.0 (s, 1F). **HRMS (APCI+)** calculated for $[C_{14}H_{11}ClF]^+$ 233.0528 *m/z*; found $[M + H]^+$ 233.0530.

1-Methoxy-4-(1-phenylvinyl-2-*^{13}C*) benzene (46)

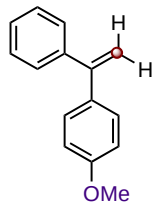

In a MW vial equipped with stirring bar, at 0 ºC potassium *tert*butoxide (166.2 mg, 1.5 mmol,1.5 equiv) was added to a solution of (methyl-^{13}C)triphenylphosphonium iodide (400.0 mg, 987.1 µmol, 1.0 equiv) in THF (2.2 mL), and the mixture was stirred for 1 hour at 25 ºC. After cooling down again the reaction mixture to 0 ºC, (4-methoxyphenyl)(phenyl)methanone (209.5 mg, 987.1 µmol, 1.0 equiv) dissolved in 0.3 ml of THF (2.5 mL of THF in total, 0.4 M) was added slowly over 10 min to it and the resulting mixture was stirred for 14 h at 25 ºC. The reaction was quenched with saturated NH_4Cl aq and subsequently extracted with Et_2O (3x). The combined organic phases were washed with saturated aq. NaCl, dried over $MgSO_4$ and concentrated under vacuum. The residue was purified by flash column chromatography on silica gel with pentane/Et_2O (20:1) to afford 1-methoxy-4-(1-phenylvinyl-2-^{13}C)benzene (164.0 mg, 776.0 µmol, 79% yield) as a white solid.

^{1}H NMR (500 MHz, $CDCl_3$) δ 7.37 – 7.31 (m, 5H), 7.30 – 7.27 (m, 2H), 6.89 – 6.85 (m, 2H), 5.54(dd, *J* = 21.4, 1.5 Hz, 1H), 5.22 (dd, *J*= 21.7, 1.4 Hz 1H), 3.83 (s, 3H). **^{13}C{^{1}H} NMR** (126 MHz, $CDCl_3$) δ 159.48, 149.92, 149.35, 141.97, 134.15, 129.53 (d, *J* = 3.3 Hz), 128.46 (d, *J* = 3.2 Hz), 128.26, 127.78, 113.67, 113.09 (^{13}C-labelled), 55.5. **HRMS** (ESI +) calculated for [C14H15O^13C]$^+$ 212.1151 *m/z*; found $[M + H]^+$ 212.1151. **M.p. =** 74–75 ºC.

Matching known analytical data for the ^{12}C-isotopologue.[78]

78 Purohit, V.C.; Allwein, S. P.; Bakale, R. P. *Org. Lett*. **2013**, *15*, 1650–1653.

1-(1-Phenylvinyl-2-^{13}C)-4-(trifluoromethyl)benzene (48)

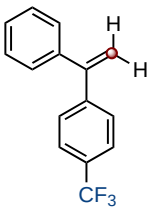

In a 10 mL 2 necked round bottom flask equipped with a stirring bar, potassium *tert*-butoxide (168.6 mg, 1.5 mmol 1.5 equiv) was added at 0 ºC to a solution of (methyl-^{13}C) triphenylphosphonium iodide (406.00 mg, 1.0 mmol, 1.0 equiv) in THF (2.5 mL, 0.4 M). The mixture was stirred for 1 h at 25 ºC. After cooling the reaction again to 0 ºC, phenyl(4-(trifluoromethyl)phenyl)methanone (250.7 mg, 1.0 mmol, 1.0 equiv) was added in portions to it and the resulting mixture was stirred for 14 h at 25 ºC. The reaction was quenched with saturated aq. NH_4Cl and extracted with Et_2O (3x). The organic layer was washed with brine, dried over $MgSO_4$, filtered, and concentrated under vacuum. The residue was flash chromatographed on silica gel with pentane to afford 1-(1-phenylvinyl-2-^{13}C)-4-(trifluoromethyl)benzene (213.0 mg, 854.6 µmol, 76% yield) as colorless oil.

^{1}H NMR (500 MHz, $CDCl_3$) δ 7.59 (d, *J* = 8.1Hz, 2H), 7.45 (d, *J* = 8.1 Hz, 2H), 7.38 – 7.29 (m, 5H), 5.70 (d, $J_{H-^{13}C}$ = 25.2 Hz, 1H), 5.38 (d, $J_{H-^{13}C}$ = 25.2 Hz, 1H). **^{13}C{^{1}H} NMR** (126 MHz, $CDCl_3$) δ 149.1 (d, *J* = 72.1 Hz), 145.3, 140.8, 129.9 (d, *J* = 32.1 Hz), 128.70 (d, *J* = 3.3 Hz), 128.5, 128.3 (d, *J* = 3.2 Hz), 128.2, 125.3 (q, *J* = 3.9 Hz), 125.3, 116.0 (^{13}C-labelled). **^{19}F{^{1}H} NMR** (471 MHz, $CDCl_3$) δ -62.5 (s, 3F).

***E* and *Z* 1-(2-Chloro-1-phenylvinyl-2-^{13}C)-4-methoxybenzene (38*E* + 38*Z*)**

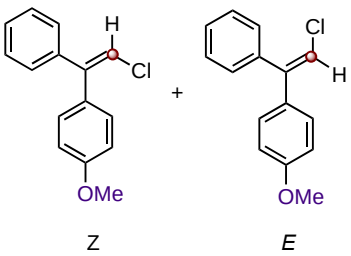

In a MW vial equipped with a stirring bar, to a solution of 1-methoxy-4-(1-phenylvinyl)benzene **46** (94.0 mg, 444.9 µmol, 1.0 equiv) in acetic acid (4.5 mL, 0.1 M), 1-chloropyrrolidine-2,5-dione (65.4 mg, 489.4 µmol, 1.1 equiv) was added in one pot. The resulting mixture was stirred at 70 °C for 4 h. Reaction was monitored by ^{1}H NMR and when no more starting material was observed, it was left to cool down to room temperature. The reaction was neutralized by slowly adding aq. $NaOH/NaHCO_3$ 1:1 (2 M) and extracted with EtOAc (3x). The combined organic layers were dried over $MgSO_4$ and concentrated under reduced pressure. Crude was purified by SiO_2 flash column chromatography (pentane/Et_2O, 5:1) to obtain a mixture of the two stereoisomers of 1-(2-chloro-1-phenylvinyl)-4-methoxybenzene **38** (70.0 mg, 0.3 mmol, 64% yield) as a colorless oil.

The two isomers were separated through HPLC: Chiralpak IJ 4.6mmx250mml, 5µl, HEX/IPA 95:5, Isocratic 1 ml/min VWD: 300nm.

The stereoselective synthesis of (*Z*)-1-(2-chloro-1-phenylvinyl-2-^{13}C)-4-methoxybenzene (38 *Z)* can be achieved following an equivalent procedure to the one used for the synthesis of (*Z*)-4-(2-chloro-1-phenylvinyl-2-^{13}C) phenol. Using anisole instead of phenol (58.9 mg, 544.7 µmol, 1.2 equiv), 1-chloro-2-phenyl-alkyne-1-^{13}C (62.0 mg, 453.9 µmol, 1.0 equiv), iPrAuCl (2.8 mg, 4.5 µmol, 10 mol%) and

$NaBAr^F$ (4.0 mg, 4.5 μmol, 10 mol%) in 1.1 ml of dichloroethane (0.4 M). With this procedure, product **38** *Z* was obtained as a white sticky solid in 36% yield.

38 ***Z***: **^{1}H NMR** (500 MHz, $CDCl_3$) δ 7.32 – 7.26 (m, 5H), 7.23–7.19 (m, 2H), 6.95 – 6.91 (m, 2H), 6.51 (d, $J_{H-^{13}C}$ = 195.1 Hz, 1H), 3.84 (s, 3H). **^{13}C{^{1}H} NMR** (126 MHz, $CDCl_3$) δ 159.4, 143.9, 143.2, 140.7 (d, *J* = 5.9 Hz), 131.4 (d, *J* = 2.8 Hz), 130.0, 128.5, 128.2, 128.0 (d, *J* = 4.1 Hz), 115.3 (^{13}C-labelled), 113.7, 55.4. **HRMS** (APCI+ calculated for $[C_{14}H_{14}ClO^{\wedge 13}C]^+$ 246.0761 *m/z*; found $[M + H]^+$ 246.0756. **M.p.**= could not be measured because the product appeared as a sticky solid.

38 ***E:*** **^{1}H NMR** (500 MHz, $CDCl_3$) δ 7.42 – 7.38 (m, 2H), 7.38 – 7.29 (m, 3H), 7.15 – 7.11 (m, 2H), 6.85 – 6.81 (m, 2H), 6.51 (d, $J_{H-^{13}C}$ = 194.7 Hz, 1H), 3.80 (s, 3H). **^{13}C{^{1}H} NMR** (126 MHz, $CDCl_3$) δ 159.7, 143.5 (d, $J_{C-^{13}C}$ = 83.1 Hz), 138.0, 132.9 (d, $J_{C-^{13}C}$ = 5.5 Hz), 130.0 (d, $J_{C-^{13}C}$ = 2.8 Hz), 129.0 (d, $J_{C-^{13}C}$ = 4.2 Hz) 128.3, 128.0, 114.4 (^{13}C-labelled), 114.0, 55.5. **HRMS** (APCI+ calculated for $[C_{14}H_{14}ClO^{\wedge 13}C]^+$ 246.0761 *m/z*; found $[M + H]^+$ 246.0756. **M.p.** = 55–56 ºC.

***E* and *Z*-1-(2-Chloro-1-phenylvinyl-2-*^{13}C*)-4-(trifluoromethyl)benzene (49*E* + 49*Z*)**

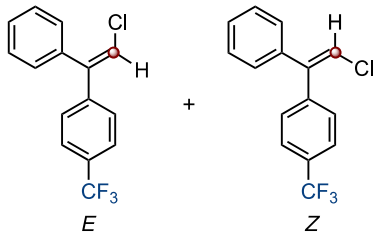

In a MW vial equipped with a stirring bar, to a solution 1-(1-phenylvinyl-2-^{13}C)-4-(trifluoromethyl)benzene (205.0 mg, 822.5 μmol, 1.0 equiv) in acetic acid (8.2 mL, 0.1 M), 1-chloropyrrolidine-2,5-dione (164.7 mg, 1.2 mmol, 1.5 equiv) was added in one pot. The resulting mixture was stirred at 90 °C for 16 h. Reaction was monitored by ^{1}H NMR and when no more starting material was observed, it was left to cool down to room temperature. The reaction was neutralized by slowly adding aq. NaOH/$NaHCO_3$ 1:1 (2 M) and extracted with EtOAc (3x). The combined organic layers were dried over $MgSO_4$ and concentrated under reduced pressure. Crude was purified by SiO_2 flash column chromatography (pentane/Et_2O, 10:1) to obtain a mixture of the two stereoisomers of 1-(2-chloro-1-phenylvinyl-2-*^{13}C*)-4-(trifluoromethyl)benzene (100.0 mg, 352.5 μmol, 43% yield) as a colorless oil.

Z isomer was separated from the mixture through HPLC: Chiralpak IC 0.46x25cm, 5μl, H_2O/ACN 45:55, Isocratic 1 ml/min VWD: 254nm. Enough amount of *E* isomer to be used in synthesis could not be isolated.

49 ***Z***: **^{1}H NMR** (500 MHz, $CDCl_3$) δ 7.66 (d, *J* = 8.1 Hz, 2H), 7.45 (d, *J* = 8.0 Hz, 2H), 7.34 – 7.30 (m, 3H), 7.20 – 7.16 (m, 2H), 6.66 (d, $J_{H-^{13}C}$ = 194.9 Hz, 1H). **^{13}C{^{1}H} NMR** (126 MHz, $CDCl_3$) δ 143.2, 142.6, 141.4, 139.4, 130.5 (d, $J_{C-^{13}C}$ = 3.2 Hz), 128.8, 128.6, 127.8 (d, $J_{C-^{13}C}$ = 4.2 Hz), 125.4 (q, J_{C-F} = 3.7 Hz) 117.2 (^{13}C-labelled). **^{19}F{^{1}H} NMR** (471 MHz, $CDCl_3$) δ –63.0. **M.p.** = > 340 ºC.

The stereochemistry was confirmed via NOESY and GOESY (nOe) irradiation experiments (Figures 18, 19 and 20).

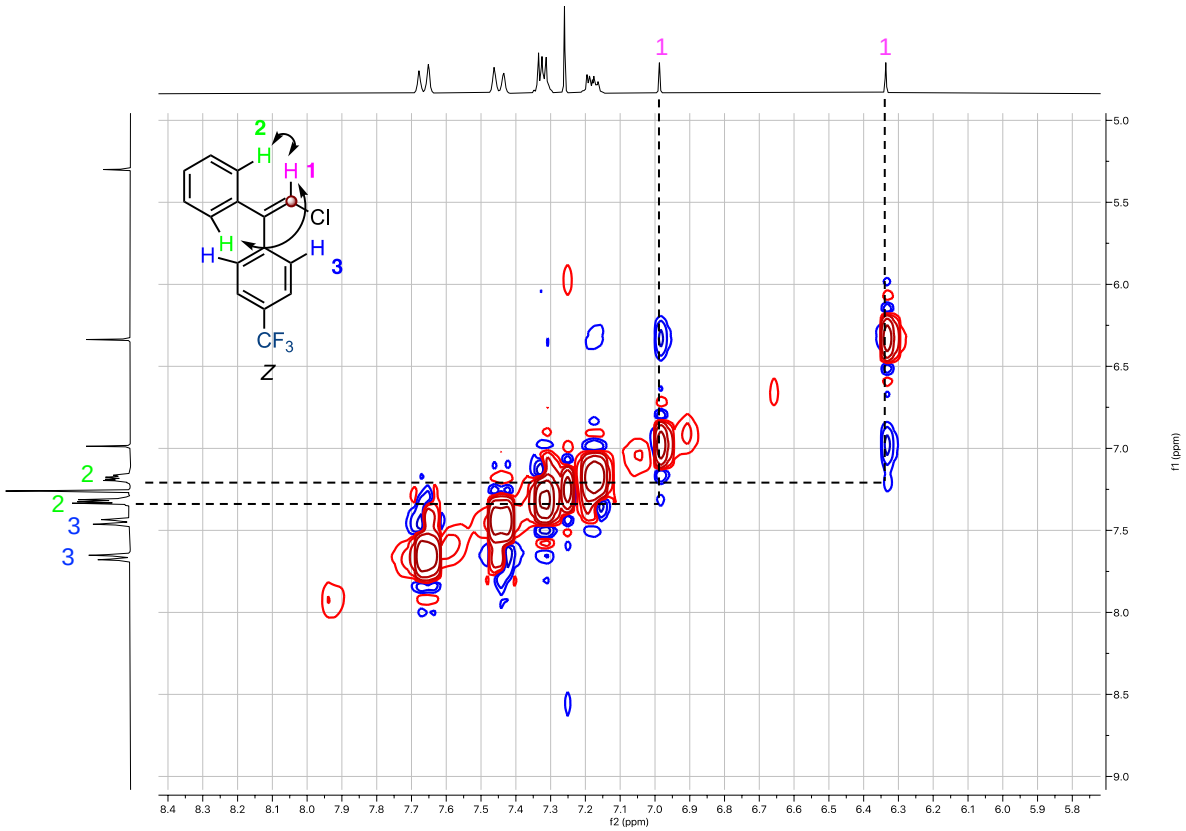

Figure 18. NOESY experiment.

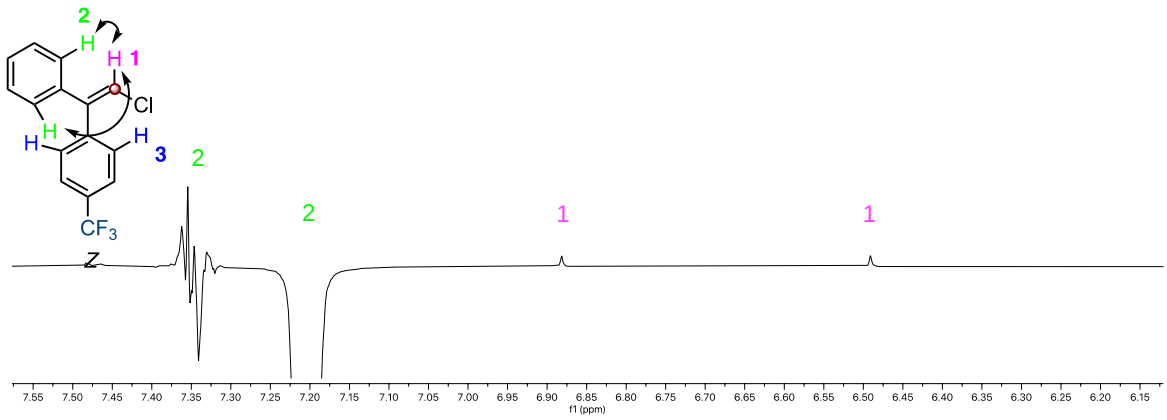

Figure 19. GOESY (nOe) Irradiation on H2 (7.20 ppm).

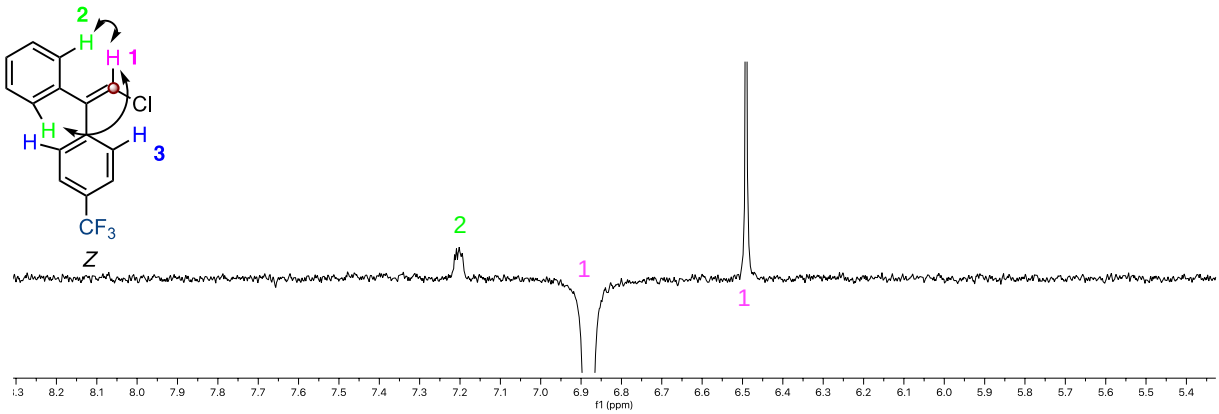

Figure 20. GOESY (nOe) Irradiation on H1 (6.88 ppm).

4,4'-(2,2-dichloroethene-1,1-diyl)bis(methoxybenzene) (64)

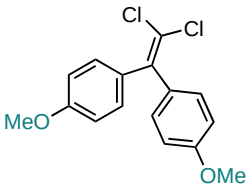

A MW vial equipped with a stirring bar was charged with triphenyl phosphine (433.1 mg, 1.65 mmol, 4.0 equiv) and dichloromethane (826 µL, 0.5 M). The solution was cooled down to 0 ºC and bis(4-methoxyphenyl)methanone (100 mg, 412.8 µmol, 1.0 equiv) and perchloromethane (127.8 mg, 80.4 µL, 825.5 µmol, 4.0 equiv) were added sequentially by syringe while keeping the reaction stirring at 0 ºC. Then the reaction was allowed to warm to room temperature and monitored by TLC. Solution turned yellow and then red overtime, after 3 h, TLC (5:1, cyclohexane/EtOAc, stained in DNP) showed no remaining starting material. The reaction mixture was quenched with water and the product was extracted with Et_2O (3x), organic phases were washed with water (2x). The combined organic phases were dried over Na_2SO_4 filtered and concentrated. The crude material was purified by SiO_2 flash column chromatography (pentane/Et_2O, 5:1) to provide 4,4'-(2,2-dichloroethene-1,1-diyl)bis(methoxybenzene) (41.0 mg, 0.13 mmol, 32% yield) as a colorless oil.

^{1}H NMR (400 MHz, $CDCl_3$) δ 7.24 – 7.12 (m, 4H), 6.91 – 6.65 (m, 4H), 3.81 (s, 6H).

Characterization was consistent with the reported data. [79]

General procedure A for the synthesis of gold(I) vinylidenoids

In a flamed and dried Schlenk flask equipped with a stirring bar and under Ar atm the corresponding 1-diaryl-2-chloroalkene (1.0 equiv) was dissolved in a mixture of dry THF/Et_2O/Hexane 4:1:1 (0.3 M/0.4 M) and cooled down to –90 ºC. At this temperature, *n*-BuLi (1.1 equiv) was added dropwise. After 1 hour stirring at –90 ºC, JohnPhosAuCl (1.0 equiv) dissolved in the minimum amount of dry THF was added. Reaction was stirred at –90 ºC for 30 minutes and followed by ^{31}P{H} NMR. When no JohnPhosAuCl was detected, the reaction was warmed up to room temperature and concentrated under vacuum to obtain a yellow oil. The yellow oil was dissolved in a minimum amount of CH_2Cl_2 and

79 Mahato, S. B.; Manfal, N. B.; Pal, A. K.; Maitra, S. K. *Journal of Organic Chemistry* **1984**, *49*, 718–720.

directly submitted to purification via nitrogen flash Al_2O_3 column chromatography with a mixture of pentane/Et_2O (attention, charge of the column via a Al_2O_3 plug lead to decomposition of the products).

Gold(I) Vinylidenoid 30

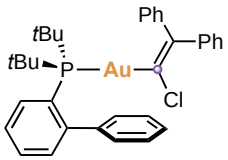

The title complex was synthesized according to the general procedure A from (2-chloroethene-1,1-diyl)dibenzene (70.0 mg, 326.0 µmol, 1.0 equiv), *n*-BuLi (134.0 µL, 2.4 molar, 326.0 µmol, 1.0 equiv), dry THF/Et_2O/Hexane 4:1:1 (518:129:129 µL, 0.4 M) and JohnPhosAuCl (173.0 mg, 326.0 µmol, 1.0 equiv) dissolved in 0.5 mL of dry THF. The crude product was purified via nitrogen flash Al_2O_3 column chromatography using a 10:1 mixture of pentane/Et_2O to obtain the title product (103.0 mg, 145.3 µmol, 44% yield) as a white solid.

^{1}H NMR (500 MHz, CD_2Cl_2) δ 7.91 – 7.85 (m, 1H), 7.52 – 7.42 (qt, *J* = 7.7, 1.6, 2H), 7.41 – 7.36 (tt, J=7.7, 1.3 1H), 7.36 – 7.25 (m, 6H), 7.25 – 7.16 (m, 4H), 7.17 – 7.07 (m, 3H), 7.07 – 7.01 (m, 2H), 1.35 (s, 9H), 1.32 (s, 9H). **^{13}C{^{1}H} NMR** (126 MHz, CD_2Cl_2) δ 174.1 (d, *J* = 131.8 Hz), 150.7 (d, *J* = 15.7 Hz), 147.1 (d, *J* = 5.8 Hz), 146.1 (d, *J* = 1.8 Hz), 144.0 (d, *J* = 5.1 Hz), 143.1 (d, *J* = 5.9 Hz), 135.1, 133.2 (d, *J* = 7.4 Hz), 130.6, 130.4 (d, *J* = 2.3 Hz), 129.8, 129.3, 128.9, 128.2, 128.1, 128.0, 127.7, 127.6, 126.9 (d, *J* = 5.6 Hz), 126.3, 126.1, 37.5 (d, *J* = 20.8 Hz), 31.0(d, *J* = 7.0 Hz). **^{31}P{^{1}H} NMR** (202 MHz, CD_2Cl_2) δ 66.25. **HRMS** (ESI+) calculated for [$C_{34}H_{38}AuClP$] 709.2060 *m/z*; found [M + H]$^+$ 709.2057. **M.p. =** > 125 ºC (decomposition).

^{13}C Gold(I) Vinylidenoid 42

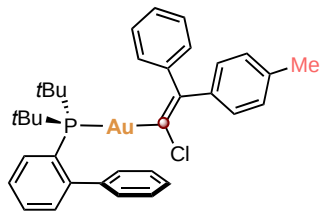

The title complex was synthesized according to the general procedure A from (*Z*)-1-(2-chloro-1-phenylvinyl-2-^{13}C)-4-methylbenzene (19.2 mg, 83.6 µmol, 1.0 equiv), *n*-BuLi (40.1 µL, 2.3 M, 91.9 µmol, 1.1 equiv), dry THF/Et_2O/Hexane 4:1:1 (160.0:40.0:40.0 µL, 0.3 M) and JohnPhosAuCl (44.4 mg, 83.6 µmol, 1.0 equiv) dissolved in 0.2 mL of dry THF. The crude product was purified via nitrogen flash Al_2O_3 column chromatography using a 10:1 to 4:1 mixture of pentane/Et_2O to obtain the title product (12.3 mg, 17.0 µmol, 21% yield) as a white solid. The ^{12}C-isotopologue was parallelly synthesized to facilitate the characterization of the compound.

^{1}H NMR (500 MHz, CD_2Cl_2) δ 7.87 (td, *J* = 7.2, 1.7 Hz, 1H), 7.49 – 7.43 (m, 2H), 7.36 (tt, *J* = 7.5, 1.2 Hz, 1H), 7.31 – 7.24 (m, 4H), 7.22 – 7.19 (m, 1H), 7.16 – 7.05 (m, 7H), 7.04 – 7.00 (m, 2H), 2.35 (s, 3H), 1.32 (d, *J* = 14.7 Hz, 18H). **^{13}C{^{1}H} NMR** (126 MHz, CD_2Cl_2) reported from the ^{12}C-isotopologue for clarity δ 173.9 (J_{C-P} = 131.9 Hz), 150.7, 150.6, 146.9 (d, J = 5.3 Hz), 146.3 (d, *J* =1.7 Hz), 143.1 (d, J = 5.5 Hz), 141.0 (d, J = 5.1 Hz), 136.0, 135.1, 133.2 (d, J = 7.8 Hz), 130.4, 129.8, 129.3, 128.9, 128.7, 128.3, 128.0, 127.7, 127.6, 127.0 (d, J = 6.5 Hz), 126.0, 37.6, 37.4, 31.0, 30.9, 21.3. **^{13}C{^{1}H} NMR**

(126 MHz, CD_2Cl_2) ^{13}C-isotopologue δ 173.9 ($J_{C–P}$ = 131.9 Hz) (^{13}C-labelled). **^{31}P{^{1}H} NMR** (202 MHz, CD_2Cl_2) δ 66.2 (d, *J* = 131.4 Hz). **HRMS** (ESI+) calculated for $[C_{34}H_{40}AuClP^{\wedge 13}C]^+$ 724.2250 *m/z*; found $[M + H]^+$ 724.2245. **M.p. =** 147–148 ºC.

^{13}C Gold(I) Vinylidenoid 43

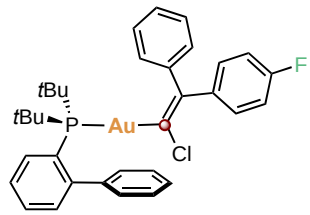

The title complex was synthesized according to the general procedure A from (*Z*)-1-(2-chloro-1-phenylvinyl-2-^{13}C)-4-fluorobenzene (10.5 mg, 44.9 µmol, 1.0 equiv), *n*-BuLi (19.9 µL, 2.5 M, 49.4 µmol, 1.1 equiv), dry THF/Et_2O/Hexane 4:1:1 (120:30:30 µL, 0.3 M) and JohnPhosAuCl (23.9 mg, 44.9 µmol, 1.0 equiv) dissolved in 0.2 ml of dry THF. The crude product was purified via nitrogen flash Al_2O_3 column chromatography using a 10:1 to 4:1 mixture of pentane/Et_2O to obtain the title product (22.0 mg, 30.0 µmol, 67 % yield) as a white solid. The ^{12}C-isotopologue was parallelly synthesized to facilitate the characterization of the compound.

^{1}H NMR (500 MHz, CD_2Cl_2) δ 7.87 (td, *J* = 8.3, 1.6 Hz, 1H), 7.50 – 7.42 (m, 2H), 7.37 – 7.33 (m, 1H), 7.30 – 7.24 (m, 4H), 7.22 – 7.16 (m, 3H), 7.15 – 7.07 (m, 3H), 7.05 – 6.99 (m, 4H), 1.34 (s, 9H), 1.31 (s, 9H).**^{13}C{^{1}H} NMR** (101 MHz, CD_2Cl_2) δ 174.6 (d, $J_{C–P}$ =131.4 Hz) (^{13}C-labelled) 161.6 (d, $J_{C–F}$ = 243.8 Hz), 150.6 (d, $J_{C–P}$ = 15.7 Hz), 143.1 (d, $J_{C–P}$ = 5.8 Hz), 135.1, 133.3, 133.2, 132.2 (dd, $J_{C–P, C-F}$ = 7.8, 2.8 Hz), 130.5 (d, J_{C-F} = 2.2 Hz), 129.8 (d, $J_{C–P}$ = 4.6 Hz), 129.3, 128.9, 128.2, 127.8, 127.7, 127.6, 126.9 (d, $J_{C–P}$ = 5.7 Hz), 126.2, 116.5, 114.7 (d, $J_{C–F}$ = 21.1 Hz), 37.6, 37.4, 31.0, 30.9. **^{31}P{^{1}H} NMR** (202 MHz, CD_2Cl_2) δ 66.2 (d, $J_{C–P}$ = 131.4 Hz).**^{19}F{^{1}H} NMR** (471 MHz, CD_2Cl_2) δ – 117.6. **HRMS** (ESI+) calculated for $[C_{33}H_{36}AuClFNaP^{\wedge 13}C]^+$ 750.1819 *m/z*; found $[M + Na]^+$ 750.1807. **M.p.** = 191–192 ºC.

^{13}C Gold(I) Vinylidenoid 44 *E*

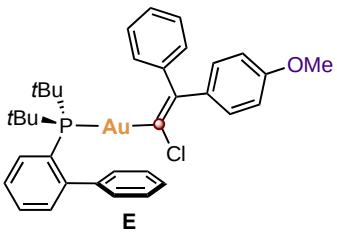

E

The title complex was synthesized according to the general procedure A from (*Z*)-1-(2-chloro-1-phenylvinyl2-^{13}C)-4-methoxybenzene (9.8 mg, 45.6 µmol, 1.0 equiv), *n*-BuLi (20.2 µL, 2.5 M, 50.2 µmol, 1.1 equiv), dry THF/Et_2O/Hexane 4:1:1 (100:25:25 µL, 0.3 M) and JohnPhosAuCl (24.2 mg, 45.6 µmol, 1.0 equiv) dissolved in 0.2 ml of dry THF. The crude product was purified via nitrogen flash Al_2O_3 column chromatography using a 10:1 to 5:1 mixture of pentane/Et_2O to obtain the title product (5.7 mg, 7.7 µmol, 17% yield) as a white sticky solid. The ^{12}C-isotopologue was parallelly synthesized to facilitate the characterization of the compound.

^{1}H NMR (400 MHz, CD_2Cl_2) δ 7.87 (td, *J* = 7.0, 1.8 Hz, 1H), 7.50 – 7.42 (m, 2H), 7.39 – 7.33 (m, 1H), 7.30 – 7.24 (m, 4H), 7.22 – 7.18 (m, 1H), 7.15 – 7.08 (m, 5H), 7.05 – 7.00 (m, 2H), 6.89 – 6.84 (m, 2H), 3.80 (s, 3H), 1.34 (s, 9H), 1.30 (s, 9H). **^{13}C{^{1}H} NMR** (126 MHz, CD_2Cl_2) δ 173.0 (d, $J_{C–P}$ = 130.5 Hz) (^{13}C-labelled), 157.0, 149.1(d, $J_{C–P}$ = 15.3 Hz), 145.6 (d, $J_{C–P}$ = 6.1 Hz), 142.2 (d, *J* = 5.8 Hz),

134.9 (d, J = 4.6 Hz), 134.2, 132.00 (d, J = 7.5 Hz), 130.9, 129.6, 128.7, 128.1, 127.9, 127.6, 126.9, 126.6, 126.4, 126.3, 125.5, 112.2, 54.8, 36.3(d, J_{C-P} = 21.4 Hz), 29.85. **$^{31}P\{^{1}H\}$** NMR (162 MHz, CD_2Cl_2) δ 66.37 (d, J_{C-P} = 131.8 Hz). **HRMS** (ESI+) calculated for $[C_{34}H_{39}AuClNaOP^{\wedge 13}C]^+$ 762.2018 *m/z*; found $[M + Na]^+$ 762.2006.

^{13}C Gold(I) Vinylidenoid 44 *Z*

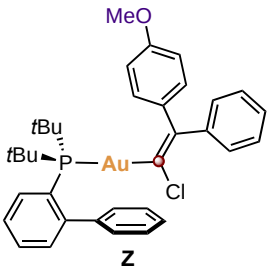

Z

The title complex was synthesized according to the general procedure A from (*E*)-1-(2-chloro-1-phenylvinyl-2-^{13}C)-4-methoxybenzene (15.0 mg, 69.9 µmol, 1.0 equiv), *n*-BuLi (31.0 µL, 2.5 M, 76.9 µmol, 1.1 equiv), dry THF/Et_2O/Hexane 4:1:1 (200:50:50 µL, 0.3 M) and JohnPhosAuCl (37.1 mg, 69.9 µmol, 1.0 equiv) dissolved in 0.2 ml of dry THF. The crude product was purified via nitrogen flash Al_2O_3 column chromatography using a 10:1 to 5:1 mixture of pentane/Et_2O to obtain the title product (15.0 mg, 30.0 µmol, 29% yield) as a white sticky solid. The ^{12}C-isotopologue was parallelly synthesized to facilitate the characterization of the compound.

^{1}H NMR (400 MHz, CD_2Cl_2) δ 7.90 – 7.85 (m, 1H), 7.51 – 7.42 (m, 2H), 7.40 – 7.35 (m, 1H), 7.35 – 7.26 (m, 4H), 7.24 – 7.16 (m, 6H), 7.07 – 7.03 (m, 2H), 6.68 – 6.64 (m, 2H), 3.72 (s, 3H), 1.35 (s, 9H), 1.32 (s, 9H). **$^{13}C\{^{1}H\}$ NMR** (126 MHz, CD_2Cl_2) 172.9 (d, J_{C-P} =132.3 Hz) (^{13}C-labelled), 158.4, 150.7 (d, J = 15.7 Hz), 146.7, 146.1, 144.2, 143.1 (d, J_{C-P} = 5.7 Hz), 138.9 (d, J_{C-P} = 10.7 Hz), 135.1, 133.2 (d, J_{C-P} = 7.4 Hz), 130.7 (d, J_{C-P} = 4.6 Hz), 130.5 (d, J_{C-P} = 2.8 Hz), 130.4 (d, J_{C-P} = 2.3 Hz), 129.3, 128.9, 128.0, 127.7, 126.9 (d, J_{C-P} = 5.6 Hz), 126.3, 113.0, 55.6, 37.5 (d, J_{C-P} = 20.7 Hz), 31.0 (d, J_{C-P} = 7.0 Hz). **$^{31}P\{^{1}H\}$ NMR** (162 MHz, CD_2Cl_2) δ 66.4 (d, J_{C-P} = 131.8 Hz). **HRMS** (ESI+) calculated for [C34H40AuClOP^13C]$^+$ 740.2199; found $[M + H]^+$ 740.2191.

^{13}C Gold(I) Vinylidenoid 50 *E*

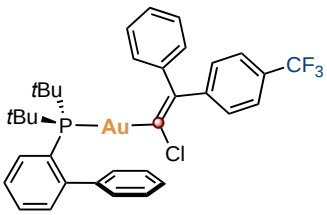

The title complex was synthesized according to the general procedure A from (*E*)-1-(2-chloro-1-phenylvinyl-2-^{13}C)-4-(trifluoromethyl)benzene (5.2 mg, 18.0 µmol, 1.0 equiv), *n*-BuLi (9.1 µL, 2.2 M, 20.0 µmol, 1.1 equiv), dry THF/Et_2O/Hexane 4:1:1 (40:10:10 µL, 0.3 M) and JohnPhosAuCl (9.7 mg, 18.0 µmol, 1.0 equiv) dissolved in 0.1 ml of dry THF. The crude product was purified via nitrogen flash Al_2O_3 column chromatography using a 10:1 to 5:1 mixture of pentane/Et_2O to obtain the title product (3.0 mg, 3.9 µmol, 21% yield) as a white solid.

^{1}H NMR (500 MHz, CD_2Cl_2) δ 7.88 (td, J = 7.1, 2.1 Hz, 1H), 7.59 (d, J = 8.0 Hz, 2H), 7.47 (qt, td, J = 7.4, 1.5 Hz, 2H), 7.38 – 7.33 (m, 3H), 7.31 – 7.25 (m, 4H), 7.23–7.19 (m, 1H), 7.16 – 7.09 (m, 3H), 7.06 – 7.01 (m, 2H), 1.34 (s, 9H), 1.31 (s, 9H). **$^{13}C\{^{1}H\}$ NMR** (126 MHz, CD_2Cl_2) δ 175.6 (d, J_{C-P} = 131.2 Hz) (^{13}C-labelled), 150.57 (d, J_{C-P} = 15.6 Hz), 147.8, 145.3, 143.2 (d, J_{C-P} = 5.9 Hz), 135.1, 133.2 (d,

J_{C-P} = 7.4 Hz), 131.1 (d, J_{C-P} = 2.7 Hz), 130.5 (d, J_{C-P} = 2.2 Hz), 129.8 (d, J_{C-P} = 4.7 Hz), 129.3, 128.9, 128.2, 128.1, 127.8, 127.6, 127.0(d, J_{C-F} = 5.6 Hz), 126.4, 125.0(q, J_{C-F} = 3.4 Hz) 123.9, 117.5, 37.5 (d, J_{C-P} = 21.0 Hz), 31.0 (d, J_{C-P} = 8.2 Hz). **^{31}P{^{1}H} NMR** (162 MHz, CD_2Cl_2) δ 66.2 (J_{C-P} = 130.9 Hz). **^{19}F{^{1}H} NMR** (376 MHz, CD_2Cl_2) δ –62.59. **HRMS** (ESI+) calculated for [C34H36AuClF3NaP^13C]$^+$ 800.1787; found [M + Na]$^+$ 800.1787. **M.p.** = 156–157 ºC.

Gold(I) Vinylidenoid 61

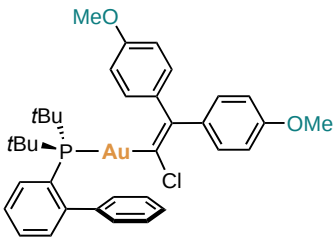

The title complex was synthesized according to the general procedure A from 4,4'-(2,2-dichloroethene-1,1-diyl)bis(methoxybenzene) (12.0 mg, 43.1 µmol, 1.0 equiv), *n*-BuLi (18.4 µL, 2.6 M, 47.5 µmol, 1.1 equiv), dry THF/Et_2O/Hexane 4:1:1 (100:25:25 µL, 0.3 M) and JohnPhosAuCl (22.9 mg, 43.1 µmol, 1.0 equiv) dissolved in 0.2 ml of dry THF. The crude product was purified via nitrogen flash Al_2O_3 column chromatography using a 10:1 to 5:1 mixture of pentane/Et_2O to obtain the title product (9.6 mg, 13.0 µmol, 30% yield) as a light yellow sticky solid.

^{1}H NMR (500 MHz, CD_2Cl_2) δ 7.94 – 7.89 (m, 1H), 7.54 – 7.46 (m, 2H), 7.40 (tt, *J* = 7.5, 1.3 Hz, 1H), 7.33 – 7.30 (m, 2H), 7.26 – 7.22 (m, 3H), 7.16 (dt, *J* = 9.50, 2.6 Hz, 2H), 7.09 – 7.06 (m, 2H), 6.89 (dt, *J* = 8.8, 2.6 Hz, 2H), 6.70(dt, *J* = 8.8, 2.4 Hz, 2H), 3.84 (s, 3H), 3.76 (s, 3H), 1.38 (s, 9H), 1.35 (s, 9H). **^{13}C{^{1}H} NMR** (Measured at 183K) (126 MHz, CD_2Cl_2) δ 172.3 (d, J_{C-P} = 131.2 Hz), 157.5 (d, J_{C-P} = 5.6 Hz), 149. 7 (d, J_{C-P} = 15.8 Hz), 145.5 (d, J_{C-P} = 5.4 Hz), 142.8 (d, J_{C-P} = 6.6 Hz), 138.38, 135.7 (d, J_{C-P} = 5.2 Hz), 134.8, 132.9, 132.59 (d, J_{C-P} = 7.1 Hz), 131.5, 130.3, 130.2, 128.7, 128.4, 127.6, 127.3, 127.2, 126.9 (d, J_{C-P} = 5.2 Hz), 114.0, 112.8, 112.3, 55.4, 36.9 (d, J_{C-P} = 20.8 Hz), 30.5. **^{31}P NMR{^{1}H}** (202 MHz, CD_2Cl_2) δ 66.3. **HRMS** (ESI+) calculated for [C36H42AuClO2P]$^+$ 769.2271; found [M + H]$^+$ 769.2279.

Gold(I) Vinylidenoid 62

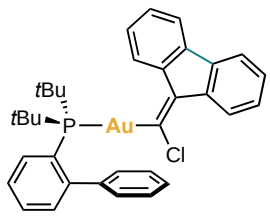

The title complex was synthesized according to the general procedure A from 9-(dichloromethylene)-9H-fluorene (70.0 mg, 283.0 µmol, 1.0 equiv), *n*-BuLi (145.0 µL, 2.0 M, 300.0 µmol, 1.1 equiv), dry THF (1.0 mL, 0.3 M) and JohnPhosAuCl (150.0 mg, 283.0 µmol, 1.0 equiv) dissolved in 0.3 ml of dry THF. The crude product was purified via nitrogen flash Al_2O_3 column chromatography using a 20:1 mixture of pentane/Et_2O to obtain the title product (56.0 mg, 79.2 µmol, 28% yield) as a pink solid.

^{1}H NMR (500 MHz, CD_2Cl_2) δ 8.74 – 8.70 (m, 2H), 7.99 – 7.95 (m, 1H), 7.80–7.75 (m, 1H), 7.72 (d, *J* = 7.5 Hz, 1H), 7.57 – 7.50 (m, 2H), 7.34 – 7.25 (m, 4H), 7.18 – 7.14 (m, 2H), 7.12 (ddd, *J* = 8.3, 7.2, 1.2 Hz, 1H), 7.05 (t, *J* = 7.7 Hz, 2H), 6.86 (tt, *J* = 7.7, Hz,1.1, 1H), 1.52 (s, 9H), 1.49 (s, 9H). **^{13}C{^{1}H} NMR** (101 MHz, CD_2Cl_2) δ 190.9 (d, J_{C-P} = 130.2 Hz), 150.7 (d, J_{C-P} = 15.5 Hz), 143.4 (d, J_{C-P} = 5.9

Hz), 141.9(d, J_{C-P} = 2.0 Hz), 140.5 (d, J_{C-P} = 6.4 Hz), 139.6, 139.0 (d, J_{C-P} = 5.5 Hz), 138.4, 135.0, 133.3 (d, J_{C-P} = 7.5 Hz), 130.7 (d, J_{C-P} = 2.2 Hz), 129.1(d, J_{C-P} = 15.0 Hz), 128.2, 127.8, 127.6, 127.2, 127.2, 126.9, 126.7, 126.5, 125.7, 122.2, 119.4, 119.1, 37.7 (d, J_{C-P} = 21.2 Hz), 31.1 (d, J_{C-P} = 6.8 Hz). **$^{31}P\{^{1}H\}$ NMR** (202 MHz, CD_2Cl_2) δ 65.4. **HRMS** (ESI+) calculated for $[C34H36AuClP]^+$ 707.1903 *m/z*; found $[M + H]^+$ 707.1900. **M.p. =** > 181 ºC (decomposition).

Aryl Migration Studies

Isotopomer ratios for η^2-diarylalkynes gold(I) complexes and free diarylalkynes were quantified by integration of the two alkynyl ^{13}C resonances (doublets for the η^2-diarylalkynes gold(I) complexes and singlets for the free alkynes). Prior studies of the group of Lloyd-Jones indicated that differences in longitudinal relaxation between the two alkynyl ^{13}C nuclei in alkynes are generally negligible.[58]

General procedure B for the migration studies

In a glovebox, the corresponding gold(I) vinylidenoid was weighed in an oven-dried standard NMR tube, dissolved in 0.4 ml of dry CD_2Cl_2 and capped with a rubber septum. Separately, $GaCl_3$ (1.1 equiv) was dissolved in dry CD_2Cl_2 (0.4 ml) in a HPLC vial and taken in a syringe with a long needle protected from air and from light.

Outside the glovebox, the capped NMR tube was cooled down to –90 ºC in an acetone/liquid nitrogen bath. Afterwards, the cold $GaCl_3$ solution was added over the mixture in the NMR tube at –90 ºC keeping the Ar atmosphere. The sample was transferred to the NMR instrument set at –90 ºC as fast as possible. The reaction was monitored by ^{1}H, $^{31}P\{H\}$, and $^{13}C\{H\}$DEPTq-135 NMR. $^{13}C\{H\}$DEPTq-135 were run instead of $^{13}C\{H\}$ NMR because they showed higher sensitivity in less time. Due to the mixture of (η^2-diphenylacetylene) gold(I) complexes, free alkynes and chloride bridge species the NMR signals of each species are difficult to account, thus only significant ones will be reported.

All the diarylakynes generated have been previously reported and the main characteristic signals of the products formed matches the reported ones.

Aryl migration of Gold(I) vinylidenoid 30

Treatment of gold(I) vinylidenoid **30** (5.0 mg, 7.0 μmol, 1.0 equiv) with $GaCl_3$ (1.4 mg, 7.8 μmol, 1.1 equiv) following procedure B, led to formation of (η^2-diphenylacetylene)gold(I) complex **32**, which after the increase of the temperature decomposes in chloride bridge **33** and diphenylacetylene. The small amount of chloride bridge **33** observed at –90ºC is formed during the transferring of the NMR tube from the cold bath at –90ºC to the NMR apparatus.

$^{13}C\{H\}$ NMR signals of expected product gold(I) vinylidene **31** were computed using DFT (303.1 ppm for C1), however any matching signal at this downfield was observed in the $^{13}C\{^{1}H\}$ spectra. Considering the expected reactivity, $^{13}C\{^{1}H\}$ NMR signals of (η^2-diphenylacetylene)gold(I) complex **32** were also computed. In this case, matching signals were found (Figure 21).

The formation of (η^2-diphenylacetylene)gold(I) complex was confirmed by treating JohnPhos gold(I) chloride with diphenylacetylene in the presence of $GaCl_3$ (Figure 22, bottom). The comparison of the low temperature $^{31}P\{^{1}H\}$ NMR of this reaction with the one of the treatment of gold(I) vinylidenoid **30** with $GaCl_3$ shows the same signals (Figure 22, up). This experiment confirmed the formation of (η^2-darylacetylene)gold(I) complexes in the aryl migration reactions studied, allowing the comparison between the migration trends of the two different aryl substituents in the coordinated and the free alkyne.

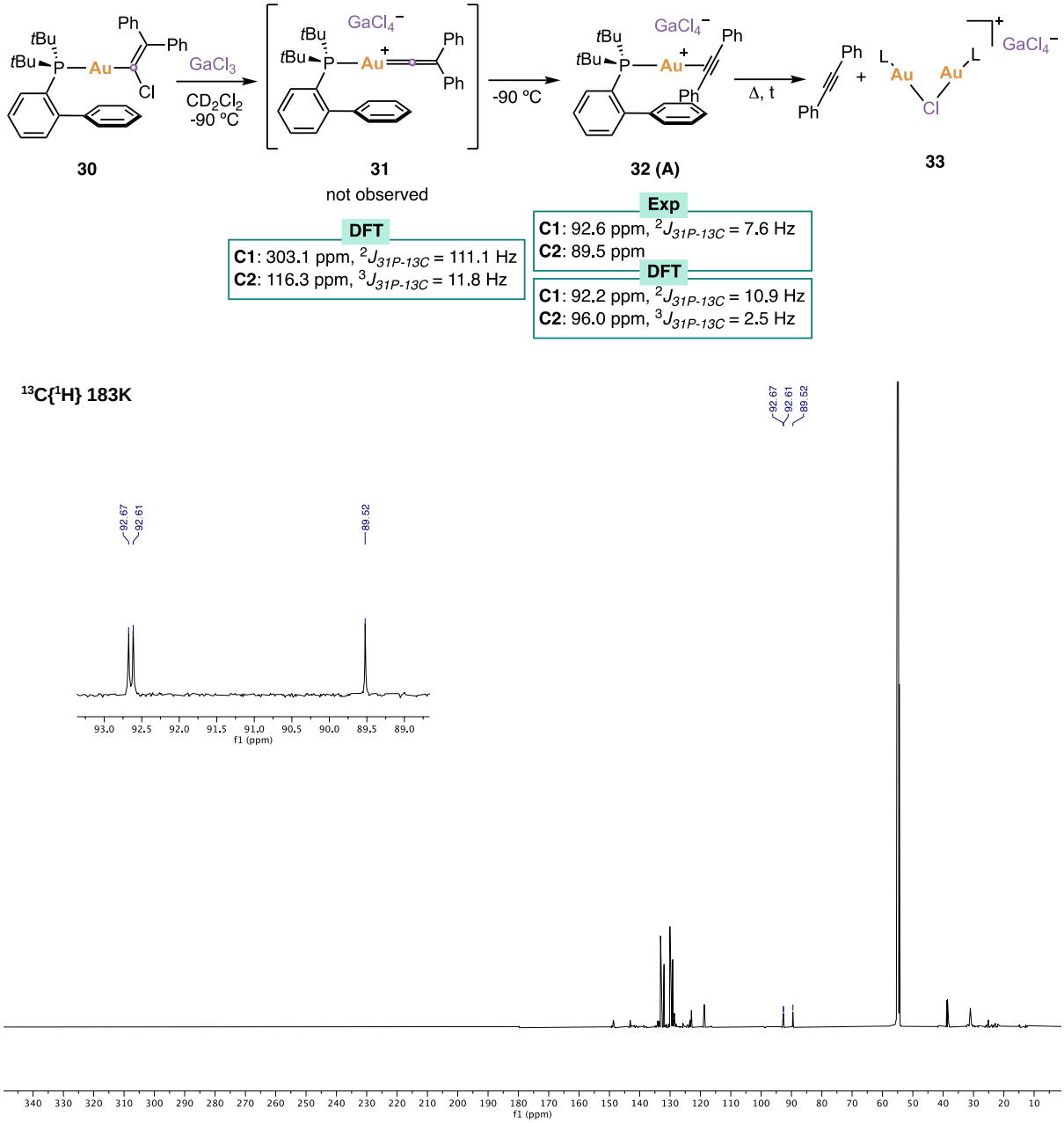

Figure 21. $^{13}C\{^{1}H\}$ NMR of treatment of vinylidenoid **30** with $GaCl_3$.

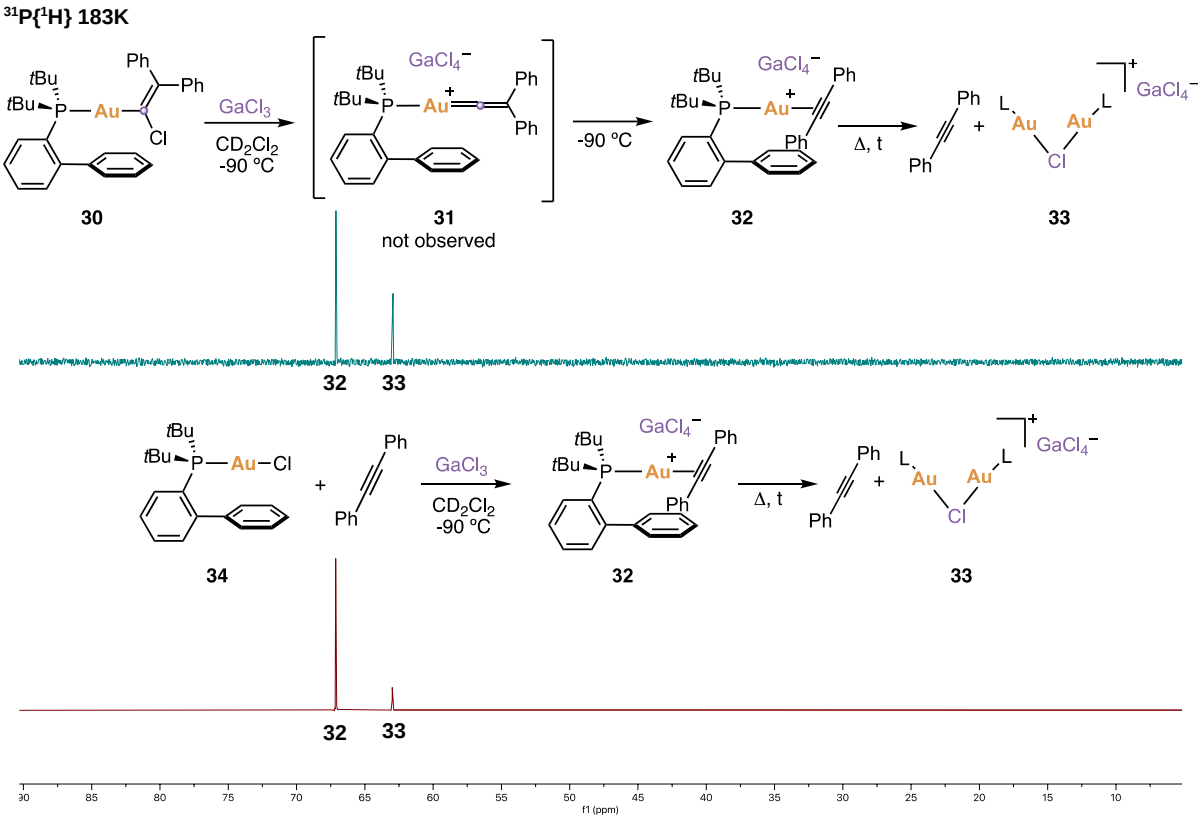

Figure 22. Confirmation of the formation of (η^2-darylacetylene)gold(I) complexes after treatment of the gold(I) vinylidenoids with $GaCl_3$.

Aryl migration of gold(I) vinylidenoid 42

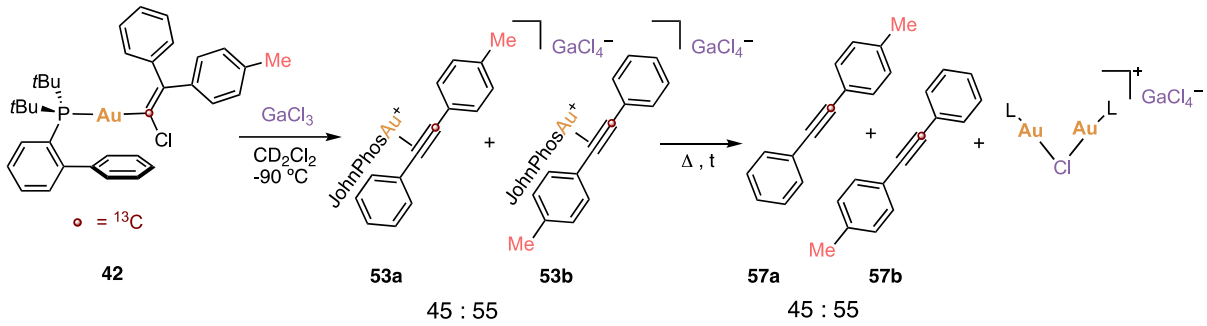

Treatment of gold(I) vinylidenoid **42** (6.0 mg, 8.3 μmol, 1.0 equiv) with $GaCl_3$ (1.6 mg, 9.1 μmol, 1.1 equiv) following procedure B, led to formation of isotopomers (η^2-diarylacetylene)gold(I) complexes **53a** and **53b**, which after the increase of the temperature decomposes in the chloride bridge and diarylacetylenes **57a** and **57b**. The isotopomer ratios of diaryl η^2-diarylalkynes gold(I)complexes **53a** and **53b** and diarylacetylenes **57a** and **57b** discloses a migration ratio of 45:55 of the tolyl substituent to the phenyl substituent (Figure 23).

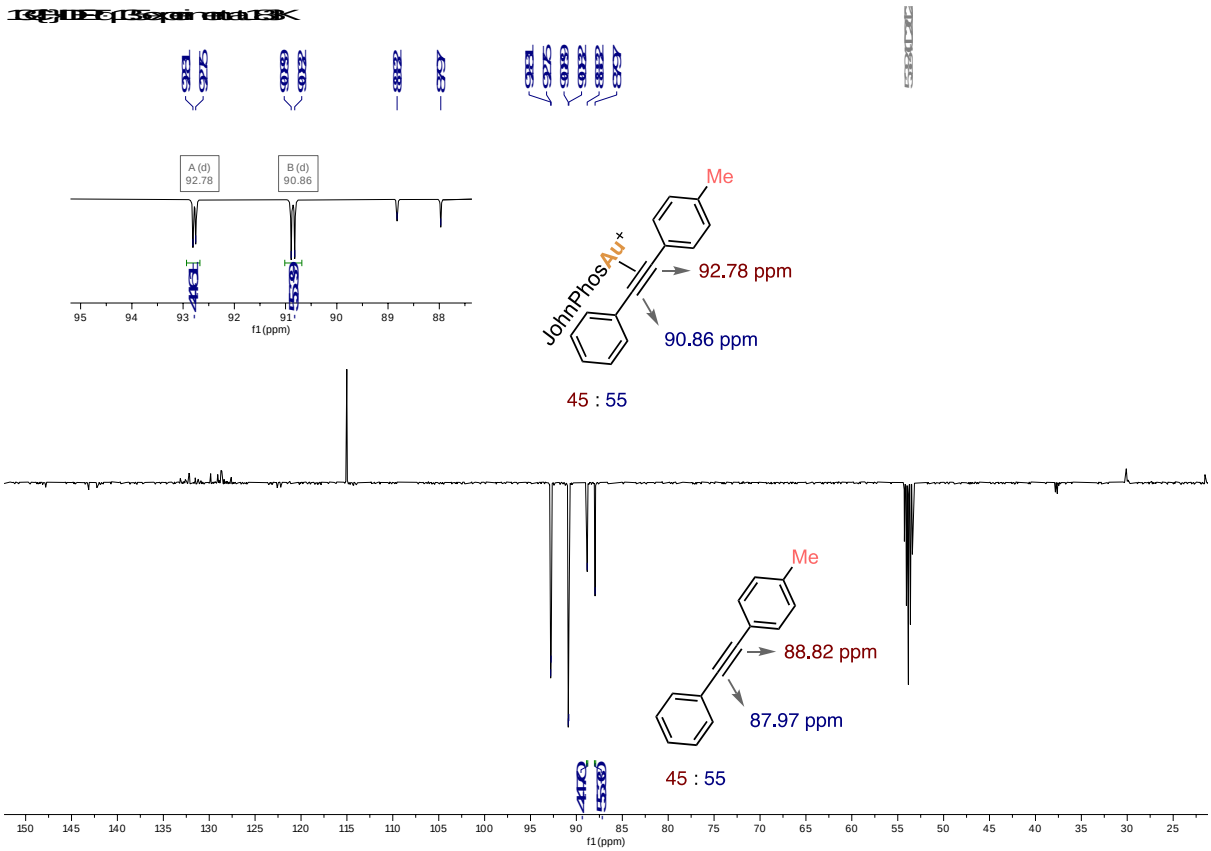

Figure 23. $^{13}C\{H\}$ DEPTq-135 NMR at 183K experiment of the treatment of gold(I) vinylidenoid **42** with $GaCl_3$.

Aryl migration of gold(I) vinylidenoid 43

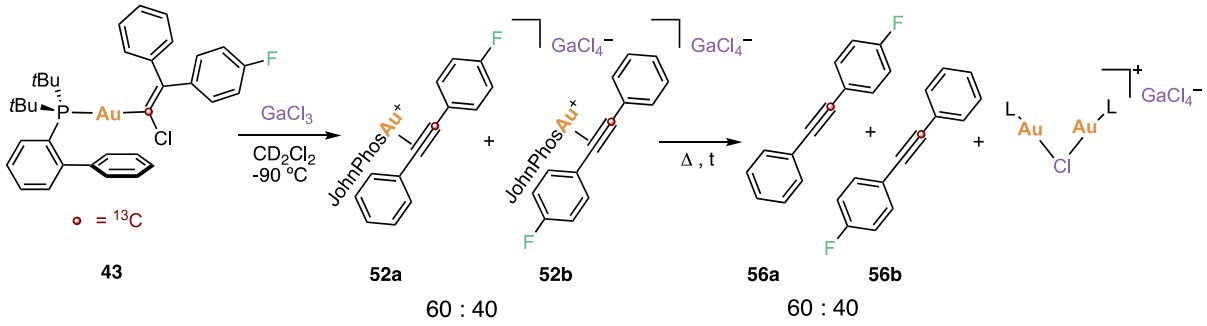

Treatment of gold(I) vinylidenoid **43** (5.6 mg, 7.7 μmol, 1.0 equiv) with $GaCl_3$ (1.5 mg, 8.5 μmol, 1.1 equiv) following procedure B, led to formation of isotopomers (η^2-diarylacetylene)gold(I) complexes **52a** and **52b**, which after the increase of the temperature decomposes in the chloride bridge and diarylacetylenes **56a** and **56b**. The isotopomer ratios of η^2-diarylalkynes gold(I)complexes **52a** and **52b** and diarylacetylenes **56a** and **56b** discloses a migration ratio of 60:40 of the fluorophenyl substituent over the phenyl substituent (Figure 24).

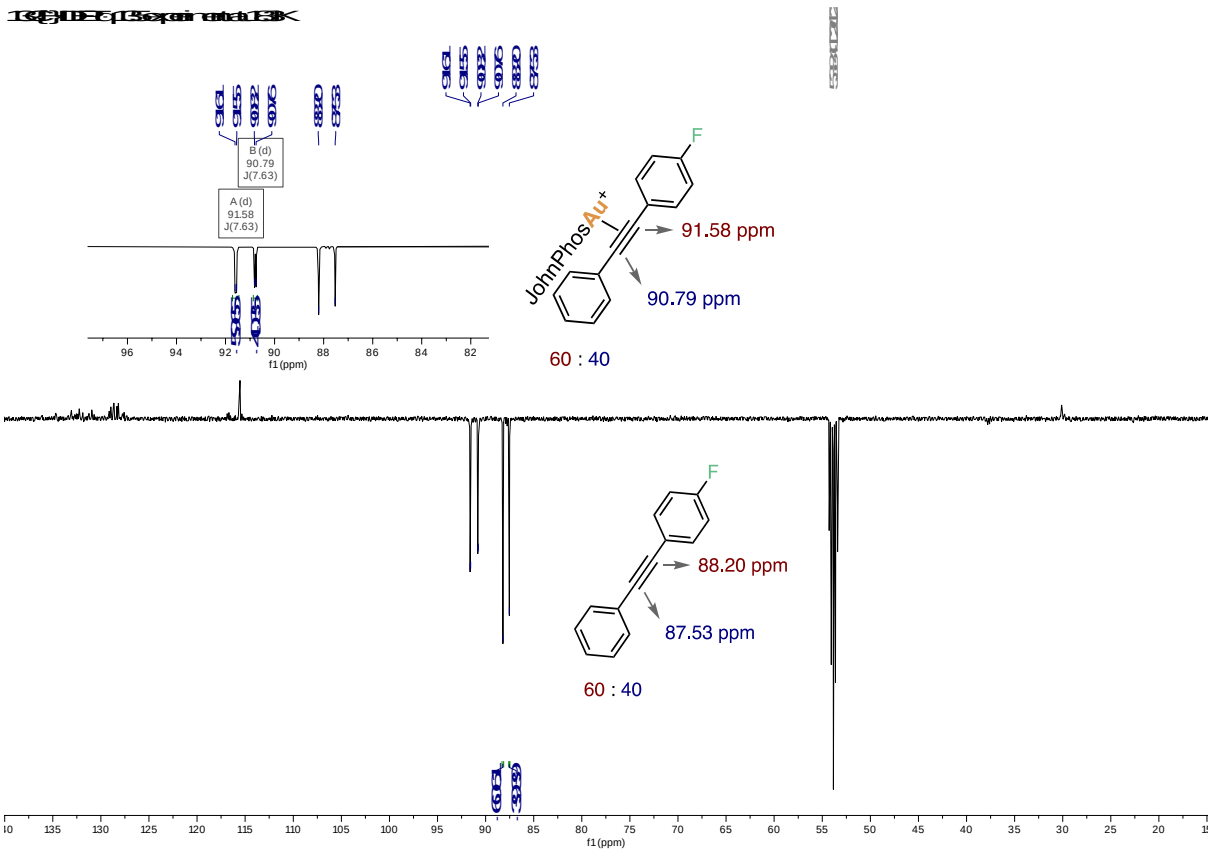

Figure 24. $^{13}C\{H\}$ DEPTq-135 NMR at 183K experiment of the treatment of gold(I) vinylidenoid **43** with $GaCl_3$.

Chapter III

Aryl migration of gold(I) vinylidenoid 44 *E*

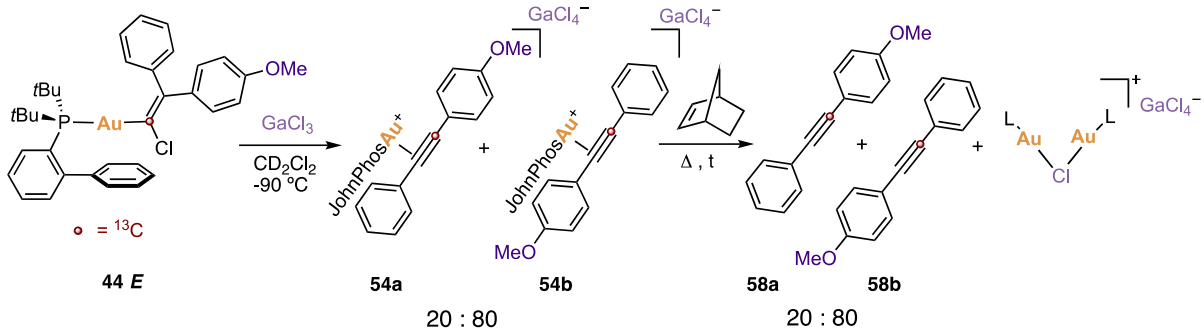

Treatment of gold(I) vinylidenoid **44 *E*** (5.0 mg, 6.8 μmol, 1.0 equiv) with $GaCl_3$ (1.3 mg, 7.4 μmol, 1.1 equiv) following procedure B, led to formation of isotopomers (η^2-diarylacetylene)gold(I) complexes **54a** and **54b**. However, in this case the signals appeared broadened, indicating a possible equilibrium with other species (Figure 25, up). The increase of the temperature instead of leading to the expected free arylalkynes **58a** and **58b** led to two unknown species which presented broad singlets (Figure 25, bottom). As it has been discussed in the results section, these signals were attributed to the species formed after coordination of gold(I) to the oxygen of the methoxy group. This coordination was broken by adding norbornene (2.1 mg, 22.0 μmol, 3.0 equiv) to the reaction, releasing diarylakynes **58a** and **58b**. The ratio of isotopomers formed was measured in both the (η^2-diarylacetylene)gold(I) complexes disclosing a migration ratio of 20:80 of the methoxyphenyl substituent to the phenyl substituent (Figure 26). This ratio is maintained when the arylalkynes **58a** and **58b** were released (22:78) the slight difference can be attributed to manual errors in the integration (Figure 27).

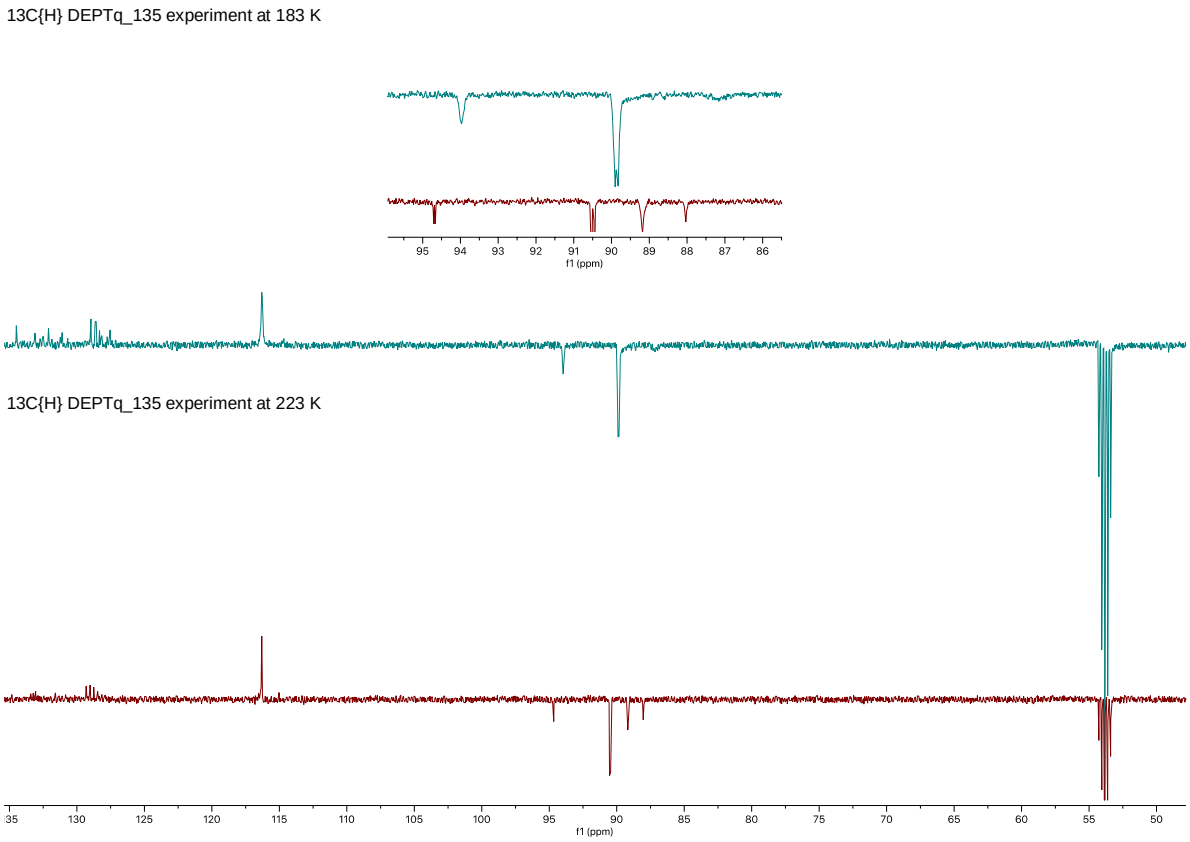

Figure 25. Treatment of gold(I) vinylidenoid **44** ***E*** with $GaCl_3$ and evolution of (η^2-diarylacetylene)gold(I) complexes to unknown species.

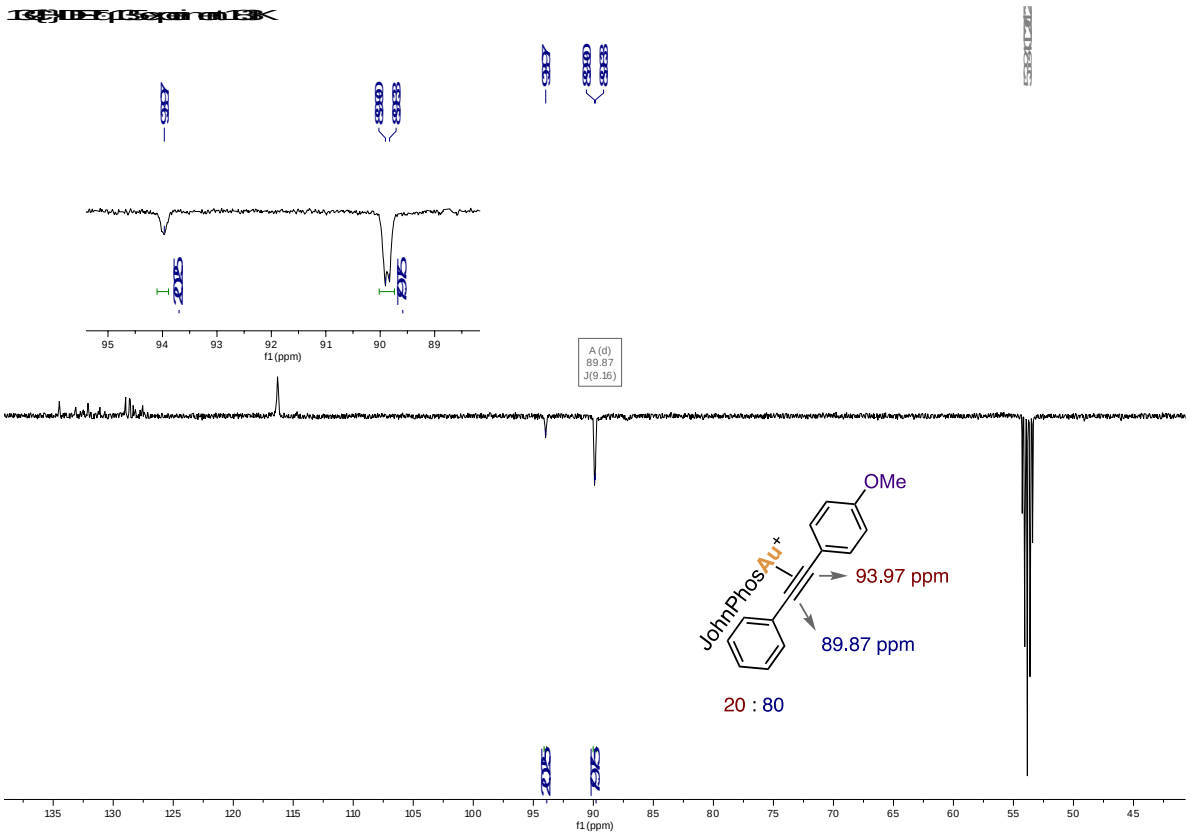

Figure 26. $^{13}C\{H\}$ DEPTq-135 NMR at 183K experiment of the treatment of gold(I) vinylidenoid **44** ***E*** with $GaCl_3$.

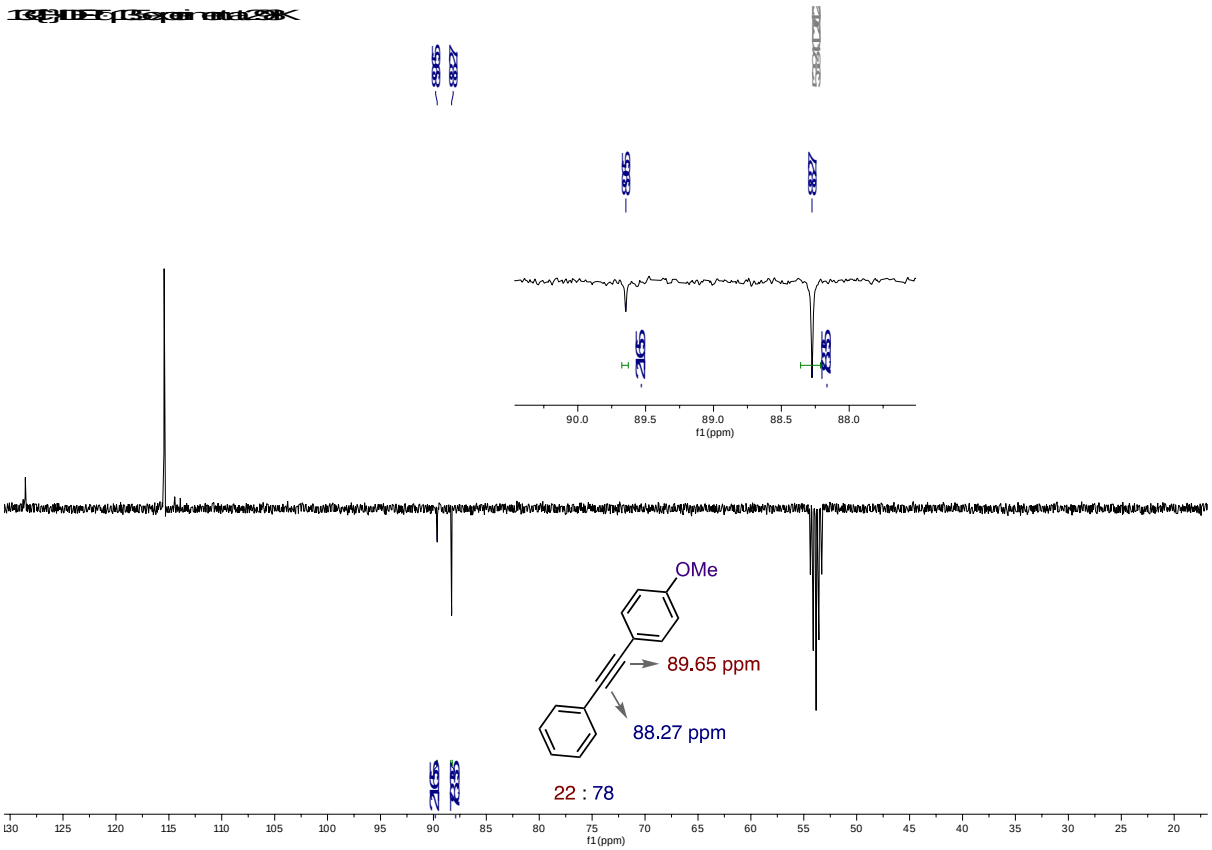

Figure 27. $^{13}C\{H\}$ DEPTq-135 NMR at 298 K of diarylacetylenes formed from treatment of vinylidenoid **44** ***E*** with $GaCl_3$.

To confirm the formation of (η^2-diarylacetylene)gold(I) complexes, this product was generated from ^{12}C isotopologue free diarylalkyne **58** and JohnPhos gold(I) chloride in the presence of $GaCl_3$ (Figure 28, down), and the $^{13}C\{^1H\}$DEPTq-135 spectra of both reactions were compared, showing matching signals (Figure 28)

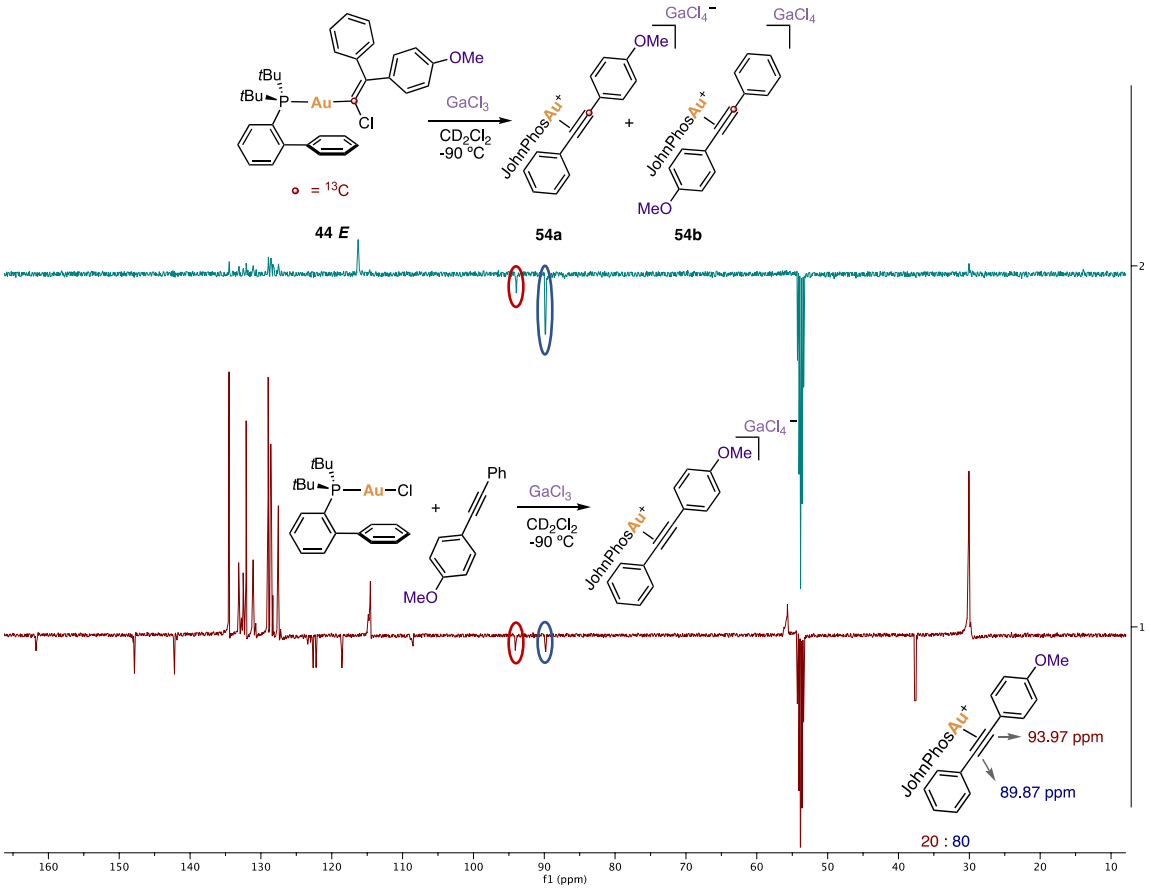

Figure 28. Confirmation of the formation of (η^2-darylacetylene)gold(I) complex **54** after treatment of gold(I) vinylidenoid **44** ***E*** with $GaCl_3$.

Aryl migration of gold(I) vinylidenoid 44 *Z*

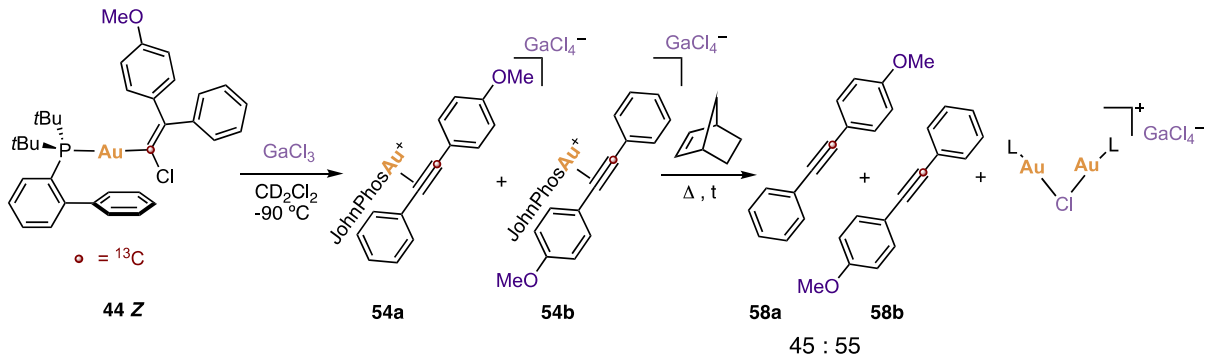

Treatment of gold(I) vinylidenoid **44** ***Z*** (6.0 mg, 8.3 µmol, 1.0 equiv) with $GaCl_3$ (1.6 mg, 9.1 µmol, 1.1 equiv) following procedure B, favored the formation of the unknown species attributed to oxygen-gold(I) coordinated species. However, the addition of norbornene (2.3 mg, 25.0 µmol, 3.0 equiv), allowed the release of diarylacetylene species **58a** and **58b**. This allowed the measurement of the ratio of isotopomers formed, which resulted in a 45:55 ratio, with a preferred migration of the phenyl substituent over the methoxyphenyl substituent (Figure 29).

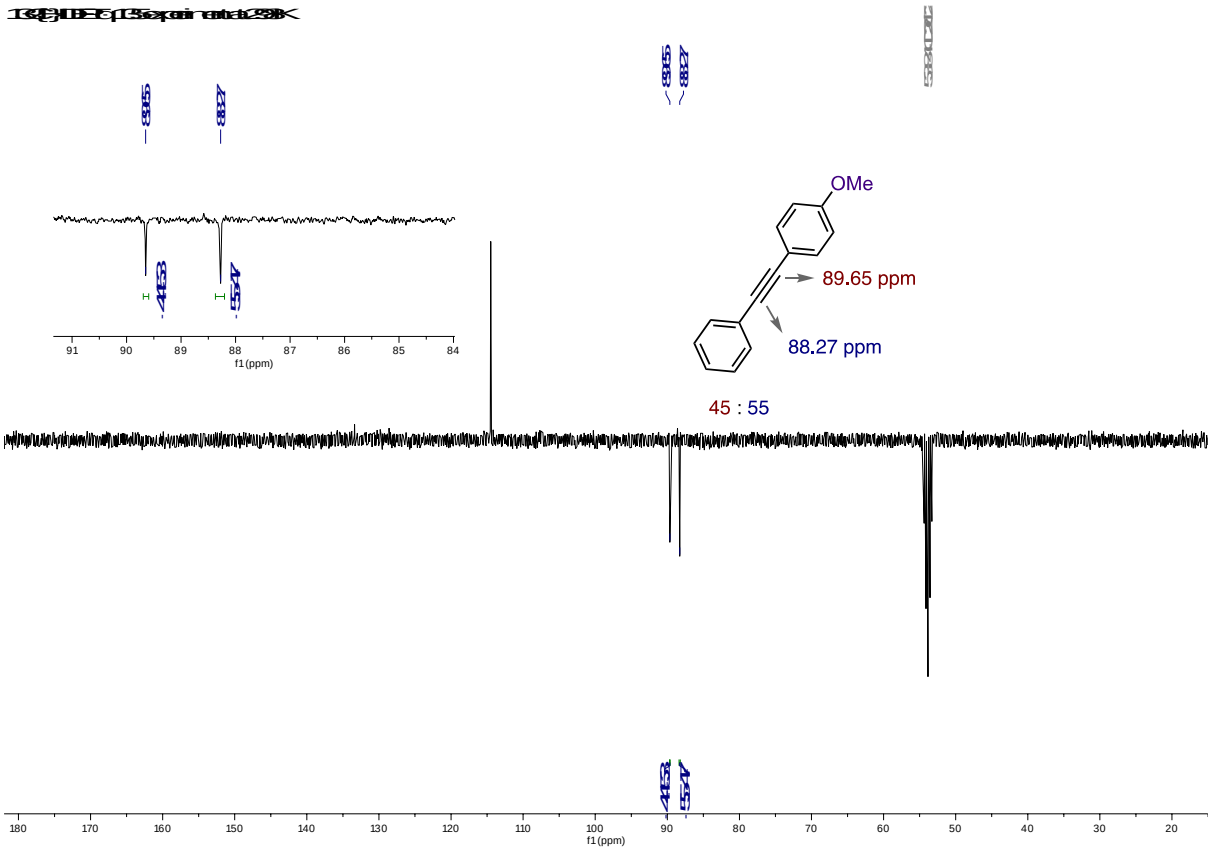

Figure 29. $^{13}C\{H\}$ DEPTq-135 NMR at 298 K of diarylacetylenes formed from treatment of vinylidenoid **44** ***Z*** with $GaCl_3$.

Aryl migration of gold(I) vinylidenoid 50 *E*

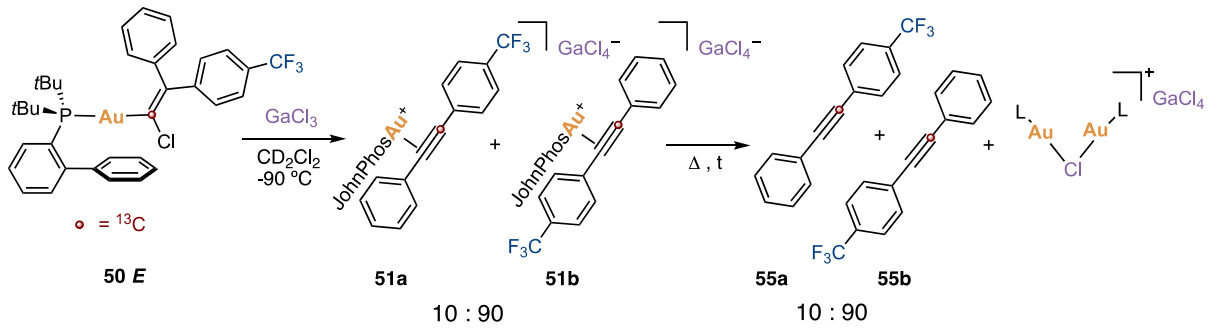

Treatment of gold(I) vinylidenoid **50** ***E*** (3.0 mg, 3.9μmol, 1.0 equiv) with $GaCl_3$ (0.8 mg, 4.3 μmol, 1.1 equiv) following procedure B, led to formation of isotopomers (η^2-diarylacetylene)gold(I) complexes **51a** and **51b**, which after the increase of the temperature decomposes in the chloride bridge and diarylacetylenes **55a** and **55b**. The isotopomer ratios of diaryl η^2-diarylalkynes gold(I)complexes **51a** and **51b** and diarylacetylenes **55a** and **55b** discloses a migration ratio of 10:90 of the trifluoromethylphenyl substituent to the phenyl substituent (Figure 30).

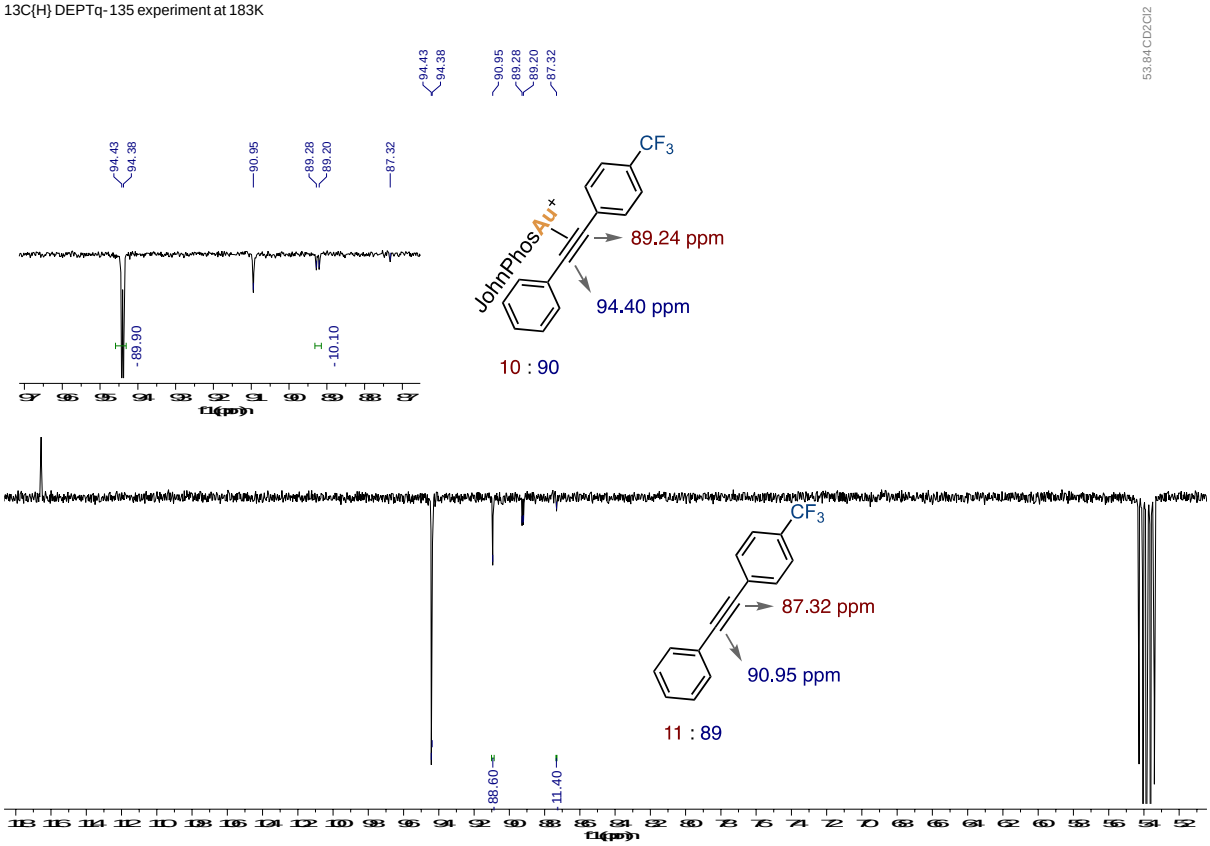

Figure 30. $^{13}C\{H\}$ DEPTq-135 NMR at 183K experiment of the treatment of gold(I) vinylidenoid **50** ***E*** with $GaCl_3$.

Crystallographic Data

Gold(I) Vinylidenoid 30

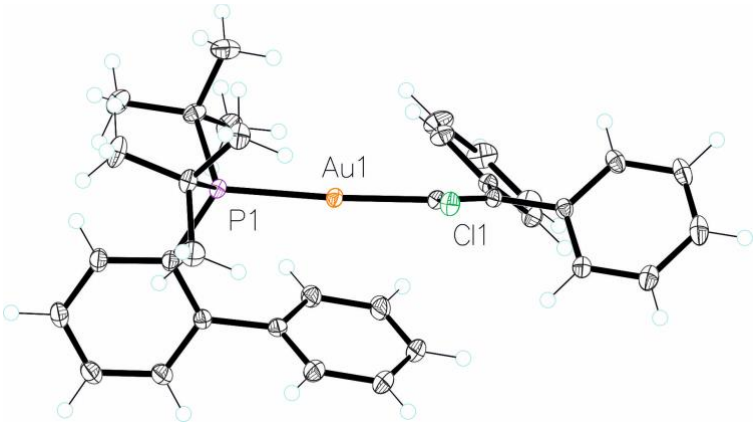

Table 13. Crystal data and structure refinement for Gold(I) Vinylidenoid **30**

Identification code	ICIQ 269a-19 AHP-06-012LT 20190617
Empirical formula	$C_{34}H_{37}AuPCl$
Formula weight	709.02
Temperature/K	100.15
Crystal system	monoclinic
Space group	$P2_1/c$
a/Å	11.25773(6)
b/Å	16.46421(9)
c/Å	16.22658(9)
α/°	90
β/°	99.8903(5)
γ/°	90
Volume/Å^3	2962.89(3)
Z	4
ρ_{calc}g/cm^3	1.589
μ/mm^{-1}	5.130
F(000)	1408.0

Crystal size/mm^3	0.3 × 0.28 × 0.15
Radiation	MoKα (λ = 0.71073)
2Θ range for data collection/°	4.428 to 74.364
Index ranges	-18 ≤ h ≤ 19, -27 ≤ k ≤ 27, -27 ≤ l ≤ 27
Reflections collected	102894
Independent reflections	14991 [R_{int} = 0.0340, R_{sigma} = 0.0215]
Data/restraints/parameters	14991/0/340
Goodness-of-fit on F^2	1.069
Final R indexes [I>=2σ (I)]	R_1 = 0.0196, wR_2 = 0.0480
Final R indexes [all data]	R_1 = 0.0230, wR_2 = 0.0489
Largest diff. peak/hole / e Å^{-3}	3.17/-1.11

Chloride bridge 33

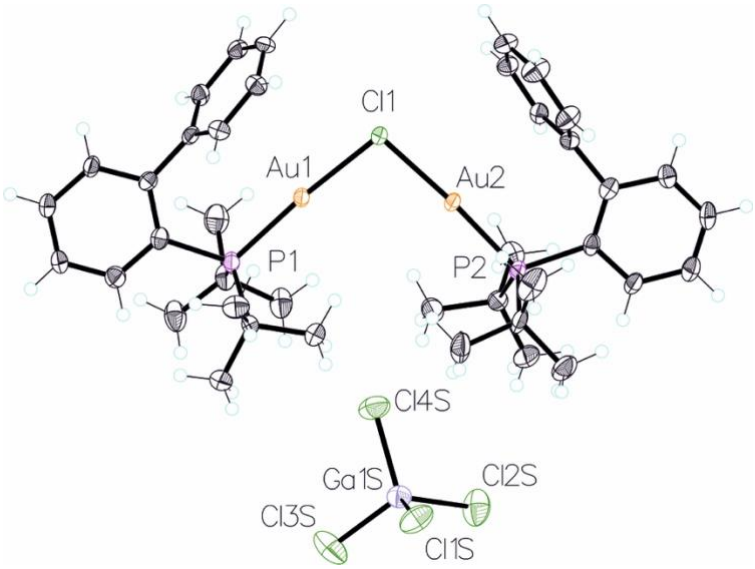

Table 14. Crystal data and structure refinement for chloride bridge **33**.

Identification code	AHP-06-028
Empirical formula	$C_{40}H_{54}P_2Cl_5GaAu_2$
Formula weight	1237.67
Temperature/K	100
Crystal system	triclinic

Space group	P-1
a/Å	11.3627(3)
b/Å	15.0280(4)
c/Å	15.7234(5)
α/°	99.892(2)
β/°	111.146(3)
γ/°	108.838(3)
Volume/$Å^3$	2240.04(12)
Z	2
$\rho_{calc}g/cm^3$	1.835
μ/mm^{-1}	7.527
F(000)	1196.0
Crystal size/mm^3	0.4 × 0.1 × 0.05
Radiation	MoKα (λ = 0.71073)
2Θ range for data collection/°	6.93 to 62.274
Index ranges	$-15 \leq h \leq 16$, $-21 \leq k \leq 20$, $-22 \leq l \leq 21$
Reflections collected	35566
Independent reflections	12913 [R_{int} = 0.0637, R_{sigma} = 0.0735]
Data/restraints/parameters	12913/0/463
Goodness-of-fit on F^2	0.946
Final R indexes [I>=2σ (I)]	R_1 = 0.0373, wR_2 = 0.0788
Final R indexes [all data]	R_1 = 0.0506, wR_2 = 0.0804
Largest diff. peak/hole / e $Å^{-3}$	2.83/-3.55

Gold(I) Vinylidenoid 42

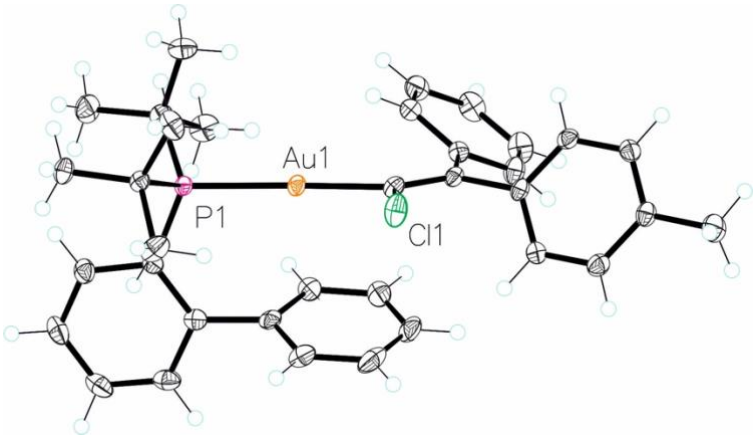

Table 15. Crystal data and structure refinement for Gold(I) Vinylidenoid **42**.

Identification code	mo_AHP06184P_0m
Empirical formula	$C_{35}H_{39}AuClP$
Formula weight	723.05
Temperature/K	100.04
Crystal system	monoclinic
Space group	$P2_1/c$
a/Å	10.8364(11)
b/Å	18.0466(18)
c/Å	16.0998(16)
α/°	90
β/°	102.209(2)
γ/°	90
Volume/Å^3	3077.3(5)
Z	4
ρ_{calc}g/cm^3	1.561
μ/mm^{-1}	4.941
F(000)	1440.0
Crystal size/mm^3	0.1 × 0.1 × 0.02
Radiation	MoKα (λ = 0.71073)

2Θ range for data collection/°	3.434 to 60.29
Index ranges	$-15 \leq h \leq 10$, $-22 \leq k \leq 25$, $-21 \leq l \leq 22$
Reflections collected	50076
Independent reflections	8986 [R_{int} = 0.0350, R_{sigma} = 0.0245]
Data/restraints/parameters	8986/0/350
Goodness-of-fit on F^2	1.044
Final R indexes [I>=2σ (I)]	R_1 = 0.0182, wR_2 = 0.0388
Final R indexes [all data]	R_1 = 0.0234, wR_2 = 0.0406
Largest diff. peak/hole / e $Å^{-3}$	1.13/-0.71

Gold(I) Vinylidenoid 43

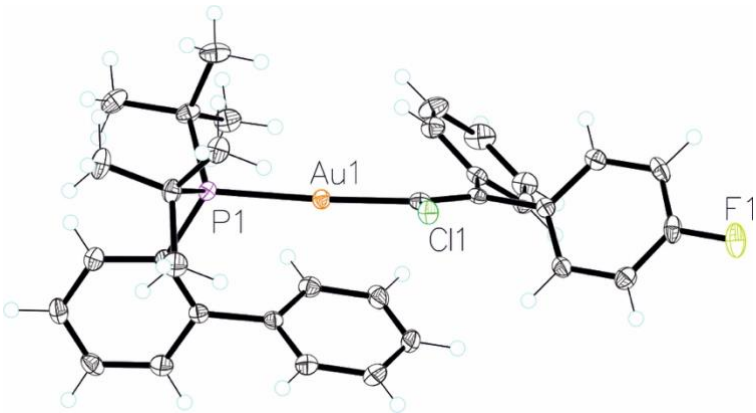

Table 16. Crystal data and structure refinement for Gold(I) Vinylidenoid **43**.

Identification code	ICIQ 43a-22 AHP-06-238LT 202202144
Empirical formula	$C_{34}H_{36}ClAuPF$
Formula weight	727.01
Temperature/K	100.15
Crystal system	monoclinic
Space group	$P2_1/c$
a/Å	11.33119(15)
b/Å	16.4646(2)
c/Å	16.2704(2)
α/°	90

β/°	98.0331(14)
γ/°	90
Volume/Å^3	3005.67(7)
Z	4
ρ_{calc}g/cm^3	1.607
μ/mm^{-1}	5.064
F(000)	1440.0
Crystal size/mm^3	0.2 × 0.2 × 0.2
Radiation	MoKα (λ = 0.71073)
2Θ range for data collection/°	4.81 to 58.634
Index ranges	-13 ≤ h ≤ 14, -22 ≤ k ≤ 22, -19 ≤ l ≤ 22
Reflections collected	35372
Independent reflections	7372 [R_{int} = 0.0319, R_{sigma} = 0.0256]
Data/restraints/parameters	7372/0/349
Goodness-of-fit on F^2	1.047
Final R indexes [I>=2σ (I)]	R_1 = 0.0181, wR_2 = 0.0404
Final R indexes [all data]	R_1 = 0.0226, wR_2 = 0.0415
Largest diff. peak/hole / e Å^{-3}	0.71/-0.54

Gold(I) Vinylidenoid 44 *Z*

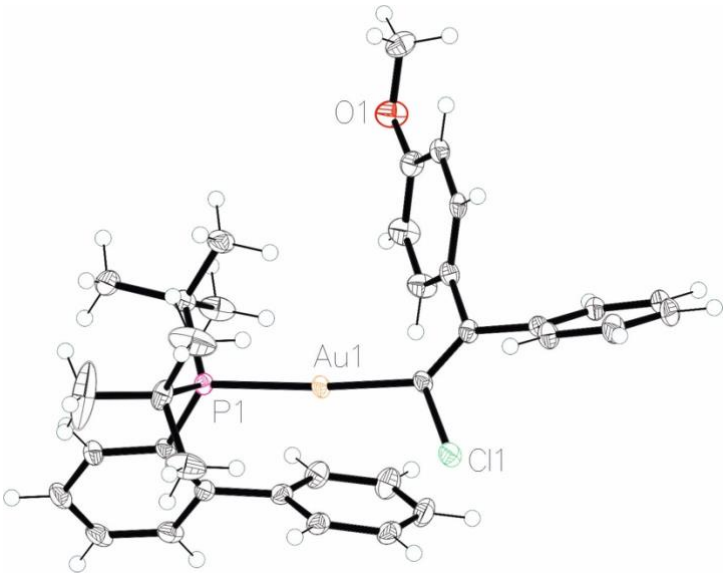

Table 17. Crystal data and structure refinement for Gold(I) Vinylidenoid **44 Z**.

Identification code	mo_AHP06284_0m
Empirical formula	$C_{35}H_{39}AuClOP$
Formula weight	739.05
Temperature/K	100.02
Crystal system	triclinic
Space group	P-1
a/Å	10.4642(7)
b/Å	12.0600(8)
c/Å	14.3546(9)
α/°	79.7997(16)
β/°	68.9427(15)
γ/°	65.6956(15)
Volume/Å^3	1539.82(18)
Z	2
ρ_{calc}g/cm^3	1.594
μ/mm^{-1}	4.942
F(000)	736.0

Crystal size/mm^3	0.1 × 0.1 × 0.01
Radiation	MoKα (λ = 0.71073)
2Θ range for data collection/°	3.708 to 62.32
Index ranges	-15 ≤ h ≤ 15, -17 ≤ k ≤ 17, -11 ≤ l ≤ 20
Reflections collected	19557
Independent reflections	9321 [R_{int} = 0.0209, R_{sigma} = 0.0316]
Data/restraints/parameters	9321/0/359
Goodness-of-fit on F^2	1.032
Final R indexes [I>=2σ (I)]	R_1 = 0.0248, wR_2 = 0.0575
Final R indexes [all data]	R_1 = 0.0304, wR_2 = 0.0597
Largest diff. peak/hole / e Å^{-3}	1.94/-1.43

Gold(I) Vinylidenoid 62

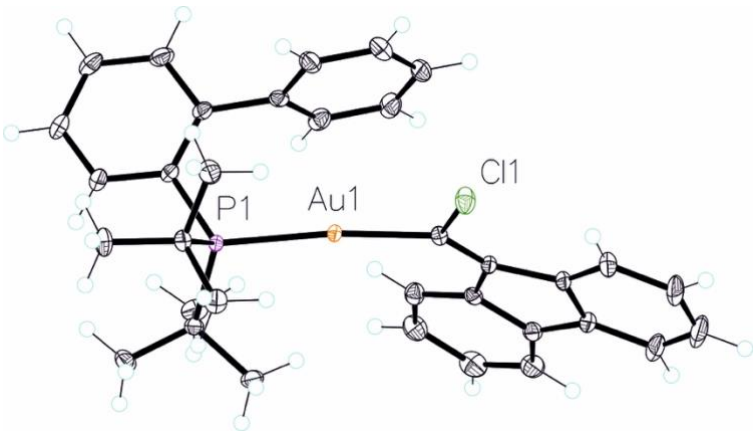

Table 18. Crystal data and structure refinement for Gold(I) Vinylidenoid **62**.

Identification code	iciq 469a-19 ahp-06-35clt 20191024
Empirical formula	$C_{11.33}H_{11.67}Au_{0.33}P_{0.33}Cl_{0.33}$
Formula weight	235.67
Temperature/K	100.15
Crystal system	triclinic
Space group	P-1
a/Å	8.58750(10)

b/Å	13.6184(2)
c/Å	13.6625(2)
α/°	69.9640(10)
β/°	80.1390(10)
γ/°	72.4300(10)
Volume/$Å^3$	1426.96(4)
Z	6
$\rho_{calc}g/cm^3$	1.645
μ/mm^{-1}	5.326
F(000)	700.0
Crystal size/mm^3	0.4 × 0.4 × 0.3
Radiation	MoKα (λ = 0.71073)
2Θ range for data collection/°	4.99 to 64.268
Index ranges	$-12 \leq h \leq 12$, $-20 \leq k \leq 20$, $-20 \leq l \leq 20$
Reflections collected	54487
Independent reflections	9556 [R_{int} = 0.0328, R_{sigma} = 0.0189]
Data/restraints/parameters	9556/0/340
Goodness-of-fit on F^2	1.061
Final R indexes [I>=2σ (I)]	R_1 = 0.0157, wR_2 = 0.0378
Final R indexes [all data]	R_1 = 0.0166, wR_2 = 0.0381
Largest diff. peak/hole / e $Å^{-3}$	1.25/-1.12

Computational Methods

Calculations were performed using Gaussian 09 suite of programs.[80] DFT was applied using B3LYP,[81] M06,[82] and B97D,[83] and PBE0[84] functionals in conjunction with Grimme's D3 dispersion correction. The SDD[85] basis set and ECP was used to describe Au. The 6-31G(d,p)[86] and 6-311+G(d,p)[87] basis sets were employed for all remaining atoms (C, H, P, O, F and Cl). Full geometry optimizations were carried out in dichloromethane, through an implicit polarizable continuum model (PCM) as implemented in Gaussian 09.[88] The stationary points were characterized by vibrational analysis. Transition states were identified by the presence of one imaginary frequency while no imaginary frequencies were found in minima. The connectivity of the transition states was confirmed by the relaxation of each transition state towards both the reactant and the product. Reported energies are potential energies (E) and free energies (G) in solution, computed at 298 K and 1 atm, unless otherwise stated. Optimized geometries were visualized using CYLview.[89]

NMR data was calculated at B3LYP/6-311+G(2d,p) level of theory in dichloromethane (PCM) using previously calculated scaling factor.[90]

---

80 Gaussian 09, Revision D.01, Frisch, M. J.; Trucks, G. W.; Schlegel, H. B.; Scuseria, G. E.; Robb, M. A.; Cheeseman, J. R.; Scalmani, G.; Barone, V.; Mennucci, B.; Petersson, G. A.; Nakatsuji, H.; Caricato, M.; Li, X.; Hratchian, H. P.; Izmaylov, A. F.; Bloino, J.; Zheng, G.; Sonnenberg, J. L.; Hada, M.; Ehara, M.; Toyota, K.; Fukuda, R.; Hasegawa, J.; Ishida, M.; Nakajima, T.; Honda, Y.; Kitao, O.; Nakai, H.; Vreven, T.; Montgomery, Jr., J. A.; Peralta, J. E.; Ogliaro, F.; Bearpark, M.; Heyd, J. J.; Brothers, E.; Kudin, K. N.; Staroverov, V. N.; Keith, T.; Kobayashi, R.; Normand, J.; Raghavachari, K.; Rendell, A.; Burant, J. C.; Iyengar, S. S.; Tomasi, J.; Cossi, M.; Rega, N.; Millam, J. M.; Klene, M.; Knox, J. E.; Cross, J. B.; Bakken, V.; Adamo, C.; Jaramillo, J.; Gomperts, R.; Stratmann, R. E.; Yazyev, O.; Austin, A. J.; Cammi, R.; Pomelli, C.; Ochterski, J. W.; Martin, R. L.; Morokuma, K.; Zakrzewski, V. G.; Voth, G. A.; Salvador, P.; Dannenberg, J. J.; Dapprich, S.; Daniels, A. D.; Farkas, O.; Foresman, J. B.; Ortiz, J. V.; Cioslowski, J.; Fox, D. J. Gaussian, Inc., Wallingford CT, **2013**.

81 (a) Becke, A. D. J. *Chem. Phys.* **1993**, *98*, 5648–5652. (b) Lee, C.; Yang, W.; Parr, R. G. *Phys. Rev. B.* **1988**, *37*, 785–789. (c) Stephens, P. J.; Devlin, F. J.; Chabalowsky, C. F.; Frisch, M. J. *J. Phys. Chem.* **1994**, *98*, 11623–11627.

82 Zhao, Y.; Truhlar, D. G. *Theor. Chem. Account.* **2008**, *120*, 215–241.

83 Grimme, S. *J. Comput. Chem*. **2006**, *27*, 1787–1799.

84 Adamo, C. *J. Chem. Phys.* **1999**, *110*, 6158–6170.

85 Andrae, D.; Haussermann, U.; Dolg, M.; Stoll, H.; Preuss, H. *Theor. Chim. Acta* **1990**, *77*, 123–141.

86 Hehre, W. J.; Ditchfield, R.; Pople, J. A. *J. Chem. Phys*. **1972**, *56*, 2257–2261.

87 Krishnan, R., Binkley, J. S., Seeger, R., Pople, J. A. *J. Chem. Phys.* **1980**, *72*, 650–654.

88 Cancès, M. T.; Mennucci, B. B.; Tomasi, J. *J. Chem. Phys.* **1997**, *107*, 3032−3041.

89 CYLview20; Legault, C. Y., Université de Sherbrooke, **2020** (http://www.cylview.org).

90 Pierens, G. K. J. *Comput. Chem*. **2014**, *35*, 1388–1394.

Benchmarks

Table 19. Benchmark of absolute calculated energy values of 1,2-aryl migration process from gold(I) vinylidene **XII**.

	XVIa	**TS $_{XIIa-XVIa}$**	**XIIa**	**TS $_{XIIa-XIIb}$**	**XIIb**	**TS $_{XIIb-XVIb}$**	**XVIb**
B3LYP 6-31G**	-3550643.0	-3550616.2	-3550621.0	-3550620.3	-3550622.6	-3550616.7	-3550643.7
PBE0 6-31G**	-3548851.2	-3548825.4	-3548829.4	-3548826.9	-3548830.7	-3548826.3	-3548851.7
M06 6-31G**	-3549736.6	-3549709.0	-3549712.2	-3549710.2	-3549712.8	-3549709.8	-3549736.9
B97D 6-31G**	-3550691.9	-3550666.8	-3550671.4	-3550670.4	-3550673.0	-3550667.3	-3550692.4
B3LYP 6-311+G**	-3552250.8	-3552222.5	-3552226.8	-3552226.6	-3552228.7	-3552222.5	-3552250.8
PBE0 6-311+G**	-3550429.7	-3550402.7	-3550406.2	-3550404.1	-3550407.7	-3550403.0	-3550429.6
M06 6-311+G**	-3551344.4	-3551314.6	-3551317.4	-3551315.8	-3551317.7	-3551314.7	-3551343.8
B97D-6-311+G**	-3552293.3	-3552267.2	-3552271.1	-3552270.6	-3552273.0	-3552267.1	-3552293.2

All the energies are given in kcal/mol.

Table 20. Benchmark of absolute calculated energy values of 1,2-aryl migration process from gold(I) vinylidene **XIII**.

	XVIIa	**TS $_{XIIIa-XVIIa}$**	**XIIIa**	**TS $_{XIIIa-XIIIb}$**	**XIIIb**	**TS $_{XIIIb-XVIIb}$**	**XVIIb**
B3LYP 6-31G**	-3560245.8	-3560218.8	-3560224.8	-3560221.2	-3560223.6	-3560218.3	-3560245.4
PBE0 6-31G**	-3558430.7	-3558404.0	-3558404.0	-3558404.2	-3558407.4	-3558404.3	-3558429.1
M06 6-31G**	-3559312.8	-3559285.0	-3559290.3	-3559284.3	-3559286.9	-3559285.2	-3559312.1
B97D 6-31G**	-3560278.3	-3560253.1	-3560258.7	-3560254.8	-3560257.5	-3560252.4	-3560277.6
B3LYP 6-311+G**	-3561850.0	-3561821.9	-3561827.4	-3561824.1	-3561826.4	-3561849.2	-3561849.2
PBE0 6-311+G**	-3560005.4	-3559977.8	-3559983.7	-3559977.8	-3559981.0	-3559977.8	-3560003.6
M06 6-311+G**	-3560918.9	-3560889.2	-3560894.0	-3560887.9	-3560890.4	-3560888.8	-3560917.6
B97D-6-311+G**	-3561876.3	-3561850.3	-3561855.5	-3561851.8	-3561854.4	-3561849.4	-3561875.4

All the energies are given in kcal/mol.

Table 21. Benchmark of absolute calculated energy values of 1,2-aryl migration process from gold(I) vinylidene **XIV**.

	XVIIIa	**$TS_{XIVa-XVIIIa}$**	**XIVa**	**$TS_{XIVa-XIVb}$**	**XIVb**	**$TS_{XIVb-XVIIIb}$**	**XVIIIb**
B3LYP 6-31G**	-3699867.7	-3699839.9	-3699845.6	-3699845.5	-3699847.6	-3699840.1	-3699870.1
PBE0 6-31G**	-3697935.2	-3697908.8	-3697912.4	-3697911.9	-3697915.1	-3697909.5	-3697938.0
M06 6-31G**	-3698911.9	-3698883.8	-3698886.3	-3698886.1	-3698887.4	-3698884.8	-3698911.9
B97D 6-31G**	-3699835.5	-3699809.9	-3699815.0	-3699814.7	-3699817.4	-3699809.9	-3699838.2
B3LYP 6-311+G**	-3701524.6	-3701495.4	-3701500.9	-3701501.3	-3701503.5	-3701495.9	-3701527.6
PBE0 6-311+G**	-3699559.5	-3699532.0	-3699535.4	-3699535.2	-3699538.5	-3699532.7	-3699562.8
M06 6-311+G**	-3700561.4	-3700531.5	-3700533.7	-3700533.8	-3700534.7	-3700532.1	-3700561.8
B97D-6-311+G**	-3701486.4	-3701459.7	-3701464.5	-3701464.7	-3701467.6	-3701460.0	-3701489.8

All the energies are given in kcal/mol.

Table 22. Low temperature frequency calculations to discard artefacts due to the temperature parameter.

	XVII a	**$TS_{XIIIa-XVIIa}$**	**XIII a**	**$TS_{XIIIa-XIIIb}$**	**XIII b**	**$TS_{XIIIb-XVIIb}$**	**XVII b**
PBE0 25 ºC	-20.5	6.2	0.0	6.0	2.7	5.9	-19.0
PBE0 –90 ºC	-15.3	5.7	0.0	6.2	2.2	5.9	-15.9

All the energies are given in kcal/mol.

Computed Structures and Energies (B3LYP-D3)

Gold(I) vinylidene 31

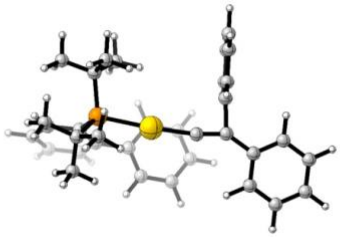

E = -1795.03695806 Hartrees
G = -1794.494270 Hartrees

TS_{31-32}

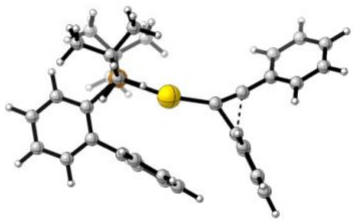

E = -1795.02973140 Hartrees
G = -1794.485943 Hartrees

(η^2-diphenylacetylene) gold(I) complex 32

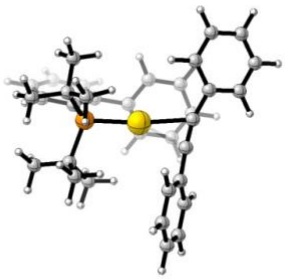

E = -1795.07697599 Hartrees
G = -1794.532794 Hartrees

III' *Z*

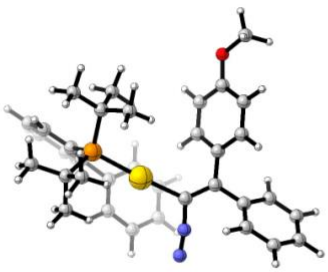

E = -2019.10494977 Hartrees
G = -2018.520816 Hartrees

III' *E*

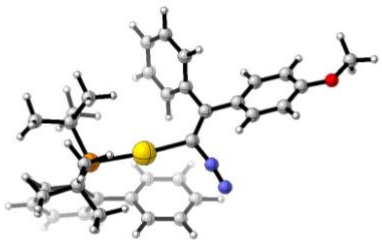

E = -2019.10484988 Hartrees
G = -2018.520345 Hartrees

Gold(I) vinylidene IVa

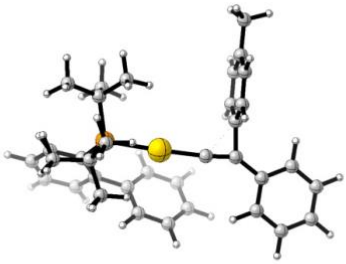

E = -1834.36424291 Hartrees
G = -1833.796635 Hartrees

Gold(I) vinylidene IVb

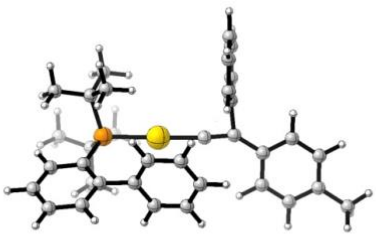

E = -1834.36249029 Hartrees
G = -1833.794635 Hartrees

$TS_{IVa-VIIa}$

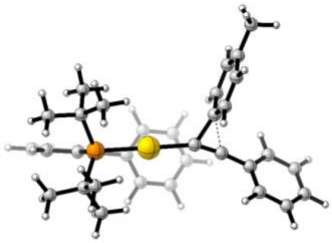

E = -1834.35530756 Hartrees
G = -1833.786515 Hartrees

$TS_{IVb-VIIb}$

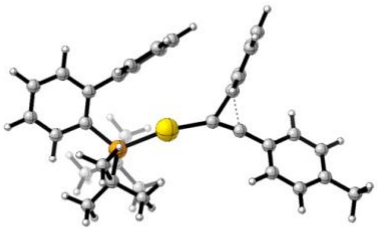

E = -1834.35435243 Hartrees
G = -1833.785198 Hartrees

(h^2-diarylacetylene) gold(I) complex VIIa

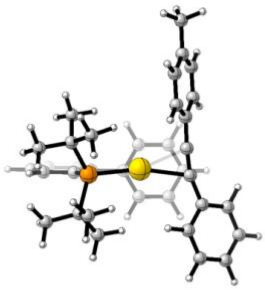

E = -1834.40093653 Hartrees
G = -1833.833462 Hartrees

(h^2-diarylacetylene) gold(I) complex VIIb

E = -1834.40133266 Hartrees
G = -1833.832863 Hartrees

Gold(I) vinylidene Va

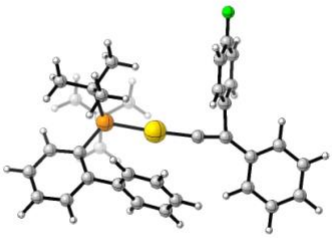

E = -1894.26927477 Hartrees
G = -1893.735994 Hartrees

Gold(I) vinylidene Vb

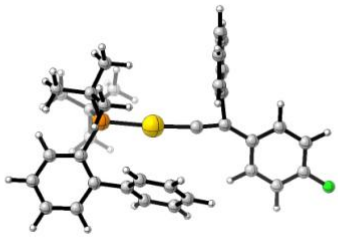

E = -1894.26870393 Hartrees
G = -1893.735462 Hartrees

$TS_{Va-VIIIa}$

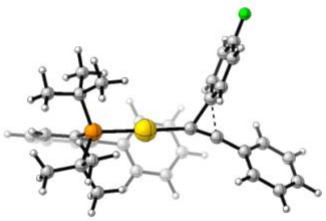

E = -1894.26054674 Hartrees
G = -1893.726727 Hartrees

$TS_{Vb-VIIIb}$

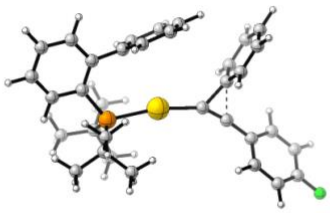

E = -1894.26016964 Hartrees
G = -1893.726694 Hartrees

(η^2-diarylacetylene) gold(I) complex VIIIa

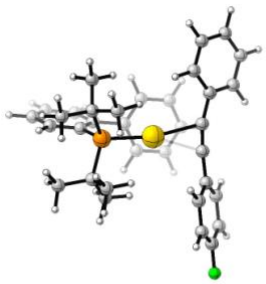

E = -1894.30700539 Hartrees
G = -1893.773925 Hartrees

(η^2-diarylacetylene) gold(I) complex VIIIb

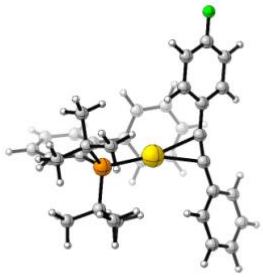

E = -1894.30738897 Hartrees
G = -1893.772738 Hartrees

Gold(I) vinylidene VIa

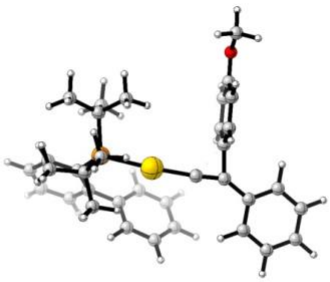

E = -1909.57420984 Hartrees
G = -1909.002169 Hartrees

Gold(I) vinylidene VIb

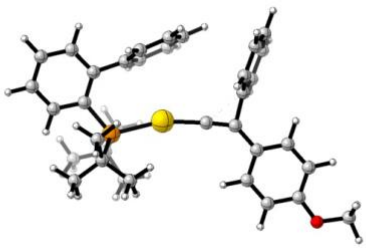

E = -1909.56812778 Hartrees
G = -1908.995330 Hartrees

$TS_{VIa-IXa}$

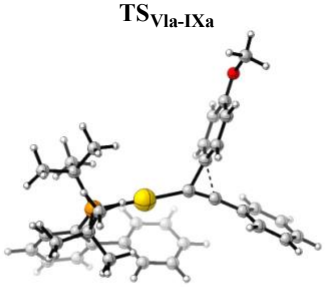

E = -1909.56432120 Hartrees
G = -1908.992066 Hartrees

$TS_{VIb-IXb}$

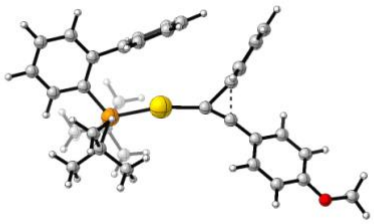

E = -1909.56167114 Hartrees
G = -1908.988901 Hartrees

(η^2-diarylacetylene) gold(I) complex IXa

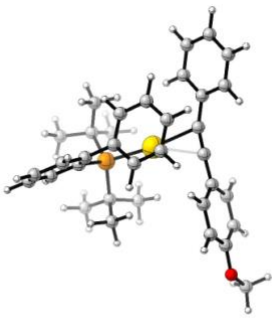

E = -1909.60862991 Hartrees
G = -1909.036273 Hartrees

(η^2-diarylacetylene) gold(I) complex IXb

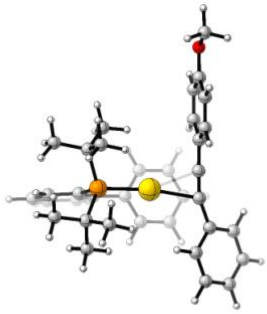

E = -1909.60832994 Hartrees
G = -1909.035084 Hartrees

Gold(I) vinylidene XIa

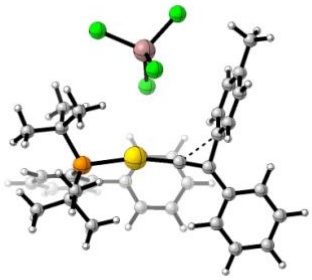

E = -5598.37365792 Hartrees
G = -5597.814371 Hartrees

Gold(I) vinylidene XIb

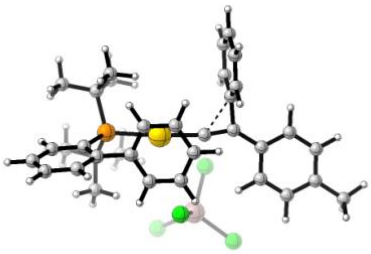

E = -5598.37500713 Hartrees
G = -5597.815898 Hartrees

$TS_{XIa-XIb}$

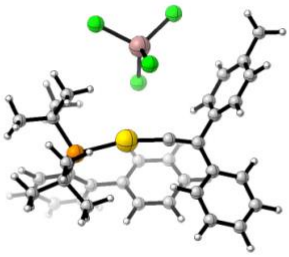

E = -5598.37193634 Hartrees
G = -5597.811089 Hartrees

$TS_{XIa-XVa}$

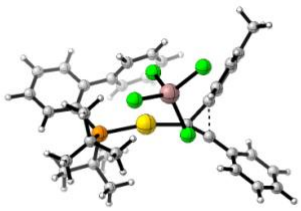

E = -5598.36570183 Hartrees
G = -5597.806831 Hartrees

$TS_{XIb-XVb}$

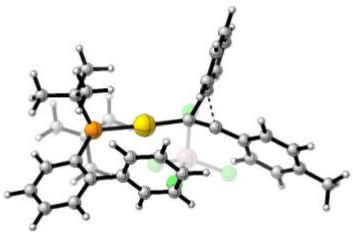

E = -5598.36615147 Hartrees
G = -5597.807722 Hartrees

(h^2-diarylacetylene) gold(I) complex XVa

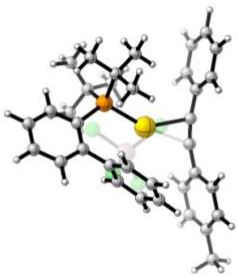

E = -5598.40908958 Hartrees
G = -5597.849208 Hartrees

(h^2-diarylacetylene) gold(I) complex XVb

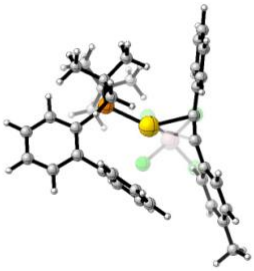

E = -5598.40893881 Hartrees
G = -5597.849043 Hartrees

Gold(I) vinylidene XIIa

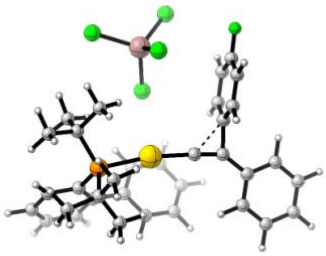

E = -5658.27925860 Hartrees
G = -5657.757012 Hartrees

Gold(I) vinylidene XIIb

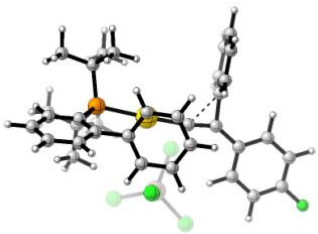

E = -5658.28168850 Hartrees
G = -5657.759395 Hartrees

$TS_{XIIa-XIIb}$

E = -5658.27805754 Hartrees
G = -5657.751919 Hartrees

$TS_{XIIa-XVIa}$

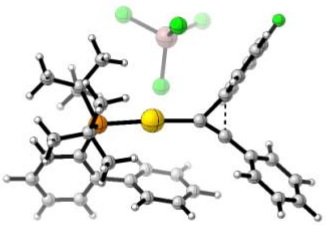

E = -5658.27156578 Hartrees
G = -5657.746514 Hartrees

$TS_{XIIb-XVIb}$

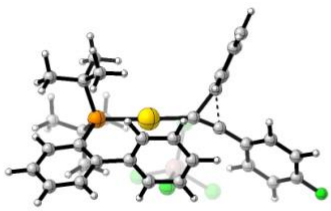

E = -5658.27253665 Hartrees
G = -5657.747400 Hartrees

(h^2-diarylacetylene) gold(I) complex XVIa

E = -5658.31442567 Hartrees
G = -5657.791677 Hartrees

(h^2-diarylacetylene) gold(I) complex XVIb

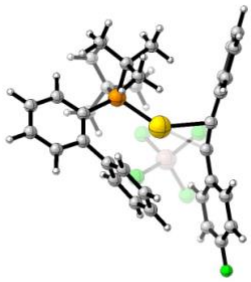

E = -5658.31521271 Hartrees
G = -5657.791495 Hartrees

Gold(I) vinylidene XIIIa

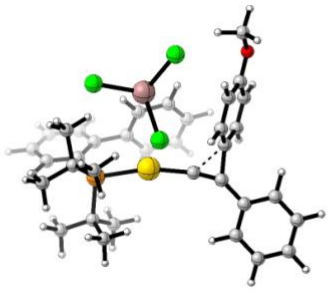

E = -5673.58382725 Hartrees
G = -5673.018834 Hartrees

Gold(I) vinylidene XIIIb

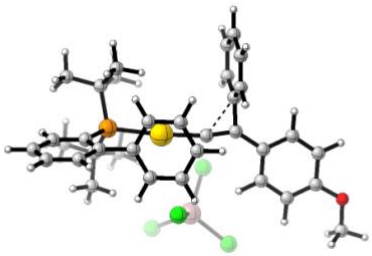

E = -5673.58194209 Hartrees
G = -5673.018681Hartrees

$TS_{XIIIa-XIIIb}$

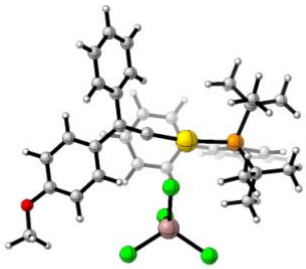

E = -5673.57811469 Hartrees
G = -5673.011621 Hartrees

$TS_{XIIIa-XVIIa}$

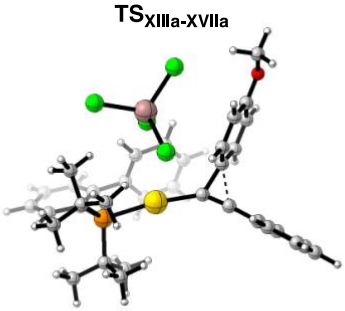

E = -5673.57427089 Hartrees
G = -5673.011675 Hartrees

$TS_{XIIIb-XVIIb}$

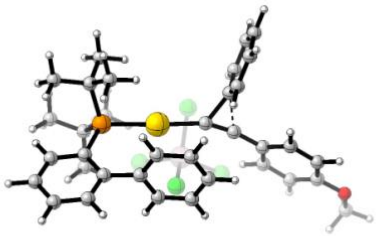

E = -5673.57383085 Hartrees
G = -5673.009114 Hartrees

(h^2-diarylacetylene) gold(I) complex XVIIa

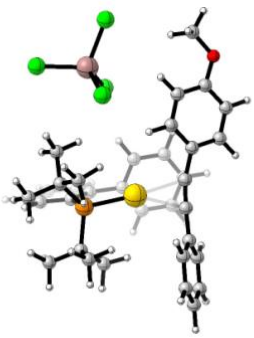

E = -5673.61726370 Hartrees
G = -5673.056258 Hartrees

(h^2-diarylacetylene) gold(I) complex XVIIb

E = -5673.61654541 Hartrees
G = -5673.051948 Hartrees

Gold(I) vinylidene XIVa

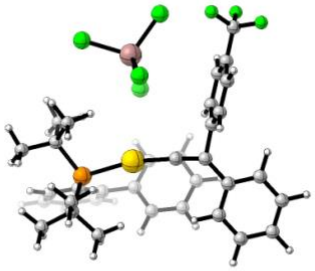

E = -5896.08380195 Hartrees
G = -5895.548171Hartrees

Gold(I) vinylidene XIVb

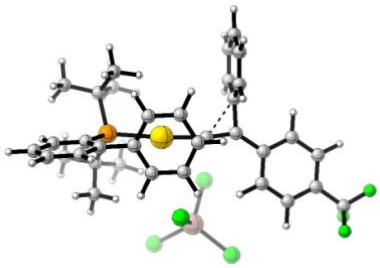

E = -5896.08695834 Hartrees
G = -5895.555654 Hartrees

$TS_{XIVa-XIVb}$

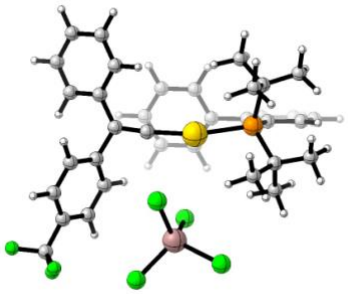

E = -5896.08363977 Hartrees
G = -5895.547649 Hartrees

$TS_{XIVa-XVIIIa}$

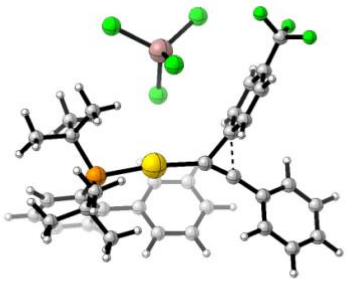

E = -5896.07481056 Hartrees
G = -5895.540802 Hartrees

$TS_{XIVb-XVIIIb}$

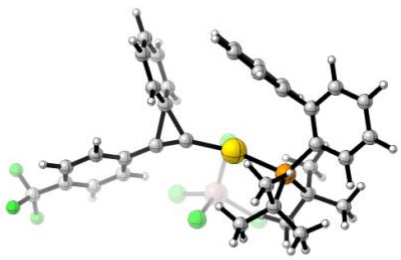

E = -5896.07523528 Hartrees
G = -5895.542917 Hartrees

(h^2-diarylacetylene) gold(I) complex XVIIIa

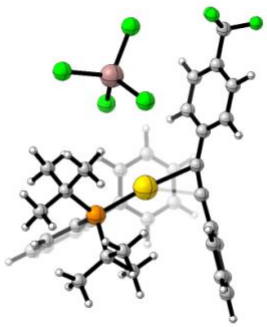

E = -5896.11914101 Hartrees
G = -5895.584198 Hartrees

(h^2-diarylacetylene) gold(I) complex XVIIIb

E = -5896.12292484 Hartrees
G = -5895.588609 Hartrees

Chapter III

General Conclusions

General Conclusions

The research developed in this Doctoral Thesis has led to the following results:

Two new members of the family of chiral pyrrolidinyl biaryl phosphine complexes has been designed and developed by amplifying the central ring (Scheme 1). This work has unblocked a new modular synthetic route which can be used to implement further modifications in this family of chiral gold(I) complexes. The performance of the new complexes has been tested in five different reactions, comparing their reactivity to the one disclosed by the first generation of this family of complexes.

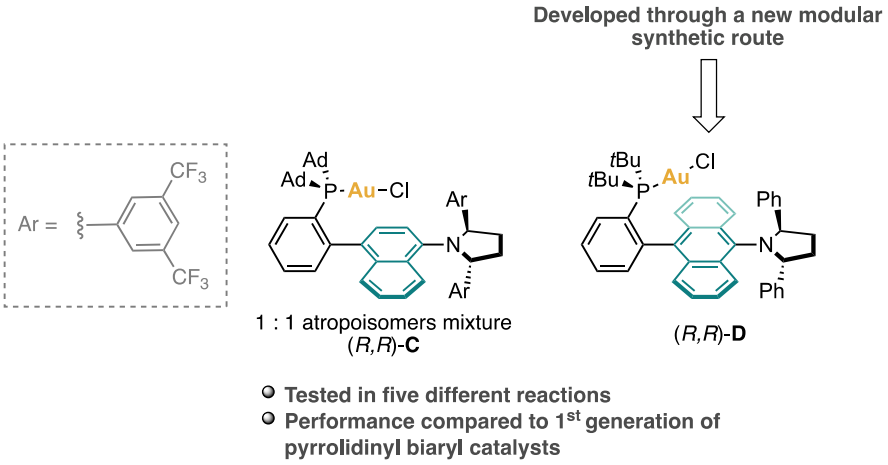

Scheme 1. Expansion of the family of pyrrolidinyl-biaryl phosphine gold(I) complexes.

The synthesis of these catalysts has given us information on how expanding the central ring of these structures affects the enantio-induction of this family of complexes.

The nature of gold(I) vinylidenes has been studied through their relationship with gold(I) vinylidenoids (Scheme 2). In this sense, a family of gold(I) vinylidenoids has been synthesized and their structural and reactivity features have been analyzed. The synthesized gold(I) vinylidenoids present matching parameters with other metal vinylidenoids and with gold(I) carbenoids, which make them suitable candidates for the generation of gold(I) vinylidenes. Additionally, they showed vinylidene typical reactivity, undergoing 1,2-shift reaction to form η^2-diarylacetylene gold(I) complexes. As far as we know, this would be the first time in which 1,2-aryl migration through gold(I) vinylidenes has been observed.

The study of the migration aptitudes of the aryl substituents via low temperature NMR, together with DFT analysis have supported the participation of gold(I) vinylidenes in these transformations. Calculation displayed that the studied gold(I) vinylidenes presented two conformational isomers a and b which ability of interconversion highly affects the reaction outcome. Additionally, DFT analysis has shown the high instability of these intermediates compere to their η^2-alkyne tautomers (a' and b'), which prevents their detection via low temperature NMR. Finally, DFT analysis of the computed structures

for these diaryl gold(I) vinylidenes a and b evidenced a higher stabilization from the diaryl groups than from the gold(I) unit.

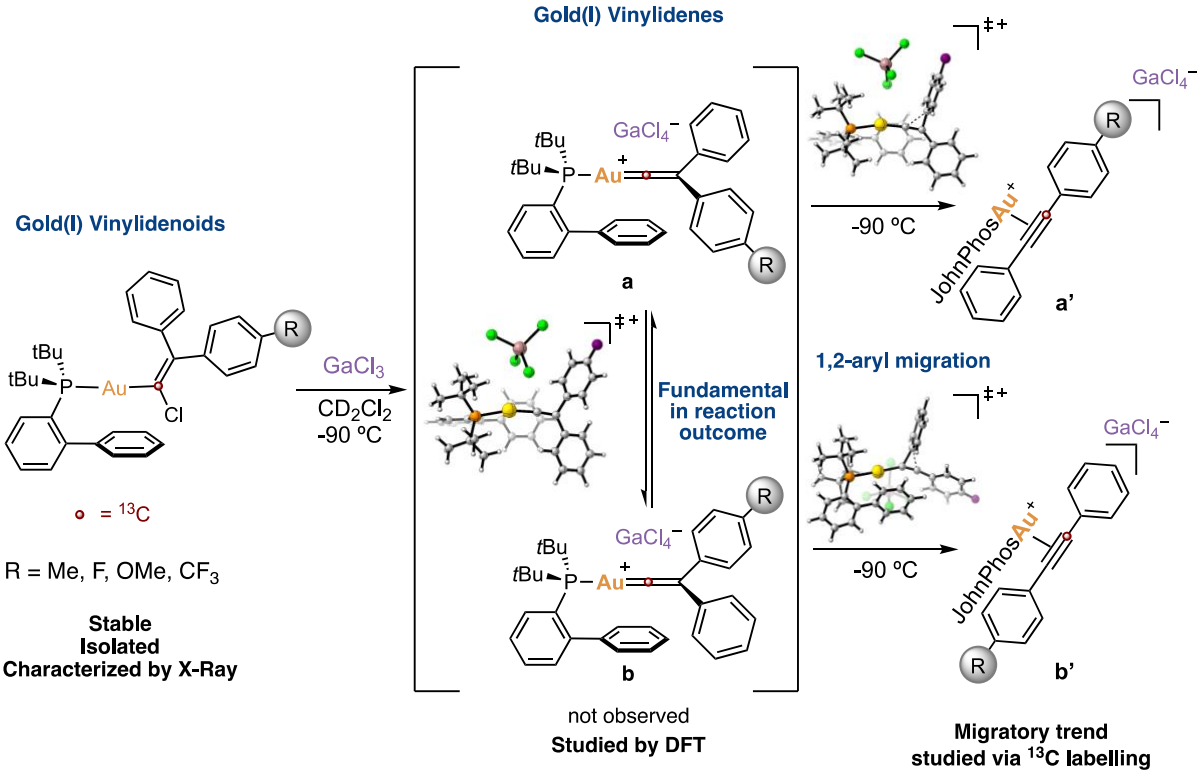

Scheme 2. On the nature of gold(I) vinylidenes.

UNIVERSITAT
ROVIRA i VIRGILI